Investigating the role of hypoxia in CML metabolism

Daniele Sarnello

Thesis submitted to the University of Glasgow in accordance with the requirements for the degree of Doctor of Philosophy

School of Cancer Sciences

College of Medical, Veterinary and Life Sciences

University of Glasgow

September 2024

University of Glasgow

CANCER RESEARCH UK

Abstract

Chronic myeloid leukaemia (CML) is a blood cancer arising from a haematopoietic stem cell (HSC) carrying the aberrant chromosomal translocation t (9;22) (q34; q11). The resulting "Philadelphia Chromosome" hosts the fusion oncogene *BCR::ABL1*, which encodes for a constitutive active non-receptor tyrosine kinase: BCR::ABL1. The gold-standard treatment of CML are tyrosine kinase inhibitors (TKIs), such as Imatinib mesylate. However, TKI treatment does not lead to complete eradication of CML cells as shown by relapse upon treatment suspension. Indeed, the main limitation of TKIs regimen is related to the presence of drug-resistant leukaemic stem cells (LSCs).

The bone marrow (BM) hypoxic microenvironment is an essential niche for the self-renewal and survival of primitive HSCs. Oxygen levels in the BM range from <1% to 6% in the sinusoidal cavity. Hematopoietic cells cultured *in vitro* under hypoxic conditions are mostly in the G_0 phase of the cell cycle and, hence, slow proliferating.

Hypoxia (0.5% O_2) enhances CML LSCs stem cell properties, clonogenicity and engraftment in immunocompromised mice despite effective TKI-mediated inhibition of downstream BCR::ABL1 signaling. Low O_2 levels reduce the pro-apoptotic effect of Imatinib, resulting in the selection of resistant progenitor cells. However, current research suggests that the transcriptional activity of HIF-1α (master regulator of the hypoxia response) is reduced by Imatinib treatment, implying that persistence of CML LSCs in the hypoxic BM microenvironment could be induced by other mechanisms, whose regulation might be independent of this transcription factor.

Despite numerous studies investigating the metabolic profile of CML LSCs, details on how CML LSCs reprogram their metabolic activity once exposed to hypoxia are lacking. Knowing this could help to better understand how this resistant cellular reservoir can properly function in the BM microenvironment.

In this work we initially show that both short-term and long-term hypoxia promotes transcriptional changes in metabolic genes in CML LSCs. Moreover, via metabolomics studies, we demonstrate that CML cells rewire their mitochondrial metabolic activity when exposed to low oxygen levels. Indeed, while glucose is mostly used for lactate production and secretion, hypoxic CML cells increase glutamine uptake and use it to fuel the tricarboxylic acid cycle via both oxidative and reductive metabolism. Interestingly, we demonstrate that pharmacological inhibition of glutaminase 1 significantly kills CML cells when exposed to hypoxia.

With the attempt to understand deeper the molecular mechanisms involved in this metabolic shift, we observed that the receptor-mediated mitophagy genes BNIP3 and BNIP3L (NIX) are upregulated in CML LSCs compared to non-CML cells. Moreover, we show that BNIP3 is required for proper mitochondrial turnover even under normoxia and erythroid differentiation under hypoxia in CML cells.

Furthermore, via extensive metabolic analysis of CML cells, we suggest a novel role of BNIP3-dependent mitophagy in promoting glutamine anaplerosis and reductive carboxylation in CML cells during their adaption to hypoxia. Of note, mice transplantation with BNIP3 depleted CML cells we prove the importance of BNIP3-mediated mitophagy in survival and tumour formation in an *in vivo* setting

Together our results indicate a novel role of BNIP3-mediated mitophagy in metabolic reprogramming and sustaining the survival of CML cells in the hypoxic microenvironment by promoting glutaminolysis and reductive carboxylation.

Table of Contents

List of Figures

Author’s declaration

I hereby testify that all the work presented in this thesis is my own, unless otherwise stated. I confirm that this work has not been previously submitted for consideration of any other degree.

Daniele Sarnello

Acknowledgments

Special thanks go to my primary supervisor Professor Vignir Helgason for giving me the opportunity to undertake a PhD in his research group with a prestigious CRUK PhD Scholarship and for his support and guidance during this journey. I would also like to thank my secondary supervisor Dr Thomas MacVicar for the helpful conversations on mitochondria and his valuable suggestions.

I would like to thank all members of the Helgason lab and all the people that I met in WWCRC for their support and the great moments shared together.

I would like to acknowledge all the people who help me to realise this work, such as the Beatson metabolic team for LC-MS experiments and Mrs Karen Dunn for her support with the *in vivo* models.

Lastly, I would like to thank my family for their unconditional support.

Abbreviations

5-mC	5-methylcytosine
α-KG	Alpha ketoglutarate
2OGDDs	2-oxoglutarate dioxygenases
7AAD	7-Aminoactinomycin D
ABL1	ABL Proto oncogene-1, non-receptor tyrosine kinase
Ac-COA	Acetyl-COA
ACLY	Adenosine triphosphate citrate lyase
ACSS2	Acetyl-CoA synthetase 2
ADP	Adenosine diphosphate
AK4	Adenylate kinase 4
Akt	Protein kinase t
ALL	Acute lymphoblastic leukaemia
AML	Acute myeloid leukaemia
AMP	Adenosine monophosphate
AMPK	AMP-activated protein kinase
ASCT2	Alanine/serine/cysteine-preferring transporter 2
ATG7	Autophagy related protein 7
ATG12	Autophagy related protein 12
ATG13	Autophagy related protein 13
ATG14	Autophagy related protein 14
ATP	Adenosine triphosphate
BCA	Bicinchoninic acid
BCR	Breakpoint cluster region
BIT	BSA insulin and transferrin
BM	Bone marrow
BNIP3	BCL2 interacting protein 3
BNIP3L/NIX	BCL2 interacting protein 3-like
BPTES	Bis-2-(5-phenylacetamido-1,2,4-thiadiazol-2-yl)ethyl
BSA	Bovin serum albumin

CaCl2	Calcium chloride
CALCOCO2	Calcium binding and coiled-coil domain 2
CBP	CREB binding protein
CCCP	Carbonyl cyanide m-chlorophenyl hydrazone
ccRCC	Clear cell renal carcinoma
CD235a	Glycophorin A
CD34	Cluster of differentiation 34
CD38	Cyclic ADP ribose hydrolase
CD71	Transferrin receptor 1
CD90	Cluster of differentiation 90
CDP	Cytidine diphosphate
c-kit	Stem cell factor receptor
CLP	Common lymphoid progenitor
CML	Chronic myeloid leukaemia
CML-BP	Chronic myeloid leukaemia blast phase
CML-CP	Chronic myeloid leukaemia chronic phase
CMP	Common myeloid progenitor
CNS	Central nervous system
CO2	Carbon dioxide
CoA	Coenzyme A
COX4l1/2	Cytochrome c oxidase subunit 4l1/2
CREB	Cyclic adenosine monophosphate response element binding protein
Cryo-EM	Cryogenic electron microscopy
CTP	Cytidine triphosphate
DMEM	Dulbecco's modified eagle medium
DMSO	Dimethyl sulfoxide
DNA	Deoxyribonucleic acid
DPBS	Dulbecco's phosphate-buffer saline
Drp1	Dynamin-1-like-protein
DTG	Double transgenic
EPO	Erythropoietin

ETC	Electron transport chain
ETV4	ETS Variant Transcription Factor 4
FA	Faty acid
FAD	Flavin adenine dinucleotide
FAO	Fatty acid oxidation
FASN	Fatty acid synthase
FBXL4	F-box and leucine rich repeat protein 4
FH	Fumarate hydratase
FIH1	Factor inhibiting HIF1
Flt3	Fms related receptor tyrosine kinase 3
FUNDC1	FUN14 Domain Containing 1
GAC	Glutaminase C
GLIPR2	Golgi-associated protein named glioma pathogenesis related 2
GLS	Glutaminase
GLUD	Glutamate dehydrogenase
GlyA	Glycophorin A
GPNA	l-γ-glutamyl-p-nitroanilide
GSH	Glutathione
GTP	Guanosine5’-triphosphate
H	Hydrogen
HCQ	Hydroxychloroquine
HSC	Haematopoietic stem cell
HIF	Hypoxia inducible factor
HREs	Hypoxia responsive elements
hiPSCs	Human induced pluripotent stem cells
IDH 1/2/3	Isocitrate dehydrogenase 1/2/3
IMM	Inner mitochondrial membrane
JNK	c-Jun N-terminal kinase
KDM	Histone (lysine) demethylase
KGA	Kidney-type glutaminase
LC3-II	Microtuble-associated protein light chain 3-II

LDHA	Lactate dehydrogenase A
L-2HG	L-2Hydroxyglutarate
LIR	LC3-interacting region
LSC	Leukaemic stem cell
MAPK	Mitogen-activated protein kinase
ME	Malic enzyme
MCT4	Monocarboxylate transporter 4
MFN2	Mitofusin-2
MIRO	Mitochondrial Rho GTPase 1
MMP	Mitochondrial membrane potential
MPC	Mitochondrial pyruvate carrier
mtDNA	Mitochondrial DNA
mTORC (1-2)	Mammalian target of rapamycin (1-2)
NAD	Nicotinamide adenine dinucleotide
NADH	NAD + H
NDUFA4L2	NADH dehydrogenase (ubiquinone) 1α subcomplex, 4- like 2
OAA	Oxaloacetate
OGDC	Oxoglutarate dehydrogenase complex
OMM	Outer Mitochondrial Membrane
OPTN	Optineurin
OXPHOS	Oxidative Phosphorylation
PARL	PINK/PGAM5-associated rhomboid-like
PC	Pyruvate carboxylase
PDAC	Pancreatic ductal adenocarcinoma
PDH	Pyruvate Dehydrogenase
PDK1	Pyruvate Dehydrogenase Kinase 1
PGAM5	PGAM family member 5
PGC1α	Peroxisome proliferator-activated receptor-gamma coactivator 1 alpha
PHDs	Prolyl hydroxylases
PINK1	PTEN-induced putative kinase 1

RAS	Ras sarcoma virus
RC	Reductive carboxylation
Rheb	Ras homolog enriched in brain
ROS	Reactive oxygen species
SCF	Cullin, F-box containing complex.
SCD	Stearoyl- CoA desaturase
SDH	Succinate dehydrogenase
SLC1A3	Solute carrier family 1 member 3
SREBP-1	Sterol regulatory element-binding protein-1
TBK1	TANK-binding kinase 1
TOM	Translocase of the outer membrane
TCA	Tricarboxylic acid
TKI	Tyrosine kinase inhibitor
TM	Transmembrane
TMT	Tandem mass tag
Ub	Ubiquitin
UPS	Ubiquitin-proteasome system
VEGF	Vascular endothelial growth factor

Chapter 1 Introduction

1.1 Haematopoiesis and Haematopoietic Stem Cells

1.1.1 Definition and discovery of HSCs

Haematopoietic stem cells (HSCs) are Bone Marrow (BM)-resident, rare and immature cells that can develop into all types of blood cells (characteristic known as multi-potency) and can regenerate themselves (ability known as self-renewal)[1].

The discovery of HSCs was due to pioneering studies of BM allogenic transplantation into immunocompromised mice and guinea pigs[2,3]. Subsequently it was discovered that a single HSC gives origin to a multilineage progeny of cells which can still retain the parental cell properties[4,5]. Later, thanks to the improvements in cell-surface markers identification and hence more advanced isolation and purification techniques, it was discovered that HSCs can regenerate all blood cells after transplantation[6]. Based on these previous studies the HSC roadmap was established.

1.1.2 Haematopoietic hierarchy roadmap

The haematopoietic hierarchy is represented as a branched roadmap that describes the differentiation steps from HSCs to all the blood cell types.

Originally HSCs were subdivided into two different subpopulations: long-term HSCs (LT-HSCs) and short-term HSCs (ST-HSCs)[7,8,9,10]. While LT-HSCs can permanently reconstitute the BM and are quiescent[11,12,13], ST-HSCs have only short-term reconstitution capability. ST-HSCs can either undergo symmetric cell division to self-renew or differentiate into Multipotent progenitors (MPPs) via asymmetric cell division, that have no self-renewal ability and can further differentiate due to their higher cell-cycle progression compared to HSCs[14,15,16]. From MPPs two differentiation branches are derived: the common lymphoid progenitors (CLPs), that can further develop into lymphocytes and the common myeloid progenitors (CMPs), that can diverge into megakaryocytes/erythrocytes progenitors (MEPs) and granulocyte/macrophage progenitors (GMPs) [17,18]. A Schematic of the HSCs tree is provided in figure 1.

Haematopoiesis is a continuous and strictly regulated differentiation process. Every day an average adult is estimated to generate more than 10^{11} blood cells[19].

However, thanks to the most recent advancements in single cell omics technologies, this classical hierarchy model has been updated since HSCs and their downstream progenies are more heterogeneous[16]. For example, Intermediate Term HSCs (IT-HSCs) have been identified as HSCs with self-renewal ability between LT-HSCs and ST-HSCs. Moreover, MPPS can be subdivided into 4 different subpopulations (MPP1, MPP2, MPP3, MPP4) or lymphoid-primed multipotent progenitors (LMMP) have been discovered as MPPs overexpressing fms related receptor tyrosine kinase 3 (Flt3) gene and preferentially differentiating into the lymphoid lineage [20,21,14].

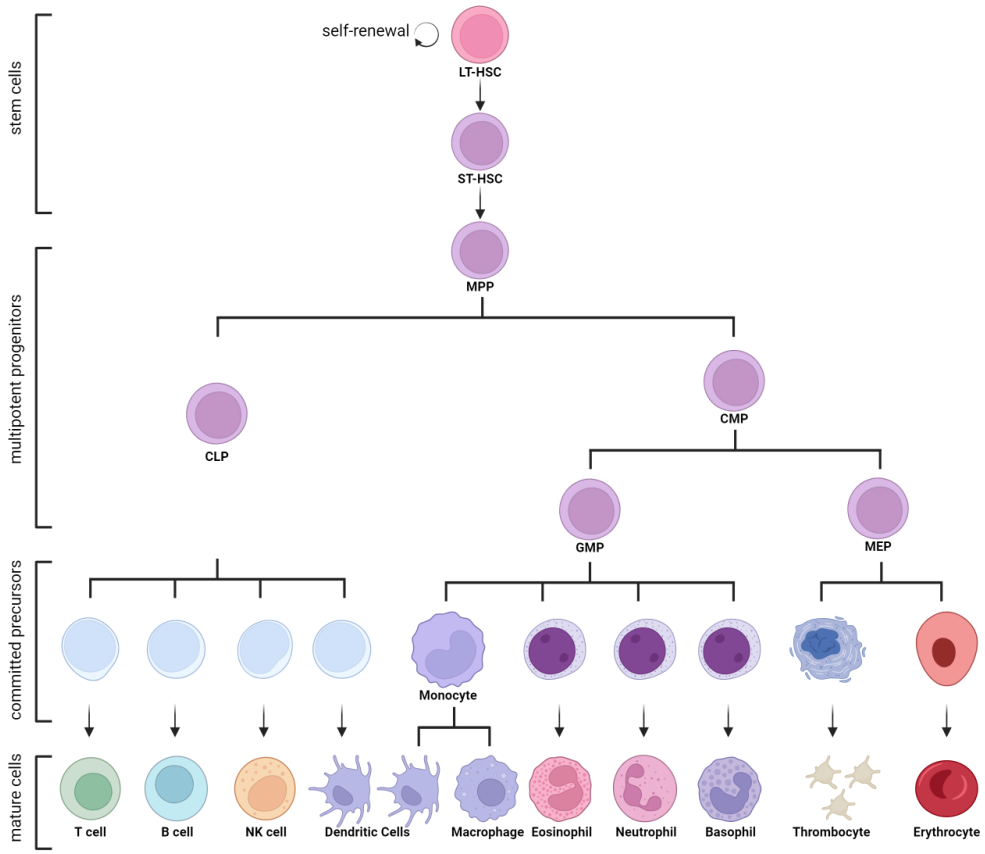

Figure 1 The HSCs tree. HSC; Haematopoietic Stem Cell. LT-HSC; Long Term HSC. ST-HSC; Short Term HSC. MPP; Multipotent progenitor. CLP; Common Lymphoid progenitor. CMP; Common Myeloid progenitor. GMP; Granulocyte/Macrophage progenitors. MEP; Megakaryocytes/erythrocytes progenitor. This figure was made by Dr Desiree Zerbst.

1.1.3 HSCs cell surface markers

A major challenge in the study of HSCs is their identification and isolation from bulk samples. As said before, HSCs represent a rare blood population (1 cell over 100.000 cells in the blood). Therefore, fluorescent activated cell sorting (FACS) has been exploited to identify and isolate HSCs via the identification of cell surface markers and cluster of differentiation antigens.

Although a very rare population of HSCs are $CD34^-$ cells and have been shown to be above the $CD34^+$ HSCs in the hierarchical roadmap[22], most of the haematopoiesis is guided by $CD34^+$ HSCs. CD34 gained interest into the HSCs studies since $CD34^+$ cells are able to reconstitute the BM when transplanted into patients undergoing autologous BM reinfusion after myeloablation[23]. Apart from CD34, the CD38 surface marker has been associated to HSCs when lowly expressed. Indeed, $CD34^+CD38^-$ HSCs could give sequential haematopoietic colonies[24].

1.1.4 Regulation mechanisms of HSCs

Mitochondrial metabolism

During the development of the haematopoietic system, embryonic and neonatal HSCs must proliferate rapidly, while adult HSCs are quiescent and rarely divide[25,26]. Therefore, the transition from embryonal/neonatal stage to adult stage is characterised by a drastic metabolic reprogramming, that mostly culminates in lower mitochondrial content[27]. Moreover, while primitive HSCs are associated to reduced mitochondria levels and rely on glycolysis for their survival and self-renewal properties, differentiating HSCs and HPCs have increased mitochondrial levels and metabolic activity. In this regard, regulation of mitochondrial biogenesis in HSCs is regulated by mammalian target of rapamycin (mTOR), that can regulate the transcriptional levels of peroxisome proliferator-activated receptor gamma coactivator 1-alpha (PGC1α)[28]. Interestingly, it has been observed that LT-HSCs retain low active mitochondria, and that lower mitochondrial activity is essential to sustain HSCs reconstitution[29,30]. Fine-tuned regulation of HSCs metabolic activity is essential for the BM microenvironment.

HSCs reside in the BM microenvironment, where the oxygen levels are low (a condition known as hypoxia). Hypoxia supports anaerobic glycolysis and low-profile metabolic activity of HSCs[31]. Initially it was observed that maintenance of quiescence and stem cell properties were mainly regulated by the high expression of Hypoxia Inducible Factors 1α (HIF1α) and 2α (HIF2α) in adult BM-resident HSCs[32,33]. However, more recent advances have shown that the HIFs are dispensable for the maintenance of HSCs[34]. Therefore, further research is needed to properly understand the molecular signalling induced by low oxygen levels in HSCs.

Other metabolic pathways play an important role in the regulation of HSCs metabolism. For example, HSCs activation and increased proliferation have been linked to glutaminase regulation via alternative polyadenylation[35]. In addition, removal of peroxisome proliferator–activated receptor gamma (PPARγ) and loss of fatty acid oxidation (FAO) inhibited HSCs BM restoration[36].

An important role in the regulation of HSCs biology is played by reactive oxygen species (ROS), a byproduct of oxidative phosphorylation (OXPHOS) given by the leak of electrons from the electron transport chain (ETC), and their regulatory mechanisms. Due to the hypoxic microenvironment of the BM, HSCs must minimise their oxidative stress to

keep their quiescent state, while increased OXPHOS and ROS levels are highly associated with their differentiation[37,38].

Autophagy and mitophagy

Autophagy involves a series of intracellular mechanisms that are essential for the proper regulation of cellular stress and metabolic activity via lysosomal degradation of cellular material, especially organelles (i.e. mitochondria) after their engulfment in double-membrane structures known as autophagosomes. Autophagy is a crucial survival mechanism during conditions of nutrient deprivation and other stressors, such as hypoxia[39,40].

Autophagy plays a key role in HSCs aging and maintenance via regulation of their metabolism. Indeed, loss of autophagy related 12 (*Atg12*) gene in mice led to abnormal accumulation of mitochondria with consequent overactivated metabolism and promoted myeloid differentiation because of reduced stem-cell self-renewal activity and regeneration. The consequence of mitochondrial accumulation in HSCs resulted in increased mitochondrial respiration, ROS levels and mitochondrial membrane potential[41]. Similarly, loss of autophagy related 7 (*Atg7*) gene led to accumulation of mitochondria, ROS and abnormal increased proliferation of DNA-damaged HSCs. Moreover, transplantation of ATG7 knock-out (KO) cells in immunodeficient mice resulted in failed reconstitution of BM[42]. Therefore, the role of autophagy in HSCs is related to the maintenance of their quiescence and low metabolic activity[43] and may represent a protective mechanism to prevent the development of haematopoietic malignancies[42].

Interestingly, autophagy has also been reported to be crucial for regulating embryonic haematopoiesis since removal of autophagy related 5 (*Atg5*) gene inhibited the development of pre-HSCs[44]. Overall, regulation of autophagy and mitochondrial quality control are extremely important for the correct functioning of HSCs.

Mitophagy is the selective removal of mitochondria via the autophagy machinery and has been the focus of studies on HSCs maintenance[45]. The different mechanisms of mitophagy will be better discussed later in this chapter. Here we will mostly report the current state of the art regarding the role of mitophagy in HSCs.

A recent study reported that HSCs exploit the transcription factor NK2 homeobox-1 (Nkx2) to control the expression of unc-51 like autophagy activating kinase 1 (ULK1), the main transcription factor of autophagy and mitophagy regulation. More precisely, ablation of Nkx2 led to reduced expression and protein levels of ULK1 and consequent accumulation of metabolically active mitochondria due to inhibited mitophagy[46]. Also, other mitophagy mechanisms are involved in promoting HSCs function and homeostasis.

For instance, TEK receptor tyrosine kinase 2 $(Tie2)^{+}$ murine HSCs preserve their self-renewal ability via recruitment of Parkin to their mitochondria that is under the control of PPARγ–FAO pathway[47].

Moreover O-linked N-acetylglucosamine (O-GlcNAc) transferase (OGT) was shown to promote high levels of the transcriptional activating histone modification H3K4me3 at PTEN-induced putative kinase 1 (PINK1) promoter and, consequently, induce mitophagy in HSCs. Increased PINK1-mediated mitochondrial quality control was then essential for the maintenance of HSCs[48].

1.2 Hypoxia metabolism and reductive carboxylation

1.2.1 Introduction to mitochondrial metabolism

The tricarboxylic acid (TCA) cycle, also known as citric acid cycle or Krebs cycle represents the major hub for the complete oxidation of the main carbon sources of the cell, i.e. carbohydrates, fatty acids and amino acids. In brief, the TCA cycle starts with the combination of two available carbons from acetyl-CoA molecule, whose total number of carbon atoms is 23, previously generated by the oxidation of carbon fuels and a four-carbon oxaloacetate (OAA) molecule to generate the six-carbon molecule citrate. Next, citrate in converted into its isomer isocitrate. Subsequently, the cycle is characterised of 2 decarboxylation reactions: the first converting the isocitrate into a five-carbon alpha-ketoglutarate (α-KG), the second promoting the generation of the four-carbon succinyl-CoA molecule. The result of these latter steps is the release of two CO_2 molecules and the generation of two reduced nicotinamide adenine dinucleotide-H (NADH) molecules. Next, succinyl-CoA is converted into succinate in a reaction that promotes the generation of 1 molecule of guanosine-5'-triphosphate (GTP), which is further converted in adenosine triphosphate (ATP). Succinate is then oxidised to produce the four-carbon molecule fumarate. During this reaction 2 hydrogen atoms are removed from succinate and donated to flavin adenine dinucleotide (FAD) in order to generate $FADH_2$. Next, fumarate is converted into malate and finally into OAA, which can restart the cycle combining with another acetyl-CoA molecule[49,50].

The net result of the TCA cycle is represented by 1 ATP molecule and high energy electrons in the form of 3 NADH and 1 $FADH_2$, that pass electrons to the ETC complex I (also known as NADH dehydrogenase) and complex II (Succinate dehydrogenase, SDH) respectively. Interestingly, SDH is the only enzyme of the TCA cycle that also belongs to the ETC machinery. Finally, electrons from complex I and complex II are subsequently donated to the ETC and used to synthetise ATP via OXPHOS[49,50]. Electrons are then transferred to coenzyme Q (also known as ubiquinone), to complex III, to cytochrome c and finally to complex IV where the final electron acceptor O_2 is reduced to H_2O. The transport of high-energy electrons is coupled to the pumping of hydrogen protons (H^+) from the mitochondrial matrix to the cytoplasmic side of the inner mitochondrial membrane, generating an electrochemical gradient known as proton-motive force characterised of a H^+ gradient and a membrane potential. This mitochondrial membrane potential allows the H^+ to flow back into the mitochondria via complex V or ATP synthase,

providing the energy to allow the synthesis of ATP[49,51,52]. A schematic of TCA cycle and OXPHOS is provided in figure 2.

Importantly, while the TCA cycle runs in loop, some metabolites can be shuttled away from the mitochondria and take part in other biosynthetic pathways. One example is citrate, that can be transported in the cytosol, where it is further converted into OAA and acetyl-CoA to initiate synthesis of nucleotides and lipids. Therefore, it is important for the TCA cycle to be replenished of its intermediates via a process known as anaplerosis. The two most important anaplerotic mechanisms are the conversion of pyruvate into OAA via pyruvate carboxylase (PC) and glutaminolysis (which will be discussed in further details later)[50,53].

The TCA cycle is tightly regulated via positive and negative allosteric regulators. For example, NADH can negatively regulate all the enzymes of the cycle, while ATP can inhibit pyruvate dehydrogenase (PDH) and isocitrate dehydrogenase (IDH). Finally, succinyl-CoA can inhibit citrate synthase and α-KG dehydrogenase to slow the cycle down. Conversely, high levels of AMP activate the regulatory enzymes of the TCA cycle due to a higher demand of ATP for cellular processes. Higher levels of acetyl-CoA inhibit PDH but activate PC to increase the production of OAA and counterbalance the amount of the two initiators of the cycle[49,50,53].

To satisfy their need to rapidly grow and expand, many cancer cells are characterised of dysregulated metabolism which is the result of metabolic reprogramming[54–59].

In 1920 Otto Warburg discovered that cancer cells preferentially use glycolysis over mitochondrial metabolism to generate ATP despite the presence of oxygen. Therefore, some cancer cells were observed to accumulate lactate, which is then secreted in the extracellular environment, instead of being converted to pyruvate. This cancer cell related abnormal metabolic rewiring has been indicated as “Warburg effect” or aerobic glycolysis since then. A possible explanation of the Warburg effect could be due to the presence of dysfunctional mitochondria due to mutations in key enzymes of mitochondrial respiration, such as SDH, fumarase, pyruvate dehydrogenase kinase (PDK) or IDH[49,50,53,60,61]. However, more recent studies have highlighted the importance of mitochondrial metabolism as a fundamental anabolic process to support tumour growth. For instance, mitochondrial respiration has been shown to support aspartate biosynthesis, which in turn is used to synthetise nucleotides[62].

Therefore, mitochondrial respiration is not only important for the generation of ATP molecules but represents a key process to support cancer cells growth via increased

anabolic activity. However, most of the studies in the field of cancer metabolism have been carried out at the presence of standard oxygen levels and have not taken into account the role of more physiological oxygen levels, generally indicated as hypoxia, which has been studied more recently. Low oxygen levels have a significative impact on cellular metabolism, especially in cancer cells that may require adaptation to survive in hypoxic cores or hypoxic microenvironments[54–56].

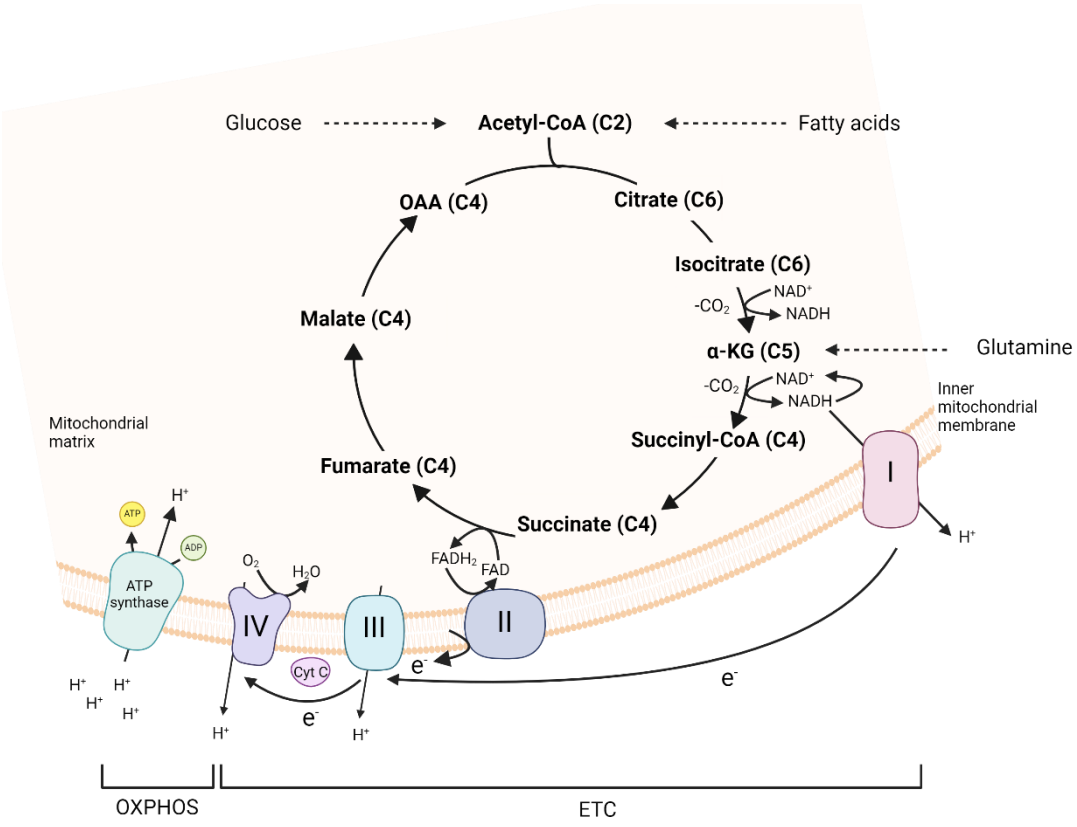

Figure 2. Schematic of the TCA cycle, ETC and OXPHOS. TCA; Tricarboxylic acid, ETC; Electron transport chain, OXPHOS; Oxidative phosphorylation.

1.2.2 Hypoxia regulation and HIFs

To switch their metabolic activity and survive in low oxygen environment, cells rely on the role of the hypoxia master regulators: HIF1 and HIF2.

HIFs are heterodimers constituted of HIFα transcription factors, whose stabilization and expression are regulated by low oxygen levels, and HIF1β, also known as aryl hydrocarbon receptor nuclear translocator (ARNT), which is constitutively expressed. Once in the nucleus HIFα interacts with HIF1β and induces the expression of many genes involved in metabolism and regulation of the molecular response to hypoxia upon binding of the transcription factor on the Hypoxia Responsive Elements (HREs) of the target genes[56,63–66]. Three different HIFα isoforms have been identified so far: HIF1α, HIF2α, HIF3α[67]. While the precise role and function of HIF3α have not been discovered yet, more is known about the activity of HIF1α and HIF2α. Both share some gene targets, such as erythropoietin (EPO) and vascular endothelial growth factor (VEGF)[68], but they can also have different functions. For instance, HIF1α can promote the expression of inducible nitric oxide synthase (iNOS), while HIF2α promotes the expression of arginase 1[69]. Moreover, HIF1α is expressed in almost all cell types, while HIF2α's expression is more tissue specific[70].

As shown in figure 3, at atmospheric oxygen levels, HIFα subunits are hydroxylated on two proline residues by the prolyl hydroxylases (PHDs), enzymes belonging to the 2-oxoglutarate dioxygenases (2OGDDs) family. The hydroxylation reaction requires the decarboxylation of α-ketoglutarate to succinate and CO_2[57,71]. There are three PHDs isoforms (PHD 1-2-3) and all of them require oxygen, iron ($F3^{2+}$) and α-ketoglutarate for their activity. Once hydroxylated, HIFα subunits can interact with the von-Hippel Lindau (pVHL) complex, which promotes their polyubiquitylation for subsequent proteasomal degradation[54,72–74]. An alternative regulatory mechanism of HIFα activity if given by factor inhibiting HIF1 (FIH1), an asparaginyl hydroxylase also belonging to the 2OGDDs family which catalyses the hydroxylation of an asparaginyl residue on the C-terminal domain of HIF1α or HIF2α. This reaction prevents the recruitment of the co-activators p300-CBP and further inhibits the transcriptional activity if HIFs[75–77].

The stability of HIFα subunits can also be modulated by ROS levels[78]. Indeed, during hypoxia (starting from 5%O_2) mitochondrial complex III[79–81] can generate ROS that can promote the oxidation of the cysteine residues of PHDs, hence inactivating them[82].

Furthermore, PHDs activity can be inhibited by succinate[83], fumarate[84,85] and L-2Hydroxyglutarate (L-2HG)[86] since these (onco-)metabolites act as competitive inhibitors

of α-ketoglutarate. The accumulation of succinate or fumarate in normoxia is usually related to mutations of TCA enzymes, such as SDH or Fumarate Hydratase (FH) respectively as it has been shown in neuroendocrine and renal tumours[84,85].

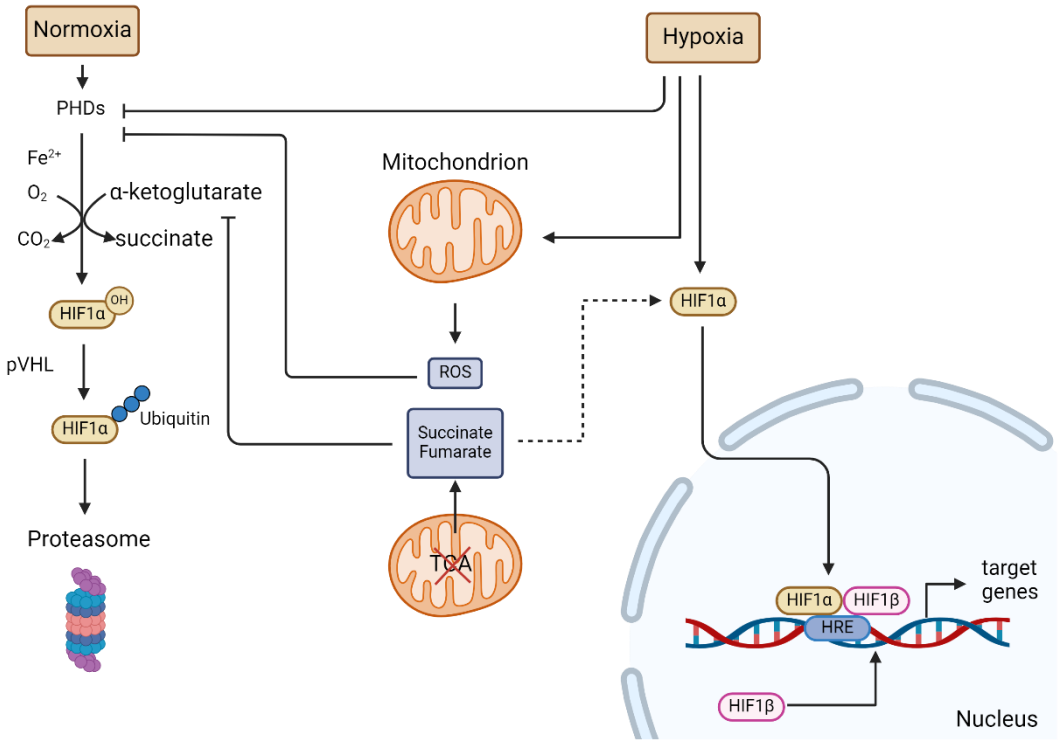

Figure 3. HIF1α stabilization. PHD; prolyl hydroxylase. pVHL; Von Hippel-Lindau

1.2.3 Hypoxia and metabolism

Oxygen is essential for many cellular functions and especially for the generation of ATP via OXPHOS as it is the last electron acceptor of the ETC in the mitochondria. Therefore, the ETC is highly affected by low oxygen levels and its activity slows down after prolonged time. Interestingly the ETC complexes can still work under hypoxia and at oxygen levels close to anoxia, as the activity of the hypoxic ETC is regulated by changes in cellular transcriptional activity[87]. Under acute hypoxia the cytochrome c oxidase subunit 4l1 (COX4l1) subunit of Complex IV is substituted with COX4l2, which allows a better electron transfer to oxygen during acute hypoxia, while during prolonged hypoxia ETC activity is drastically reduced thanks to the over-expression of NADH dehydrogenase (ubiquinone) 1α subcomplex, 4- like 2 (NDUFA4L2)[88]. The reduced ETC activity during hypoxia is also required to avoid excessive oxidative stress[89].

While decreasing the ETC activity, under low oxygen conditions cells also drastically minimise pyruvate oxidation into the TCA cycle (figure 4). Mechanistically HIFs promote the expression of lactate dehydrogenase A (LDHA), which converts pyruvate into lactate. Moreover, the overexpression of pyruvate dehydrogenase kinase 1 (PDK1) promotes the inhibition of pyruvate dehydrogenase (PDH) and hence the entrance of pyruvate into the mitochondrial matrix and its oxidation into the TCA cycle with consequent reduced generation of reducing equivalents NADH and $FADH_2$ and slower ETC[56,90,91].

An important aspect of the hypoxia-reduced TCA activity is that aspartate levels are sharply reduced leading to slower cell proliferation due to lower nucleotide levels[92,93]. Therefore, aspartate is a limiting factor for cells exposed to low oxygen. In a recent study, Garcia-Bermudez *et al*. revealed that cancer cells upregulate the expression of an aspartate-glutamate transporter solute carrier family 1 member 3 (SLC1A3) to import it and sustain their growth *in vitro* and *in vivo* xenografts. Moreover, inhibition of SLC1A3 negatively affected cancer cells growth under low oxygen and sensitised them to ETC inhibitors[94]. HIFs are the major regulators of the "Warburg effect", which can also be indicated as aerobic glycolysis. The Warburg effect happens when cancer cells mostly rely on glycolysis instead of OXPHOS to support their needs of rapid proliferation despite oxygen availability[95–97].

The hypoxic microenvironment can also promote lipid metabolism. Indeed, via HIF1α activity to induce the upregulation of sterol regulatory element-binding protein (SREBP)-1, hypoxic cells can increase *de novo* lipid synthesis due to the higher expression of fatty acid

synthase (FASN)[98,99]. Lipids can be an important source of energy storage, cell membrane formation and a fuel to support ATP production via fatty acid oxidation (FAO)[98,100]. Another important enzyme involved in lipid metabolism is adenosine triphosphate citrate lyase (ACLY), which catalyses the conversion of citrate and CoA into acetyl-CoA and oxaloacetate. Although the proper regulatory mechanisms of ACLY in cancers are not completely understood yet, it has been shown that the enzyme is involved in the regulation of the oncogenic ETS Variant Transcription Factor 4 (ETV4) and hypoxia-induced apoptosis in solid cancer cells[101].

Low oxygen availability triggers the expression and activity of stearoyl- CoA desaturase (SCD). This enzyme catalyses the conversion of saturated fatty acids to monounsaturated fatty acids (FA) and its activity has been linked to poor prognosis and tumour recurrence[102,103]. Interestingly, SCD overexpression promoted migration of metabolically adapted acute lymphoblastic leukaemia (ALL) cells to the hypoxic central nervous system (CNS) *in vivo*, while its inhibition reduced the leukaemic cell burden[104]. In a model of clear cell renal carcinoma (ccRCC), a cancer driven by aberrant constitutive HIF2α expression, Bacigalupa *et al*. have recently discovered that inhibition of acetyl-CoA synthetase 2 (ACSS2) disrupts glycolysis and cholesterol synthesis and successfully kills cancer cells[105].

All these studies suggest that hypoxia exert a strong pressure on non-cancer and cancer cells, that can quickly adapt to this challenging microenvironment. Therefore, studying metabolic adaptions of cancer cells to hypoxia could help to identify novel therapeutic targets.

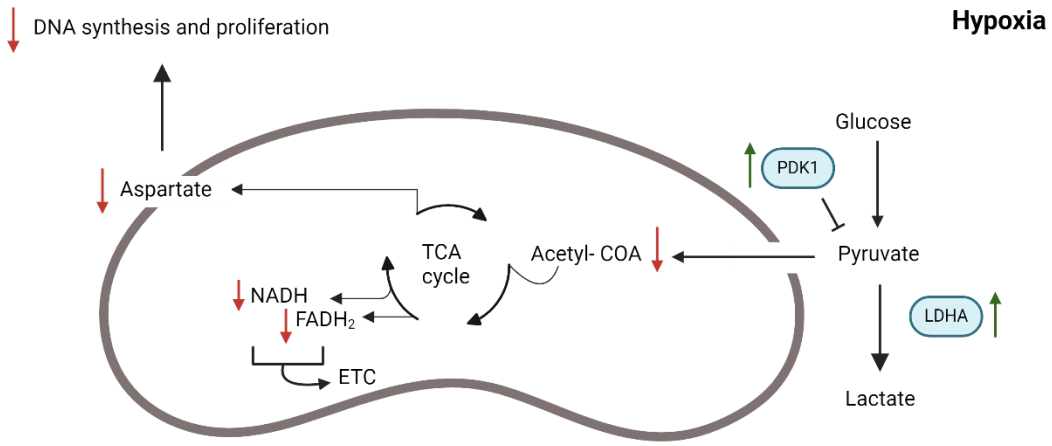

Figure 4. Mitochondrial metabolism changes during hypoxia. ETC; Electron transport chain**.**

1.2.4 Overview of glutamine metabolism in cancer

Glutamine is the most abundant non-essential amino acid in the human plasma[106] and has been shown to be an important carbon and nitrogen source for biosynthetic pathways especially in cancer cells. Indeed, many cancers show oncogene-dependent addictions to glutamine[107].

It is indeed known that the proto-oncogene c-MYC promotes the expression of amino acid transporters as the alanine/serine/cysteine-preferring transporter 2 (ASCT2 or SLC1A5) which can also be used by many cancer cells to sustain glutamine uptake[108]. Moreover, a mitochondrial variant of the SLC1A5 (called as SLC1A5_var) was discovered to be upregulated by pancreatic ductal adenocarcinoma (PDAC) cells under hypoxia and due to the activity of HIF2α. Increased SLC1A5_var activity promoted ATP and glutathione production with consequent gemcitabine resistance in pancreatic cancer cells[109]. Moreover, some rat sarcoma virus (RAS)-driven cancers can exploit autophagy to degrade intracellular proteins and promote glutamine uptake to sustain their abnormal mitochondrial metabolism[110,111].

Overall, inhibition of glutamine uptake has been investigated for long time as a putative anti-cancer treatment strategy. Indeed, small molecule SLC1A5 inhibitors as benzyl serine, l-γ-glutamyl-p-nitroanilide (GPNA), and V-9302 have been used[112–114]. However, glutamine can also be exported in the extracellular environment by the antiporter L-type / large neutral amino acid transporter 1 (LAT1) in exchange of other amino acids, such as leucine, to promote mTORC1 activation[115] or once converted in glutamate by the xCT antiporter for cysteine[116].

Glutamine catabolism (schematic shown in figure 5) is due to the activity of glutaminase (GLS) of which there are two isoforms: kidney-type GLS1 and liver-type GLS2[117]. While GLS1 is predominantly expressed in many tissues, GLS2 expression is more tissue-specific; indeed, GLS2 is present in liver, brain, pituitary gland and pancreas[112]. Interestingly, GLS1 expression levels are under the transcriptional control of c-MYC[118,119], while the tumour-suppressor p53 is involved in the upregulation of GLS2[120]. Moreover, due to alternative splicing two isoforms of GLS1 can be generated: glutaminase C (GAC) and kidney-type glutaminase (KGA)[121–123]. Using cryogenic electron microscopy (Cryo-EM) it has been recently revealed that GAC and GLS2 form filaments to increase their catalytic activity[124]. Moreover, mitochondria containing filamentous GLS showed

decreased mitophagy flux and mitochondrial turnover when cells where starved of glutamine[125].

While both GLS1 and GL2 can be activated by inorganic phosphate[122], GLS1 is allosterically inhibited by its product glutamate[126].

However, all GLS enzymes catalyse the hydrolysis of glutamine to glutamate and an ammonium ion[120,127]. Additional post-translational regulation mechanisms are for GLS the inhibitory Sirtuin 5 (SIRT5)-mediated desuccinylation[128,129] or the activatory SIRT3 deacetylation of GLS2 during calorie restriction[130].

Once generated, glutamate can be converted into α-KG and enter the TCA cycle to generate ATP, NADH and $FADH_2$[112]. A-KG can be generated in two different ways: the first is via glutamate dehydrogenase (GLUD), which promotes the release of ammonia during the process and the second is via several aminotransferases, such as glutamate-pyruvate transaminase (GPT, also known as alanine aminotransferase) or glutamate-oxaloacetate transaminase (GOT, also known as aspartate aminotransferase), with reactions that do not release ammonia groups during their reaction and support the synthesis of other amino acids transferring nitrogen from glutamate[131,132]. Moreover, the prevalence of one pathway or the other has been seen to be cell-type dependent[133].

Glutamine-derived metabolites are important for many essential mechanisms in several cancer cells[112]. As an example, glutamate plays a role in the cellular antioxidant response as a precursor for the biosynthesis of glutathione (GSH). GSH is a tripeptide (Glu-Cys-Gly) involved in the response to cellular oxidative stress induced by peroxide free radicals[134]. Moreover, glutamate is an important donor of amino groups for nonessential amino acids synthesis. Finally, glutamate is the main source of α-KG. As discussed before, this TCA-derived metabolite is extremely important for the regulation of the 2-OGDDs enzymes, being their substrate. This enzyme family is composed of histone demethylases (KDMs), 5-methylcytosine (5-mC) hydroxylases and PHDs. Therefore α-KG is not only important for the regulation of cellular signalling and epigenetics, but also for the regulation of HIF-1α stability, and hence the overall hypoxia response[135,136]. Another interesting fate of glutamine metabolism in cancers is to be converted to pyruvate via malic enzyme (ME)[137] This pathway has been observed initially in glioblastoma cells exhibiting aerobic glycolysis (i.e. Warburg effect) and served to generate NADPH for lipid biosynthesis and fuel the TCA cycle[137]. As an example of the importance of ME activity in cancers, it was reported that AML cells sustain mitochondrial biogenesis and the synthesis

of mitochondrial DNA (mt-DNA) exploiting ME2 activity, whose activation is dependent on fumarate[138].

Given that many cancer cells are "glutamine addicted", several molecular targets have been under investigation to develop possible anti-cancer therapeutic strategies. One of the mostly studied and more promising glutamine-related drug targets is indeed GLS[139]. The effective and broad anti-cancer effect of GLS inhibition in cancers is usually due to the reduced synthesis of antioxidant molecules like GSH[108,112,140].

Several small molecule inhibitors of this enzyme have been developed and some of them have also reached clinical trials. One of the most used compounds to inhibit GLS is Bis-2-(5-phenylacetamido-1,2,4-thiadiazol-2- yl)ethyl (BPTES), which showed promising results in the treatment of human lymphoma B cells and ovarian cancer[141,142]. Furthermore, the more recent telaglenastat or CB-839, that is a potent and highly specific allosteric GLS inhibitor and has also shown encouraging anti-tumour activity with no significant side effects in clinical trials[143–145].

Normally mammalian cells produce citrate via decarboxylation of pyruvate, mainly derived from glycolysis. However, during hypoxia or mitochondrial dysfunction, citrate is generated via reductive carboxylation of α-ketoglutarate. This reaction can be mediated by either the NADP+-dependent IDH1 in the cytoplasm or IDH2 in mitochondria[146,147]. Both these enzymes mediated the conversion of α-KG into citrate but can also work in the opposite direction, catalysing both the oxidative and reductive reactions. Another IDH isoform (IDH3) is mitochondrial and NAD+-dependent and can only catalyse the oxidative reaction[148]. Moreover, in many cancers IDH1 or IDH2 mutations promote the production of L-2HG, which is responsible for oncogenesis via epigenetics changes[149].

Reductive carboxylation (schematic shown in figure 5) has been discovered as an IDH1-dependent alternative pathway to promote the generation of acetyl-CoA moieties for lipid biosynthesis when cells are exposed to low oxygen environments. Indeed, Metallo *et al*. proposed a model where reductive carboxylation of amino acids could be used by cells located in poorly vascularised microenvironments with low glucose permeation[150]. Independently, Mullen *et al*. observed that glutamine-dependent reductive carboxylation also happens in conditions of ETC complex I and III mutations, mutations in FH or in cells treated with ETC inhibitors. Also in this study, reductive carboxylation was observed to happen as an alternative to glucose oxidation and to promote the synthesis of citrate for further lipid synthesis[151]. Although, reductive carboxylation can also occur in the absence of lipogenesis, as it has been shown in FASN deficient cells[152].

Under normoxic conditions the pVHL tumour suppressor directs the hydroxylated HIF-1α subunit for ubiquitylation and subsequent proteasomal degradation. Therefore, cells lacking pVHL can stabilise HIFs even when exposed at atmospheric oxygen levels, condition known as pseudohypoxia[153]. Interestingly, human renal carcinoma cells expressing pVHL mutants showed enhanced reductive carboxylation activity due to HIFs stabilization and could form xenografts when transplanted into mice. Moreover, their growth *in vivo* was inhibited by treatment with GLS inhibitors[154]. In order to produce the reducing equivalents, such as NADPH, necessary for the proper functioning of IDH2 in the mitochondria and promote reductive carboxylation, cells with mitochondrial defects can oxidize part of the glutamine derived α-KG via AKG dehydrogenase (also known as oxoglutarate dehydrogenase complex, OGDC) into succinyl-CoA to produce NADH and, therefore, sustain the reductive flux[155].

Recently, it has been discovered that reductive carboxylation is also involved in epigenetics regulation. More precisely, Jaccard *et al*. have shown that $CD8^+$ T cells require glutamine IDH2-mediated reductive carboxylation to be locked into a terminally effector differentiation program. Moreover, manipulation of reductive carboxylation via inhibition of IDH2 hijacks the development of $CD8^+$ T effector cells, inducing a memory phenotype with increased anti-tumour activity *in vivo*[156]. Moreover, Jiang et al. have discovered that using mitochondrial uncouplers, kidney cancer cells could redirect α-KG from the reductive flux to the oxidative on of the TCA via an increase in the NAD^+/NADH ratio and stop their growth[157].

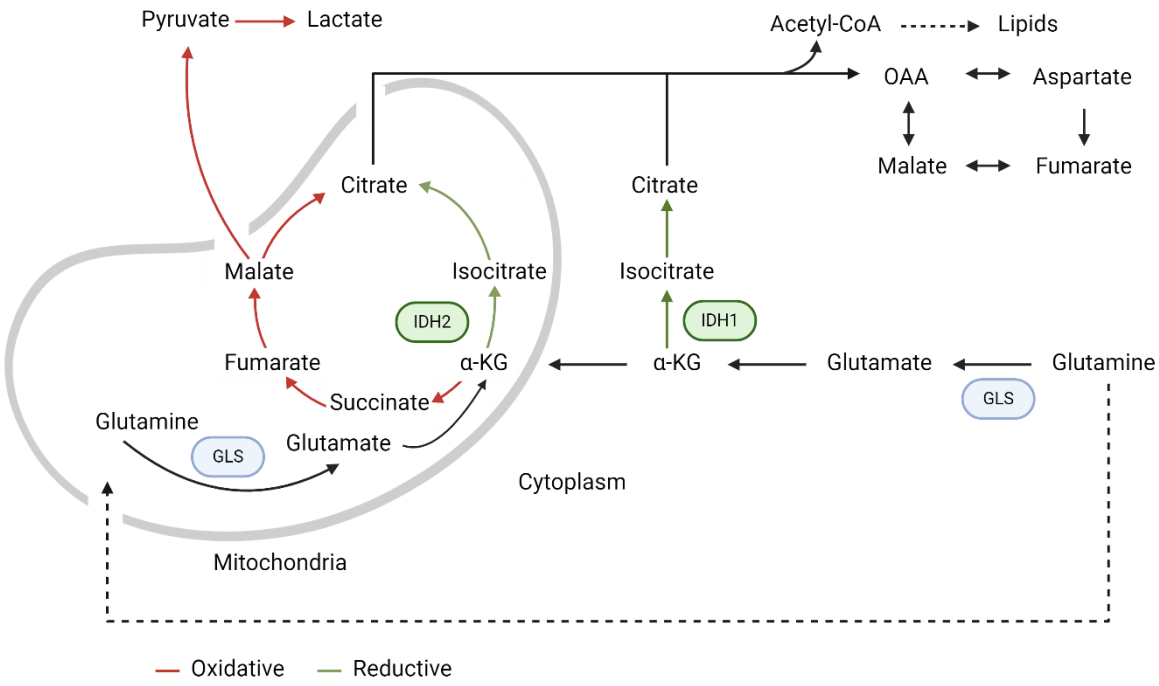

Figure 5. Schematic of glutamine oxidative (red) and reductive (green) metabolism.

1.3 Overview of receptor-mediated mitophagy

There are two different types of autophagy: non-selective autophagy, which is mostly related to starvation and energy deprivation, and cargo-specific autophagy, which instead is important for the proper removal of damaged or superfluous organelles[158,159]. Mitophagy is the selective removal of mitochondria via the autophagy machinery. Mitophagy can be used to promote mitochondrial turnover, adjust the number of mitochondria according to changing metabolic requirements[160] or to tigger differentiation, like in the final stages of red blood cells maturation[161,162]. Therefore, mitophagy plays a critical role as a cellular protective mechanism which removes potentially harmful damaged mitochondria[163,164].

Mitophagy is usually preceded by mitochondrial fission, which fragments the mitochondria making them of manageable size for the membrane engulfment thanks to the activity of the GTP-ase dynamin-1-like protein (Drp1)[165–167]. Moreover, mitochondrial dynamics and metabolic rewiring are highly related. In this regard, many recent advancements in the understanding of how cells induce metabolic rewiring have been made. For instance, while differentiating into the endothelial lineage, human induced pluripotent stem cells (hiPSCs) promote mitophagy and subsequently mitochondrial biogenesis to replenish with new mitochondria that will be metabolically adapted to the needs of the differentiated cells. During this switch the phosphatase PGAM family member 5 (PGAM5) is cleaved and can trigger PGC1α activation via β-catenin to start mitochondrial biogenesis[168]. However, a different non-conventional model of a Drp1-independent mitochondrial division occurring synchronically with the generation of autophagic membranes at the mitochondria has been proposed[169].

As shown in figure 6, there are two different mitophagy pathways: the PINK1-Parkin pathway, which is very well known and explored and is also known as ubiquitin-dependent pathway, and the receptor-mediated pathway.

PINK1 is a mitochondrial protein whose localisation can change between the outer mitochondrial membrane (OMM) and the inner mitochondrial membrane (IMM) according to its activation state[170]. Indeed, in healthy mitochondria PINK1 is translocated into the IMM, where it is cleaved by PINK/PGAM5-associated rhomboid-like (PARL) and hence inactivated. However, as soon as there is a drop in the mitochondrial membrane potential (MMP), PINK1 accumulates at the OMM, where it can form complexes with translocase of the outer membrane (TOM) and be activated via autophosphorylation on Ser228[159,170–172]. Once activated PINK1 promotes phosphorylation of ubiquitin (Ub) on Ser65 acquiring

high binding affinity for Parkin, which is recruited from the cytosol on the mitochondria[173]. Therefore, the activated Parkin can recruit more Ub subunits on mitochondria and, hence, PINK1 has more substrate for phosphorylation, resulting a positive feed-back loop. Finally, Ub chains on the OMM promote the recruitment of both the ubiquitin-proteasome system (UPS) and the autophagy machinery[173,174]. Several autophagy receptors are then recruited at the OMM to amplify the "eat me" signal initially generated by PINK1, such as Voltage-dependent anion-selective channel 1 (VDAC1), Mitofusin-2 (MFN2), TANK-binding kinase 1 (TBK1), and Mitochondrial Rho GTPase 1 (MIRO)[175]. Finally, thanks to the interactions between the Ub and Microtubule-associated protein 1A/1B-light chain 3 (LC3), the autophagosome can engulf the mitochondria, that will be degraded once the autophagosomes will fuse with the lysosomes[176].

The PINK1-Parkin mitophagy pathway has been associated with tumour-suppressing roles due to the reduced number of dysfunctional mitochondria and, hence, reduced ROS production and overall mitochondrial improved activity[177–179]. However, PINK1 was reported to be dispensable *in vivo* to induce mitophagy. Indeed, metabolically active tissues could still promote basal mitophagy despite the loss of PINK1. These fundings paved the way for the investigation of novel mitophagy pathways[180].

Indeed, mitophagy cargo receptors can directly interact with the processed LC3-II on the autophagosome due to a highly conserved LC3-interacting region (LIR) domain[181]. There are several autophagy/mitophagy cargo receptors, such as the ubiquitin-binding protein p62 or sequestosome-1 (SQSTM1), optineurin (OPTN), calcium binding and coiled-coil domain 2 (CALCOCO2, also known as NDP52) and FUN14 Domain Containing 1 (FUNDC1)[170,172,182–187].

However, for the scope of this thesis we will mainly discuss BCL2 interacting protein 3 (BNIP3) and BCL2 interacting protein 3-like (BNIP3L/NIX) and their role in mitophagy. These are mitochondrial receptors localised on the OMM via a C-terminal transmembrane (TM) domain and their expression can be induced by several stressors, such as hypoxia, increased ROS levels, DNA damage and changes in nutrient availability[188]. Both share homology with BCL2, having a BH3 domain, which can induce both autophagy and cell death[189], and are direct targets of HIF-1 transcriptional activity[190]. The induction of mitophagy and mitochondrial turnover are due to the direct interaction of LC3, and their LIR domain localised at the N-termini. Moreover, it has been shown that both BNIP3 and NIX can form homodimers[191]. A recent study also showed that NIX requires homodimerization to properly drive the recruitment of the autophagic machinery due to

increased avidity to LC3-II[192]. However, formation of BNIP3/NIX heterodimers has been observed, but the functional role of this process has not been fully understood yet[193]. Interestingly, both NIX and BNIP3 are related to the adjustment of the cellular metabolic activity during stress or environmental changes[194]. For instance, both BNIP3 and NIX activity were increased in differentiating cardiomyocytes, supporting the idea that HIF1α-dependent mitophagy is required to regulate metabolic reprogramming[195].

Moreover, in cells with high OXPHOS activity, i.e. when cultured in the presence of galactose or increasing glutamine concentrations, the GTP-ase Ras homolog enriched in brain (Rheb) is recruited on the mitochondria and promotes mitophagy via interaction with NIX and LC3. Therefore, Rheb-induced mitophagy could help the cells to sustain functional mitochondria during nutrient switches or cellular stress conditions[196]. On the other hand, it was observed that BNIP3 can bind to Rheb and inhibit it, disrupting mTOR activity under hypoxia[197]. Indeed, Rheb plays a crucial in the regulation of mTOR activity as their interaction at the lysosome promotes cellular growth[198].

Despite the numerous studies regarding the outcome of receptor-induced mitophagy and subsequent removal of mitochondria, less is known about the initial activation steps of this process. Some studies have proposed that under hypoxia BNIP3 protein stability is preserved via its phosphorylation by key cellular kinases, such as c-Jun N-terminal kinases (JNK)1/2[199] or ULK1[200]. Indeed, several kinase-specific phosphorylation sites can be found on BNIP3 and NIX protein sequences[199,200]. However, additional studies would be needed in order to understand if the regulation of hypoxia-induced mitophagy via BNIP3 or NIX is regulated by their interaction with a specific kinase, or if their activation is the result of a more complex set of kinase activity. More is known in the context of FUNDC1-mediated mitophagy (another mitochondrial cargo receptor whose activation is triggered by hypoxia). Indeed, it was shown that, after recruitment in the mitochondria, ULK1-mediated phosphorylation of FUNDC1 on Ser17 at the promotes its interaction with LC3 and, subsequently, the mitophagy flux[201]. Conversely, the inhibition of BNIP3 and NIX at cellular steady-state conditions has been reported to be mediated by a protein ubiquitin ligase complex known as SCF^{FBXL4} (SCF; Skp, Cullin, F-box containing complex. FBXL4; F-box and leucine rich repeat protein 4), which would promote their ubiquitylation and constant proteasomal degradation at the OMM[202].

While the function of NIX is mostly linked to erythroid cell differentiation[161,190,203], it has been reported to play a crucial role in Kirsten rat sarcoma virus (KRAS)-driven PDAC, supporting cancer cells mitochondrial metabolism and growth[204], and promoting survival

of glioblastoma in hypoxic niches[205]. Using iron-chelation to promote HIF1α stabilisation and mimic hypoxia, Wilhelm et al. have recently demonstrated that NIX plays a dual role in mediating both the selective removal of mitochondria via receptor-mediated mitophagy and peroxisome via a process named pexophagy. Under more physiological conditions NIX-mediated pexophagy was shown to be involved in cardiomyocytes and erythrocytes differentiation[206].

BNIP3 activity has been mostly characterised in the liver and liver-associated pathologies[161,191,203,207]. For instance, in response to nutrient deprivation BNIP3 is necessary for glucagon-induced mitophagy via initially the promotion of LC3 translocation from the nucleus to the cytosol and subsequent interaction on the autophagosome in the liver[208]. Interestingly, in a model of hepatocellular carcinoma BNIP3 was shown to act as a tumour suppressor as it can reduce lipid accumulation promoting autophagy-mediated degradation of lipid droplets[209]. However, in the context of melanoma BNIP3 showed to elicit cancer migration[210] and sustain cancer cells migration and metabolic rewiring[211].

Therefore, despite the most recent advances in mitophagy related research, further research is required to properly understand the role of mitophagy in regulating cellular metabolism and support the development of metabolic-related diseases and cancer. Indeed, many cancers show significant alterations of their mitochondrial functions. Therefore, the role of mitophagy and mitochondrial dynamics in tumorigenesis and cancer progression has become thriving field of scientific research[186].

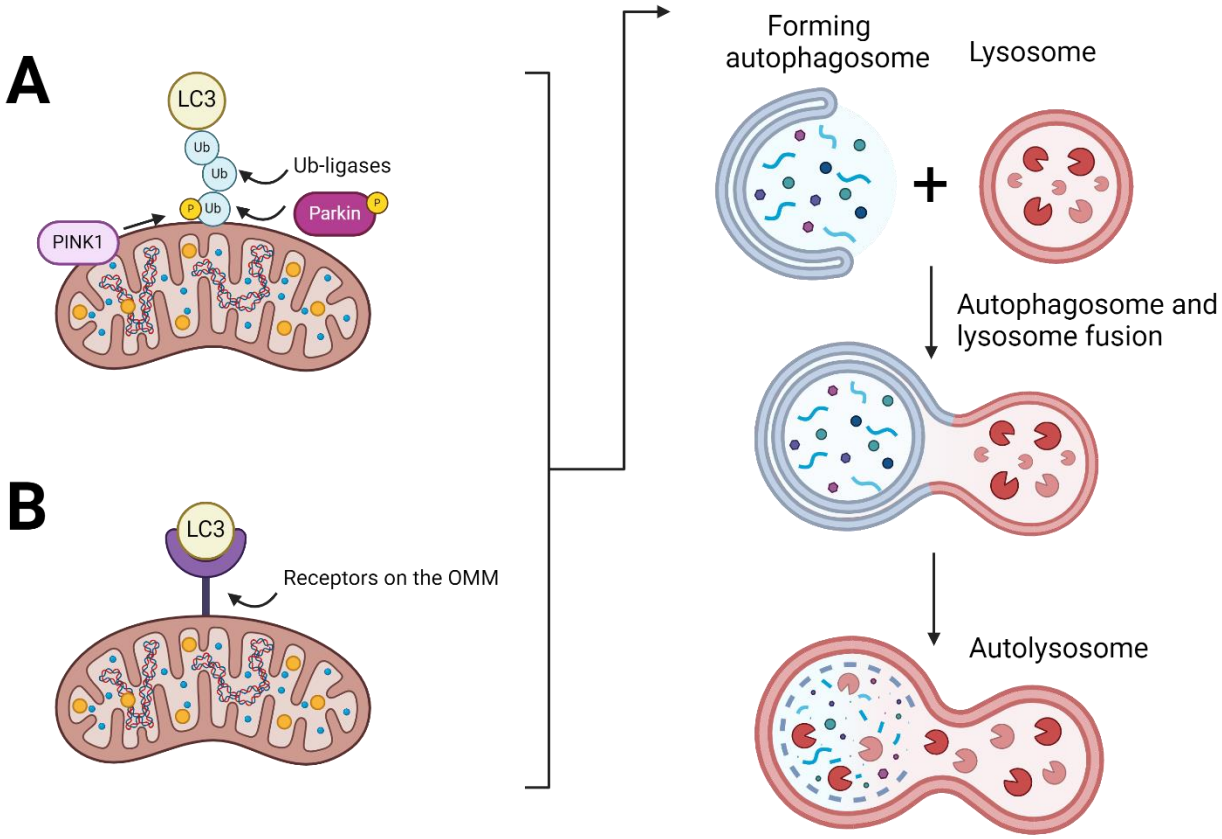

Figure 6. Schematic of the main mitophagy pathways. A) Ubiquitin-dependent mitophagy. B) Receptor-mediated mitophagy. OMM; outer mitochondrial membrane.

1.4 Chronic Myeloid Leukaemia

1.4.1 Introduction

Chronic myeloid leukaemia (CML) is a blood cancer arising from a haematopoietic stem cell (HSC) carrying the aberrant chromosomal translocation t (9;22) (q34; q11)[212,213]. The resulting "Philadelphia Chromosome" hosts the fusion oncogene *BCR::ABL1*, which encodes for a constitutive active non-receptor tyrosine kinase: BCR::ABL1. The disease is prevalently diagnosed in the Chronic Phase (CP), characterized by abnormal proliferation of differentiated myeloid cells. If left untreated, CML progresses to Blast Crisis (BC), showing a more aggressive clinical picture resembling the one of acute myeloid leukaemia (AML)[214,215].

CML is a relatively rare blood cancer. For instance, in Europe 0.7-1 per 100.000 individuals are affected by the disease and the average age at diagnosis is 60 years. Moreover, it has been observed higher incidence in males than in females[216].

1.4.2 BCR::ABL1 pathways

BCR::ABL1 is fusion oncoprotein with constitutive active non-receptor tyrosine kinase activity. The CML phenotype is mostly dependent on ABL aberrant tyrosine activity, which is triggered by the juxtaposition of BCR[217]. Moreover, while in physiological conditions ABL can move from cytosol to nucleus, this property is lost once fused to BCR. The aberrant tyrosine activity promotes generation of dimers or tetramers offering more docking sites for SH2 domains of other proteins. These new interactions dramatically perturbate essential cellular processes. For example, abnormal MAPK pathway leads to uncontrolled proliferation, or the perturbation of the JAK-STAT pathway promotes atypical transcriptional activity[218,219].

The phosphorylation site on the N-terminal domain of BCR (Tyr177) is essential for leukemogenesis as it works as an interaction site for the recruitment of the GRB2 adaptor proteins. Therefore, BCR::ABL1 can form many protein super complexes to induce dysregulated signalling pathways with the final outcome of sustaining the uncontrolled proliferation of the leukaemic clone[220].

Another important player in the CML-induced molecular pathway is signal transducer and activator of transcription 5 (STAT5). This transcription factor can be activated via interaction with BCR::ABL1 on its phosphorylated tyrosines and the SH2 domain of STAT5. Thus, STAT5 becomes constitutively active and, contrary to what happens in non-pathological scenarios, does not require cytokines for its activation. The role of STAT5 in CML biology is mostly associated with inhibition of apoptosis due to upregulation of the antiapoptotic protein B-cell lymphoma extra-large (BCL-xL) and inactivation of the proapoptotic protein BCL2-associated death promoter (BAD) by Akt[218].

1.4.3 TKI therapy

The gold-standard treatment of CML is mediated by tyrosine kinase inhibitors (TKIs). TKIs have been traditionally classified in two groups: first-generation Imatinib and second-generation nilotinib, dasatinib, bosutinib[221,222]. Moreover, Ponatinib has been more recently shown to potently target the T315I BCR::ABL1 mutants[223].

TKIs compete with the binding of ATP in the ATP-binding pocket of BCR::ABL 1, resulting in efficient blockade of the downstream signalling pathways and consequent apoptosis of CML cells. CML patients can survive due to a life-long administration of TKIs. However, TKI treatment does not lead to complete eradication of CML cells as shown by relapse upon treatment suspension, which is observed in roughly 50% of patients with deep enough response to be able to suspend therapy[224–227]. Consequently, the lifelong TKI therapy can lead to insurgence of side effects and represent an economical burden on the health care system.

Besides possible BCR::ABL1 dependent mechanisms conferring drug resistance, such as mutations in the ATP-binding site[228] or the expression of drug transporters that can promote the efflux of such compounds from the targeted cells[229],the main limitation of TKIs regimen is related to the presence of drug-resistant leukaemic stem cells (LSCs)[230]. Indeed, pioneering research in the field defined these as “non oncogene addicted” and, using a mouse model of inducible BCR::ABL 1 expression, demonstrated how these cells are persistent but more quiescent following removal of their oncogene. These data suggest that BCR::ABL1 independent mechanisms are responsible of LSCs resistance and could represent survival pathways[231,232].

Recently, a phase 3 randomized clinical study of newly diagnosed CP CML patients showed the greater efficacy of a novel TKI called asciminib when compared to other TKIs (Imatinib included). Moreover, asciminib showed improved safety and side-effect profile[233]. Asciminib targets the BCR::ABL1 myristoyl pocket, blocking it via allosteric inhibition and therefore, it is still active against mutated forms of the kinase, such as the BCR::ABL1^{T315I} mutations which confers drug resistance to almost all the approved TKIs, apart from ponatinib[234,235].

1.4.4 Metabolism of CML LSCs

One of the properties conferring TKI-resistance in CML LSCs is their ability to metabolically adapt to adverse environments and conditions, such as treatments. This is achieved via exploitation of intrinsic metabolic rewiring[236,237].

Using mRNA microarray analysis, an early study showed that CP CML LSCs overexpress genes related to the mitochondrial respiratory chain, i.e. genes encoding for mitochondrial complexes I, II, III, IV and V. Moreover, treatment with Imatinib did not affect the expression of the MRC genes[238]. In this regard, Kuntz et al. have shown that bulk $CD34^+$ CML LSCs have increased mitochondrial mass and mitochondrial membrane potential with consequent enhanced TCA cycle flux and OXPHOS when compared to their $CD34^-$ counterpart. Moreover, OXPHOS reliance was particularly evident also in more primitive CML $CD34^+CD38^-$ cells but not in non-CML ones. Inhibition of mitochondrial transcription using tigecycline, a potent inhibitor of mitochondrial ribosomes, promoted the eradication of CML LSCs both *in vitro* and *in vivo*[239]. Subsequently, it was shown that increased OXPHOS in CML LSCs was sustained by SIRT1 as it can trigger gene expression and activity of PGC1α that, in turn, would promote the expression of mitochondrial genes involved in respiration and ETC activity[240]. Interestingly, Upregulation of OXPHOS in BCR::$ABL1^+$ LSCs was confirmed via single cell RNA sequencing in a more recent study[241]. However, tigecycline failed to reach target inhibitory efficacy at the maximal tolerated dose in patients with AML[242]. An alternative strategy to inhibit the ETC in leukaemia is to use more recently developed ETC inhibitors, such as the complex I inhibitor IACS-01075[243]. However, two recent clinical trials have questioned the therapeutic role of ETC inhibitors, as IACS-01075 showed dose-dependent toxicity and induced lactate acidosis and neurotoxicity leading to its discontinuation[244]. Therefore, there is still the need to further investigate the metabolic vulnerabilities in LSCs and identify novel druggable targets.

In this regards, deeper investigation has revealed that CML LSCs not only rely on TCA cycle to fuel OXPHOS but that they also have Imatinib-insensitive increased pyruvate anaplerosis shown by increased Mitochondrial Pyruvate Carriers 1 and 2 (MPC1 and MPC2) and PC levels and activity. Moreover, treatment with MPC1/2 inhibitor MSDC-0160 showed promising results in targeting Imatinib-insensitive CML LSCs in preclinical models[245].

Since the discovery of the high availability of lipids in the hypoxic BM[246], many researchers have sought to investigate the role of fatty acid metabolism in LSCs. Fatty acids can sustain OXPHOS and therefore sustain mitochondrial energetics in both HSCs and LSCs[237]. Fatty acids uptake is promoted by CD36. Indeed, in the adipose tissue niche, $CD36^{+}CD34^{+}$ LSCs undergo abnormal lipolysis, which is triggered by pro-inflammatory cytokines, and constitute a metabolically distinct population with increased resistance to current chemotherapy[247]. Recently, lipidomic experiments carried out in K562 cells exposed to hypoxia uncovered increased levels of peroxisome-derived saturated lipids and lipid droplets formation due to hypoxia-induced inhibition of Stearoyl-CoA desaturase [248].

Finally, it has been shown that to promote their proliferation, CML LSCs exploit the folate metabolism pathway, often referred to as one carbon metabolism (1C), which is required for nucleotide biosynthesis. Folate metabolism related genes are highly upregulated in LSCs and can be exploited as a druggable vulnerability to promote cytostatic effect on cancer cells[249].

Overall, all these studies have shown how LSCs rely on several metabolic pathways and switch their metabolism according to specific needs.

1.4.5 CML and Hypoxia

The first evidence of the importance of hypoxia in CML biology was provided by Desplat et al., who observed that patient derived $CD34^+$ CML cells cultured under $1\%O_2$ were characterised by increased $CD34^+$ expression, lower BCR::ABL1 driven hyperphosphorylation of cellular protein-hence reduced oncogene activity- and slower cell growth when compared to CML cells cultured under atmospheric oxygen levels[250]. Years later, Ng et al reported that hypoxia promoted persistence of $CD34^+$ CML cells in a BCR::ABL1 independent manner. Indeed, despite TKI mediated suppression of the oncogene activity, CML cells showed enhanced clonogenicity and engraftment in immunocompromised mice. Moreover, this study revealed that HIF1α signalling was only partially attenuated by Imatinib. Indeed, treatment with Imatinib and hypoxia promoted gene expression of different genes, suggesting the existence of oncogene-independent mechanisms that could promote CML persistence in the BM microenvironment[251].

Subsequently, it has been reported that inhibition of HIF1α using the inhibitor acriflavine promotes eradication of TKI-insensitive CML LSCs *in vivo*[252]. Interestingly, more recent discoveries of metabolic reprogramming of TKI-resistant CML cells have once again highlighted the importance of hypoxia in supporting quiescent CML cells. Indeed, long-term TKI treatment triggered metabolic reprogramming in murine CML progenitors, resulting in increased expression and activity of HIF1α. Also in this study, pharmacological inhibition of the transcription factor using echinomycin led to suppression of human CML LSCs growth, potentially due to increased cellular ROS stress[253]. Another recent study has shown that CML LSCs overexpress HIF2α. Moreover, both its pharmacological targeting and genetic ablation sensitise LSCs to TKI treatment, induce metabolic changes via suppression of glycolysis and induction of OXPHOS with consequent increase in ROS levels[254].

Overall, all these studies suggest the existence of hypoxic or pseudo-hypoxic molecular mechanisms inducing TKI-resistance and persistence of CML LSCs. However, targeting HIFs might not represent a suitable therapeutic strategy, given that these transcription factors are essential for the regulation of the hypoxic response also in non-CML cells. Therefore, CML specific hypoxia driven mechanisms of drug resistance warrants deeper investigation.

Another interesting study has identified hypoxia-driven mTORC2 activation and protein kinase t (Akt)-signaling as a potential TKI-resistance mechanism used by CML LSCs when

exposed to hypoxia. The activation of mTORC2 happens when mTORC1 is inactivated by indirect targets of HIF1α, such as DDIT4. However, there are no anti-mTORC2 specific small molecules yet available[255].

Interestingly, in the context of AML leukemogenesis, it has been elegantly demonstrated that inhibition of PHD2 is a highly promising anti-leukaemia treatment as it can effectively inhibit the initiation and propagation of AML cells without affecting non leukaemic cells and haematopoiesis. The authors propose a model in which via inhibition of PHD2 with IOX5, HIF1α is stabilised and promotes a pro-apoptotic signaling via BNIP3. Moreover, PHD2 inhibition sensitise AML cells to venetoclax following a combination treatment strategy[256].

Aims of the thesis

In this study we initially aimed to understand how hypoxia promotes metabolic changes in CML cells and identify novel potential vulnerabilities using transcriptomics and metabolomics.

Next, we aimed to investigate the molecular mechanisms involved in the hypoxia-induced metabolic adaption of CML cells and focussed our attention on mitochondrial biology and turnover.

The overall aim was to provide further insight into the CML cells cellular and metabolic response to a low oxygen environment mimicking a condition of the BM microenvironment.

Chapter 2 Materials and Methods

2.1 Materials

2.1.1 General Reagents

Product	Manufacturer	Catalogue number
^{13}C-Glucose	Sigma-Aldrich	389374
^{13}C-Glutamine	Sigma-Aldrich	607983
CD117 MicorBeads, mouse	Miltenyi Biotec	130-097-146
AlbuMAX II Lipid-Rich Bovine Serum Albumin (BSA)	Gibco	11021045
AG-221, Enasidenib (IDH2i-2)	Selleckchem	S8205
AGI-6780 (IDH2i-1)	Selleckchem	S7241
Ampicillin	Sigma Aldrich	A5354-10ml
Antimycin A	Sigma Aldrich	A8674
Bafilomycin A1	TOCRIS biotechne	1334
Blasticidin S hydrochloride	Fisher Scientitific	10658203
BSA insulin and transferrin (BIT) 9500 Serum Substitute	Stem Cell Technologies	9500
BsmBI Enzyme	New England BioLabs	R0580
Calcium Chloride (CaCl2)	Sigma Aldrich	1023780500
Carbonyl cyanide 3-chlorophenylhydrazone (CCCP)	Sigma Aldrich	C2759
CB-839 (Telaglenastat)	Sellckchem	S7655
CD34 MicroBead Kit	Fisher Scientific	354240
Compensation beads	Thermo Fisher Scietific	01-2222-42
Dimethyl 2-oxoglutarate	Merck	349631
Dimethyl Sulfoxide (DMSO)	Sigma Aldrich	D2660
Dialysed Foetal Bovine Serum (FBS)	Gibco	A3382001
Dulbecco's Modified Eagle Medium (DMEM)	Gibco	21969-035
Dounce homogeniser	Scientific Laboratory Supplies	HOM2570
Dulbecco's Phosphate Buffered Saline (DPBS)		
FBS	Gibco	10500064
ECL western Blotting Substrate	Fisher Scientific	10005943
Glucose	Sigma Aldrich	G7021
Hank's Balanced Salt Solution (HBSS) (10X), Calcium, magnesium, no phenol red	Gibco	14065049
HEPES	Sigma Aldrich	H3375-100G
Histopaque 1119	Sigma Aldrich	11191

Human Flt3-Ligand	PeproTech	300-19
Human granulocyte colony-stimulating factor (G-CSF)	PeproTech	300-23
Human granulocytemacrophage CSF (GMSCF)	PeproTech	300-03
Human insulin solution	Sigma Aldrich	I9278-5ML
Human interleukin-6 (IL6)	PeproTech	200-06
Human leukaemia inhibitory factor (LIF)	PeproTech	300-05
Human macrophage inflammatory protein α (MIP-1α)	PeproTech	300-08
Human stem cell factor (SCF)	PeproTech	300-07
Human Serum Albumin	National Blood Transfusion Service	
Hydroxychloroquine Sulfate	Merck	PHR1782-1G
Iscove's Modified Dulbecco's Medium (IMDM)	Gibco	21980
L-Glutamine	Life Technologies	25030-024
Low density lipoprotein	Sigma Aldrich	L4646
Luciferin Monopotassium Salt	Fisher Scientific	15225733
Magnesium chloride	Sigma Aldrich	208337
Methanol	Fisher Scientific	M/4056/17
Methanol (HPLC grade)	Fisher Scientific	67-56-1
Methocult^{TM} SF H4236	Stem Cell Technologies	04236
Mitochondria Isolation Kit	Thermo Fisher Scientific	89874
MitoSOX™ Red Mitochondrial Superoxide Indicator	Life Technologies	M36008
MitoTracker™ Green	Life Technologies	M46750
N-acetyl-L-cysteine (NAC)	Sigma Aldrich	A9165-25G
NuPAGE™ 4-12% Bis-Tris Protein Gels, 1.0 mm, 10-well	Life Technologies	NP0321BOX
NuPAGE™ LDS Sample Buffer (4X)	Life Technologies	NP0007
NuPAGE™ MES running buffer	Life Technologies	NP0002
Oligomycin	Sigma Aldrich	O4876-5MG
One Shot™ Stbl3™ Chemically Competent E. coli	Thermo Fisher Scientific	C737303
PageRuler™ Plus Prestained Protein Ladder	Thermo Fisher Scientific	26619
Pierce™ BCA Protein Assay Kit	Thermo Fischer Scientific	23225

Pierce™ BSA Standard Ampules, 2 mg/mL	Thermo Fischer Scientific	23209
PhosSTOP (phosphatase inhibitors)	Roche	4906845001
Polybrene Transfection Reagent	Merck	TR-1003-G
Potassium Chloride (KCl)	Thermo Fisher Scientific	10684732
Pre-Separation Filters (30 µm	Miltenyi Biotec	130-041-407
Protease inhibitors cocktail	Sigma	P8340
Puromycin Dihydrochloride	Life Technologies	12122530
PVDF Transfer Membrane	Thermo Fisher Scientific	88520
QIAquick Gel Extraction Kit	Qiagen	28704
Quick Ligation™ Kit	New England BioLabs	M2200S
Rotenone	Sigma Aldrich	R8875
Roswell Park Memorial Institute media (RPMI) 1640	Gibco	31870-025
Seahorse XF Base Medium	Agilent Technologies	102353
Separation columns	Miltenyi Biotec	130-042-401
Sodium bicarbonate (NaHCO3)	Sigma Aldrich	S5761
Sodium cloride (NaCl)	Sigma Aldrich	S5886
Sodium hydroxide (NaOH)	Sigma Aldrich	S0899
Sodium pyruvate	Gibco	11360070
SuperSignal™ West Femto Maximum Sensitivity Substrate	Thermo Fisher Scientific	34094
Trypsin-EDTA (0.05%), phenol red	Thermo Fisher Scientific	25300054
Tween 20	Sigma Aldrich	P9416-100ML
Seahorse XFe96 FluxPak (includes calibrant)	Agilent Technologies	102416-100
Tetramethylrhodamine, methyl Ester, Perchlorate (TMRM)	Thermo fisher Scientific	T668
Transferrin	Sigma Aldrich	T4132-100MG

2.1.2 Western blot Antibodies

Product	Manufacturer	Catalogue number
Primary Antibodies		
β-tubulin	Cell Signaling Technology	2146S
ATG7	Cell Signaling Technology	8558S
ATG14	Cell Signaling Technology	96752
p-ATG14 Ser29	Cell Signaling Technology	92340
ATP5A1	Proteintech	14676-1-AP
BNIP3	Cell Signaling Technology	44060
HIF-1α	Cell Signaling Technology	36169
HSP90	Proteintech	60318-1-Ig
LC3B	Cell Signaling Technology	2775S
MT-CO2	Proteintech	55070-1-AP
NDUFB8	Proteintech	14794-1-AP
NIX	Cell Signaling Technology	12396S
P62	BD Biosciences	610833
PGC-1α	Millipore	ST1202
SDHB	Proteintech	10620-1-AP
TOM20	Proteintech	11802-1-AP
ULK1	Cell Signaling Technology	8054S
UQCRC2	Proteintech	14794-1-AP
VDAC1	Proteintech	55259-1-AP
Secondary Antibodies		
Anti-mouse IgG, HRP-linked	Cell Signaling Technology	7076S
Anti-rabbit IgG, HRP-linked	Cell Signaling Technology	7074S

2.1.3 Flow Cytometry Antibodies

Product	Manufacturer	Catalogue number
7-AAD	BD Biosciences	559925
APC-Anti-Human Annexin V	BD Biosciences	550475
APC Anti-Human CD34	BD Biosciences	555824
APC Anti-Human CD71	Biolegend	334108
FITC Annexin V	BioLegend	640906
PE Anti-Human CD11b	BioLegend	301306
PE Anti-Human CD133	Milteney Biotec	130-113-108
PE Anti-Human CD235a (Glycophorin A)	BioLegend	349106
PE Anti-Human CD71	BD Biosciences	555537
PerCP/Cy5.5 AntiHuman CD235a (Glycophorin A)	BioLegend	349110

2.1.4 CRISPR Guides

Gene	Targeting Sequence
ATG7	5′-GAAGCTGAACGAGTATCGGC-3′
BNIP3 guide#1	5’-ATGGGATTGGTCAAGTCGGC- 3’
BNIP3 guide#2	5’-GCTGAAGTGCAGTTCTACCC-3’
NIX	5'-GTTCTGTGTCTTTAAGCATG-3'

Targeting sequence for ATG7 was designed and developed by Dr Angela Ianniciello and targeting sequence for NIX was designed and developed by Dr Martha Zarou.

2.1.5 Cell lines

All cell lines (K562, KCL22, THP1, MOLM13, MV-411, OCI-AML3 and HEK293FT) were available in-house. All cell lines were routinely tested for mycoplasma contamination.

2.1.6 Primary cells

2.1.7 Equipment

Name	Supplier
7000 Series Triple Quadrupole MS	Agilent
7890A GC system A	Agilent
Attune NxT Flow Cytometer	Thermo Fisher Scientific
Biochemistry Analyser	YSI
CASY Cell Counter and Analyser	Roche
Whitley H35 hypoxystation	Don Whitley Scientific
FACS Verse	BD Biosciences
Infinite M200 Pro Plate Reader	Tecan
Nanodrop 2000	Thermo Fisher Scientific
Odyssey FC	LiCor
Peltier Thermal Cycler PTC 225	MJ Research
Q Exactive Orbitrap MS sysytem	Thermo Fisher Scientific
Seahorse XFe96 Analyser	Agilent
Ultimate 3000 HPLC System	Thermo Fisher Scientific

2.2 Composition of buffers and Cell Culture Media

Complete RPMI

Name	Final Concentration
RPMI 1640	N/A
FBS, heat inactivated	10%
L-Glutamine	2mM
Penicillin-Streptomycin (Pen/Strep)	100 IU/mL

Complete DMEM

Name	Final Concentration
DMEM 1X with Sodium Pyruate	N/A
FBS, heat inactivated	10%
L-Glutamine	2mM
Pen/Strep	100 IU/mL

Serum free medium (SFM)

Name	Final Concentration
IMDM	N/A
BIT (BSA/Insulin/Transferrin)	20%
2-Mercaptoethanol	0.2%
Low Density Lipoprotein	40µg/ml
L-Glutamine	2mM
Pen/Strep	100 IU/mL

SFM supplemented with physiological growth factors (φGF)

Name	Final Concentration
SFM	N/A
SCF	0.2ng/ml
IL-6	1ng/ml
G-CSF	1ng/ml
GM-CSF	0.2ng/ml

MIP-a	1ng/ml
LIF	0.05ng/ml

DAMP solution

Name	Final Concentration
DPBS	N/A
Magnesium Chloride	1M
Trisodium Citrate	0.155M
Human Serum Albumin	0.2
DNase I	2500U/ml

Plasmax (primary cells)

As described by Vande Voorde et al.[257], Plasmax was formulated as follows: glucose-free Earle's Balanced Salt Solution (EBSS) was supplemented with amino acids, vitamins, salts, trace elements and uric acid. Plasmax was further supplemented as follows:

Name	Final Concentration
Plasmax base media	N/A
Glucose	5.560 mM
L-Glutamine	0.65mM
Pyruvate	100µM
Pen/Strep	100IU/mL
AlbuMAX II Lipid-Rich BSA	0.50%
Insulin	10µg/mL
Transferrin	7.5µg/mL
2-Mercaptoethanol	0.2%
ϕGF cocktail	as described

Seahorse XF media (Mito Stress Test)

Name	Final Concentration
XF Seahorse Base Media	N/A
Glucose	11.1 mM
L-Glutamine	2mM

Protein Lysis Buffer

Name	Final Concentration
RIPA Buffer	N/A
PhosphoSTOP	10%
Protease Inhibitor	10%
SDS	10%

10 X TBS (pH=7.5)

Name	Final Concentration
H2O	1L
Tris	60.5g
NaCl	87.6g

TBST

Name	Final Concentration
H2O	900ml
10x TBS	100ml
Tween20	1ml

Blocking Buffer

Name	Final Concentration
TBST	N/A
BSA	2%

2X HEPES-Buffered Saline (HBS) (pH=7.0-7.1)

Name	Recipe for 500ml
H2O	480ml
NaCl	8g
KCl	0.37g
Glucose	1g
HEPES	5g
Na2HPO4*7H2O (100x	500µl

2 X $CaCl_2$

Name	Recipe for 500ml
H2O	500ml
CaCl2*2H2O	147g

2.3 Methods

2.3.1 Human primary samples

2.3.1.1 Origin of the primary samples

Patient samples were kindly donated after ethical approval and consent (REC 10/S0704/60 & REC 15/WS/0077). CML samples were obtained at the time of diagnosis after leukapheresis from Chronic Phase Ph^+ patients and before they started TKI treatment.

2.3.1.2 Isolation of $CD34^+$ cells

Isolation of $CD34^+$ cells from CML patient samples was performed by Dr Alan Hair. Briefly, after centrifuging mononuclear cell layer for 10 min at 400g, cells were resuspended in 300µl PBS and 100µl of FcR blocking reagent. Then 100µl of CD34 Microbeads from CD34 Microbead Kit were added to the mix and left at 4°C for 30 min. Cells were washes in PBS, centrifuged for 10 min at 300g and finally resuspended in 500µl of fresh PBS and added to the magnetic column for separation. After three washes, the magnetically labelled cells were collected by pushing the plunger into the column.

2.3.2 Cell culture

2.3.2.1 Primary cells and cell lines culture

CML (K562 and KCL22) and AML (THP1, MOLM13, MV-411, OCI-AML3) cell lines were cultured in complete RPMI at 5% CO_2, 37°C. Cells were passaged every 2-3 days and kept at 0.2-0.3x10^6 cells/ml. HEK293FT were cultured in complete DMEM and passaged every 2-3 days with the addition of trypsin-EDTA to detach the cells form the plastic and maintained at 0.5x10^6 cells/ml. Primary human cells were cultured in SFM+φGFs in non-adherent tissue culture flasks at 1.6x106 cells/ml to achieve overnight recovery after thawing. Hypoxic treatment (0.5-1%O_2 and 5%CO_2 at 37°C) was performed in a humidified H35 Hypoxystation (Don Whitley Scientific).

2.3.2.2 Cryopreservation of cells

Cell lines were cryopreserved by suspending cell pellets in a freezing medium with 90% FBS and 10% DMSO. Cell suspensions collected in cryopreservation vials and transferred to -80°C. The following day, cryovials were transferred into liquid nitrogen containers.

2.3.2.3 Recovery of cells

To recover cell lines, frozen vials were placed in a 37°C water bath for one min. Cells were then washed in pre-warmed complete medium to remove DMSO and allowed to recover in culture overnight.

Vials of primary cells were initially placed in a 37°C and washed with DAMP solution. More precisely 10ml of DAMP solution was added dropwise over 20 min and centrifuged. This process was repeated other two times. Finally, DAMP was removed by centrifugation at 300g for 10 min. Recovery of primary cells was then achieved by resuspending the cells in SFM+φGFs and let grow overnight.

2.3.2.4 Drug preparation

Most drugs used in this thesis were dissolved in DMSO or water at a concentration of 10mM and the stock solutions were stored at -20°C for a maximum of three months.

2.3.2.5 Cell line growth rate

K562/KCL22, K562/KCL22 BNIP3 KO, K562 overexpressing the ULK1 SMARTvector were plated at 3x10^4 cells/ml in 6 ml and let grow in normoxia (21%O_2) and hypoxia (0.5%O_2) for 6 days. Cell counts were obtained at 48h intervals using the CASY automated cell counter.

2.3.3 Flow cytometry

2.3.3.1 Apoptosis assay

Apoptosis can be monitored using Annexin V, which is a calcium-dependent phospholipid-binding protein which has a high binding affinity for phosphatidylserine. Indeed, the translocation of phosphatidylserine to the outer cell membrane is an indicator of early-stage apoptosis. Moreover, the identification of apoptotic cells can be improved by using a combination of Annexin V and a cell impermeable viability dye, 7AAD. While $AnnexinV^+$ $7AAD^+$ cells are considered to be in late apoptosis, $AnnexinV^+$ $7AAD^-$ are considered to be in early apoptosis.

To measure apoptosis approximately $2x10^5$ cells were washed twice in PBS and then resuspended in a staining mix solution composed of: 3µl Annexin V, 3µl of 7AAD and 44µl of HBSS $Ca2^+$ $Mg2^+$. Staining was conducted in the dark for 15-20 min at Room temperature (RT). After staining 200µl of HBSS were added to each sample and subjected to flow cytometry analysis.

2.3.3.2 Erythroid maturation analysis

K562 tend to promote erythroid differentiation when treated with several conditions or compounds and are a good *in vitro* model to study erythropoiesis. To assess erythroid differentiation glycophorin A (CD235a, a sialoglycoprotein in the membrane of erythrocytes) and CD71 (transferrin receptor protein) cell markers were used. Both represent well-known erythroid markers.

Approximately $2x10^5$ K562 cells were washed twice with PBS and stained with 3µl of CD71 (PE) and 3µl of GlyA (PerCP/Cy5.5) in a total volume of 50µl PBS. Staining was conducted in the dark for 15-20 min at Room temperature (RT). Finally, cells were washed in 1 ml PBS to remove excessive fluorescent probe and then resuspended in 300µl of PBS for flow cytometry analysis.

2.3.3.3 Mitochondrial ROS

To assess mitochondrial ROS content MITOSOX Red staining was used. MITOSOX Red is a permeable dye that specifically targets mitochondria binding to triphenyl phosphonium cations. Fluorescence is produced after its oxidation due to the presence of superoxides.

$3x10^5$ cells were stained with 1ml of 5µM MITOSOX Red PBS mix. Cells were incubated for 30min at 37°C and 5% CO_2 in the dark. Cells were then washed twice in PBS and resuspended in 300µl PBS for Flow cytometry analysis.

2.3.3.4 Measurement of mitochondrial content

To assess mitochondrial mass/content mitotracker green was used. Mitotracker green is a cell-permeant dye that selectively bind to mitochondria and its fluorescence is directly correlated to cellular mitochondrial content.

Approximately $3x10^5$ cells were stained with 100nM of mitotracker green PBS mix and incubated for 30min at 37°C and 5% CO_2 in the dark. Cells were incubated for 30min at 37°C and 5% CO_2 in the dark. Cells were then washed twice in PBS and resuspended in 300µl PBS for Flow cytometry analysis.

2.3.3.5 Measurement of mitochondrial membrane potential

To assess mitochondrial membrane potential in live cells, Tetramethylrhodamine methyl ester (TMRM) was used. TMRM is a cell-permeable red-orange emitting fluorescent dye that accumulates in active mitochondria with intact membrane potential.

Approximately $3x10^5$ cells were stained with 100nM of TMRM PBS mix and incubated for 30min at 37°C and 5% CO_2 in the dark. Cells were incubated for 30min at 37°C and 5% CO_2 in the dark. Cells were then washed twice in PBS and resuspended in 300µl PBS for Flow cytometry analysis.

2.3.3.6 MitoKeima assay

To assess mitophagy flux in live cells, mitochondrial target keima (mt-Keima) assay was used. Mt-Keima is a pH sensitive mitochondrial protein, which can be detected in the mitochondrial matrix due to its fusion with the mitochondrial targeting sequence of cytochrome c oxidase subunit VIII. Increased mitophagy flux can be easily detected via measurement of the shift in excitation peak of Keima from 440 nm (pH=7) to 586 nm (pH=4), when the mitochondria are inside the lysosome[258].

Around $3x10^5$ K562 cells overexpressing mKeima plasmid were washed in PBS and resuspended in 300µl of PBS for flow cytometry analysis using Attune NxT Flow Cytometer.

2.3.3.7 Mito-Timer assay

To assess mitochondrial turnover in live cells, Mito-Timer expressing cells were used. Mito-Timer is characterized of a time-sensitive fluorescent protein (Timer), which has been fused with the mitochondrial targeting sequence of COX VIII, hence Mito-Timer. Fine-tuned control of Mito-Timer protein expression is achieved via a doxycycline-inducible vector, here referred as DOX pulse. Once pulsed with DOX, fluorescence of the Mito-Timer protein can be monitored over time. After the initial DOX pulse, cells overexpressing the Mito-Timer construct show green florescence because of induced transcription and protein-translation. Over time the red fluorescence becomes predominant[259–261].

Around $3x10^5$ K562 and K562 BNIP3-KO cells overexpressing Mito-Timer plasmid were washed in PBS and resuspended in 300µl of PBS for flow cytometry analysis. To monitor mitochondrial turnover, the analysis was repeated at 24h intervals for a total of 72 hours. To monitor mitochondrial biogenesis, a second DOX pulse was induced after 48h from the first one. Cells were then assessed for mitochondrial biogenesis after 24h.

2.3.3.8 expression of stem cell markers in primary cells

$CD34^+CD133^+$ cells are considered a primitive population of LSCs. Approximately $2x10^5$ CML cells were stained with 3µl of CD34 (APC) and 3µl of CD133 (PE) in a total of 50µl of PBS and left incubating at RT for 20 min in the dark. Following staining cells were washed and resuspended in 300µl of PBS for flow cytometry analysis.

2.3.4 Western Blotting

2.3.4.1 Protein lysis

After treatments, cells were counted and collected. Cells were washed with ice-cold PBS and transferred to a 1.5ml Eppendorf tube for a second wash with ice-cold PBS. Cell pellets or mitochondrial-enriched fractions were suspended in 120-150µl of RIPA lysis buffer. Tubes were kept on ice for 15 min and then centrifuged at 16,000g for 20 min at 4°C. Finally, supernatants were collected and stored at -80°C.

2.3.4.2 Protein quantification

Proteins were quantified using the bicinchoninic acid (BCA) assay.

Following defrosting of lysates on ice, 2µL x3 of each sample were placed into a 96 well plate. A standard curve was generated at 2µg to 0µg by 1:2 serial dilution of standard albumin (BSA) in water. For protein quantification, the Pierce™ BCA Protein Assay Kit was used according to manufacturer's instructions. Briefly, 98% (v/v) Reagent A was mixed with 2% (v/v) Reagent B and 198µl of the Reagent A+ Reagent B were distributed into each sample previously spread in a 96-well plate. Following incubation of the plate at 37°C for 30 min, absorbance was measured at OD 562nm using a spectrophotometer plate reader. The concentration of each sample was determined by interpolating their absorbance values with the standard curve.

2.3.4.3 Sodium dodecyl sulfate polyacrylamide gel electrophoresis (SDS-PAGE)

10-20µg of protein from each sample were mixed with 4xLDS sample buffer and an appropriate volume of water for a total volume of 20µl. Samples were boiled at 95°C for 5 min to achieve protein denaturation. Samples were loaded into pre-cast 4-12% gels in presence of 1X running buffer at 120V for 60-90 min in order to achieve the desired separation into a mini-cell electrophoresis system. To assess the proteins molecular weight, 4µl of protein molecular weight ladder from 10-250KDa were loaded into the first well of the gel.

2.3.4.4 PVDF transfer

Following the SDS-page running, proteins were transferred onto a PVDF membrane, which was previously activated in methanol, using a "sandwich" wet transfer system. The "sandwich" was assembled as follows: from cathode (-) - 1 sponge- 2 paper Whatman – gel – PVDF membrane – 2 paper Whatman – 1 sponge – anode (+). Finally, the "sandwich" was placed in a transfer tank in presence of 1X transfer buffer. The transfer setup was 120V, 400mA for 90 min.

2.3.4.5 Immunoblotting

The membrane was blocked in blocking buffer solution for 1 hour with slow rocking. After blocking, the membrane was incubated overnight with primary antibody diluted 1:500-1:1000 in blocking buffer at 4°C with gentle rolling. The day after, the membrane was washed three times x 5 min with TBST and incubated with the secondary HRP-conjugated antibody at a dilution of 1:5000 for 1 hour. The membrane was then washed at least three times with TBST. Membrane was then incubated with equal volumes of the luminol-enhancer and peroxide solute of the SuperSignalTM Femto Maximum Sensitivity Substrate or ECL western Blotting Substrate and developed using the Odyssey FC imaging system.

2.3.4.6 Isolation of mitochondria

Mitochondrial- enriched fractions were isolated from K562 cells using the Thermo Mitochondrial Isolation kit according to manufacturer instructions. Briefly, 800µl of mitochondria isolation reagent A with protease inhibitors was used to resuspend a pellet of $20x10^6$ cells. Cells were then homogenised with 60-80 strokes using a dounce homogeniser to ensure complete lysis of the cells. Then the lysed cells were returned to a 2ml tube with 800µl of mitochondria reagent C with protease inhibitors. Tubes were centrifuged at 700g for 10 min at 4°C. the supernatant containing the cytosol-enriched fraction was transferred to a new tube, while the pellet containing the mitochondria-enriched fraction was kept on ice for downstream processing.

2.3.6 Generation of CRISPR-Cas9 KO cell lines

2.3.6.1 Cloning of the guide RNA into LentiCRISPR plasmid

This cloning protocol was readapted from O'Prey and colleagues[262].

Initially the LentiCRISPR v2 carrying a puromycin-resistance marker was digested for 2h at 37°C with the following reaction:

5µg	LentiCRISPR v2
2µl	BSMBI enzyme (NEB)
5µl	10X buffer 3.1 (NEB)
Xµl	dH_2O
50µl	Final volume

Once digested, the plasmid was run in a 2% agarose gel and the digested fraction of ~11Kb was gel-purified using the QIAquick Gel Extraction Kit (Qiagen). The product was then quantified using the NanoDrop 2000 Spectrophotometer (Thermo Fisher Scientific).

Oligos were then phosphorylated and annealed as follow:

1µl	Forward gRNA oligo (100µM)
1µl	Reverse gRNA oligo (100µM)
1µl	10X T4 Ligation Buffer (NEB)
0.5µl	T4 polynucleotide kinase (NEB)
6.5µl	dH_2O

Annealing was performed in a thermal cycler as follows:

Step 1 37°C 30min

Step 2 95°C 5 min

Ramp down to 25°C at 5°C/min

Annealed oligos were then diluted at 1:200 in dH_2O. subsequently the digested lentiCRISPR v2 was ligated with annealed oligos for 15 min at RT with the following reaction:

50ng	Digested LentiCRISPR v2
1µl	Oligos duplex
5µl	2X Quick Ligase Buffer (NEB)
1µl	Quick Ligase (NEB)
Xµl	dH_2O to reach a 10µl final volume

The product of the ligation reaction was then transformed into Stbl3 competent bacteria and cultured overnight at 37°C into ampicilling-containing agar plates. Sigle colonies were picked and amplified by growing into 200 ml of lysogeny broth (LB) at 37°C at 225rpm for 24h. DNA plamid was then isolated using a Maxiprep kit (Qiagen).

2.3.6.2 Viral production and transduction

Initially, $1x10^6$ HEK293FT cells were plated in a $10cm^2$ Petri dish and left in culture for 3-4 days until they reached 70-80% confluency. The day of the transfection, exhausted DMEM medium was replaced with 9ml of fresh one and a DNA transfection mix was prepared as follows:

Recombinant vector	14.2µg
Packaging plasmid	12.4µg
Envelope plasmid (pVSVg)	4.5µg
dH_2O	Up to 1.3ml

Subsequently, 1.5ml of 2X HSBS and 183µl of CaCl2 were added dropwise. The solution was then incubated at 37°C for 30 min.

Once ready, the solution was added to the HEK293FT cells dropwise and cells were incubated overnight. Following the incubation time, medium was removed and replaced with 10mil of fresh DMEM medium. After 48h of incubation, DMEM containing viral particles was collected and filtered using a 0.45µm filter. Virus particles were then added to $0.5x10^6$ of target cells (K562 or KCL22). After 3 days the medium was removed and cells were selected with the appropriate antibiotic (when applicable) in fresh culture medium for 48h or let recover and washed three times with PBS before been subjected to FACS.

2.3.5 Plasmid Vectors

2.3.5.1 LentiCRISPR V2 vector Plasmid #52961 addgene (puromycin resistance marker)

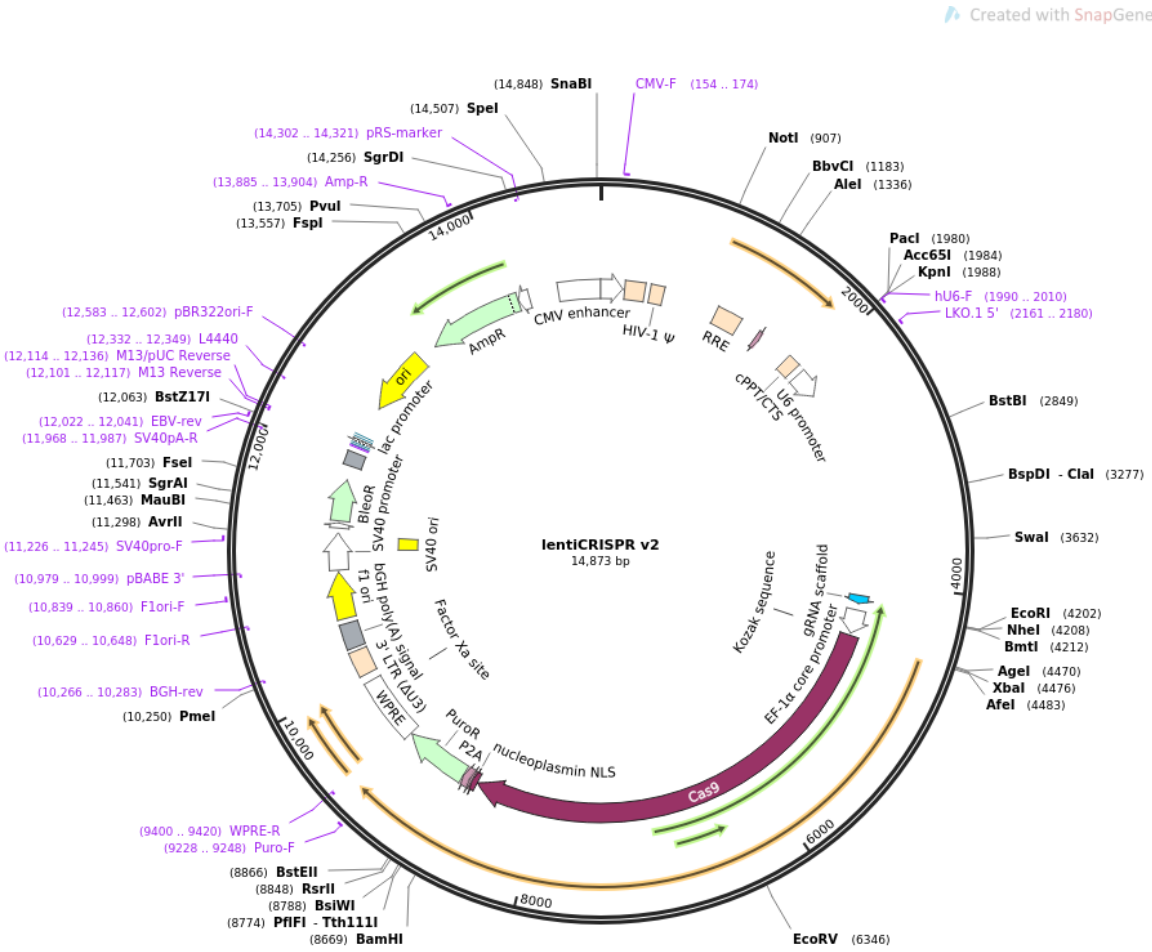

2.3.5.2 psPAX2 Plasmid #12260 addgene

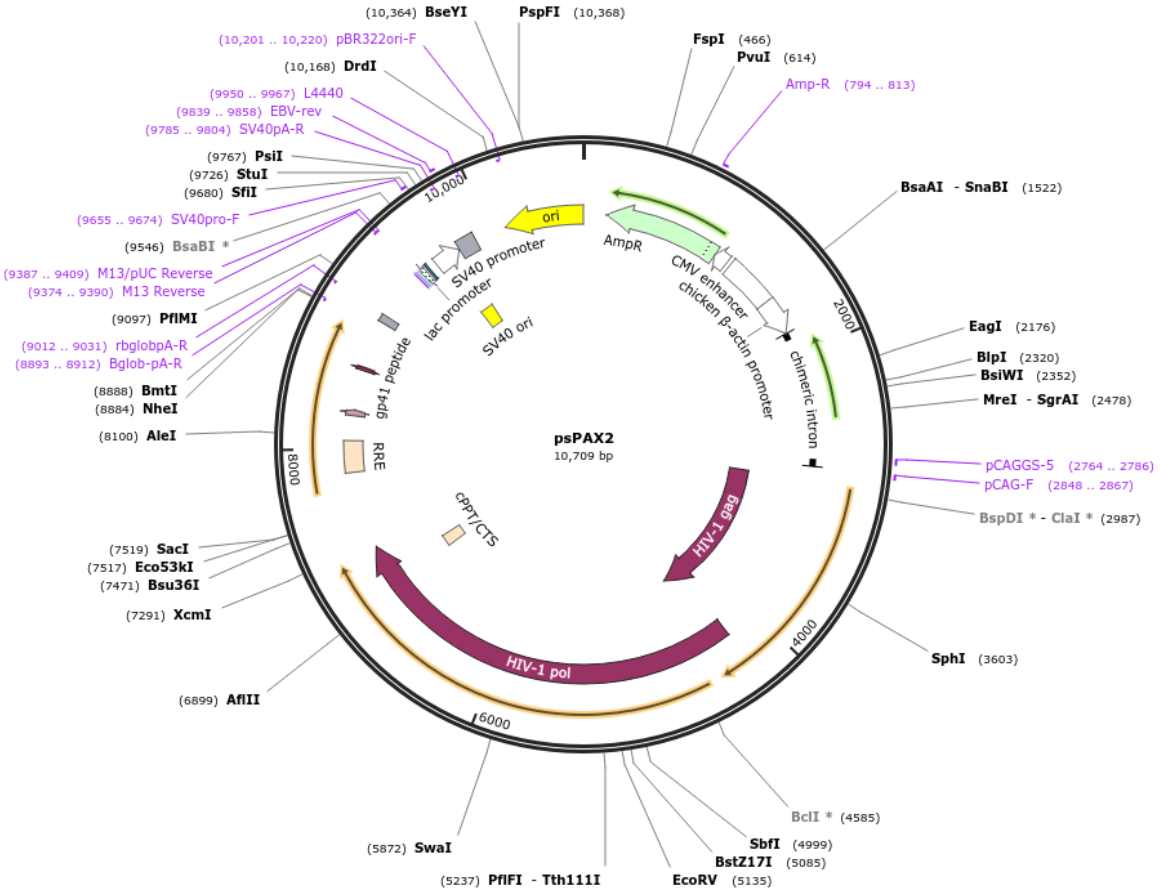

2.3.5.3 pCMV-VSV-G Plasmid #8454 addgene

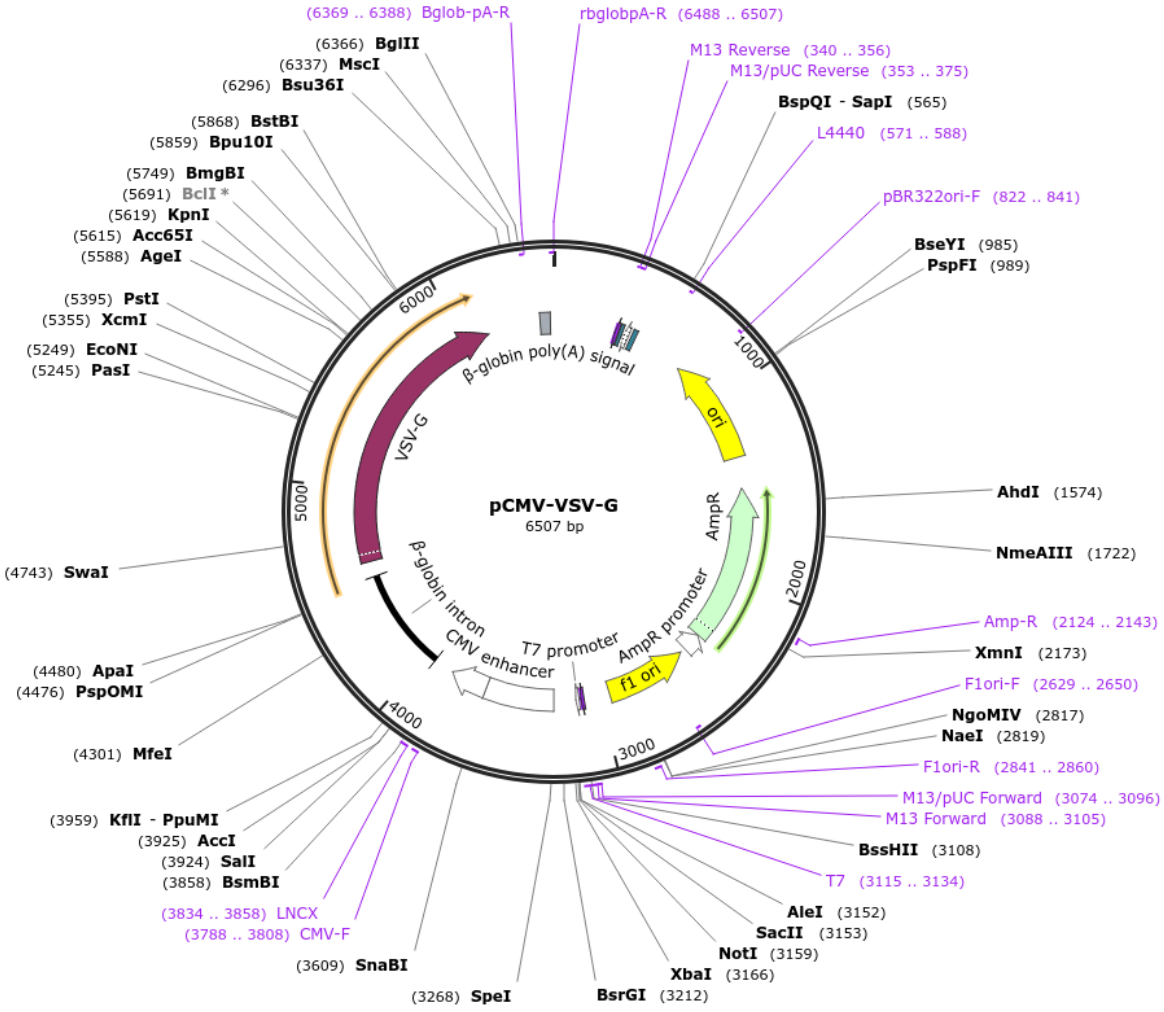

2.3.5.4 p-BS-gagpol Plasmid #35614 addgene

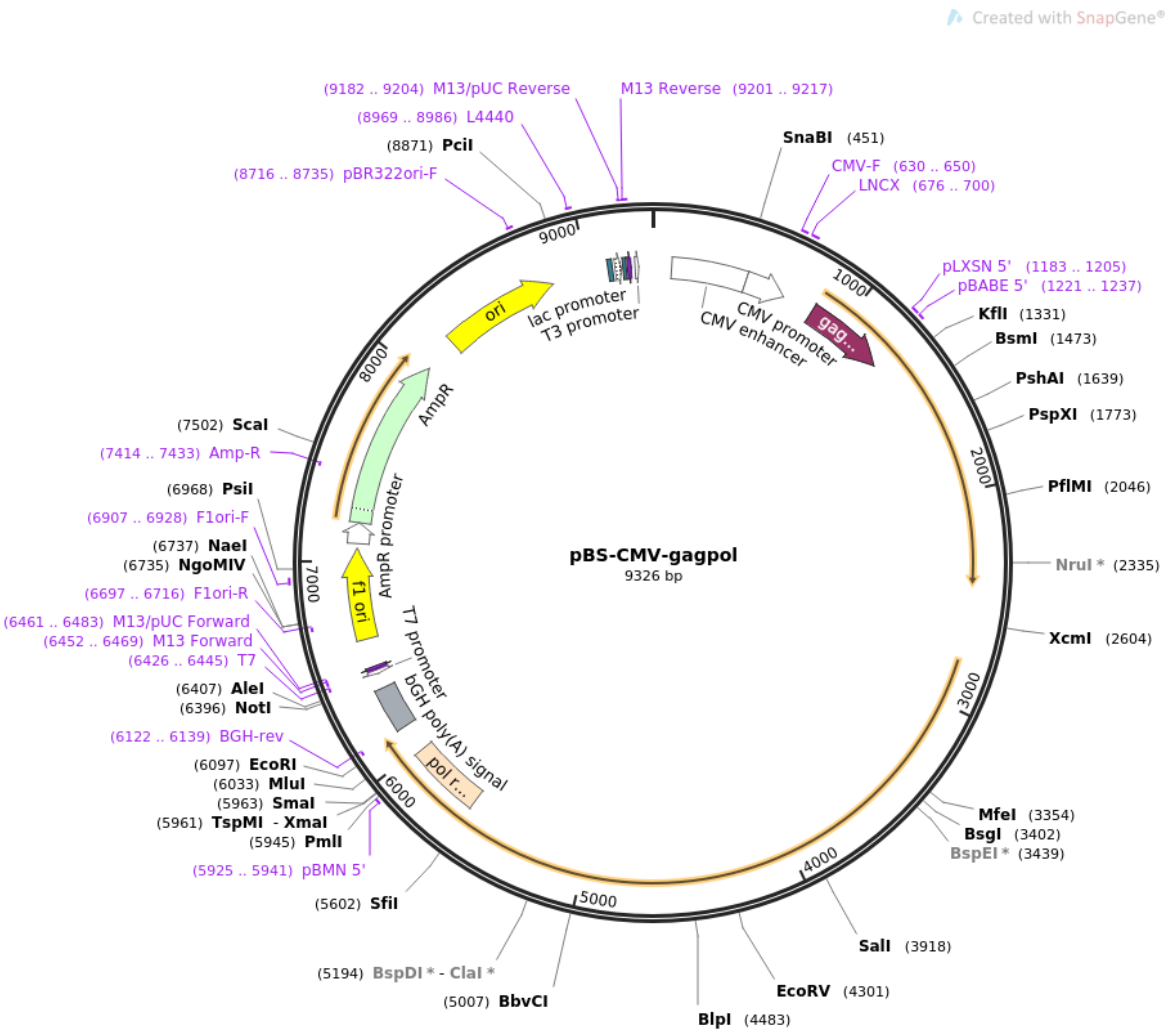

2.3.5.5 mKeima-Red-Mito-7 Plasmid #56018 addgene

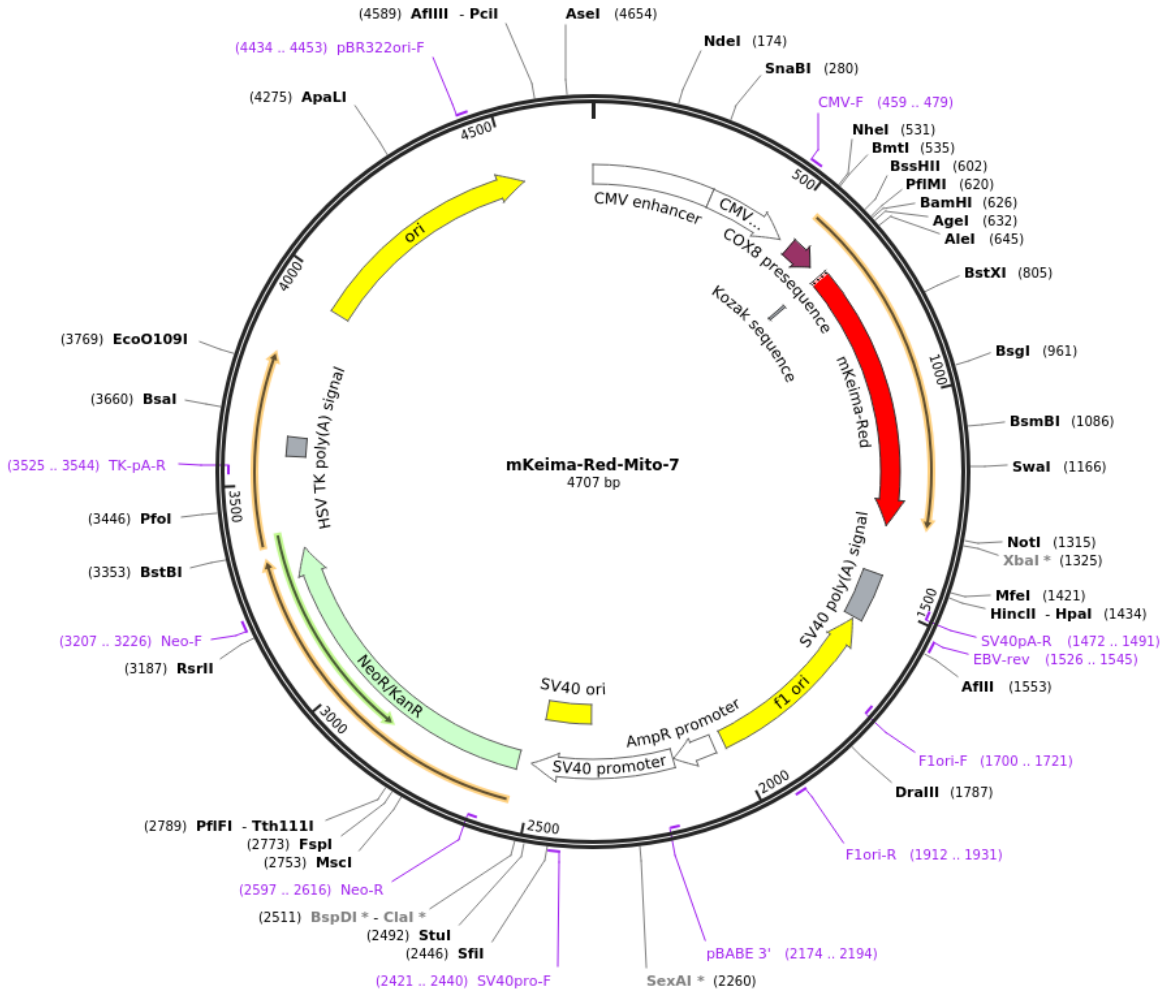

2.3.5.6 pLVX Mito-Timer

For representative purposes we are showing here a map of the original vector (pTRE-Tight Mito Timer, plasmid #50547 addgene). However, a pLenti version of this plasmid was kindly provided by Dr Garcia Vega Garcia-Escudero[263].

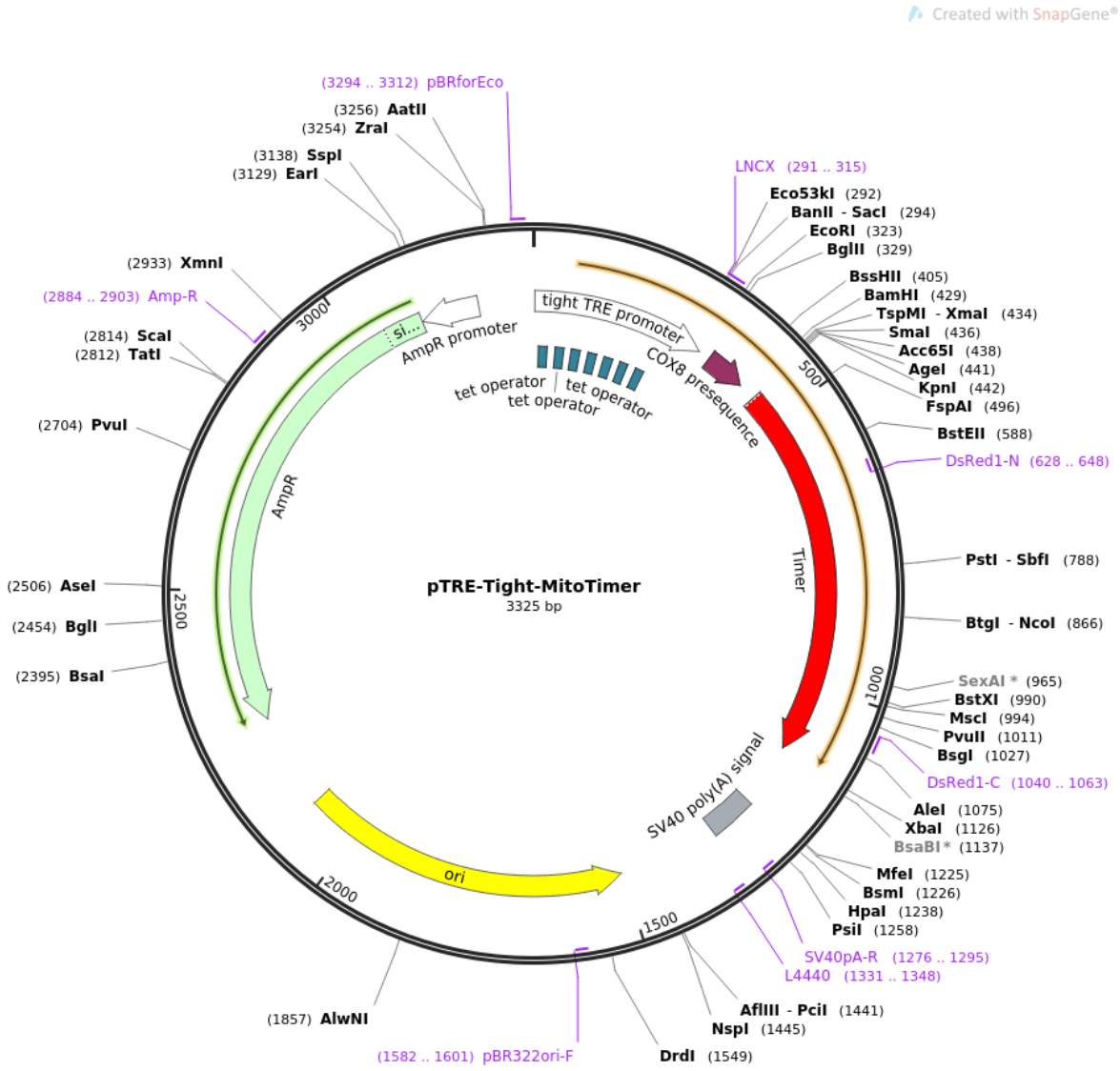

.

2.3.5.7 SMARTvector™ inducible lentiviral shRNA (horizon™)

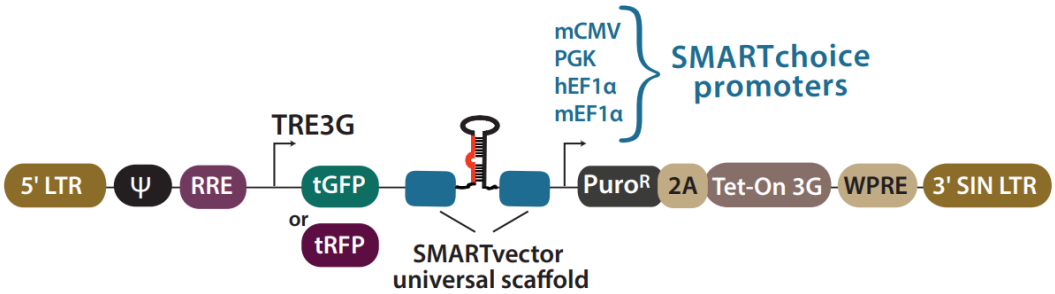

SMARTvector™ containing shRNA targeting sequences NTC (control TurboGFP, ID:VSC11653) and ULK1#1-2 (https://horizondiscovery.com/en/gene-modulation/knockdown/shrna/products/smartvector-inducible-lentiviral-shrna?nodeid=entrezgene-8408#resources) were ordered from horizon™.

K562 SV-NTC and SVULK1#1-2 were generated by Dr Martha Zarou following viral production and transfection as in 2.3.6.2. ULK1 Knock Down cells were validated by immunoblotting.

2.3.6 Metabolomics

2.3.6.1 Intracellular metabolite extraction

At the beginning of the experiment, cells were plated in normoxia (21%O_2) or hypoxia (0.5%O_2) and treated or left untreated with appropriate drugs according to the experimental setup at a concentration of $1.5x10^5$ in a 12-well plate in a total volume of 2 ml per condition. 24h or 48h later cell concentration was measured with CASY automated cell counter and cells were washed 2x with ice-cold PBS and extracted with ice-cold extraction solvent: MeOH/Acetonitrile/H_2O (ratio 50:30:20). The metabolite extraction was left incubating on ice for 5 min and centrifuged at 18,000g for 5 min at 4°C. the supernatant was transferred in LC-MS (Liquid Chromatography-Mass Spectrometry) glass vials and stored at -80°C until measurement was performed.

2.3.6.2 LC-MS analysis

The LC-MS set-up consisted of a Thermo Ultimate 3000 High pressure liquid chromatography (HPLC) system (Thermo Scientific) and a Q Exactive Orbitrap mass spectrometer (Thermo Scientific). The HPLC system consisted of a ZIC-pHILIC column (SeQuant, 150 x 2.1mm, 5µm, Merck KGaA), with a ZIC-pHILIC guard column (SeQuant, 20 x 2.1mm) and an initial mobile phase of 20% 20mM ammonium carbonate, pH 9.4, and 80% acetonitrile. Metabolite extracts (5µL) were injected into the system, and metabolites were separated over a 15min mobile phase gradient decreasing the acetonitrile content to 20%, at a flow rate of 200µl/min and a column temperature of 45ºC. Metabolites were then detected using the mass spectrometer with electrospray ionization and polarity switching. All metabolites were detected across a mass range of 75 - 1000m/z at a resolution of 35,000 (at 200m/z), and with a mass accuracy below 5ppm.

Data acquisition and analysis of metabolites' peak areas was performed using Skyline software (https://skyline.ms/project/home/software/Skyline/begin.view). Peak areas were normalised to cell number and volume measured before extraction.

2.3.6.3 Fumarate analysis

Fumarate analysis was carried out as in Mahmood et al.[264].

The setup consisted of a Q Exactive Orbitrap mass spectrometer (Thermo Scientific) coupled to an Ultimate 3000 high-performance liquid chromatography system (Thermo Fisher Scientific). Metabolite separation was done using a HILIC-Z column (InfinityLab Poroshell 120, 150 × 2.1mm, 2.7µm, Agilent) with a mobile phase consisting of a mixture of A (40mM ammonium formate, pH 3) and B (90% ACN / 10% 40mM ammonium formate). The flow rate was set to 200µl/min and the injection volume was 5µl. The gradient started at 10% A for 2 min, followed by a linear increase to 90% A for 15 min; 90% A was then maintained for 2 min, followed by a linear decrease to 10% A for 2 min and a final re-equilibration step with 10% A for 5 min. The total run time was 25 min. The Q Exactive mass spectrometer was operated in negative mode with a resolution of 70,000 at 200 m/z across a range of 100 to 150 m/z (automatic gain control) target of 1×10^6 and maximum injection time of 250 ms.

Data acquisition and analysis of metabolites' peak areas was performed using Skyline software. Peak areas were normalised to cell number and volume measured before extraction.

2.3.6.4 Analysis of extracellular metabolites

Cells were counted, collected in 1.5ml Eppendorf tubes and centrifuged at 500g x 5 min (4°C). The supernatant was collected in new tubes, which were centrifuged again at 500g x 5 min (4°C) to remove residual cells and supernatant was collected in fresh tubes. Tubes were stored at -80°C until analysis. On the day of the analysis, 300µl of medium were transferred in a 96-well plate and extracellular metabolites were analysed using a Biochemistry Analyser. Metabolites concentrations were calculated relative to media only samples (baseline) and normalised to cell proliferation. The exchange rate per 48h or 72h for a specific metabolite (x) was obtained with the following equation as in Rattigan et al.[265] :

Δmetabolite/(cell number day0 + cell number day 2 or 3)/2

Where Δmetabolite = ((x) mmol spent medium – (x) mmol cell-free medium).

2.3.6.5 Seahorse assay

Oxygen Consumption Rate (OCR) was measured using a Seahorse XFe96 Analyser (Agilent) as a readout of OXPHOS activity.

Initially a Seahorse 96 well plate was coated with a 0.02mg/ml $NaHCO_3$ (pH 7.4) Cell-Tak solution. And left incubating for 30 min. Cell-Tak was discarded and the plate was washed 2x with dH_2O and left at RT to air dry. A XF96 sensor cartridge was left hydrating overnight with calibrant solution in a non-humified CO2-free incubator at 37°C.

The following day, cells were counted and resuspended in Seahorse medium to seed 100,000 cells per well. The plate was centrifuged at 200g x 1 min without brakes. Cells were incubated in non-humified CO2-free incubator at 37°C for 30 min.

Oligomycin (1µM), CCCP (1µM), rotenone (1µM) and antimycin A (1µM) were prepare in Seahorse medium and transferred into the sensor cartridge. The sensor cartridge was left in the instrument for calibration, then followed by cell plate for cell readings.

Data were analysed using the Seahorse software Wave. Cell proliferation was used for normalisation of the assay's results.

2.3.7 Animal work

Animal experiments were conducted in accordance with the Animals Scientific Procedures Act 1986 and UK Home Office regulations. All experiments were conducted using personal licence number I30902590 and project licence PP2518370 held by Professor Vignir Helgason. Animals of both sexes were housed in a specific pathogen-free facility and kept in day/night cycles (12 hours each). Mice were fed *ad libitum* with food and water.

2.3.7.1 NRGW^{41} mouse model

NOD.Cg-Rag1^{tm1Mom} Kit^{W-41J} Il2rg^{tm1Wjl}/EavJ (NRGW^{41}) is an immunocompromised mouse model lately established in Dr. Connie Eaves lab[266]. These mice don't carry the Prkdc^{scid} allele which increases sensitivity to ionizing radiation, supporting engraftment of human cells for PDX studies with or without sub-lethal irradiation. These mice lack the stem cell growth factor KIT, resulting in high levels of chimerism. Moreover, the lack of interleukin-2 (IL2) and recombination activating gene 1 (Rag1) results in impairment of T and B cells.

2.3.7.2 KCL22 xenograft experiment

4 x10^6 KCL22 WT and KCL22 BNIP3 KO cells were resuspended in 200µl of PBS and transplanted via tail vein in NRGW^{41} mice (females and males) aged 8-12 weeks. Mice were monitored for tumour growth and sacrificed once tumour burden reached the experimental threshold. Tumour size was measured with a calibre and tumour volume was calculated with the following formula:

Volume = 0.5 x (length x width^2).

2.3.7.3 *In vivo* tracing experiment

In vivo tracing experiments were performed by using intraperitoneal bolus injections of $^{13}C_5$-glutamine (200µl each, 50 mg/mL) dissolved in Hank's Balanced Salt Solution (Sigma) in 8-12 weeks old NRGW^{41} mice. Mice were euthanized 20 minutes after the injection. Blood was directly lysed in extraction solvent, while spleen and bones were collected for isolation of c-kit$^+$ cells using CD117 mouse MicroBeads (#130-097-146, Miltenui Biotec). Cells were then processed for extraction of intracellular metabolites as in 2.3.6.2 and stored at -80 ºC before LC-MS analysis was performed.

2.3.8 Bioinformatics

RNA-seq dataset (GSE144527): raw data were downloaded from GEO database and raw counts obtained following the Galaxy pipeline Package *Deseq2* was used for both pre-processing and differential gene expression analysis.

ILLUMINA microarray dataset (GSE48294): data were downloaded from GEO database. Analysis was performed using Bioconductor. Package *limma* was used for both pre-processing and differential gene expression analysis.

Affymetrix microarray dataset (E-MTAB-2581): data were downloaded from Array Express database. Analysis was performed using Bioconductor (adapted from An End to End Workflow for Differential Gene Expression Using Affymetrix Microarrays, n.d.). Packages *oligo* and *arrayQualityMetrics* were used for quality control and pre-processing, while *limma* for differential gene expression analysis.

In house single cell data were generated by Dr Amy Dawson[268] and analysed by Mr Kiron Roy.

2.3.9 Graphical representation and statistical analysis

Data were plotted and analysed using GraphPad Prism (software 10.2.3). statistical tests employed are indicated in the figure legends. Results were considered statistically significant when p-value were < 0.05.

Chapter 3. Hypoxia influences CML mitochondrial metabolism

3.1 Introduction

As previously mentioned, the role of the microenvironment in CML metabolism remains underexplored. Our lab has identified mitochondrial metabolism as a targetable vulnerability in CML LSCs. More precisely, $CD34^{+}CD38^{-}$ LSCs showed higher mitochondrial mass and activity when compared to progenitor cells or non-CML stem cells[239]. Of note, most of the studies aiming at understanding LSCs metabolism were performed using conventional tissue culture techniques, i.e. under atmospheric oxygen levels. However, LSCs reside in the BM, which is hypoxic (1-5% O_2). Moreover, low oxygen incubation (0.5%O_2) has been shown to induce increased clonogenicity *in vitro* and improved engraftment in immunocompromised mice and consequent reduced responsiveness to conventional TKI therapy in CML[269]. Nonetheless, whether BM hypoxia promotes metabolic reprogramming of CML LSCs is yet not known.

This is hinting on a potential role of hypoxia in manipulating CML metabolism and promote different adaption mechanisms to physiologic-like environments.

To gain better understanding into the role of hypoxia in CML, we initially used a transcriptomic approach where we compared expression of metabolic genes in CML cells cultured under hypoxic conditions to conventional tissue culture, using a publicly available dataset. Secondly, we investigated the metabolic changes in CML cells exploiting a metabolomic approach. These results showed that hypoxic CML cells rewire their metabolic activity to promote glutaminolysis and glutamine reductive carboxylation.

To support our findings, we decided to inhibit glutaminolysis in CML cells using CB-839, a clinically relevant and selective GLS1 inhibitor.

3.2 CML cells preferentially use glutamine as a carbon fuel in hypoxia

3.2.1 Hypoxia reduces mitochondrial glucose oxidation in CML cells

Previous studies from our lab and others have shown that leukaemic cells rely on mitochondrial metabolism and OXPHOS to survive[239]. More precisely, CML LSCs showed increased mitochondrial mass and metabolic activity when compared to CML progenitor cells or normal HSCs[239]. However, these studies did not consider the limited oxygen levels that characterises the BM microenvironment and how this condition could affect cellular metabolic activity. Indeed, as previously discussed, the BM is hypoxic and represents an essential niche for the self-renewal and survival of primitive HSCs and LSCs[270,271,272].

Moreover, hypoxia (0.5% O_2) enhances CML LSCs properties, clonogenicity and engraftment in immunocompromised mice despite effective TKI-mediated inhibition of downstream BCR::ABL1 signaling. Low O_2 levels reduce the pro-apoptotic effect of Imatinib, resulting in the selection of resistant progenitor cells[251]. Furthermore, although inhibition of HIF-1α using acriflavine in combination with Imatinib showed reduced LSC burden in a CML mouse model, no evidence of improved survival with long-term HIF-1α inhibition was observed and possible off-target effects were shown[252]. Despite numerous studies investigating the metabolic profile of CML LSCs, investigation of the metabolic adaptations undergoing into CML LSCs exposed to hypoxia is warranted, which could help to improve our knowledge of how this resistant cellular reservoir properly functions in the BM microenvironment.

Initially, to gain better understanding into the effect of hypoxia on CML cells gene expression, we performed computational analysis on a publicly available dataset (GEO: GSE144527) characterised of K562 exposed to hypoxia (1% O_2) for 1, 3 and 6 days, with focus on main metabolic pathways. As shown in figure 7a, hypoxia resulted in the consistent upregulation of many glycolytic genes over time, such as SLC2A1 (glucose transporter 1, GLUT1), SLC2A3 (glucose transporter 3, GLUT3) and Hexokinase 2 (HK2). Moreover, the increased levels of lactate dehydrogenase A (LDHA) and SLC16A3 (also known as monocarboxylate transporter 4, MCT4) expression (figure 7c) suggested promotion of anaerobic glycolysis and lactate secretion into the extracellular environment respectively. Interestingly, this is in line with the observed increased expression of PDK1 and PDK3, both known to promote the inhibition of PDH activity and, hence, pyruvate oxidation in mitochondria (figure 7b). As a result, most of the TCA cycle genes were

downregulated, apart from IDH2 (figure 7d). Finally, we also explored the Pentose Phosphate Pathway genes, but their expression levels were not consistently changed over time (figure 7e).

Our analysis showed that CML cells downregulate gene expression of genes involved in mitochondrial metabolism and promote the transcription of genes related to glycolysis. Therefore, CML cells might lose their oxidative dependency when exposed to physiologic oxygen conditions. These results raise new questions regarding CML metabolic plasticity and ability to adapt to different environmental conditions.

To validate our *in-silico* findings, we exposed K562 cells to low oxygen levels (0.5 $\%O_2$, hereafter referred to as hypoxia or H) for 3 days and assessed their mitochondrial respiration. We decided to use 0.5% O_2 oxygen levels for our experiments as this oxygen concentration was previously used in CML in vitro model[269]. We observed decreased basal, maximal, and ATP-linked OCR (figure 8a-b). This would hint to reduced OXPHOS dependency in low oxygen environment. Next, we monitored cellular growth over time in both normoxia and hypoxia. Hypoxia significantly decreased cellular proliferation in both K562 and KCL22 cells (figure 8c-d). The slower cellular growth could be due to reduced ATP levels given the lower oxygen levels and pyruvate mitochondrial oxidation into the TCA cycle as suggested by our previous bioinformatic analysis.

LC-MS analysis of TCA cycle metabolites revealed that CML cells accumulate intracellular levels of α-KG (figure 9b), succinate (figure 9c) and fumarate (figure 9d) after 2 days of hypoxia exposure, while malate (figure 9e) and citrate (figure 9a) levels were reduced. While lower citrate is in line with the reduced mitochondrial oxidative profile of hypoxic cells, the increased levels of fumarate and succinate, known to be mitochondrial-resident metabolites, suggested that hypoxic CML cells still use mitochondrial metabolism to sustain their growth. However, it has been shown in other cancer models that hypoxia not only promotes glycolysis but also induces a metabolic switch towards glutamine or other alternative carbon sources to support their mitochondrial activity[273,274].

To confirm reduced glucose mitochondrial oxidation in CML cells under low oxygen condition, we performed fully labelled glucose tracing. As shown in Figure 10b, hypoxia promoted increased incorporation of glucose-derived carbons in pyruvate and lactate, hence confirming anaerobic glycolysis. Moreover, hypoxic cells significantly promoted secretion of lactate in the extracellular environment (figure 10b). Interestingly, reduction in glucose derived $^{13}C_2$ labelling into citrate (figure 10d) was in line with our transcriptomic analysis. Furthermore, as a readout of oxidative metabolism and glycolysis, we assessed

the ratio between the glucose-derived carbons into the TCA cycle-derived amino acid glutamate ($^{13}C_{2\text{-}5}$-Glutamate) and the glycolytic end-product lactate ($^{13}C_3$-Lactate), shown in figure 10c. This showed that hypoxia significantly decreased the ratio of glucose-derived glutamate over glucose-derived lactate, in line with the reduced glucose oxidation in mitochondria.

However, despite lower incorporation of glucose-derived carbons in all TCA-related metabolites, hypoxic K562 cells still showed high intracellular total and unlabelled levels of α-KG, succinate, and fumarate (figure 10d). Consequently, we speculated if glutamine could represent an alternative carbon source for reductive carboxylation to fuel mitochondrial metabolism under low oxygen tension.

Of note, similar results were obtained exposing patient derived $CD34^+$ samples to hypoxia. Indeed, low oxygen tension increased anaerobic glycolysis (figure 11a), decreased glucose oxidation in the TCA cycle (figure 11b-d). Moreover, hypoxia promoted increased α-KG/Citrate ratio (figure 11c), which is indicative of metabolic reprogramming and, more precisely, of glutamine reductive carboxylation[275]. This prompted us to investigate glutaminolysis in hypoxic CML cells.

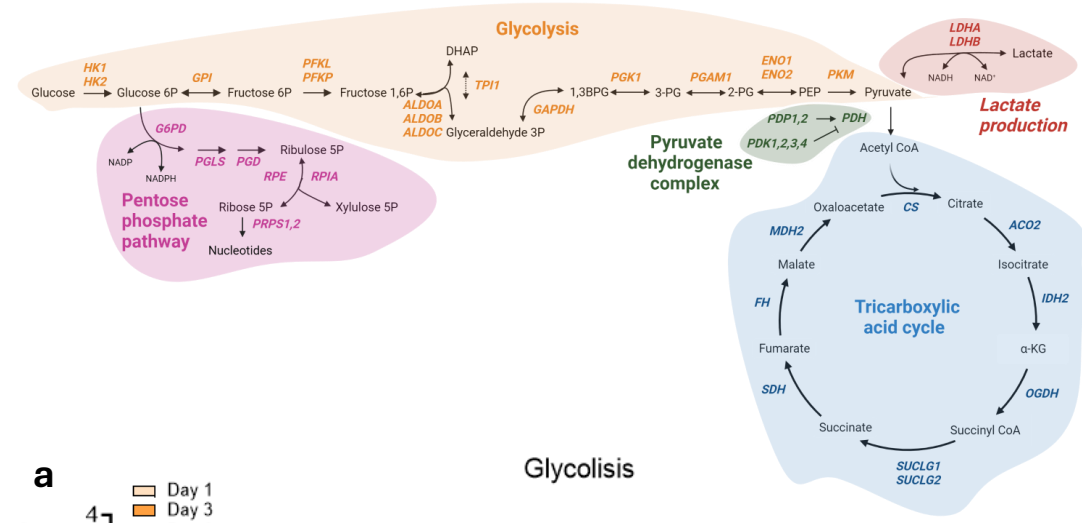
Glycolysis
Glucose
HK1
HK2
Glucose 6P
GPI
Fructose 6P
PFKL
PFKP
Fructose 1,6P
DHAP
TPI1
ALDOA
ALDOB
ALDOC
Glyceraldehyde 3P
GAPDH
1,3BPG
PGK1
3-PG
PGAM1
2-PG
ENO1
ENO2
PEP
PKM
Pyruvate
LDHA
LDHB
Lactate
NADH
NAD+
Lactate production
G6PD
NADP
NADPH
PGLS
PGD
Ribulose 5P
RPE
RPIA
Ribose 5P
Xylulose 5P
PRPS1,2
Nucleotides
Pentose phosphate pathway
PDP1,2
PDH
PDK1,2,3,4
Pyruvate dehydrogenase complex
Acetyl CoA
Oxaloacetate
CS
Citrate
ACO2
Isocitrate
IDH2
α-KG
OGDH
Succinyl CoA
SUCLG1
SUCLG2
Succinate
SDH
Fumarate
FH
Malate
MDH2
Tricarboxylic acid cycle

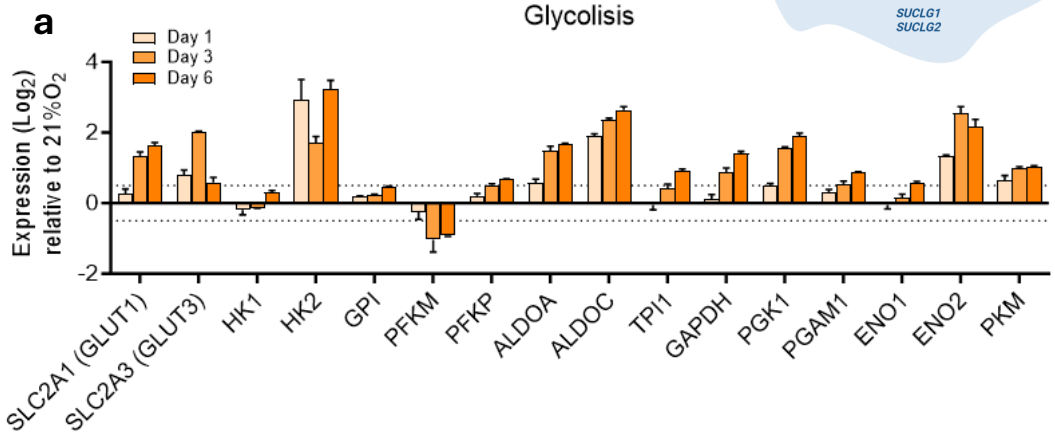
a
Glycolisis
Day 1
Day 3
Day 6
Expression (Log2) relative to 21%O2
SLC2A1 (GLUT1)
SLC2A3 (GLUT3)
HK1
HK2
GPI
PFKM
PFKP
ALDOA
ALDOC
TPI1
GAPDH
PGK1
PGAM1
ENO1
ENO2
PKM

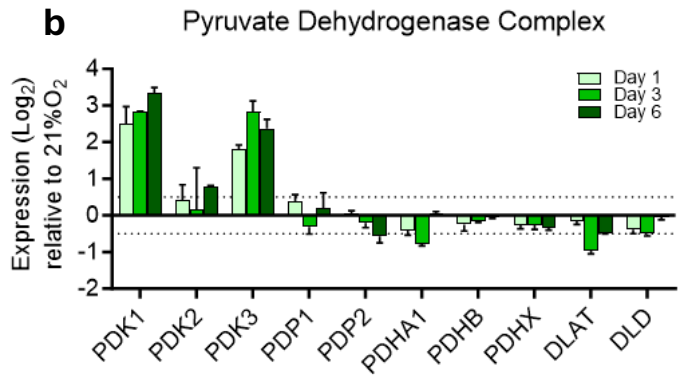
b
Pyruvate Dehydrogenase Complex
Day 1
Day 3
Day 6
Expression (Log2) relative to 21%O2
PDK1
PDK2
PDK3
PDP1
PDP2
PDHA1
PDHB
PDHX
DLAT
DLD

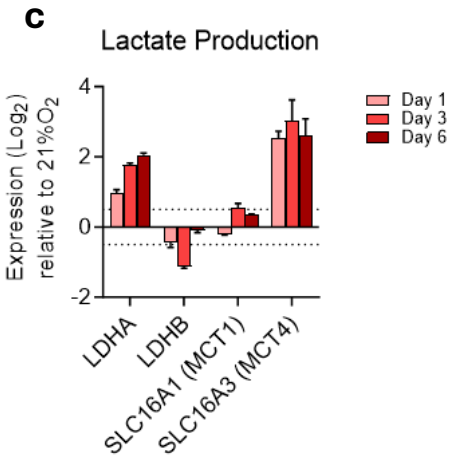
c
Lactate Production
Day 1
Day 3
Day 6
Expression (Log2) relative to 21%O2
LDHA
LDHB
SLC16A1 (MCT1)
SLC16A3 (MCT4)

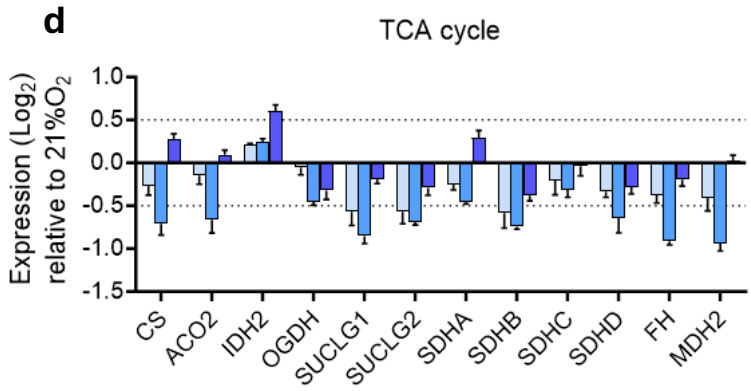
d
TCA cycle
Day 1
Day 3
Day 6
Expression (Log2) relative to 21%O2
CS
ACO2
IDH2
OGDH
SUCLG1
SUCLG2
SDHA
SDHB
SDHC
SDHD
FH
MDH2

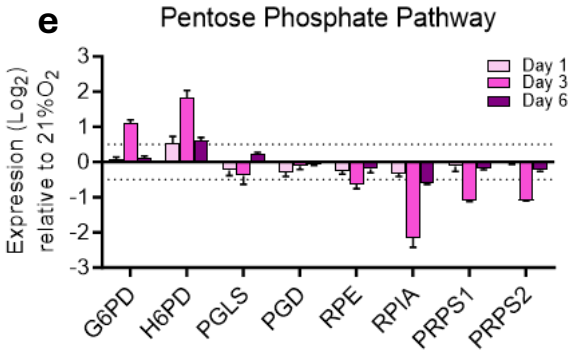

Figure 7: Hypoxia promotes changes in metabolic gene transcript levels in CML cells. Expression levels of key genes involved in major cellular metabolic pathways are shown. a) Enzymes involved in Glycolysis (orange). b) Enzymes involved in Pyruvate dehydrogenase complex (green). c) Enzymes involved in Lactate Production (red). d) Enzymes involved in TCA cycle (blue). e) Enzymes involved in Pentose Phosphate Pathway (purple). Bars represent SD. All genes whose Log_2 Fold Change that are above the 0.5 (upregulated) or below the -0.5 (downregulated) are significant and their adjusted P-values were calculated using the DESeq2 pipeline in R.

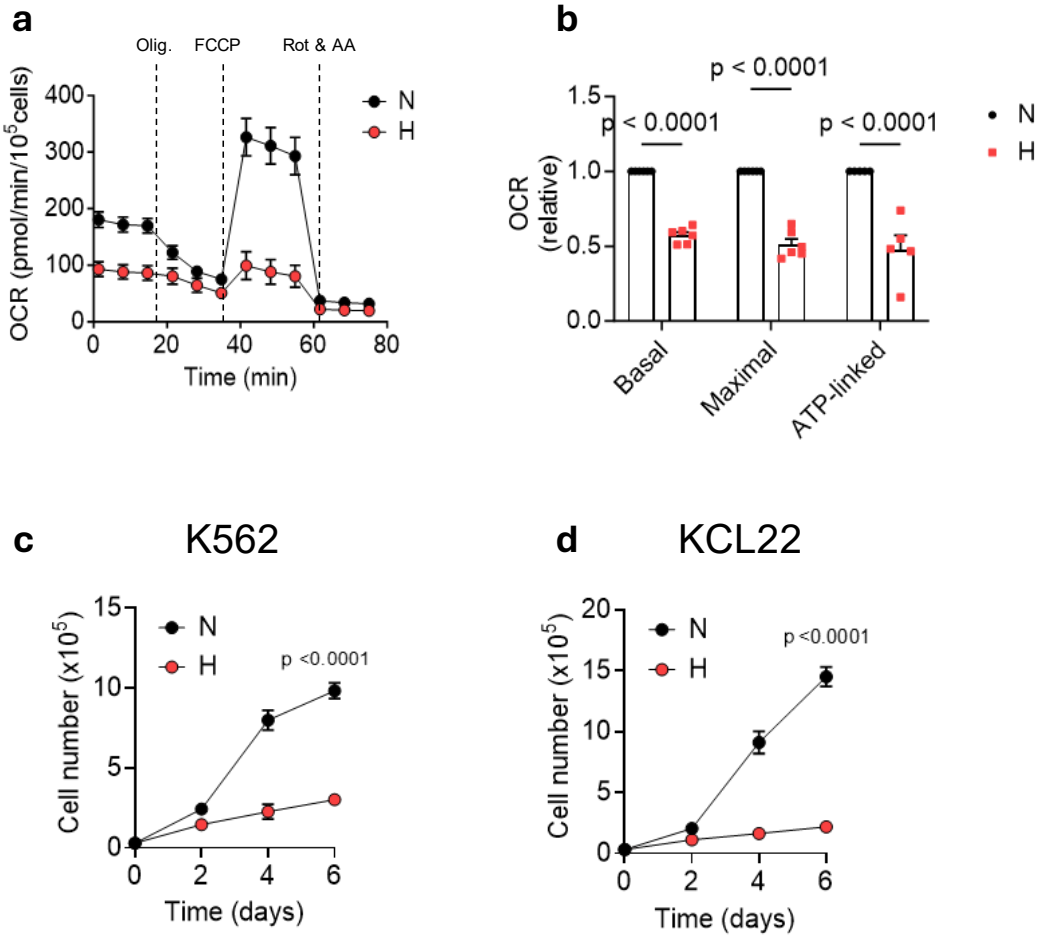

Figure 8: Hypoxia reduces OXPHOS and cell proliferation in CML cells. a) Seahorse profile of K562 cells exposed to 21% O_2 (N) or pre-exposed to 0.5% O_2 (H) for three days. b) quantification of basal, maximal and ATP-linked OCR. c) growth curves of K562 and d) KCL22 exposed to 21% O_2 (N) or 0.5% O_2 (H) for 2,4 and 6 days. P values showed in (b) were calculated with a 2-way ANOVA with Sidak's multiple comparison test. Data in (b) are plotted as mean ± SEM. Data in (c) and (d) are plotted as mean ± SD of n=4 independent cultures. P values were calculated with a 2-way ANOVA using Šídák's multiple comparisons test.

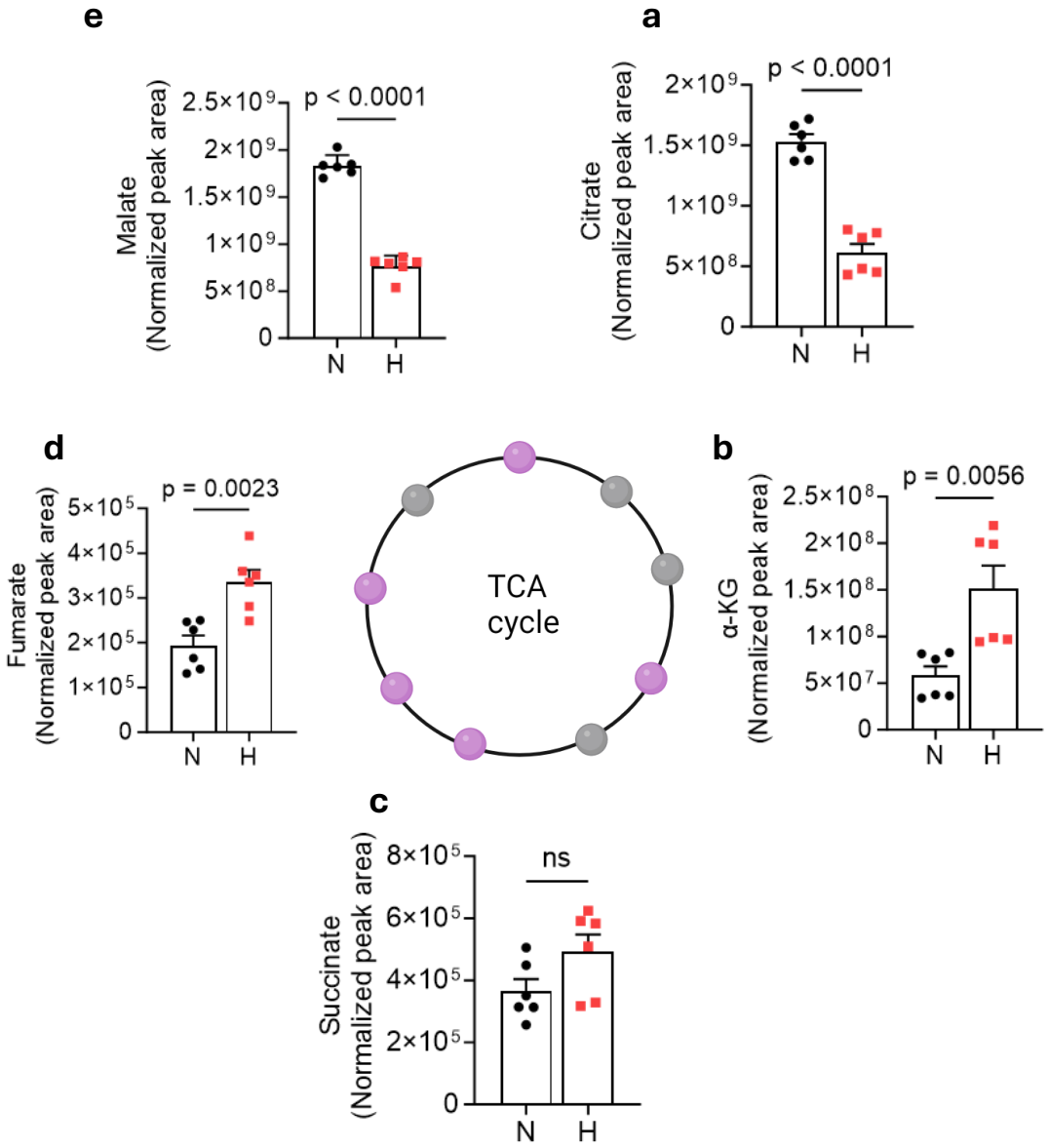

Figure 9: Hypoxia leads to changes in metabolites levels in CML cells. Representative graphs of peak areas of (a) citrate, (b) α-KG, (c) succinate, (d) fumarate, (e) malate in K562 cells exposed to 21% O_2 (N) or 0.5% O_2 (H) for 2 days. Data are plotted as mean ± SEM of n=2 independent cultures (n=6 technical replicates, 3 each). P values were calculated with a pair t-test.

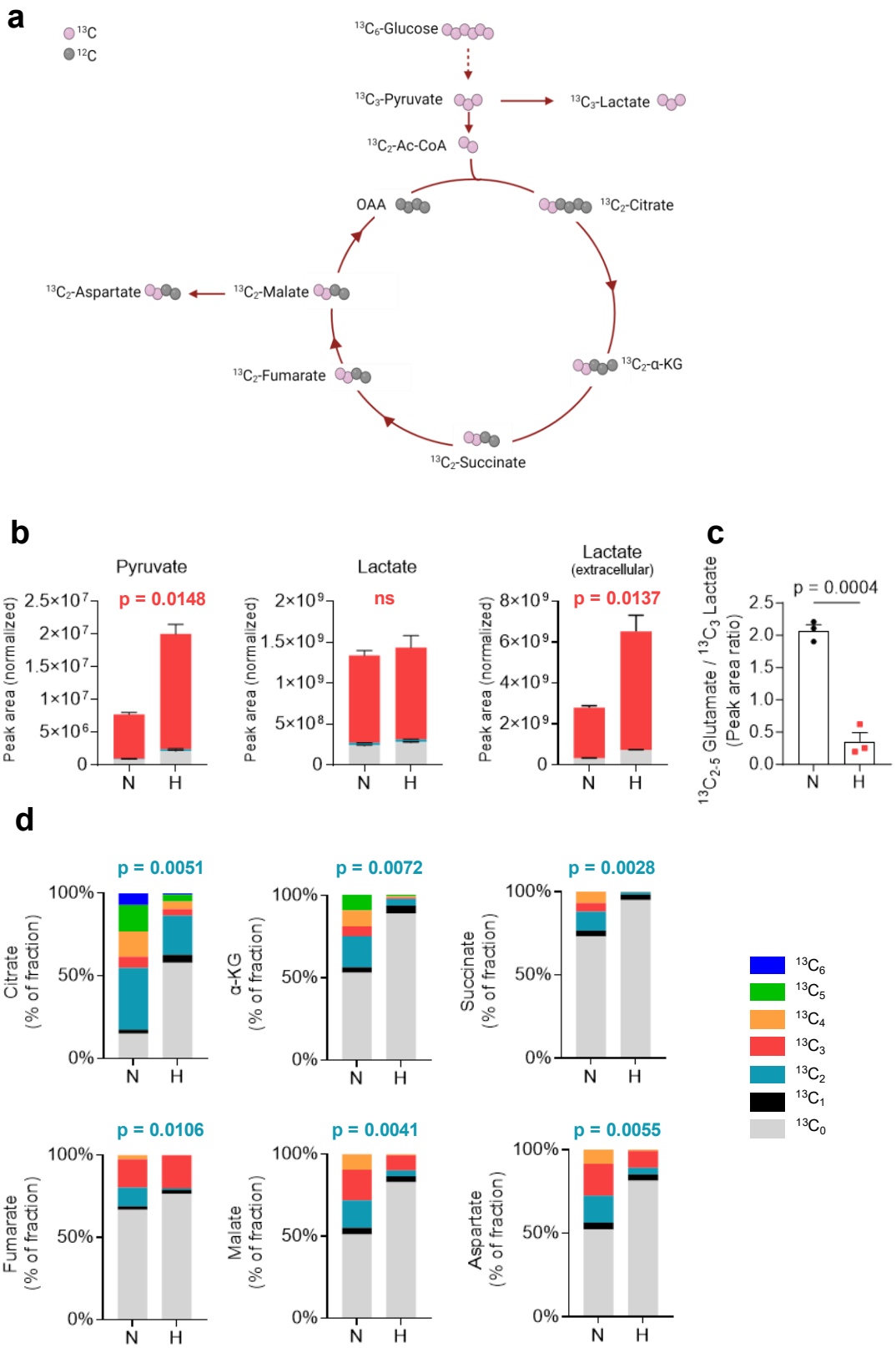
a
^{13}C
^{12}C
$^{13}C_6$-Glucose
$^{13}C_3$-Pyruvate
$^{13}C_3$-Lactate
$^{13}C_2$-Ac-CoA
OAA
$^{13}C_2$-Citrate
$^{13}C_2$-α-KG
$^{13}C_2$-Succinate
$^{13}C_2$-Fumarate
$^{13}C_2$-Malate
$^{13}C_2$-Aspartate
b
Pyruvate
p = 0.0148
Lactate
ns
Lactate (extracellular)
p = 0.0137
Peak area (normalized)
N
H
c
p = 0.0004
$^{13}C_{2-5}$ Glutamate / $^{13}C_3$ Lactate (Peak area ratio)
d
p = 0.0051
p = 0.0072
p = 0.0028
p = 0.0106
p = 0.0041
p = 0.0055
Citrate (% of fraction)
α-KG (% of fraction)
Succinate (% of fraction)
Fumarate (% of fraction)
Malate (% of fraction)
Aspartate (% of fraction)
100%
50%
0%
$^{13}C_6$
$^{13}C_5$
$^{13}C_4$
$^{13}C_3$
$^{13}C_2$
$^{13}C_1$
$^{13}C_0$

Figure 10: Hypoxia reduces glucose oxidation in CML cells. A) Schematic of $^{13}C_6$ glucose tracing into TCA cycle metabolites. Ac-CoA; Acetyl-CoA, OAA; oxaloacetate, α-KG; alpha-ketoglutarate. b) Representative graphs of normalized peak areas of Pyruvate, Lactate (intracellular) and Lactate (extracellular) in K562 cells following exposure to 21% O_2 (N) or 0.5% O_2 (H) and cultured with custom-made Plasmax containing of ^{13}C glucose for 24 hours (n=3 technical replicates). c) ratio of glucose-derived glutamate ($^{13}C_{2-5}$ Glutamate) over glucose-derived lactate ($^{13}C_3$ Lactate) in K562 cells cultured under 21% O_2 (N) or 0.5% O_2 (H) (n=3 technical replicates). d) Fractional labelling from ^{13}C glucose into indicated metabolites of K562 cells exposed to 21% O_2 (N) or 0.5% O_2 (H) for 24 hours (n=3 technical replicates). P values in b), c) and d) were calculated using calculated using paired Student's t test. For tracing experiments colour code of the P-values refers to comparisons of similarly coloured isotopologues.

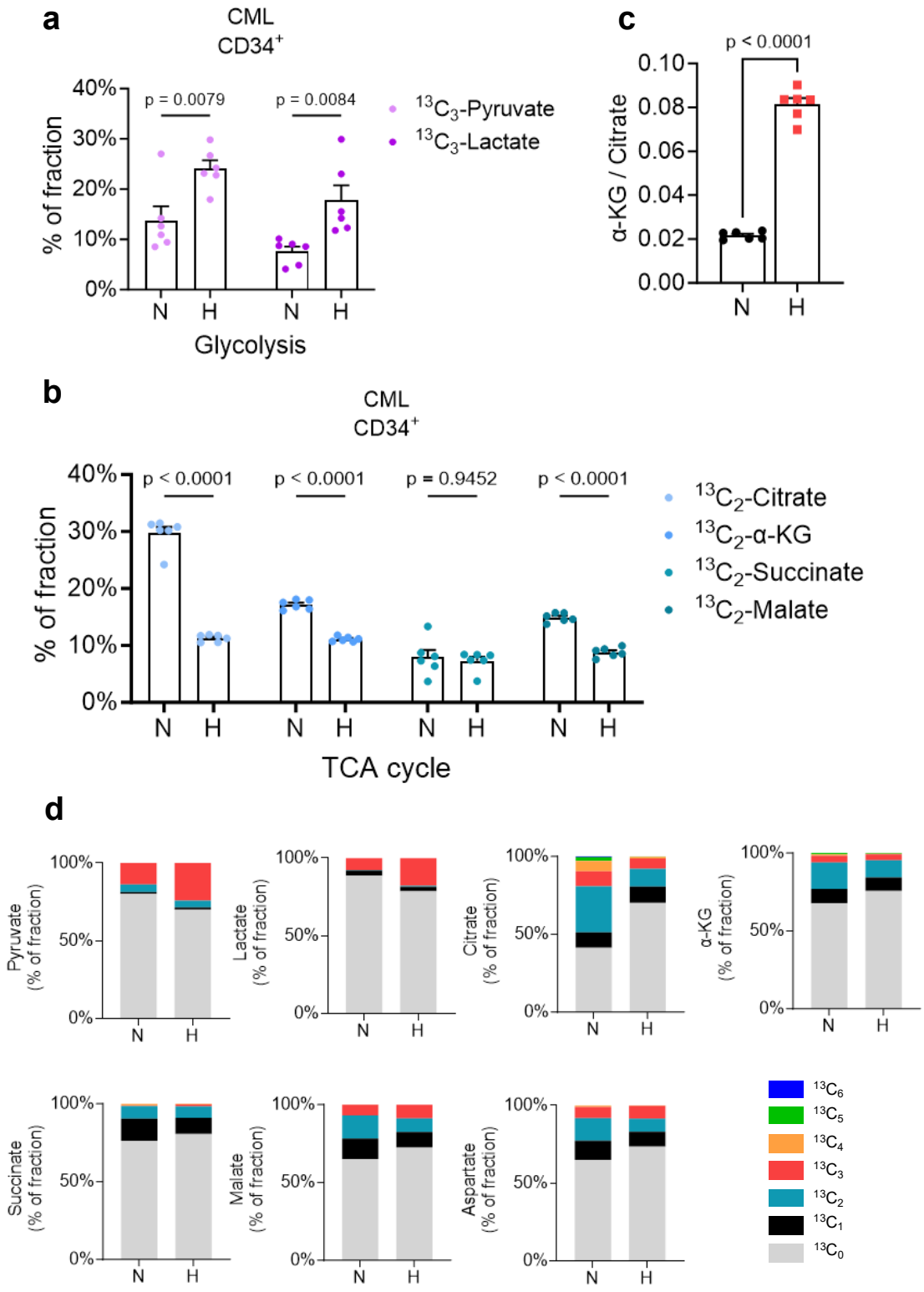
a
CML
CD34+
% of fraction
40%
30%
20%
10%
0%
p = 0.0079
p = 0.0084
N
H
N
H
Glycolysis
13C3-Pyruvate
13C3-Lactate
c
p < 0.0001
α-KG / Citrate
0.10
0.08
0.06
0.04
0.02
0.00
N
H
b
CML
CD34+
% of fraction
40%
30%
20%
10%
0%
p < 0.0001
p < 0.0001
p = 0.9452
p < 0.0001
N
H
N
H
N
H
N
H
TCA cycle
13C2-Citrate
13C2-α-KG
13C2-Succinate
13C2-Malate
d
Pyruvate (% of fraction)
Lactate (% of fraction)
Citrate (% of fraction)
α-KG (% of fraction)
Succinate (% of fraction)
Malate (% of fraction)
Aspartate (% of fraction)
100%
50%
0%
N
H
13C6
13C5
13C4
13C3
13C2
13C1
13C0

Figure 11: Hypoxia increases glycolytic flux while reduces glucose oxidation in patient derived CML cells. a-b) Fractional labelling from ^{13}C glucose into indicated metabolites of patient-derived cells exposed to 21% O_2 (N) or 0.5% O_2 (H) for 24 hours (n=3 patient samples, n=2 technical replicates). c) Ratio of α-KG over Citrate of CML patient-derived cells cultured under 21% O_2 (N) or 0.5% O_2 (H) for 24 hours (n=3 patients, n=2 technical replicates). d) Fractional labelling from ^{13}C glucose into indicated metabolites of patient-derived cells exposed to 21% O_2 (N) or 0.5% O_2 (H) for 24 hours (n=3 patients, n=2 technical replicates). Means ± SEM P values in were calculated using paired Student's t test.

3.2.2 Hypoxia promotes reductive carboxylation of glutamine in CML cells.

To confirm that hypoxic CML cells preferentially use glutamine to fuel their mitochondrial metabolism, we initially measured the levels of nutrients uptake from extracellular environment with particular focus on glutamine and glutamate. As shown in figure 12b, our results indicated that hypoxia significantly promotes glutamine uptake without affecting glutamate secretion (figure 12c), supporting our hypothesis that glutamine is indeed an alternative carbon fuel for hypoxic CML cells.

Next, we performed fully labelled glutamine ($^{13}C_5$) tracing. Interestingly, as shown in figure 12e, our results showed increased labelling of glutamine-derived carbons into glutamate (C_5) and a-KG (C_5). Furthermore, glutamine derived carbons could be identified in increased abundance in all TCA-metabolites (figure 12e). The increased influx of glutamine derived a-KG into the TCA cycle is known as glutamine anaplerosis and it is used by many cancer and non-cancer cells to replenish intermediates and promote the generation of NADPH [276]. Glutamine anaplerosis is mainly regulated by the activity of Glutaminase (GLS).

Intriguingly, we also observed increased C_5 labelling in citrate, which is indicative of reductive carboxylation (RC) of glutamine. It has been shown that RC can support the citrate pool especially in cancer cells under hypoxia or with defective mitochondria[150,275]. RC depends on the activity of two enzymes: IDH1 (cytosolic) and IDH2 (mitochondrial). In support of hypoxia-promoted RC, we observed that the only TCA-related gene to be upregulated in our transcriptomic analysis was indeed IDH2 (figure 7d). Consistently, hypoxic CML cells showed significantly higher levels of fumarate, malate and aspartate derived from reductive metabolism (glutamine derived C_3 labelling) compared to normoxic cells (figure 12e and figure 13a-d). The hypoxia-induced reductive glutamine flux was further confirmed by the increased ratio of a-KG over Citrate (figure 12d). Finally, the ratios of reductive over oxidative metabolites were significantly increased in hypoxia (figure 13e-h).

Reductive carboxylation is generally exploited by cancer cells to support the citrate pool as this metabolite represents the major source of acetyl-CoA, which, in turn, is used for lipid biosynthesis and/or epigenetic as a donor for acetylation. Indeed, hypoxic K562 were seen to accumulate lipid droplets[248]. However, how and if CML cells can reconstitute their mitochondrial network in order to promote reductive carboxylation of glutamine under hypoxia has not been addressed yet.

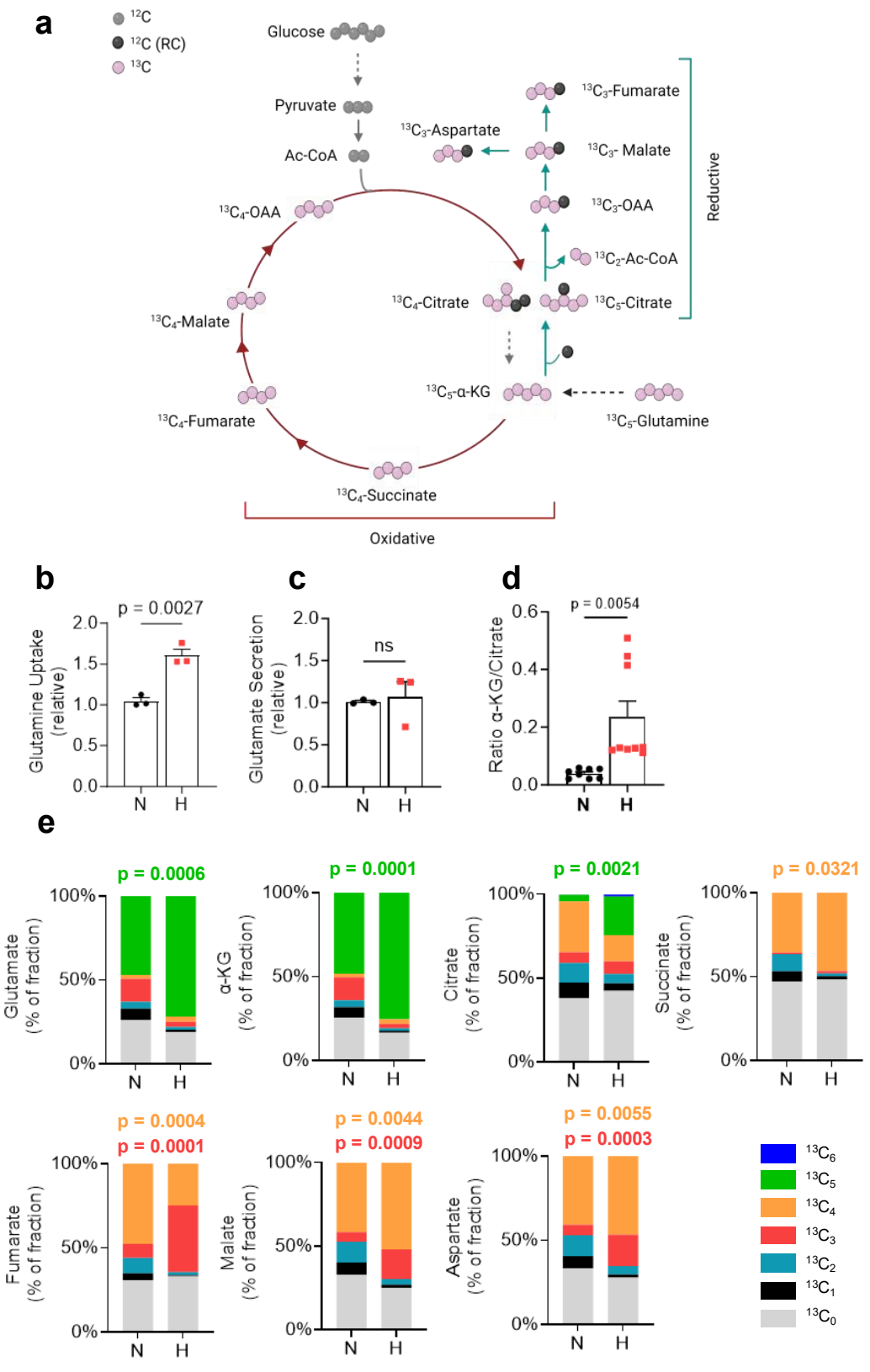
a
12C
12C (RC)
13C
Glucose
Pyruvate
Ac-CoA
13C4-OAA
13C4-Citrate
13C5-Citrate
13C4-Malate
13C4-Fumarate
13C5-α-KG
13C5-Glutamine
13C4-Succinate
13C3-Fumarate
13C3-Aspartate
13C3- Malate
13C3-OAA
13C2-Ac-CoA
Reductive
Oxidative
b
p = 0.0027
Glutamine Uptake (relative)
N
H
c
ns
Glutamate Secretion (relative)
d
p = 0.0054
Ratio α-KG/Citrate
e
p = 0.0006
Glutamate (% of fraction)
p = 0.0001
α-KG (% of fraction)
p = 0.0021
Citrate (% of fraction)
p = 0.0321
Succinate (% of fraction)
p = 0.0004
p = 0.0001
Fumarate (% of fraction)
p = 0.0044
p = 0.0009
Malate (% of fraction)
p = 0.0055
p = 0.0003
Aspartate (% of fraction)
13C6
13C5
13C4
13C3
13C2
13C1
13C0

Figure 12: CML cells preferentially use glutamine-derived carbons to fuel the TCA cycle under low oxygen conditions. a) Schematic of $^{13}C_5$- glutamine tracing following oxidative (red arrows) and reductive (green arrows) metabolism. Ac-CoA; Acetyl-CoA, OAA; oxaloacetate, α-KG; alpha-ketoglutarate. b) Relative glutamine uptake and c) glutamate secretion of K562 cells cultured under 21% O_2 (N) or 0.5% O_2 (H) for 72 hours (n=3 independent cultures). d) Ratio of α-KG over Citrate of K562 cells cultured under 21% O_2 (N) or 0.5% O_2 (H) for 72 hours (n=9 independent cultures). e) Fractional labelling from ^{13}C glutamine into indicated metabolites of K562 cells exposed to 21% O_2 (N) or 0.5% O_2 (H) for 24 hours (n=3 independent cultures). Means ± SEM P values in b), c), d) and e) were calculated using paired Student's t test. For tracing experiments colour code of the P-values refers to comparisons of similarly coloured isotopologues.

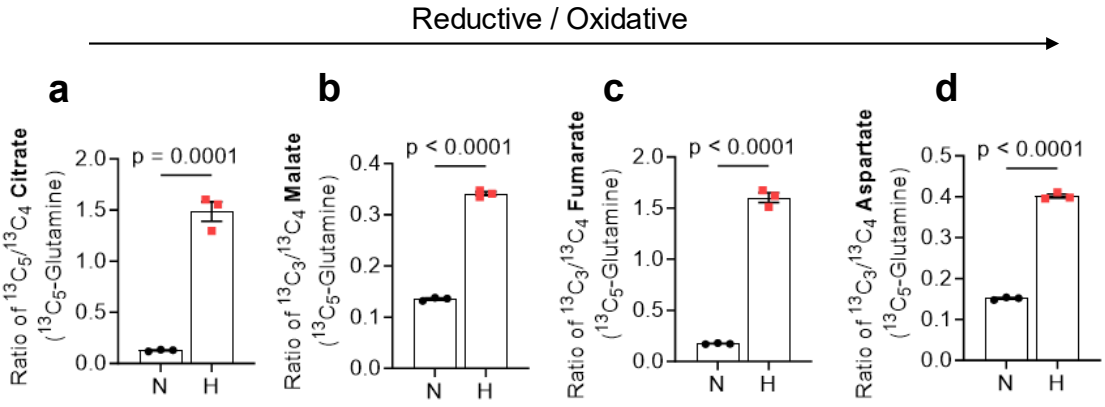
Reductive / Oxidative
a
b
c
d
Ratio of $^{13}C_5/^{13}C_4$ Citrate ($^{13}C_5$-Glutamine)
Ratio of $^{13}C_3/^{13}C_4$ Malate ($^{13}C_5$-Glutamine)
Ratio of $^{13}C_3/^{13}C_4$ Fumarate ($^{13}C_5$-Glutamine)
Ratio of $^{13}C_3/^{13}C_4$ Aspartate ($^{13}C_5$-Glutamine)
p = 0.0001
p < 0.0001
p < 0.0001
p < 0.0001
N
H

Figure 13: Hypoxic CML cells promote glutamine reductive carboxylation. a) Ratio of $^{13}C_5$ over $^{13}C_4$ Citrate, b) Ratio of $^{13}C_3$ over $^{13}C_4$ Malate, c) Ratio of $^{13}C_3$ over $^{13}C_4$ Fumarate, d) Ratio of $^{13}C_3$ over $^{13}C_4$ Aspartate of K562 cells treated as before. (n=3 independent cultures) Means ± SEM P values were calculated using paired Student's t test.

3.2.3 CML cells highly depend on GLS1 activity for their growth in hypoxia.

To assess if glutamine anaplerosis and RC may represent molecular vulnerabilities in CML under hypoxic conditions, we investigated the effects of CB-839, a selective allosteric inhibitor of GLS1, (referred to as GLS1i) and two structurally different IDH2 inhibitors (AGI-67 referred to as IDH2i-1 and AG221 or enasidenib, referred to as IDH2i-2). Both the IDH2 inhibitors have been designed to target mutated IDH2 and have showed efficacy in targeting AML cells carrying this aberrant form of the enzyme. Nevertheless, some studies have reported that IDH2i-1 and-2 can also successfully target wild-type IDH2[156]. Therefore, we monitored the cell growth of K562 and KCL22 cells upon treatment of 2 GLS1i concentrations (50 and 500 nM) or 2 μM of IDH2i-1 and IDH2i-2. Cells were grown for 4 days under normoxia or hypoxia in two different media: conventional RPMI (R in figure 14) and Plasmax (P in figure 14) since it is the cellular culture medium used in our metabolomics experiments. While CB-839 significantly reduced cellular proliferation in both CML cell lines (figure 14a-d), both the tested IDH2 inhibitors did not affect cell growth (figure 14e-h). statement removed as the difference between normoxia and hypoxia was not statistically significant.

Subsequently, we tested if CB-839 reduces reductive carboxylation in hypoxia via fully labelled glutamine tracing. As shown in figure 15b, CB-839 treated cells showed significantly lower α-KG /Citrate ratio when cells were treated under hypoxia. However, the glutamine derived labelling into TCA metabolites was not decreased (figure 15c). Furthermore, despite higher α-KG/citrate ratio and in contrast to what was previously shown in figure 12e, we did not observe a significant increased glutamine-derived labelling in α-KG under hypoxia (figure 15c). Therefore, we are planning to repeat this experiment to rule out technical issues.

Interestingly, supplementation of a supraphysiological concentration of α-KG rescued the growth of K562 cells under hypoxia (figure 16a-b). Furthermore, staining with apoptotic markers 7-AAD and annexin V showed that pharmacological inhibition of GLS1 using CB-839 significantly induces cell death under low oxygen conditions and that α-KG supplementation is sufficient to reduce its pro-apoptotic effect (figure 16c-d). However, glutamine deprivation could induce cell death but not to the same extent as GLS1 inhibition (figure 16e-f).

Given the effect that CB-839 treatment had on cell proliferation and apoptosis in K562 and KCL22 cells, we wondered whether GLS1 inhibition could promote programmed cell death in other leukaemia cell lines. Gallipoli et al.[277] showed that CB-839 treatment was effective in AML cells and could synergise with standard treatments. Therefore, we treated four AML cell lines with CB-839 in normoxia and hypoxia and assessed its pro-apoptotic effect via flow cytometry. This revealed that THP1 (figure 17a) were more sensitive to GLS1 inhibition under low oxygen conditions, while MV-411 (figure 17b) and MOLM13 (figure 17c) OCI_AML_3 (figure 17d) did not show higher apoptosis levels.

These data suggest that several leukaemic cells become dependent on GLS1 when exposed under low oxygen conditions, which can be targeted with CB-839 to induce cell death.

R = RPMI
P = Plasmax

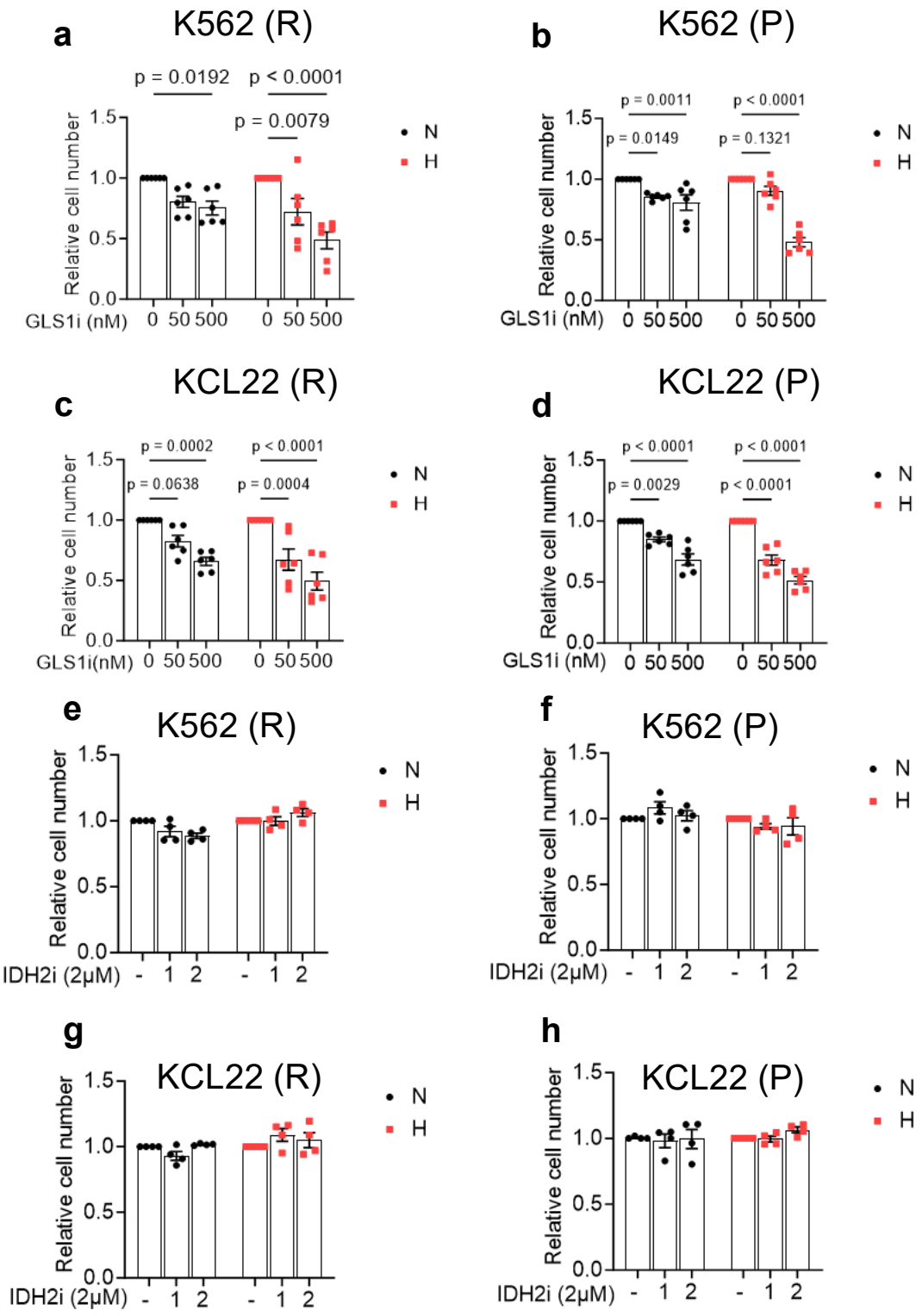

Figure 14: Inhibition of GLS1 but not IDH2 reduces the growth of CML cells. Relative cell numbers of K562 cells cultured in a) RPMI or b) Plasmax under 21% O_2 (N) or 0.5% O_2 (H) and treated or left untreated with the indicated GLS1i (CB-839) concentrations for 3 days. c) and d) as in a) and b) but in KCL22 cells. Relative cell numbers of K562 cells cultured in e) RPMI or f) Plasmax under 21% O_2 (N) or 0.5% O_2 (H) and treated or left untread with the indicated IDH2i-1 (AG-221) or IDH2i-2 (AGI-6780) concentrations for 3 days. g) and h) as in e) and f) but in KCL22 cells.

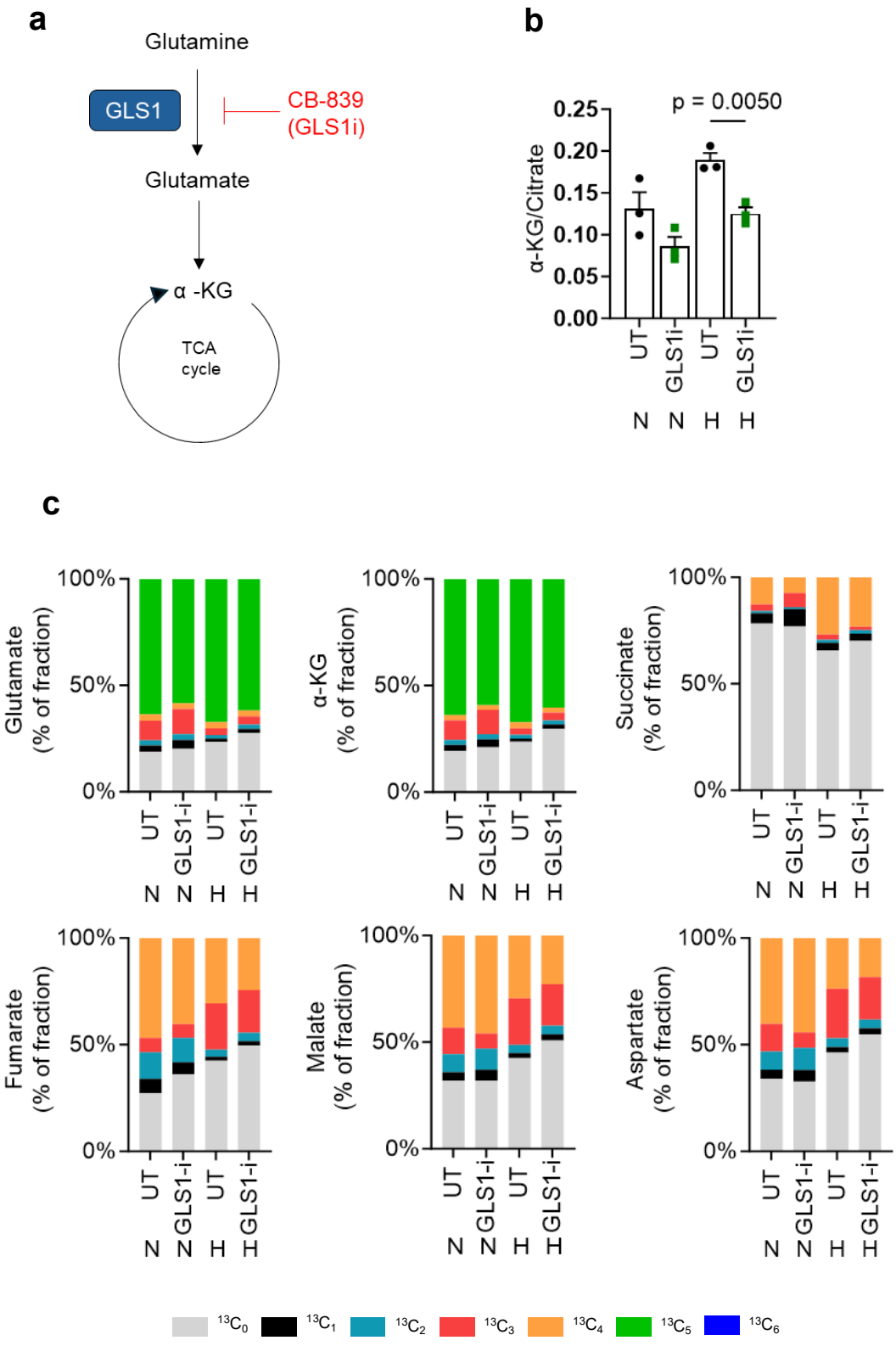
a
Glutamine
GLS1
CB-839
(GLS1i)
Glutamate
α -KG
TCA
cycle
b
p = 0.0050
α-KG/Citrate
0.25
0.20
0.15
0.10
0.05
0.00
UT
GLS1i
UT
GLS1i
N N H H
c
Glutamate (% of fraction)
α-KG (% of fraction)
Succinate (% of fraction)
Fumarate (% of fraction)
Malate (% of fraction)
Aspartate (% of fraction)
100%
50%
0%
UT
GLS1-i
UT
GLS1-i
N N H H
13C0 13C1 13C2 13C3 13C4 13C5 13C6

Figure 15: CB-839 reduces glutamine reductive carboxylation in hypoxia. a) Schematic of mechanism of action of CB-839 (=GLS1i). b) Ratio of α-KG over Citrate of K562 cells cultured under 21% O_2 (N) or 0.5% O_2 (H) treated or left untreated with 500 nM of GLS1i for 48 hours. (n=3 independent cultures). c) Fractional labelling from ^{13}C glutamine into indicated metabolites of K562 cells exposed to 21% O_2 (N) or 0.5% O_2 (H) for 24 hours (n= 3 independent cultures). Means ± SEM P values were calculated using paired Student's t test.

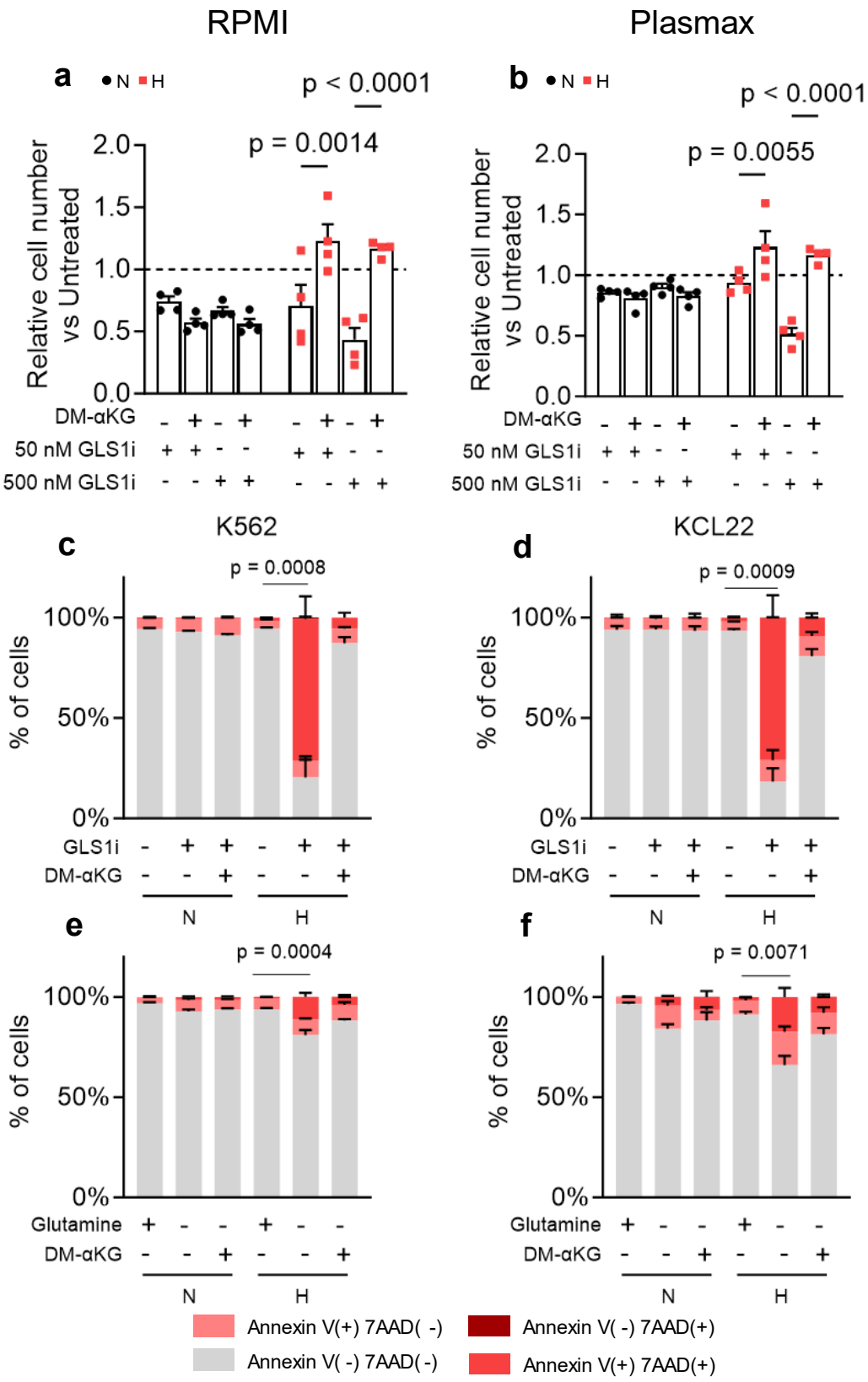
RPMI
Plasmax
a
b
N
H
p < 0.0001
p = 0.0014
p = 0.0055
Relative cell number vs Untreated
2.0
1.5
1.0
0.5
0.0
DM-αKG
50 nM GLS1i
500 nM GLS1i
K562
KCL22
c
d
e
f
p = 0.0008
p = 0.0009
p = 0.0004
p = 0.0071
% of cells
100%
50%
0%
GLS1i
DM-αKG
Glutamine
N
H
Annexin V(+) 7AAD(-)
Annexin V(-) 7AAD(-)
Annexin V(-) 7AAD(+)
Annexin V(+) 7AAD(+)

Figure 16: Inhibition of Glutaminase-1 induces cell death in CML cell lines under low oxygen levels. a) Cell numbers of K562 cells cultured in RPMI under 21% O_2 (N) or 0.5% O_2 (H) and treated or left untread with the indicated GLS1i (CB-839) concentrations for 3 days. Where indicated, inhibition of Glutaminase 1 was rescued with 3.5 mM of dimethyl alpha-ketoglutarate (DM-αKG) (n=4 independent cultures). b) Same as in a) but cells were cultured in Plasmax ((n=4 independent cultures). c) Levels of Annexin V and 7AAD positive K562 and d) KCL22 cells cultured under 21% O_2 (N) or 0.5% O_2 (H) and treated or left untread with 500 nM GLS1i (CB-839) for 3 days. Where indicated, inhibition of Glutaminase 1 was rescued with 3.5 mM of dimethyl alpha-ketoglutarate (DM-αKG) (n=4 independent cultures). e) Levels of Annexin V and 7AAD positive K562 and d) KCL22 cells cultured under 21% O_2 (N) or 0.5% O_2 (H) and depleted or not of Glutamine for 3 days. Where indicated, 3.5 mM of dimethyl alpha-ketoglutarate (DM-αKG) were added to rescue cell death (n=4 independent cultures). P values in a) and b) were calculated using 2-way ANONA using Šídák's multiple comparisons. P values in c-f) were calculated using unpaired t-test and refer to Annexin V (+) 7AAD (+) population.

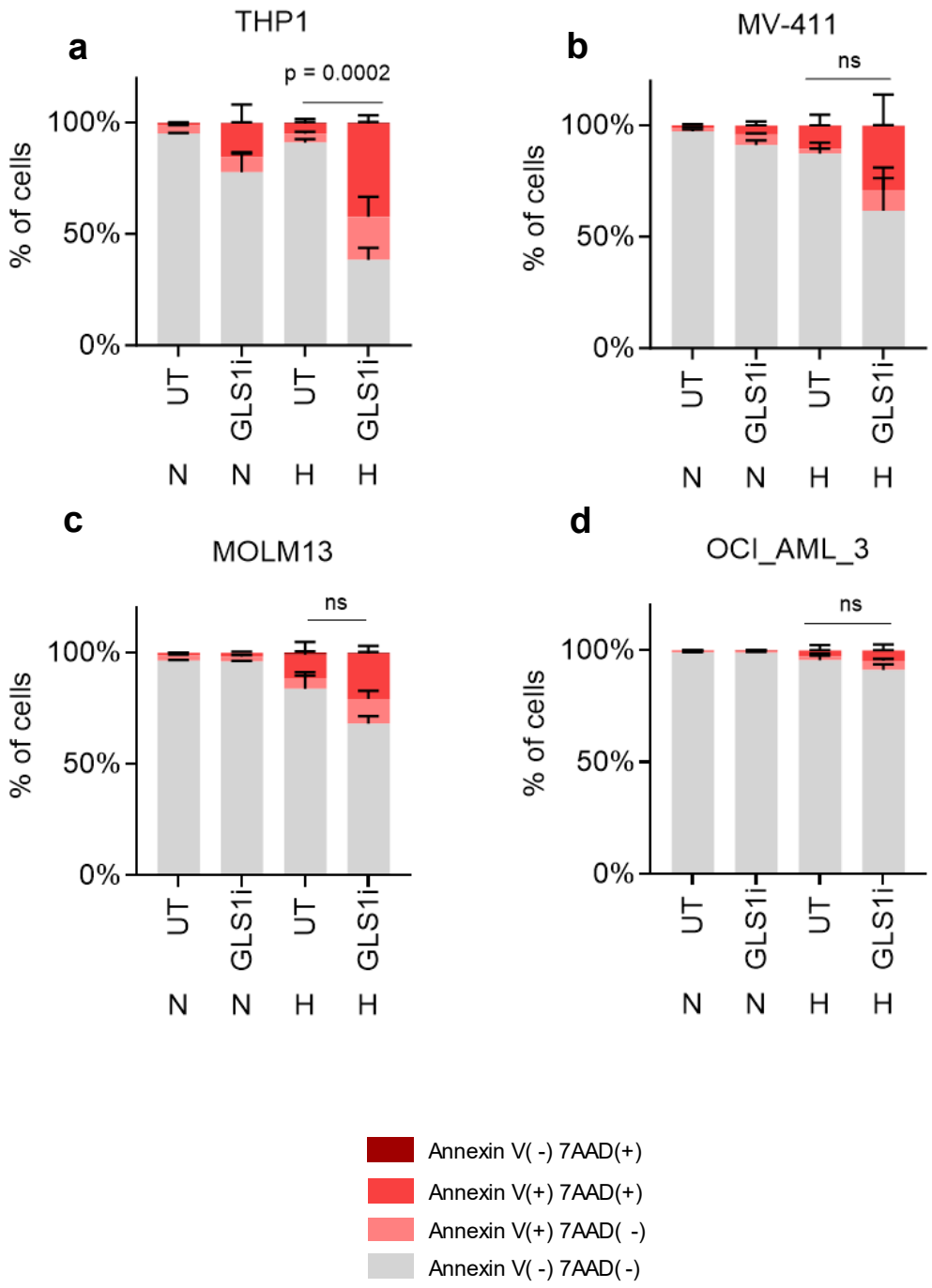
a
THP1
p = 0.0002
% of cells
100%
50%
0%
UT
GLS1i
UT
GLS1i
N
N
H
H
b
MV-411
ns
c
MOLM13
ns
d
OCI_AML_3
ns
Annexin V(-) 7AAD(+)
Annexin V(+) 7AAD(+)
Annexin V(+) 7AAD(-)
Annexin V(-) 7AAD(-)

Figure 17: Effect of CB-839 in AML cells exposed to hypoxia. Levels of Annexin V and 7AAD positive a) THP1, b) MV-411, c) MOLM13, d) OCI-AML3 cells cultured under 21% O_2 (N) or 0.5% O_2 (H) and treated or not with 500 nM GLS1i (CB-839) for 3 days. Where indicated, 3.5 mM of dimethyl alpha-ketoglutarate (DM-αKG) were added to rescue cell death (n=4 independent cultures). P values in a-d) were calculated using unpaired t-test and refer to Annexin V (+) 7AAD (+) population.

3.2.4 Establishing a protocol to study glutamine metabolism *in vivo*.

Encouraged by our promising results *in vitro,* we decided to further investigate glutamine metabolism *in vivo*, as this would represent a more suitable model to study CML cells metabolic adaption in hypoxic microenvironment. Ideally, we would like to use an established inducible CML mouse model[278]. Once leukaemia is induced, we would like to inject ^{13}C fully labelled glutamine into both CML and non-CML mice, harvest blood, bone marrow and spleen. Bone marrow and spleen would be further processed in order to isolate c-kit^{+} cells which would be then lysed for metabolites extraction.

However, before proceeding with this experiment, we sought to optimise the procedure. For this reason, we used non leukaemic NRGW[41] mice. According to Spinelli et al., mice sacrificed after only 20 minutes post-injection would be enough to observe a significative level of glutamine-derived isotopologues in different tissues[279]. Therefore, we tried this method in our experiment. Mice were intraperitoneally (IP) injected with a solution of saline containing $^{13}C_5$-glutamine (50 mg/ml). After 20 minutes, an aliquot of blood (20 µL) was taken from each mouse and directly extracted in lysis buffer and left on ice. Mice were then sacrificed, and spleen and bones were collected and subsequently processed to isolate c-kit^{+} cells. Collected cells were then lysed (schematic illustrated in figure 18a). As shown in figure 18b, LC-MS revealed detection of $^{13}C_5$ glutamine in the analysed tissues and cells. However, levels of glutamine-derived isotopologues (figure 18c-d) in glutamate and α-KG were not accumulated and were not in line with our *in vitro* data. These results suggest that further optimisation would be required to improve our *in vivo* tracing experiments.

One solution could be to use continuous infusion of the tracer after injection of the first bolus. Indeed, this has been proven to improve the labelling of glucose and acetate tracers in glioblastoma setting[280] and fully labelled serine in T-cells acute lymphoblastic leukaemia[281].

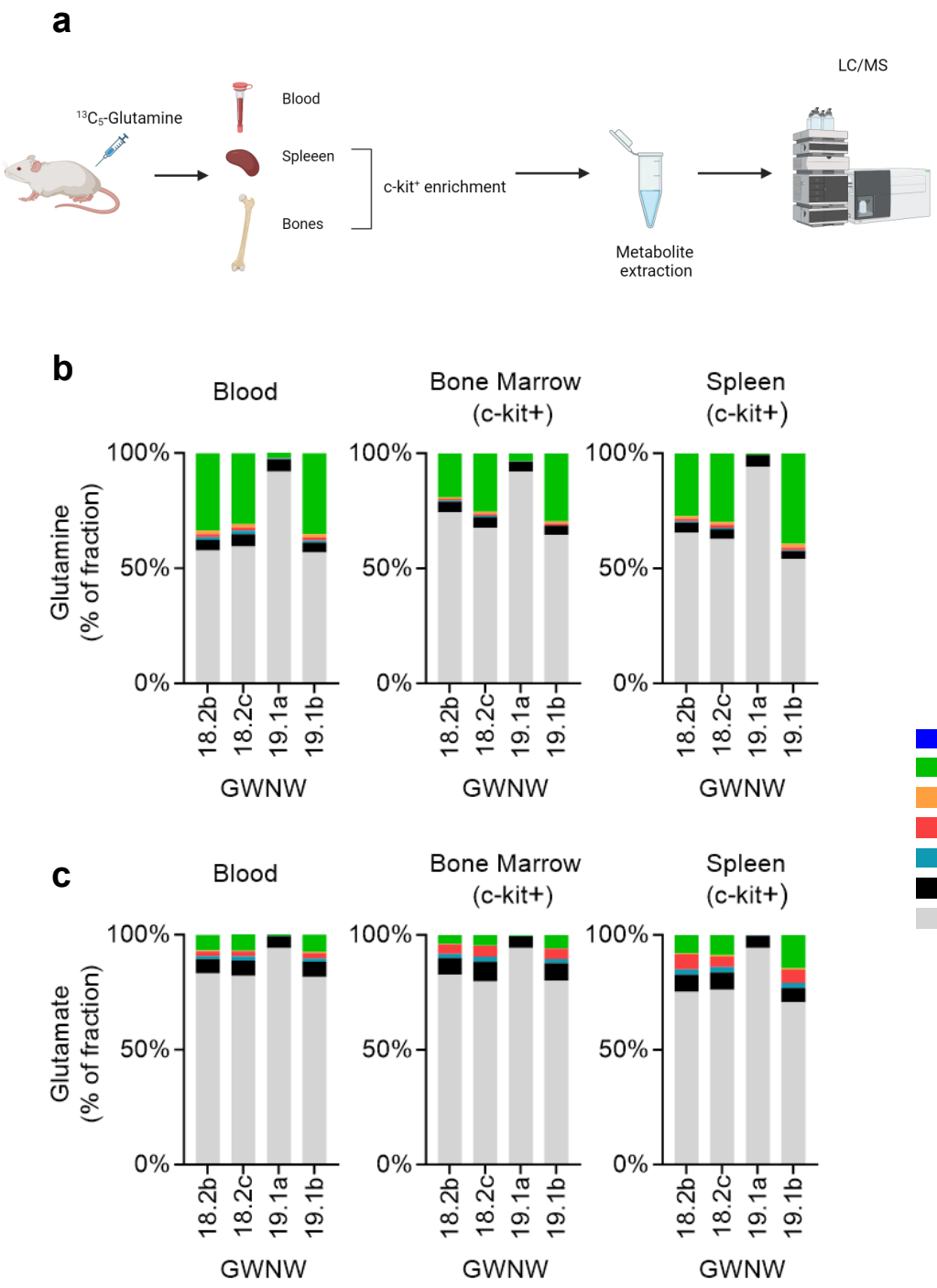
a
LC/MS
$^{13}C_5$-Glutamine
Blood
Spleeen
Bones
c-kit⁺ enrichment
Metabolite extraction
b
Blood
Bone Marrow (c-kit+)
Spleen (c-kit+)
Glutamine (% of fraction)
100%
50%
0%
18.2b
18.2c
19.1a
19.1b
GWNW
$^{13}C_6$
$^{13}C_5$
$^{13}C_4$
$^{13}C_3$
$^{13}C_2$
$^{13}C_1$
$^{13}C_0$
c
Blood
Bone Marrow (c-kit+)
Spleen (c-kit+)
Glutamate (% of fraction)

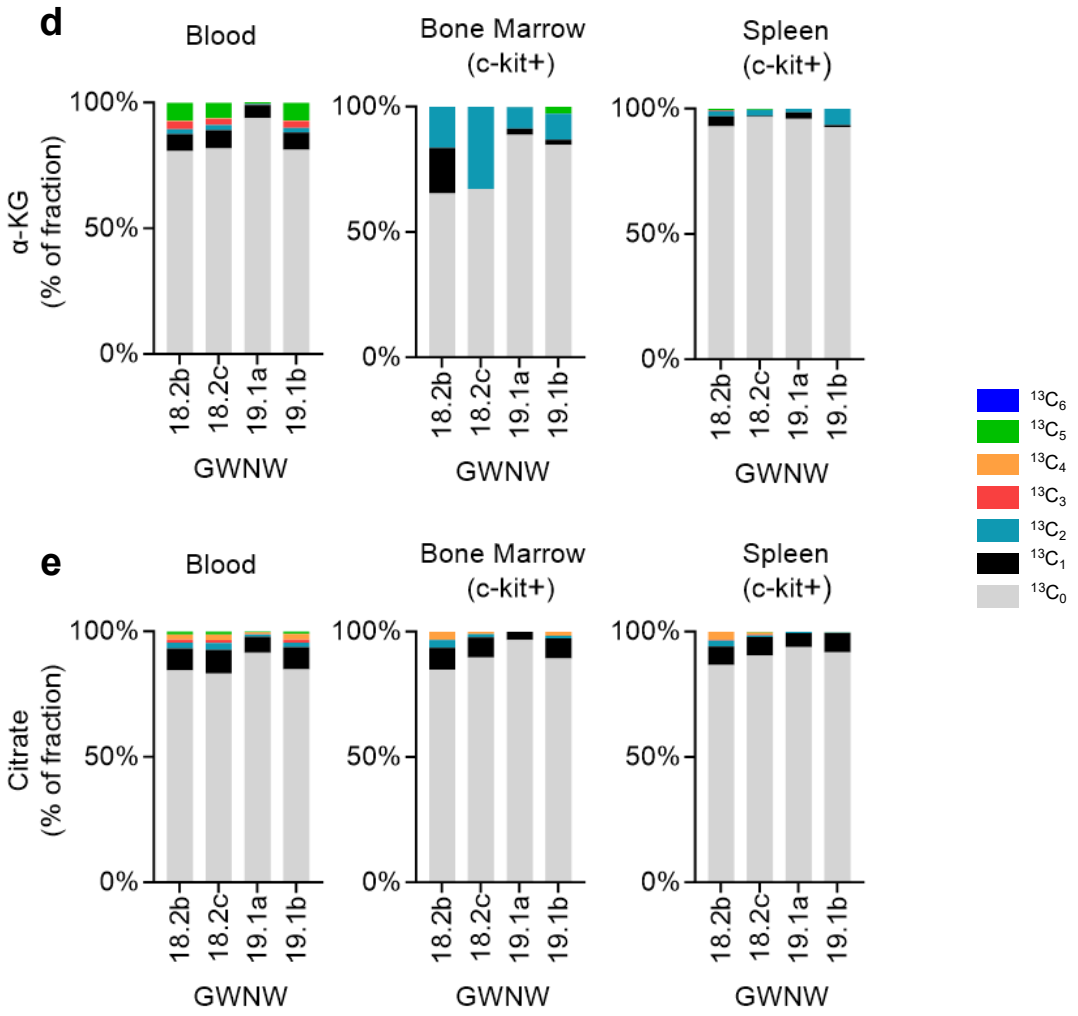
d
Blood
Bone Marrow (c-kit+)
Spleen (c-kit+)
α-KG (% of fraction)
100%
50%
0%
18.2b
18.2c
19.1a
19.1b
GWNW
e
Citrate (% of fraction)
$^{13}C_6$
$^{13}C_5$
$^{13}C_4$
$^{13}C_3$
$^{13}C_2$
$^{13}C_1$
$^{13}C_0$

Figure 18: Establishing a method to study glutamine tracing in vivo. a) schematic of ^{13}C glutamine *in vivo* tracing workflow. b-e) Fractional labelling from ^{13}C glutamine into indicated metabolites from mouse blood, spleen and bone marrow (n=4 mice). X axis are codes for mice.

3.3 Discussion

In this chapter we sought to investigate the metabolic changes happening in CML cells during the hypoxia response. Initially, we performed analysis of a publicly available dataset of CML cells exposed to hypoxia over 1,3 and 6 days to understand how they respond to both short and long-term hypoxia.

In hypoxia, CML cells upregulate the expression of genes belonging to glycolysis, PDK activation and lactate production and secretion, while genes involved in the TCA cycle are downregulated. These results are in line with the literature, showing that hypoxia promotes anaerobic respiration and slower cell proliferation[56]. Moreover, we also showed that hypoxia significantly reduces mitochondrial respiration and proliferation of CML cells.

LC-MS analysis of hypoxic CML cells showed accumulation of α-KG, succinate and fumarate. While increased α-KG levels are indicative of a change towards glutamine as a preferential carbon source, the accumulated levels of succinate and fumarate could be explained as a metabolic switch to sustain HIF1α activity and signalling since both can act as competitive inhibitors for 2OGDD activity[282]. On the other hand, lower citrate levels are indicative of reduced mitochondrial glucose oxidation and altered central carbon metabolism[283]. These findings suggest that CML cells can promptly switch their activity according to their oxygen availability. More precisely, CML cells lose their OXPHOS activity when exposed to low oxygen environment and develop new metabolic strategies to survive and slow their growth down.

Fully labelled ^{13}C glucose tracing confirmed that hypoxic CML cells increase glycolytic flux, secrete lactate in the extracellular environment and significantly reduce its mitochondrial oxidation. Of note, similar fundings were observed in $CD34^{+}$ CML patient-derived cells, supporting the idea that the hypoxia-driven metabolic rewiring happens also in more clinically relevant cancer models.

Interestingly, CML cells significantly enhance glutamine uptake and glutaminolysis (but not glutamate secretion), suggesting that glutamine represents a preferential carbon source to fuel mitochondrial metabolism in CML cells under low oxygen conditions. Indeed, using stable isotope (^{13}C) labelled glutamine tracing, we show that hypoxic CML cells revert the direction of the TCA cycle, exploiting glutamine reductive carboxylation and promote the accumulation of fumarate levels. However, further investigation is required to assess the role of fumarate in our model and to further explore the final fate of glutamine in our model, as reductive carboxylation has been previously observed to be required for lipid synthesis[284].

Moreover, in cancer cells hypoxia-induced reductive carboxylation was shown to promote production of L-2 Hydroxyglutarate via LDHA to induce histone methylation due to inhibition of histone demethylases belonging to the 2-OGDD family[285]. This represents an additional example of metabolic rewiring in low oxygen environment and might be worth more investigation in our model as well.

Furthermore, we also assessed the sensitivity of CML cell lines to IDH2 and GLS1 inhibitors. While IDH2 pharmacological inhibition did not affect cellular growth, pharmacological treatment of hypoxic CML cells with a clinically relevant glutaminase inhibitor (CB-839 or telaglenastat) significantly and selectively reduced the growth and induced apoptosis in hypoxia-exposed CML cells, highlighting that reductive glutamine carboxylation is important for leukaemic cell proliferation and metabolic activity in low oxygen environments, both in conventional RPMI cell culture medium and physiologic-like Plasmax medium. The pro-apoptotic effect of GLS1 inhibition was also observed in several AML cell lines. Therefore, hypoxia-induced glutaminolysis may represent a metabolic adaptation in several blood cancers originating in the bone marrow. To further validate these fundings, genetic ablation of GLS and other genes involved in glutamine metabolism should be performed as have been already proposed in AML and other cancers studies with promising results [142,286–290].

Finally, we aimed to establish a suitable protocol for *in vivo* fully labelled glutamine tracing. However, our preliminary results showed that further optimisation needs to be carried out to robustly monitor glutamine metabolism in our mouse model.

Chapter 4 Hypoxia induces receptor-mediated mitophagy in CML cells

4.1 Introduction

In the previous chapter we showed that CML cells adapt to hypoxia by rewiring their metabolic activity and promote reductive glutamine metabolism. Moreover, their reliance on this metabolic adaptation was confirmed via pharmacological inhibition of glutaminolysis using a GLS1 inhibitor. However, the precise mechanism applied by CML cells to re-adapt their mitochondrial network to promote this metabolic switch under low oxygen conditions is not known.

To investigate hypoxia-driven changes in mitochondrial gene expression, we initially used a transcriptomic approach looking at all mitochondrial genes in primitive CML primary samples ($CD34^{+}CD38^{-}CD90^{+}CD93^{+}$) exposed to hypoxia for 48 hours. We observed that CML LSCs upregulate BNIP3 expression when compared to non-CML cells even at basal culture conditions.

To support our *in-silico* findings, we used an *in vitro* approach to inhibit BNIP3-mediated mitophagy exploiting CRISPR-Cas9 technology. We assessed cell growth, mitochondrial biology via flow cytometry to monitor mitochondrial mass and ROS content, and mitochondrial turnover using Mito-Timer engineered cells. Next, we investigated metabolic changes of CML cell lines upon loss of BNIP3 and other autophagy/mitophagy-related proteins (i.e. ATG7, NIX) in both normoxia and hypoxia using LC-MS. Moreover, we investigated the effect of BNIP3 loss in an *in vivo* setting, by assessing xenograft formation.

Lastly, we investigated the role of BNIP3 in erythroid differentiation of K562 under hypoxic conditions.

4.2 Hypoxia reshapes the (Mito)transcriptome in CML primary cells

Primary samples were sorted into $CD34^+CD38^-CD90^+CD93^+$ populations and cultured under normoxia or hypoxia for 48 hours. It has been previously shown that $CD93^+$ CML cells are characterised by increased stem cell and engraftment properties, representing a primitive and quiescent CML LSCs population[291]. Upon culture, cells were then extracted for sc-RNA seq using SMART seq-2 technology. This experiment was originally carried out by Dr Amy Dawson, a previous PhD student in our lab[292].

We then performed analysis of this unpublished sc-RNA seq data in order to identify differentially expressed genes upon exposure to hypoxia and focussed our interest on mitochondria genes, looking at the MitoCarta 3.0 gene collection. As represented in figure 19a, hypoxia promoted downregulation of the majority of mitochondrial genes. However, two genes were highly upregulated: BNIP3 and BNIP3L (NIX). These two genes encode for mitochondrial cargo receptors localised at the outer mitochondrial membrane, promoting a process known as receptor-mediated mitophagy, which is involved in the clearance of dysfunctional mitochondria, as previously described. Moreover, the expression of these two genes is highly dependent on HIFs activity and, hence, their expression levels are promptly responsive to low oxygen conditions[293,294]. Therefore, these preliminary data suggested that CML LSCs upregulate receptor-mediated mitophagy in order to metabolically adapt to low oxygen environments.

Next, we performed analysis of another publicly available microarray dataset (E-MTAB-2581) consisting of $CD34^+CD38^-$ LSCs and HSCs. Interestingly, this analysis revealed that LSCs expressed higher levels of BNIP3 compared to non-CML cells (figure 19b), while levels of NIX were unchanged (figure 19c). Given that LSCs overexpressed BNIP3 even at basal culture conditions, we next focussed mostly on the role of this mitochondrial receptor.

Moreover, we analysed a different publicly available microarray dataset (GSE48294) of bulk $CD34^+$ CML cells exposed to normoxia or hypoxia and treated or not with Imatinib for 24 or 96 hours. This analysis revealed that BNIP3 and NIX gene expression are differently regulated by Imatinib. Indeed, while BNIP3 gene expression was downregulated in hypoxia by the TKI at both 24 and 96 hours (figure 20a-b), Imatinib alone was sufficient to drive upregulation of NIX at both time points and its increased mRNA levels were kept constant under low oxygen levels (figure 20c-d). While it is

known that Imatinib can drive autophagy [295,296], which is used as a defence mechanism by LSCs, less is known about the role of Imatinib or other TKIs to drive mitophagy.

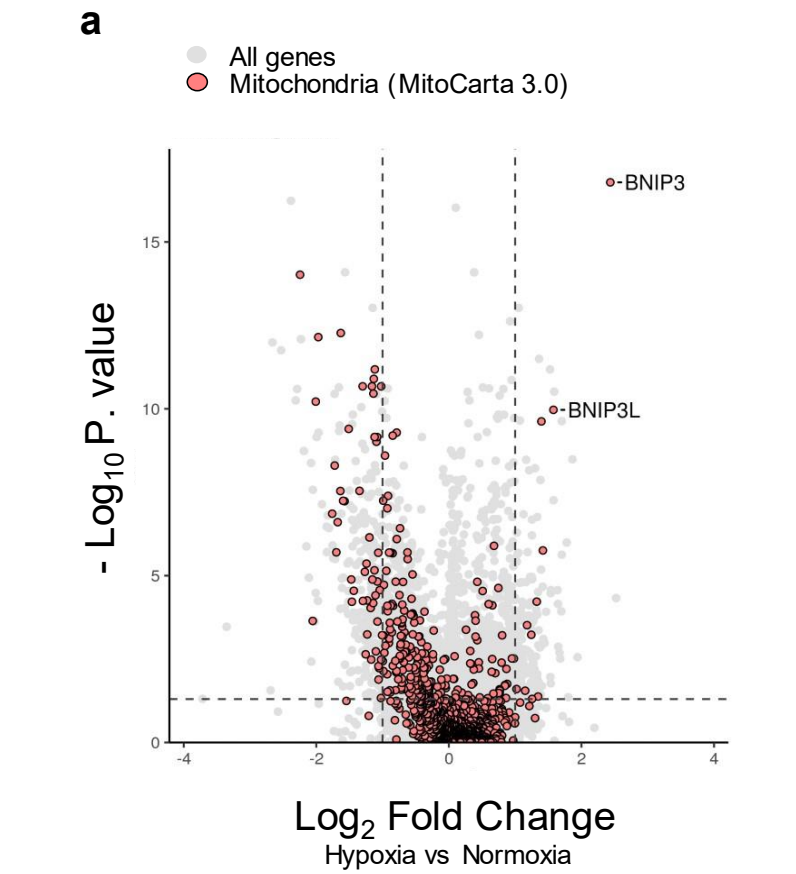
a
All genes
Mitochondria (MitoCarta 3.0)
BNIP3
BNIP3L
- Log10 P. value
Log2 Fold Change
Hypoxia vs Normoxia
b
E-MTAB-2581
p = 0.0018
Log2(BNIP3 expression)
HSC
LSC
c
E-MTAB-2581
ns
Log2(BNIP3L expression)
HSC
LSC

Figure 19: Hypoxic CML cells upregulate BNIP3 and NIX. a) Volcano plot of differentially expressed mitochondrial genes of $CD34^{+}38^{-}90^{+}93^{+}$ CML LSCs exposed to 21% O_2 or 0.5% O_2 for 48 hours in in-house single cell transcriptomic dataset. b,c) plots showing expression of (b) BNIP3 and (c) NIX in non-CML Haematopoietic Stem Cells (HSC) and Leukaemic Stem Cells (LSC) ($CD34^{+}38^{-}$) in indicated dataset (n=6). Means and P-values were calculated using unpaired t-test (two-sided).

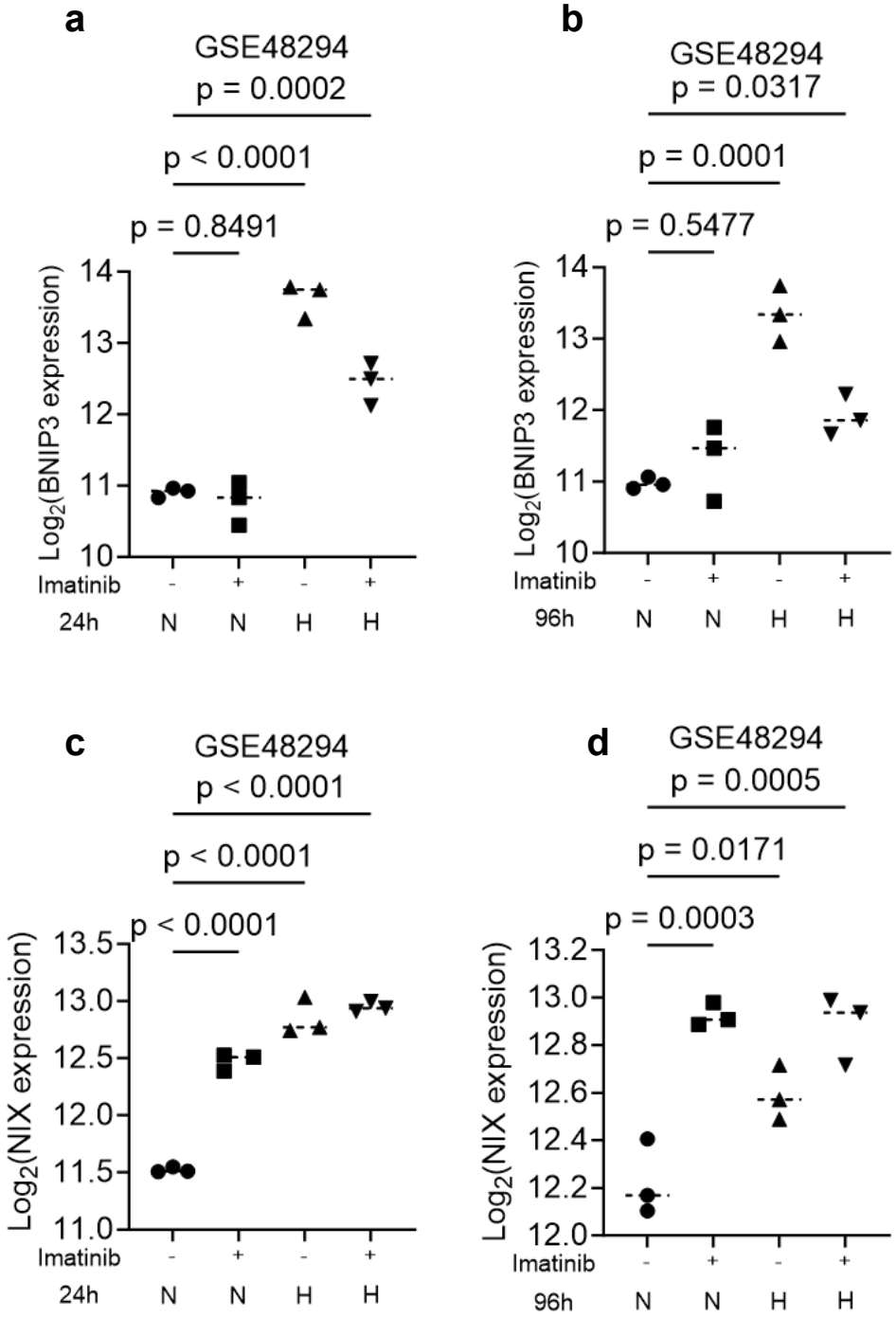

Figure 20: BNIP3 and NIX expression levels are differently regulated by Imatinib in patient derived CML cells exposed to hypoxia. a,b,c,d) plots showing expression of (a,b) BNIP3 and (c,d) NIX in bulk $CD34^+$ leukaemic cells treated or not with 5μM of Imatinib under 21% O_2 (N) or 0.5% O_2 (H) for 24 hours (a,c) and 96 hours (b,d) in indicated dataset (n=3). means and P-values were calculated using unpaired t-test (two-sided).

4.3 Hypoxia triggers BNIP3/NIX-mediated mitophagy in CML

BNIP3 and NIX are two mitochondrial receptors localized at the outer mitochondrial membrane. To induce clearance of mitochondria via mitophagy they can directly interact with LC3-II localized at phagophore membranes and recruit autophagosome on the target mitochondria[297–299] (see figure 21a for a schematic of their mechanism).

In order to validate BNIP3 and NIX expression and their mitochondrial translocation in our model, we isolated mitochondrial-enriched fractions from K562 cells following exposure to hypoxia for 24 hours. As expected, hypoxia led to further accumulation of both BNIP3 and NIX in the mitochondrial enriched fraction. Interestingly, we also observed accumulation of both BNIP3 and NIX homodimers in the isolated mitochondrial fractions (figure 21b). It has been shown that NIX forms dimers on the outer mitochondrial membrane to increase avidity and hence bind with higher affinity to LC3-II on the forming autophagosome during the mitophagy process. Therefore, dimers can be used as a redout of ongoing mitophagy flux[300].

To assess mitophagy, we initially measured mitochondrial mass via flow cytometry. After 72 hours of hypoxia exposure mitochondrial mass was significantly reduced in both K562 and KCL22, as an indication of induced mitochondrial degradation (figure 21c and d). However, hypoxia did not affect mitochondrial membrane potential ($\Delta\Psi_m$) as showed in figure 21e and f. Indeed, differently from PINK1-PRKN pathway, receptor-mediated mitophagy is not triggered by a drop in mitochondrial membrane potential[299].

To further monitor mitophagy flux we used mitochondrial target Keima (mt-Keima) expressing cells. Mt-Keima is a pH sensitive mitochondrial protein, which can be detected in the mitochondrial matrix due to its fusion with the mitochondrial targeting sequence of cytochrome c oxidase subunit VIII. Increased mitophagy flux can be detected via measurement of the shift in excitation peak of Keima from 440 nm (pH=7) to 586 nm (pH=4), when the mitochondria are inside the lysosome[301]. To test the model, both K562 and KCL22 overexpressing mt-Keima were treated with carbonyl cyanide m-chlorophenylhydrazone (CCCP), which is known to trigger depolarization of mitochondrial membrane and, hence, promote mitophagy via the PINK1-PRKN mechanism. As a negative control, cells were co-treated with bafilomycin A1 (BafA1) to abolish mitophagy flux. As shown in figure 22a-c, treatment with CCCP promoted a switch in fluorescence compared to untreated cells. Pre-treatment with BafA1, instead, reduced the switch in fluorescence as autophagy was inhibited.

K562 mt-Keima overexpressing cells were then exposed to low oxygen levels to measure hypoxia-induced mitophagy. As shown in figure 23a-b, hypoxia significantly induced mitophagy flux. Moreover, we further validated hypoxia-induced mitophagy via western blot analysis. As shown in figure 23c, hypoxia promoted degradation of p62/SQSTM1 (a selective autophagy receptor whose protein levels can be used as a readout of autophagic flux as it gets degraded when autophagy is induced[302]) over time, accumulation of LC3-II, and degradation of TOM20. As a negative control, cells were co-treated with hydroxychloroquine (HCQ) to inhibit the fusion of autophagosomes with lysosomes and, hence, autophagy. Although not significantly, TOM20 levels were partially increased upon treatment with HCQ (figure 23d). However, TOM20 levels were reduced of almost 60% in K562 cells exposed to hypoxia when compared to normoxic cells. Moreover, LC3-II protein levels were accumulated, although not significantly, at both 24 and 48 hours upon treatment with HCQ compared with untreated cells (figure 23e). This further proves the induction of autophagy (and mitophagy) upon exposure to hypoxia in our model.

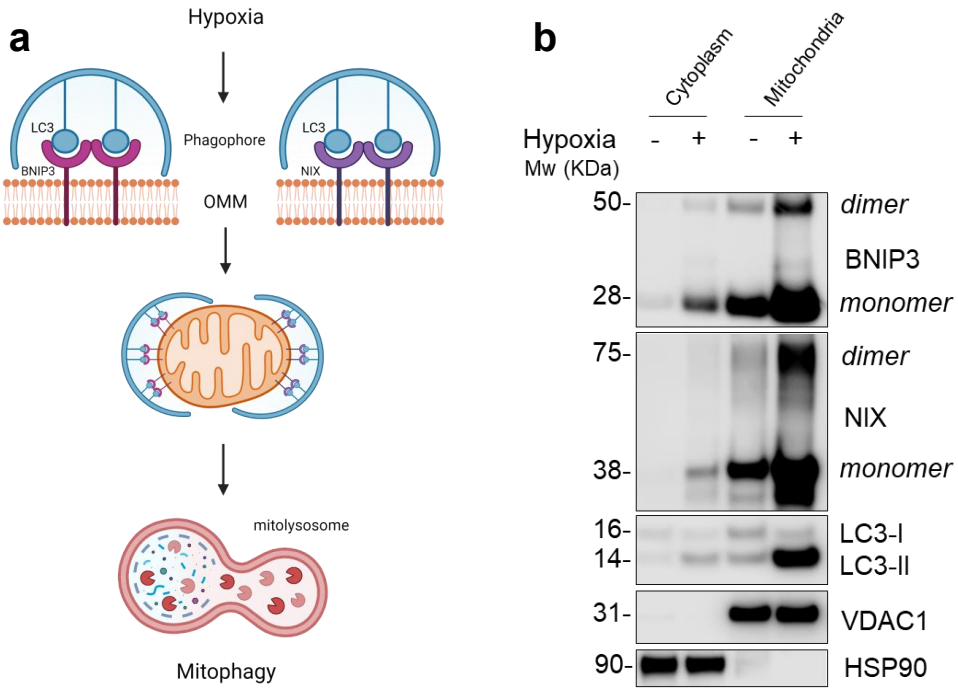

OMM = Outer Mitochondrial Membrane

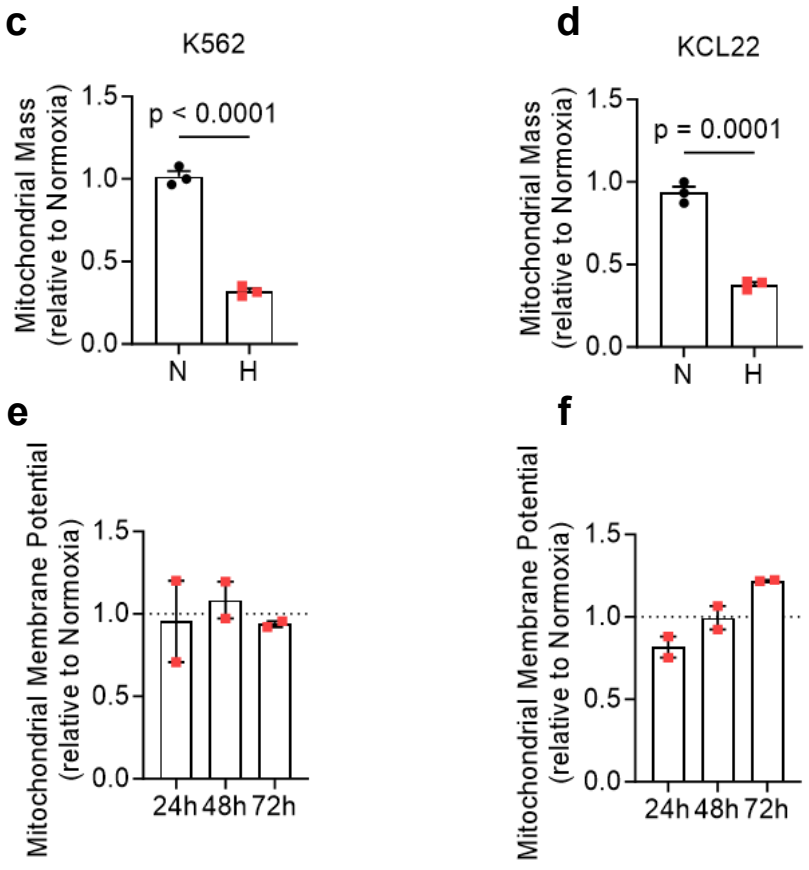

Figure 21: Upregulation of BNIP3 and NIX promote receptor-mediated mitophagy in CML under hypoxia. a) Schematic of BNIP3 and NIX receptor-mediated mitophagy mechanism. b) Western blot of isolated mitochondria from K562 cells exposed to 21% O_2 or 0.5% O_2 (Hypoxia) for 24 hours. c) MFI of Mito-tracker green in K562 cells cultured under 21% O_2 (N) or 0.5% O_2 (H) for 3 days (relative to N). d) same as in c) but in KCL22 (n=3 independent cultures). e) MFI of TMRM in K562 cells cultured under 21%O_2 (N) or 0.5% O_2 (H) for 24, 48 and 72 hours (relative to N). f) same as in e but in KCL22 (n=2 independent cultures). Data were represented as means ± SD. P-values in c) and d) were calculated using paired Student's t test.

Mt-Keima

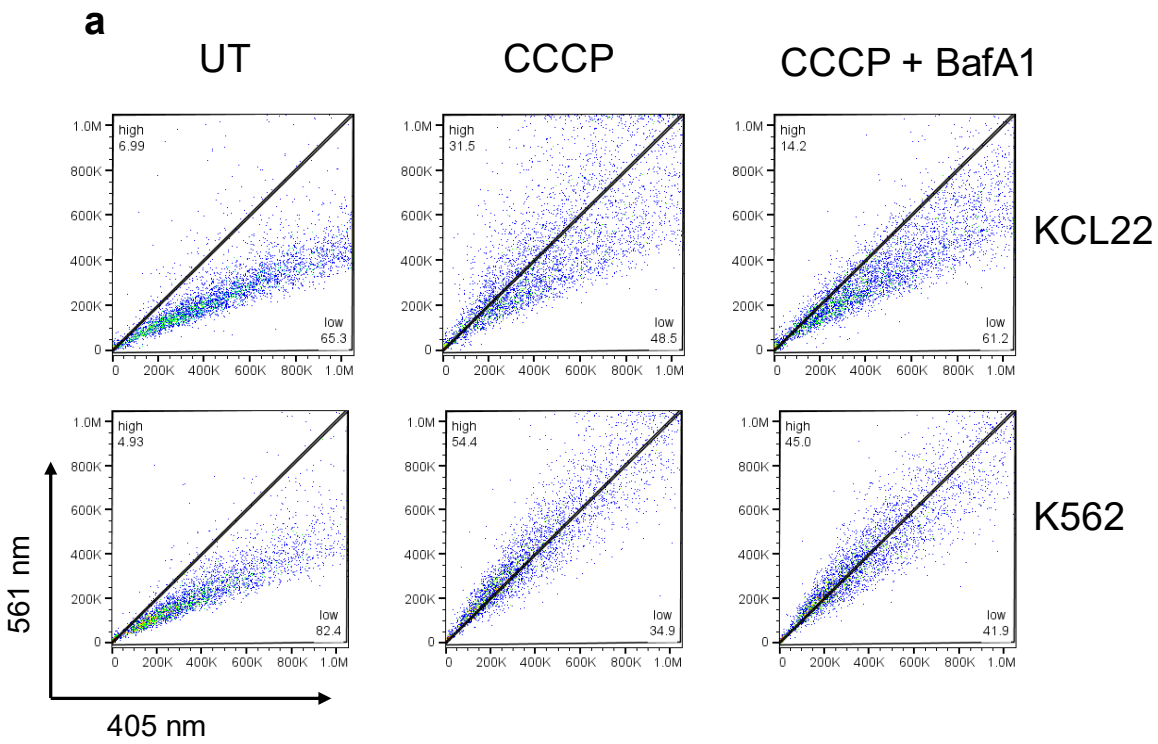
a
UT
CCCP
CCCP + BafA1
KCL22
K562
high 6.99
low 65.3
high 31.5
low 48.5
high 14.2
low 61.2
high 4.93
low 82.4
high 54.4
low 34.9
high 45.0
low 41.9
561 nm
405 nm

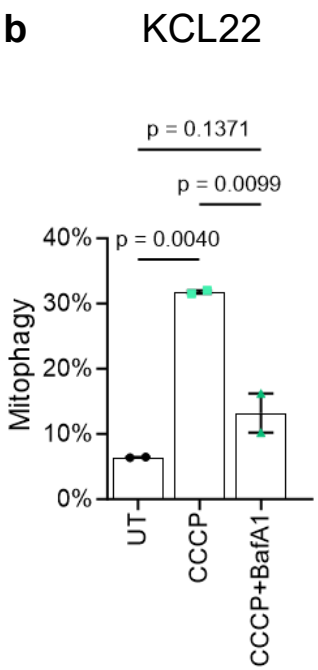
b
KCL22
p = 0.1371
p = 0.0099
p = 0.0040
Mitophagy
40%
30%
20%
10%
0%
UT
CCCP
CCCP+BafA1

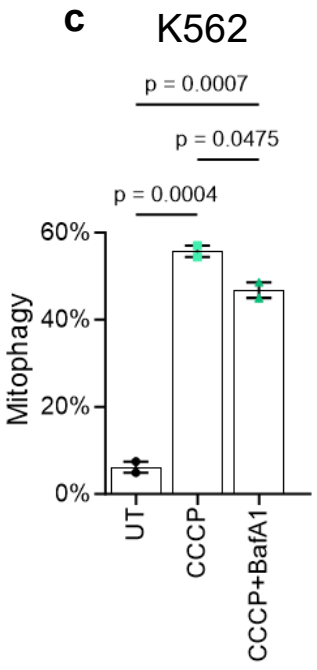
c
K562
p = 0.0007
p = 0.0475
p = 0.0004
Mitophagy
60%
40%
20%
0%
UT
CCCP
CCCP+BafA1

Figure 22: Optimization of mt-Keima to measure mitophagy flux in CML cells. a) Representative flow cytometry plots of K562 and KCL22 cells overexpressing mt-Keima and treated or not with 10μM CCCP for 6 hours to induce mitophagy. As a negative control 100 nM of Bafilomycin A1 were used to block mitophagy flux. b, c) bar plots of experiments shown in a) showing percentage of mitophagy flux in b) K562 and c) KCL22 (n=2 independent cultures). P values in b) and c) were calculated using Ordinary one-way ANOVA.

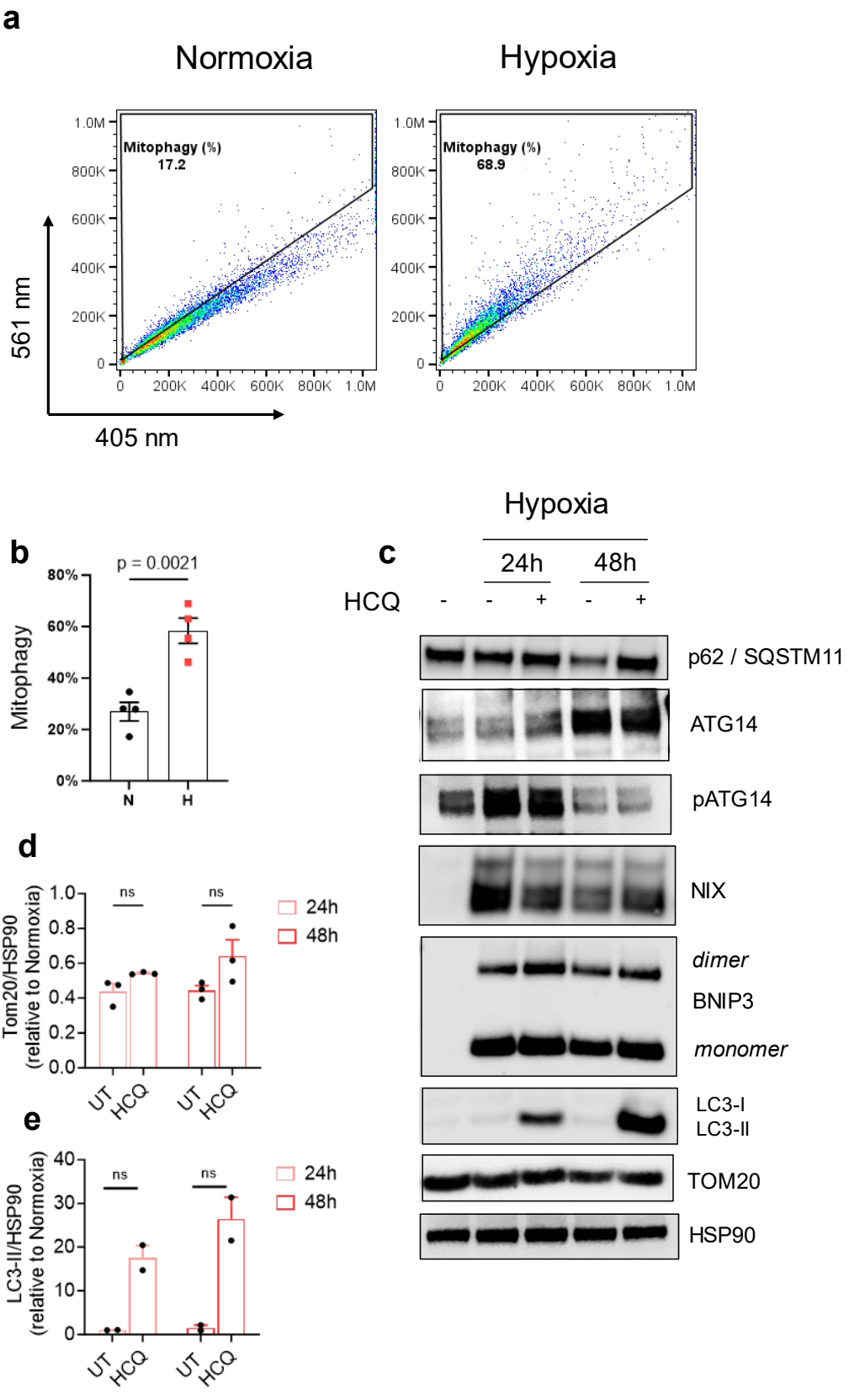
a
Normoxia
Hypoxia
Mitophagy (%)
17.2
Mitophagy (%)
68.9
561 nm
405 nm
b
p = 0.0021
Mitophagy
N
H
c
Hypoxia
24h
48h
HCQ
p62 / SQSTM11
ATG14
pATG14
NIX
dimer
BNIP3
monomer
LC3-I
LC3-II
TOM20
HSP90
d
Tom20/HSP90 (relative to Normoxia)
ns
24h
48h
UT
HCQ
e
LC3-II/HSP90 (relative to Normoxia)

Figure 23: Hypoxia promotes receptor-mediated mitophagy flux in CML cells. a) Representative flow cytometry plot of K562 cells overexpressing mt-Keima and exposed to 21% O_2 (Normoxia) 0.5% O_2 (Hypoxia) for 3 days. b) bar plots of mitophagy flux as in (a) (n=4 independent cultures). c) Western blot of K562 cells exposed to 0.5% O_2 (Hypoxia) for 24 or 48 hours and treated or not with 10μM of Hydroxychloroquine (HCQ). d) Protein levels quantification of TOM20 over HSP90 relative to Normoxia. e) protein levels quantification of LC3-II over HSP90 relative to normoxia. Data in (b), (d) and (e) were represented as mean ± SD. P-values in (b), (d) and (e) were calculated using paired Student's t test.

4.4 BNIP3-mediated mitophagy is dependent on ULK1 activity

Interestingly, we observed that hypoxia triggers ULK1-dependent phosphorylation of ATG14, as shown in figure 23c. It was previously shown that hypoxia promotes ULK1 activation and that ULK1 can protect BNIP3 from proteasomal degradation. However, the authors used only pharmacological inhibition of ULK1and did not provide evidence of the effect of ULK1 genetic ablation on BNIP3 activity[303].

To study the ULK1-BNIP3 interdependency we developed K562 expressing inducible SMARTvector (SV) lentiviral shRNA targeting ULK1 or non-targeting control (NTC) to promote inducible knock down (KD) of ULK1 upon treatment with doxycycline. Successful ULK1 KD was confirmed with immunoblotting as showed in figure 24a (realised by Dr Martha Zarou)

As shown in Figure 24b, ULK1 KD promoted slower growth of leukaemic cells in both normoxia and hypoxia.

To observe the effect of ULK1 KD on BNIP3 protein expression and dimerization, we performed immunoblot of induced ULK1 KD cells and NTC with 3 different DOX concentrations in a dose-dependent manner and exposed to hypoxia. Reduction in the p-ATG14 levels confirmed inhibition of ULK1 kinase activity. As reported in figure 24c BNIP3 protein levels dropped-both monomers and dimers-upon induction of ULK1 KD and decreased activity. Interestingly, TOM20 levels were reduced upon exposure to hypoxia in the non-induced cells, while could be rescued upon ULK1 KD. These results are in line with the literature and suggest that ULK1 activity controls BNIP3 protein stability in hypoxic CML cells.

However, more data should be generated to understand if and how ULK1 and BNIP3 interact.

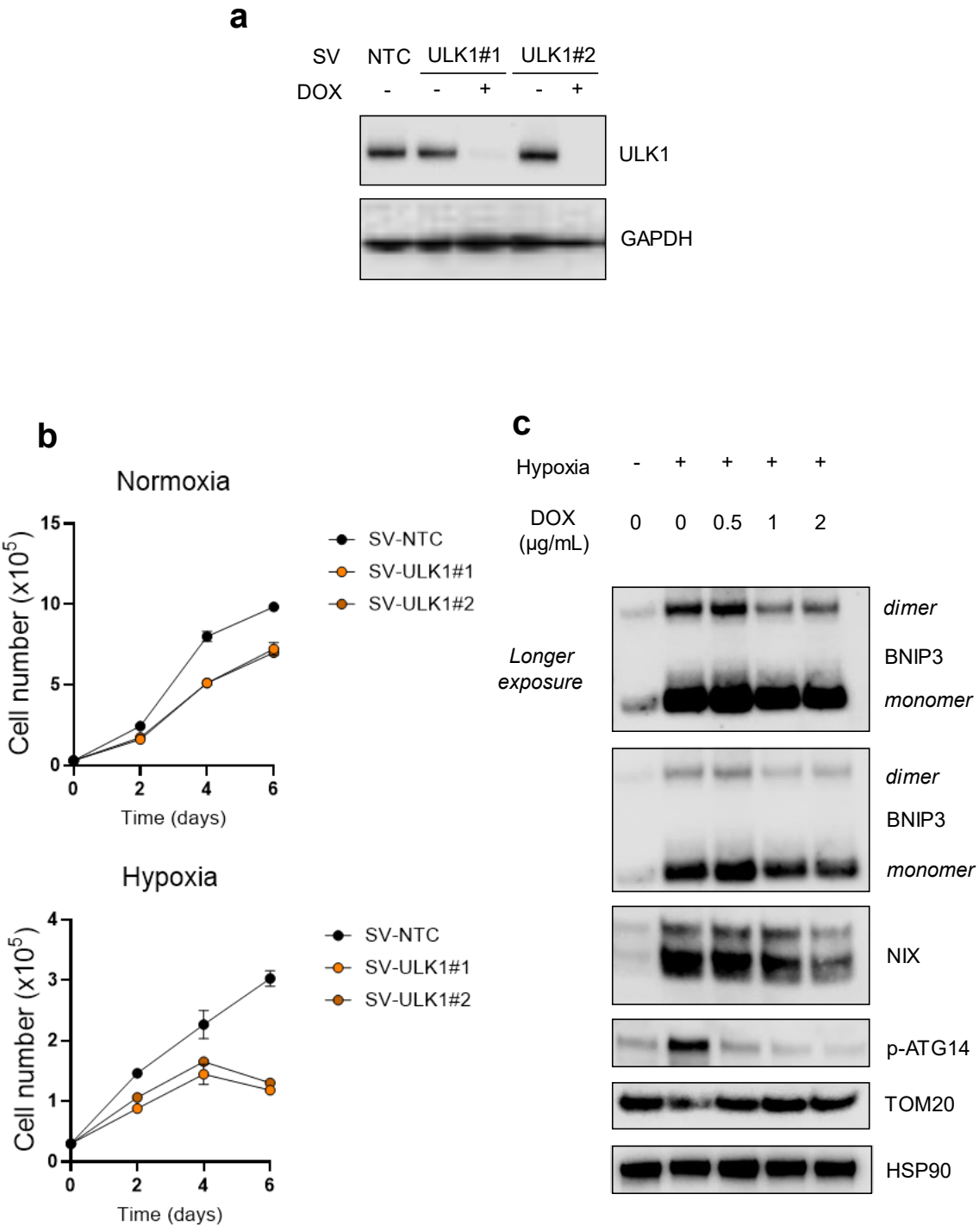
a
SV
NTC
ULK1#1
ULK1#2
DOX
-
-
+
-
+
ULK1
GAPDH
b
Normoxia
Cell number (x10^5)
Time (days)
SV-NTC
SV-ULK1#1
SV-ULK1#2
Hypoxia
Cell number (x10^5)
Time (days)
SV-NTC
SV-ULK1#1
SV-ULK1#2
c
Hypoxia
DOX (µg/mL)
0
0
0.5
1
2
Longer exposure
dimer
BNIP3
monomer
dimer
BNIP3
monomer
NIX
p-ATG14
TOM20
HSP90

Figure 24: BNIP3 protein levels and dimerization partially depend on hypoxia-induced ULK1 activity. a) Immunoblot of K562 expressing SMARTvector non-targeting control (NTC) or ULK1 targeting sequence#1 and 2 (ULK1#1/#2) treated or not with doxycycline. b) growth curves of K562 cells transfected with non-targeting control (NTC) and SMARTvector (SV) lentiviral shRNA targeting ULK1 cultured under 21%O_2 (Normoxia) or 0.5 %O_2 (Hypoxia). Cells were treated with 2µg/ml of Doxycycline (DOX) to induce ULK1 KD (n=4 independent cultures). c) Immunoblot of K562 expressing SMARTvector shRNA targeting ULK1 exposed to 0.5%O_2 (Hypoxia) and treated or not with three different DOX oncentrations. Representative image of n=2 independent cultures.

4.5 CML cells exploit autophagy to regulate mitochondrial turnover.

To investigate mitochondrial in CML cells, we used the Mito-Timer technology. Mito-Timer is characterized of a time-sensitive fluorescent protein (Timer), which has been fused with the mitochondria targeting sequence of COX VIII, hence Mito-Timer. Fine-tuned control of Mito-Timer protein expression is achieved via a doxycycline-inducible vector, here referred as DOX pulse. Once pulsed with DOX, fluorescence of the Mito-Timer protein can be monitored over time[260,261]. A schematic of the Mito-Timer workflow is depicted in figure 25 a.

After only 8 hours of DOX pulse, K562 overexpressing the Mito-Timer construct showed green florescence because of induced transcription and protein-translation. Over time the red fluorescence was predominant. The shift from green to red is given by several factors, such as heat, oxygen levels and pH. Green mitochondria are here indicated as non-mature mitochondria, while red mitochondria are indicated as mature mitochondria (figure 25b-d). The red/green ratio can be used as a redout of general mitochondrial turnover[304–306].

To assess if mitochondrial turnover in CML cells depends on autophagy, we treated DOX induced Mito-Timer-K562 cells with HCQ to block general autophagy flux and MRT-403 (here referred to as ULK1i), a selective ULK1 inhibitor. As shown in figure 25e and f, mature mitochondria were found accumulated over time in treated cells when compared to untreated ones, indicating that basal autophagy flux is indeed required to regulate mitochondrial turnover in CML cells.

Mito-Timer can be used to study mitochondrial biogenesis as well, as shown in the schematic of figure 26a. This can be done by monitoring Mito-Timer fluorescence after a second DOX pulse. After 48 hours of DOX removal from DOX pulse 1, we treated the cells with a second DOX pulse and monitored Mito-Timer fluorescence after 24 hours. Moreover, to assess if autophagy inhibition could affect mitochondrial biogenesis, cells were treated with ULK1i.

After flow cytometry analysis, we observed that the second DOX pulse is enough to detect new mitochondria, given the increased green fluorescence (figure 26b-d). Red fluorescence is indicative of old accumulated mitochondria.

Surprisingly, even though our results showed a non-significant increase in old mitochondria fluorescence, inhibition of ULK1 further promoted new mitochondria

biogenesis (figure 26e-f). This could be explained as a compensatory effect as there is a constant interplay between mitophagy and mitobiogenesis[307]. Furthermore, western blot analysis revealed that PGC1α expression (master regulator of mitochondrial biogenesis) was increased upon ULK1 inhibition in a time dependent manner (figure 26g).

Overall, our results showed that mitochondrial turnover in CML cells is regulated by basal autophagy flux. Moreover, pharmacological inhibition of ULK1 could promote mitochondrial biogenesis via PGC1α.

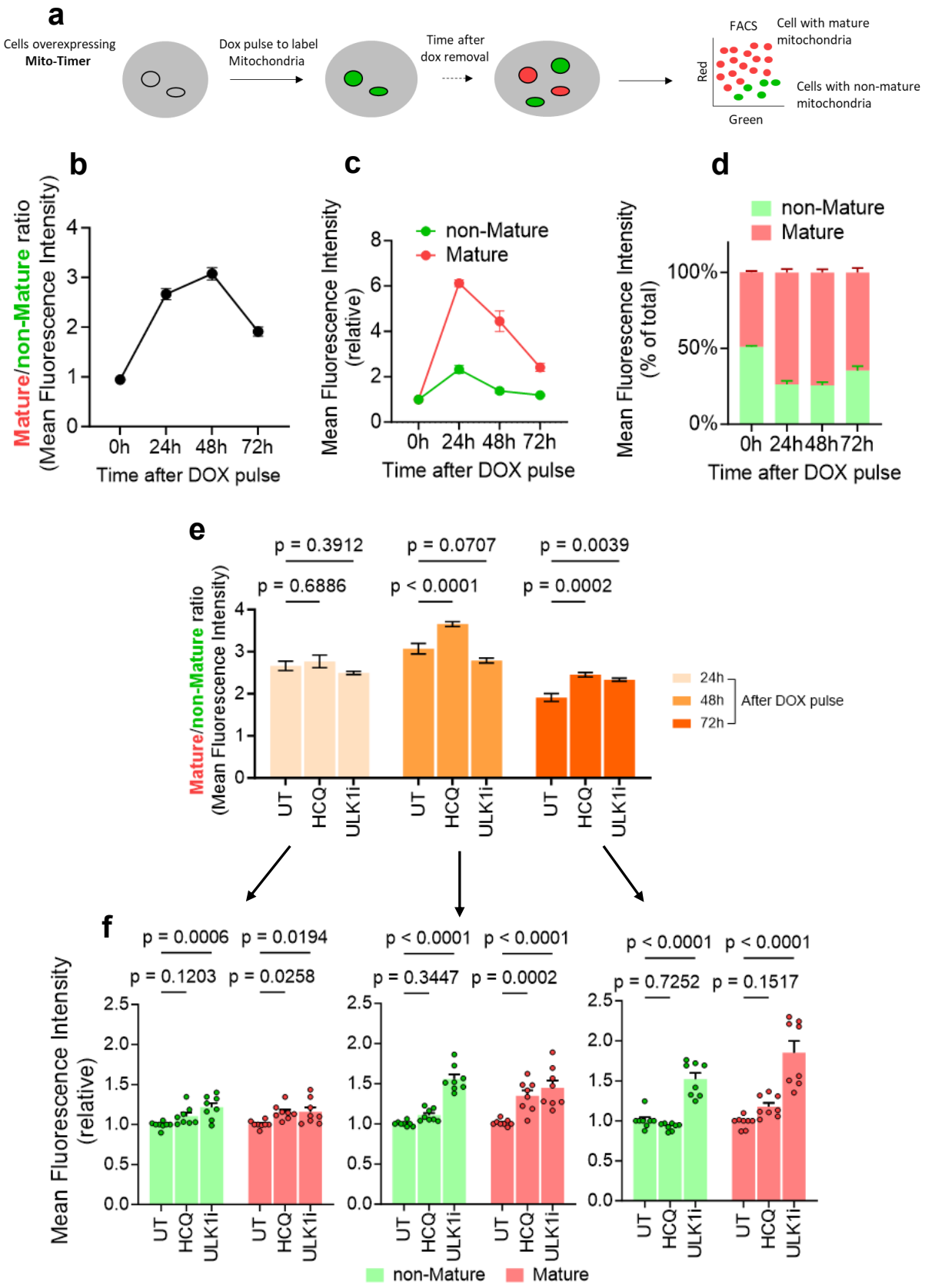
a
Cells overexpressing
Mito-Timer
Dox pulse to label
Mitochondria
Time after
dox removal
FACS
Cell with mature
mitochondria
Red
Cells with non-mature
mitochondria
Green
b
Mature/non-Mature ratio
(Mean Fluorescence Intensity)
Time after DOX pulse
0h 24h 48h 72h
c
Mean Fluorescence Intensity
(relative)
non-Mature
Mature
Time after DOX pulse
d
Mean Fluorescence Intensity
(% of total)
non-Mature
Mature
100%
50%
0%
Time after DOX pulse
e
Mature/non-Mature ratio
(Mean Fluorescence Intensity)
p = 0.3912
p = 0.6886
p = 0.0707
p < 0.0001
p = 0.0039
p = 0.0002
UT
HCQ
ULK1i
24h
48h
72h
After DOX pulse
f
Mean Fluorescence Intensity
(relative)
p = 0.0006
p = 0.1203
p = 0.0194
p = 0.0258
p < 0.0001
p = 0.3447
p < 0.0001
p = 0.0002
p < 0.0001
p = 0.7252
p < 0.0001
p = 0.1517
non-Mature
Mature

Figure 25: Mitochondrial turnover is regulated by autophagy in CML cells. a) Schematic of Mito-Timer workflow. b) Ratio of Mature to non-Mature mitochondria measured by flow cytometry using Mito-timer overexpressing K562 cells at 24, 48 and 72 hours post doxycycline (DOX) treatment. c) Mean Fluorescence Intensity (MFI) of non-Mature and Mature Mitochondria measured by flow cytometry using Mito-timer overexpressing K562 cells at 24, 48 and 72 hours post DOX treatment. d) same as in b) but shown as percentage of total MFI (n=4 independent cultures). e) Ratio of Mature to non-Mature mitochondria measured by flow cytometry using Mito-timer overexpressing K562 cells at 24, 48 and 72 hours post DOX treatment treated with or without Hydroxychloroquine (HCQ) or ULK1 inhibitor (ULK1i). f) Relative MFI of non-Mature and Mature mitochondria measured by flow cytometry using Mito-timer overexpressing K562 cells at 24, 48 and 72 hours post DOX treatment treated with or without HCQ or ULK1i (n=8 independent cultures). P-values in (e) and (f) were calculated using ordinary two-way ANOVA.

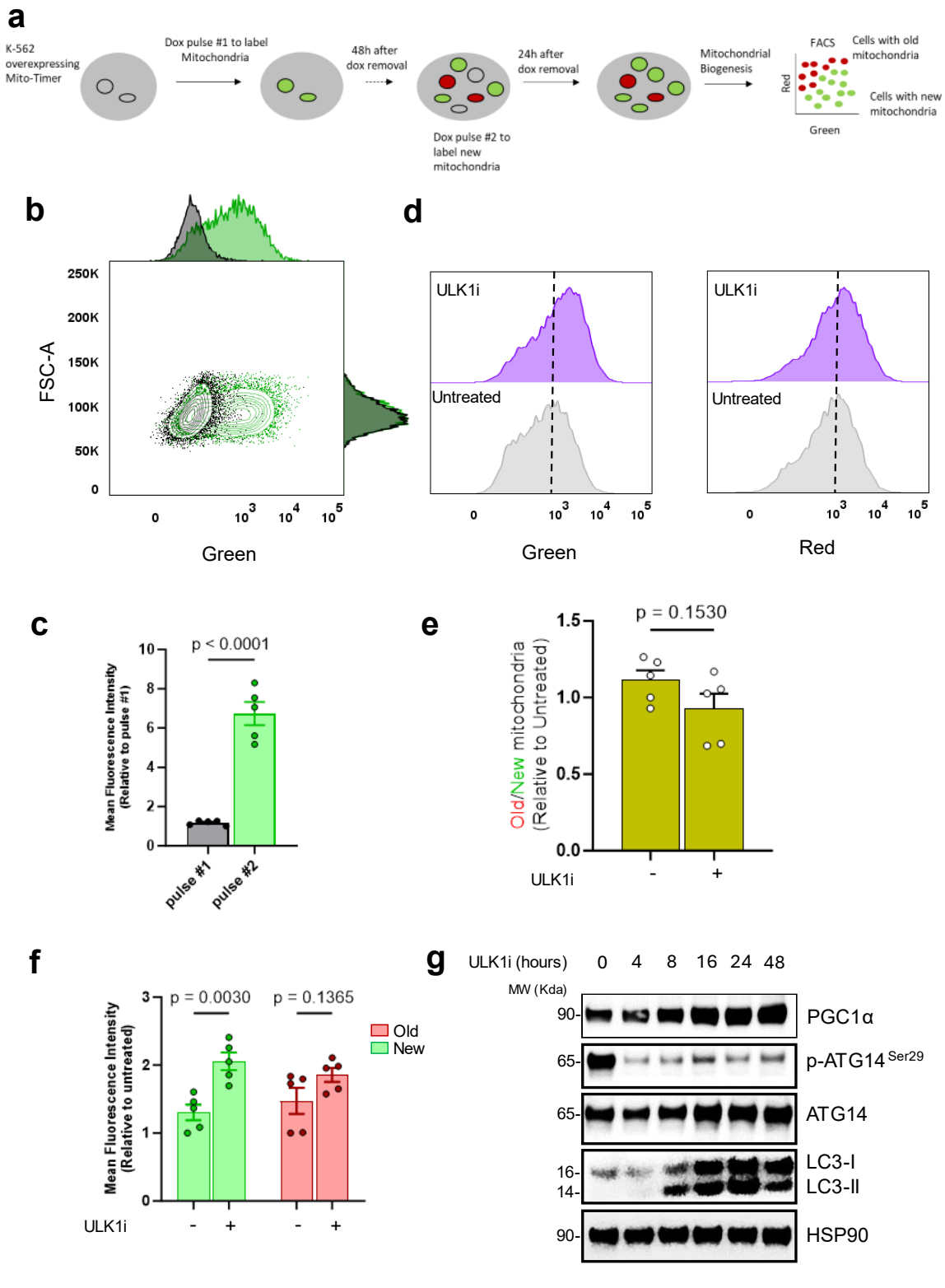
a
K-562 overexpressing Mito-Timer
Dox pulse #1 to label Mitochondria
48h after dox removal
24h after dox removal
Mitochondrial Biogenesis
FACS
Cells with old mitochondria
Cells with new mitochondria
Red
Green
Dox pulse #2 to label new mitochondria
b
FSC-A
250K
200K
150K
100K
50K
0
Green
d
ULK1i
Untreated
Green
Red
c
Mean Fluorescence Intensity (Relative to pulse #1)
p < 0.0001
pulse #1
pulse #2
e
Old/New mitochondria (Relative to Untreated)
p = 0.1530
ULK1i
f
Mean Fluorescence Intensity (Relative to untreated)
p = 0.0030
p = 0.1365
Old
New
ULK1i
g
ULK1i (hours) 0 4 8 16 24 48
MW (Kda)
PGC1α
p-ATG14 Ser29
ATG14
LC3-I
LC3-II
HSP90

Figure 26: Inhibition of ULK1 may drive mitochondrial biogenesis via PGC1a. a) Schematic of Mito-Timer workflow to study mitochondrial biogenesis**.** b) Representative flow cytometry plot of green mitochondria of MitoTimer cells pulsed once (black) or twice (green). c) bar plot of (b) (n=5 independent cultures). d) Representative histogram flow cytometry plots of green and red mitochondrial after treatment with or without ULK1i and second DOX pulse. e) Ratio of old to new mitochondria measured by flow cytometry using Mito-timer overexpressing K562 cells after 48 hours of treatment with ULK1i and second DOX pulse (n=5 independent cultures). f) Mean Fluorescence Intensity (MFI) of new and old mitochondria measured by flow cytometry using Mito-timer overexpressing K562 cells treated with ULK1i (n=5 independent cultures). g) Immunoblot representing a time course treatment of K562 with ULK1i. P-values in (c) and (e) were calculated using paired Student's t test. P-values in (f) were calculated using ordinary two-way ANOVA.

4.6 BNIP3 regulates mitochondrial turnover in CML cells

To further study the role of BNIP3 in CML cells, we generated K562 and KCL22 BNIP3 KO cells (figure 27a-b). Western blot analysis showed a delayed LC3-II maturation, which is indicative of reduced autophagy flux in BNIP3 KO K562 cells compare to mitophagy competent cells (figure 27a). Moreover, BNIP3 KO cells showed slower proliferation rate and doubling time (indicated as doublings per day) especially when cultured under hypoxic conditions (figure 27 c,d,e and f) for a long exposure time.

Furthermore, BNIP3 KO cells showed increased accumulation of mitochondrial MT-CO2 and TOM20 protein levels when exposed to hypoxia (figure 28a). Levels of mitochondrial proteins could not be rescued upon treatment with BafA1 (figure 28b). All together these data suggested impaired receptor-mediated mitophagy due to removal of BNIP3. Of note, BNIP3 KO cells did not show any impairment in HIF1α stabilization, suggesting that the mitochondrial clearance function is independent of this transcription factor.

To further validate the accumulation of mitochondria in BNIP3 deficient cells, we overexpressed Mito-Timer in BNIP3 KO cells and monitored the levels of old mitochondria over time. As expected, BNIP3 KO cells accumulated mature mitochondria (figure 28c). Interestingly, BNIP3 KO cells also showed increased mitochondrial ROS (mROS) accumulation when compared to WT cells, as a further confirmation of dysfunctional mitochondrial turnover (figure 28d).

Finally, both BNIP3 KO and ATG7 KO cells (used as control) showed increased basal and maximal OCR (figure 29a-c) and increased mitochondrial mass when compared to WT cells (figure 30a-c). These results further confirm that general autophagy and BNIP3-mediated mitophagy are necessary for mitochondrial turnover in CML cells.

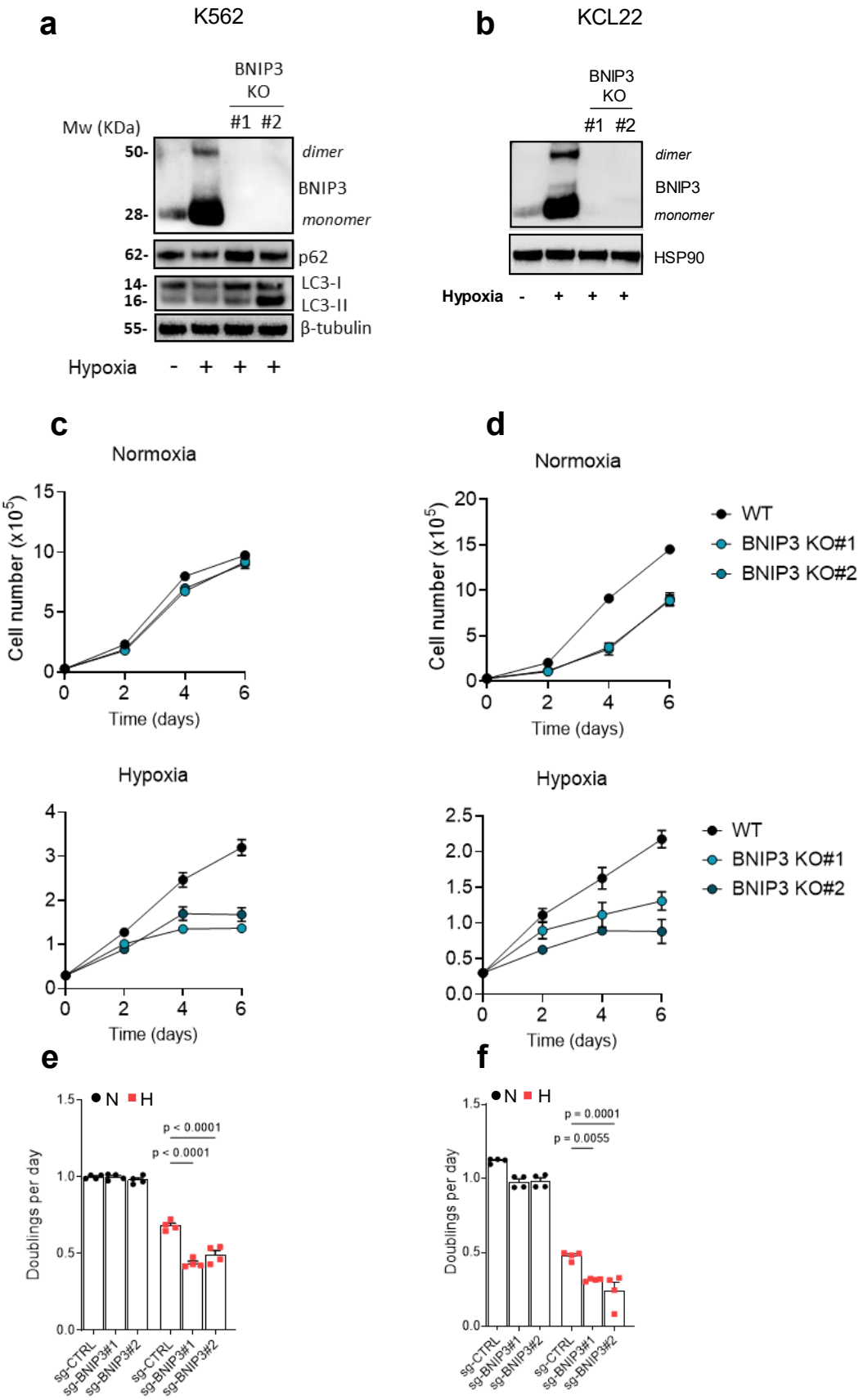
a
K562
BNIP3 KO
#1 #2
Mw (KDa)
50-
28-
62-
14-
16-
55-
dimer
BNIP3
monomer
p62
LC3-I
LC3-II
β-tubulin
Hypoxia - + + +
b
KCL22
BNIP3 KO
#1 #2
dimer
BNIP3
monomer
HSP90
Hypoxia - + + +
c
Normoxia
Cell number (x10^5)
Time (days)
Hypoxia
Time (days)
d
Normoxia
Cell number (x10^5)
Time (days)
WT
BNIP3 KO#1
BNIP3 KO#2
Hypoxia
Time (days)
WT
BNIP3 KO#1
BNIP3 KO#2
e
N H
p < 0.0001
p < 0.0001
Doublings per day
sg-CTRL
sg-BNIP3#1
sg-BNIP3#2
sg-CTRL
sg-BNIP3#1
sg-BNIP3#2
f
N H
p = 0.0001
p = 0.0055
Doublings per day
sg-CTRL
sg-BNIP3#1
sg-BNIP3#2
sg-CTRL
sg-BNIP3#1
sg-BNIP3#2

Figure 27: Genetic ablation of BNIP3 has an anti-proliferative effect on CML cells under hypoxia. a) Immunoblot analysis showing deletion of BNIP3 in K562 and (b) KCL22 cells. c) Growth curves of K562 and (d) KCL22 wild type (WT) and BNIP3 KO (#1 = guide 1 and #2 = guide 2) over 2,4 and 6 days under 21% O_2 (normoxia) or 0.5%O_2 (hypoxia). e) Proliferation rate (doublings per day) of K562 and (f) KCL22 WT and BNIP3 KO (#1 and #2) cells at 6 days as in (c) and (d) respectively. Data were represented as mean ± SD and P-values were calculated with two-way ANOVA.

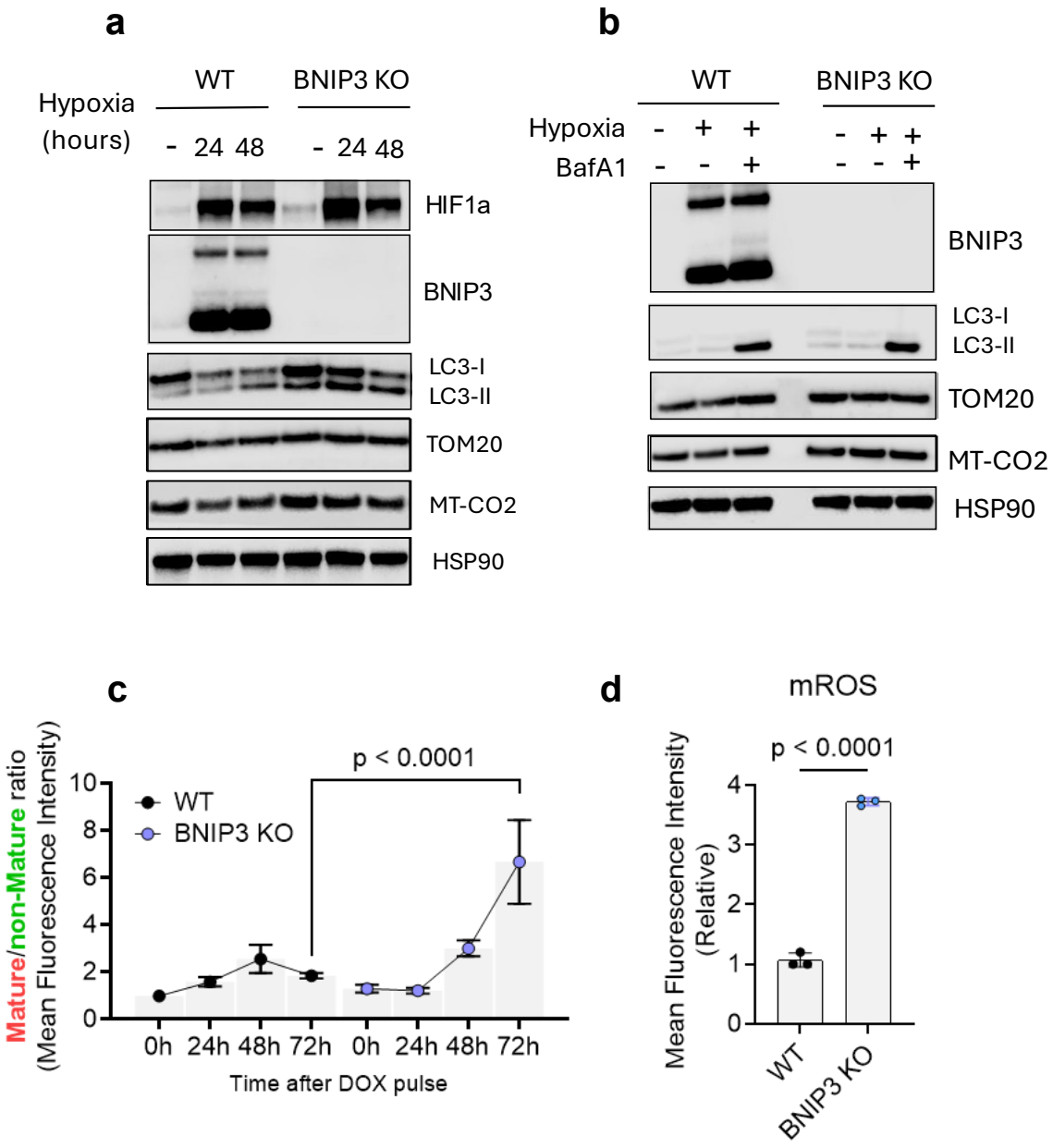
a
WT
BNIP3 KO
Hypoxia
(hours)
- 24 48
- 24 48
HIF1a
BNIP3
LC3-I
LC3-II
TOM20
MT-CO2
HSP90
b
WT
BNIP3 KO
Hypoxia
BafA1
BNIP3
LC3-I
LC3-II
TOM20
MT-CO2
HSP90
c
Mature/non-Mature ratio
(Mean Fluorescence Intensity)
p < 0.0001
WT
BNIP3 KO
0h 24h 48h 72h 0h 24h 48h 72h
Time after DOX pulse
d
mROS
p < 0.0001
Mean Fluorescence Intensity
(Relative)
WT
BNIP3 KO

Figure 28: BNIP3 loss promotes accumulation of old and dysfunctional mitochondria in CML cells. a) Immunoblot of K562 WT and BNIP3 KO cells exposed to hypoxia for 24 and 48 hours. b) Immunoblot of K562 WT and BNIP3 KO cells exposed to hypoxia for 24 hours and treated or not with 100 nM of Bafilomycin A for the last 4 hours. c) Ratio of Mature to non-Mature mitochondria measured by flow cytometry using Mito-timer overexpressing WT and BNIP3 KO K562 cells at 24, 48 and 72 hours post doxycycline (DOX) treatment (n=3 independent cultures). d) Relative MFI levels of mitoSOX (mROS) measured via flow cytometry of WT and BNIP3 KO. Data were represented as mean ± SD. P-values in (c) and were calculated using two-way ANOVA. P-values in (d) were calculated using unpaired t-test.

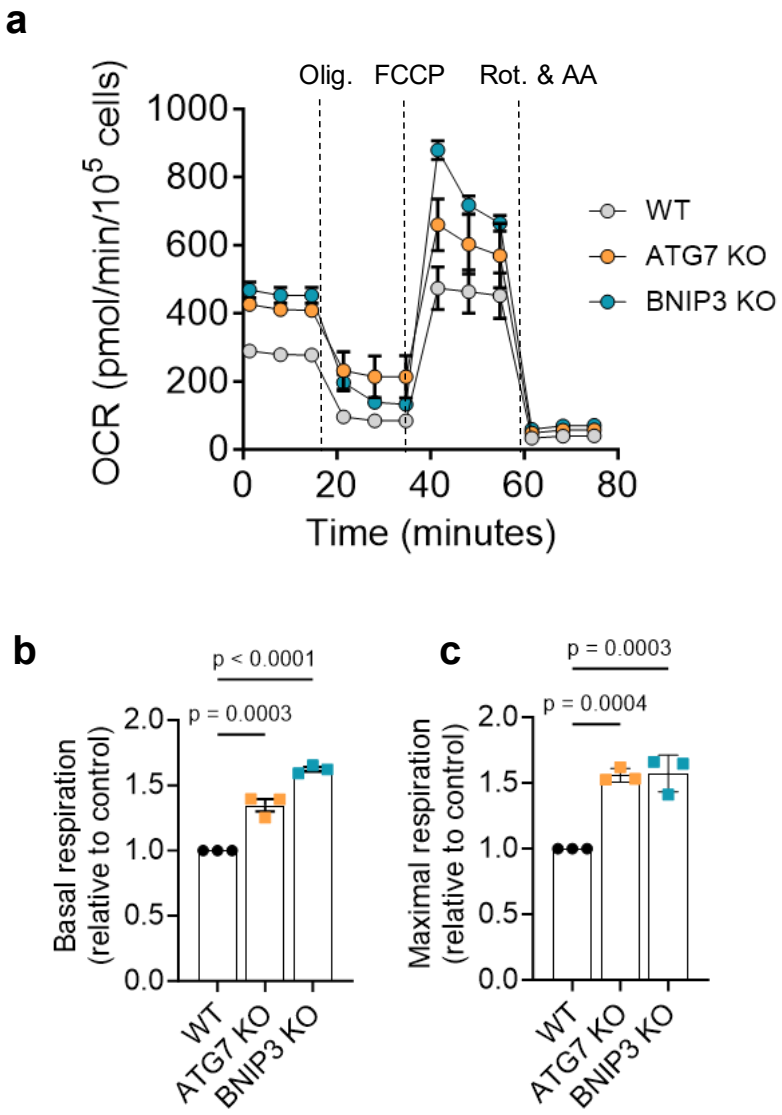

Figure 29: BNIP3 KO cells show increased OCR. a) Representative Mito Stress OCR (oxygen consumption rate) profile. b) Basal respiration and c) Maximal respiration of WT, ATG7 KO and BNIP3 KO K562 cells. Data were plotted as mean ± SD of n=3 independent cultures. P-values were calculated with a paired one-way ANOVA with Geisser-Greenhouse correction and Sidak's multiple comparison test.

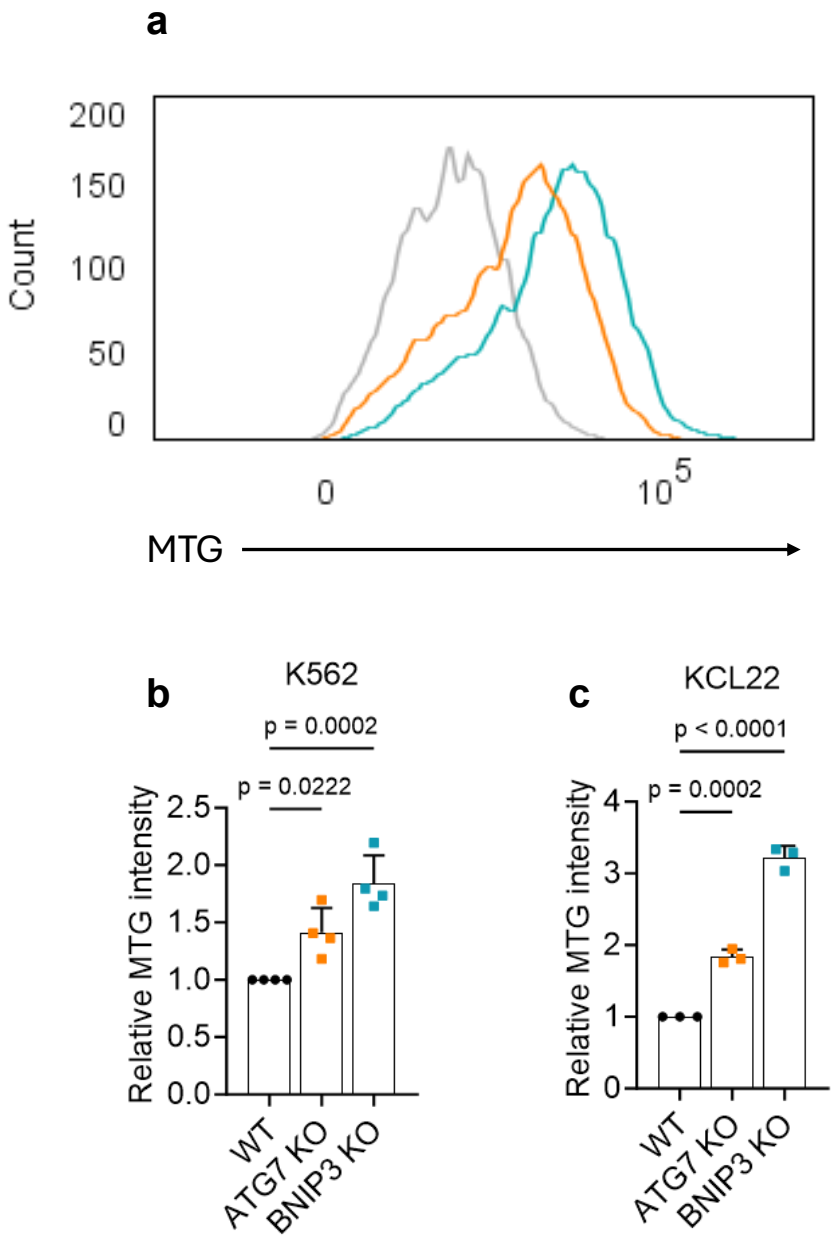

Figure 30: BNIP3 KO cells show increased mitochondrial mass. a) Representative flow cytometry plot of Mitotracker green (MTG). b) Relative MTG intensity in K562 and c) KCL22 WT, ATG7 and BNIP3 KO cells. Data were plotted as mean ± SD of n=4 in (b) and n=3 in (c) independent cultures. P-values were calculated with a paired one-way ANOVA with Geisser-Greenhouse correction and Sidak's multiple comparison test.

4.7 BNIP3 regulates glutamine metabolism in CML cells

To investigate the role of BNIP3 in regulating CML metabolism we initially assessed the uptake of extracellular metabolites in WT, ATG7 KO and BNIP3 KO cells exposed to normoxia or hypoxia for 72 hours.

While we observed increased glucose uptake and increased lactate secretion in BNIP3 KO cells (figure 31a-b), ablation of ATG7 (figure 32a-b) did not show similar results. More interestingly, we noticed reduced glutamine uptake and increased glutamate secretion in hypoxia-exposed BNIP3 KO cells, as if BNIP3 KO cells were unable to use glutamine to fuel TCA cycle (figure 31c-d) under low oxygen levels. Interestingly, also ATG7 KO cells showed reduced glutamine uptake when exposed to hypoxia, but we did not observe significative changes in glutamate secretion (figure 32c-d).

To further investigate how BNIP3 affects glutamine utilization, we performed fully labelled ^{13}C-glutamine tracing of WT and BNIP3 KO cells exposed or not to hypoxia for 24 hours after a previous exposure of additional 24 hours to allow initial adaption of cells to low oxygen atmosphere. Results from glutamine tracing are shown in figure 33. BNIP3 KO cells showed significant reduction in the α-KG/Citrate ratio (figure 33a), $^{13}C_5$-glutamate (figure 33b), and glutamine reductive carboxylation metabolites. When compared to hypoxic WT cells, BNIP3 KO cells showed reduced labelling from ^{13}C-glutamine derived carbons (figure 34) with a significant reduction of fumarate levels.

As controls, we performed the same experiments using ATG7 KO (figure 35a-c and figure 36) and NIX KO cells (figure 37a-c and figure 38). However, although ATG7 showed a significant slightly reduced α-KG/Citrate ratio (figure 35a) and significant lower levels of reductive carboxylation related metabolites (figure 35c), the effect of its ablation on glutamine metabolism was of a lower extent compared to what we previously observed in BNIP3 KO cells. Moreover, apart from an increased α-KG/Citrate ratio (figure 37a) and a slight increase in some reductive carboxylation related metabolites (figure 37c), NIX KO cells did not show other significant changes when compared to WT cells, suggesting that this mitochondrial receptor does not play a major role in supporting metabolic rewiring under low oxygen conditions in CML cells.

All together these results suggest that BNIP3-mediated mitophagy is required for CML cells to promote glutaminolysis and glutamine reductive carboxylation to successfully adapt and survive in a hypoxic environment.

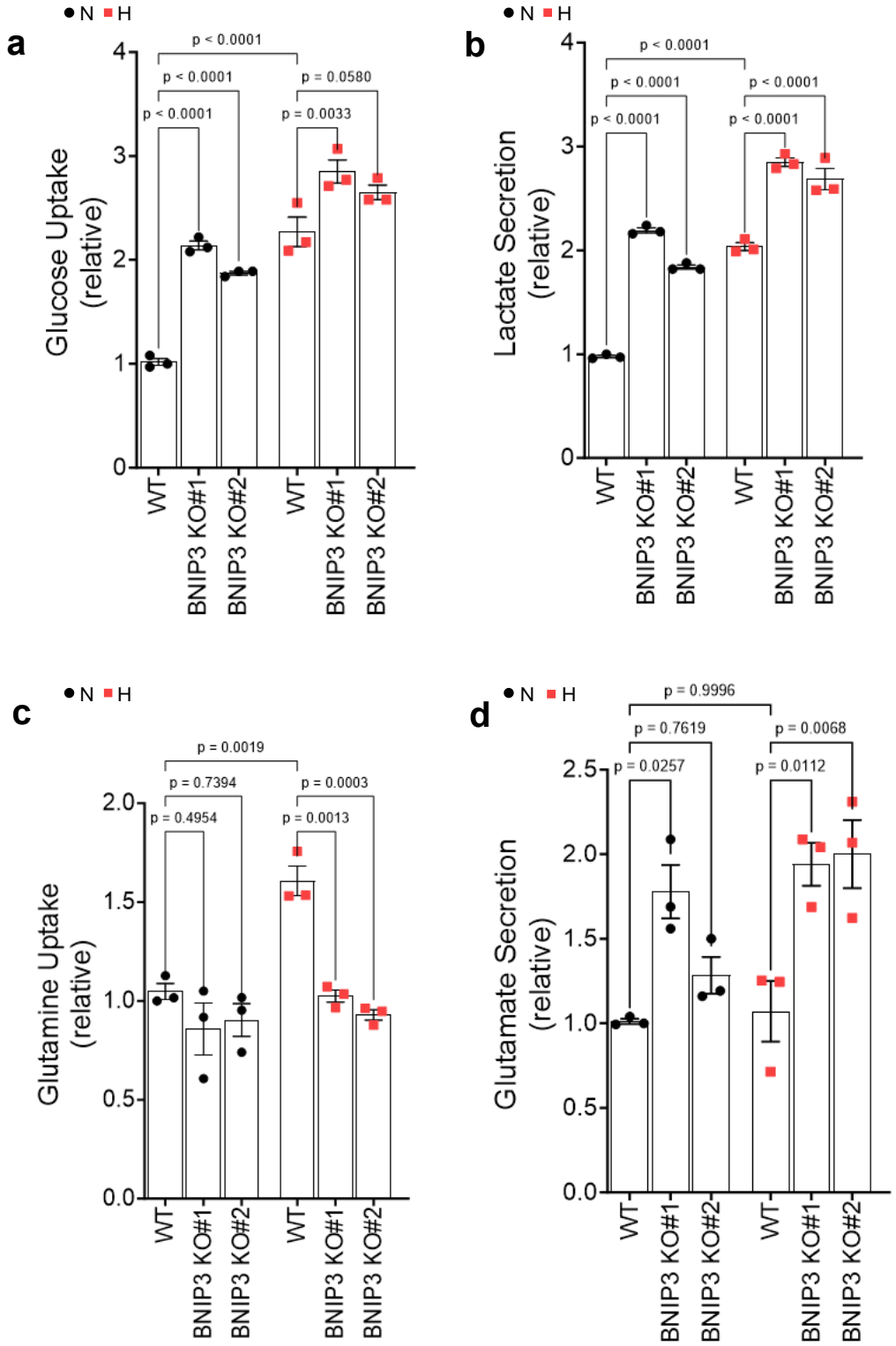
a
N H
Glucose Uptake (relative)
p < 0.0001
p < 0.0001
p < 0.0001
p = 0.0580
p = 0.0033
WT
BNIP3 KO#1
BNIP3 KO#2
WT
BNIP3 KO#1
BNIP3 KO#2
b
N H
Lactate Secretion (relative)
p < 0.0001
p < 0.0001
p < 0.0001
p < 0.0001
p < 0.0001
WT
BNIP3 KO#1
BNIP3 KO#2
WT
BNIP3 KO#1
BNIP3 KO#2
c
N H
Glutamine Uptake (relative)
p = 0.0019
p = 0.7394
p = 0.4954
p = 0.0003
p = 0.0013
WT
BNIP3 KO#1
BNIP3 KO#2
WT
BNIP3 KO#1
BNIP3 KO#2
d
N H
Glutamate Secretion (relative)
p = 0.9996
p = 0.7619
p = 0.0257
p = 0.0068
p = 0.0112
WT
BNIP3 KO#1
BNIP3 KO#2
WT
BNIP3 KO#1
BNIP3 KO#2

Figure 31: BNIP3 regulates the hypoxia-increased glutamine uptake in CML cells. Relative a) glucose uptake, b) lactate secretion c) glutamine uptake and d) glutamate secretion of WT and BNIP3 KO (guide#1 and guide#2) K562 cells cultured under 21% O_2 (N) or 0.5% O_2 (H) for 72 hours. Data were plotted as mean ± SEM of n=3 independent cultures. P-values were calculated with ordinary two-way ANOVA with Turkey's multiple comparison test.

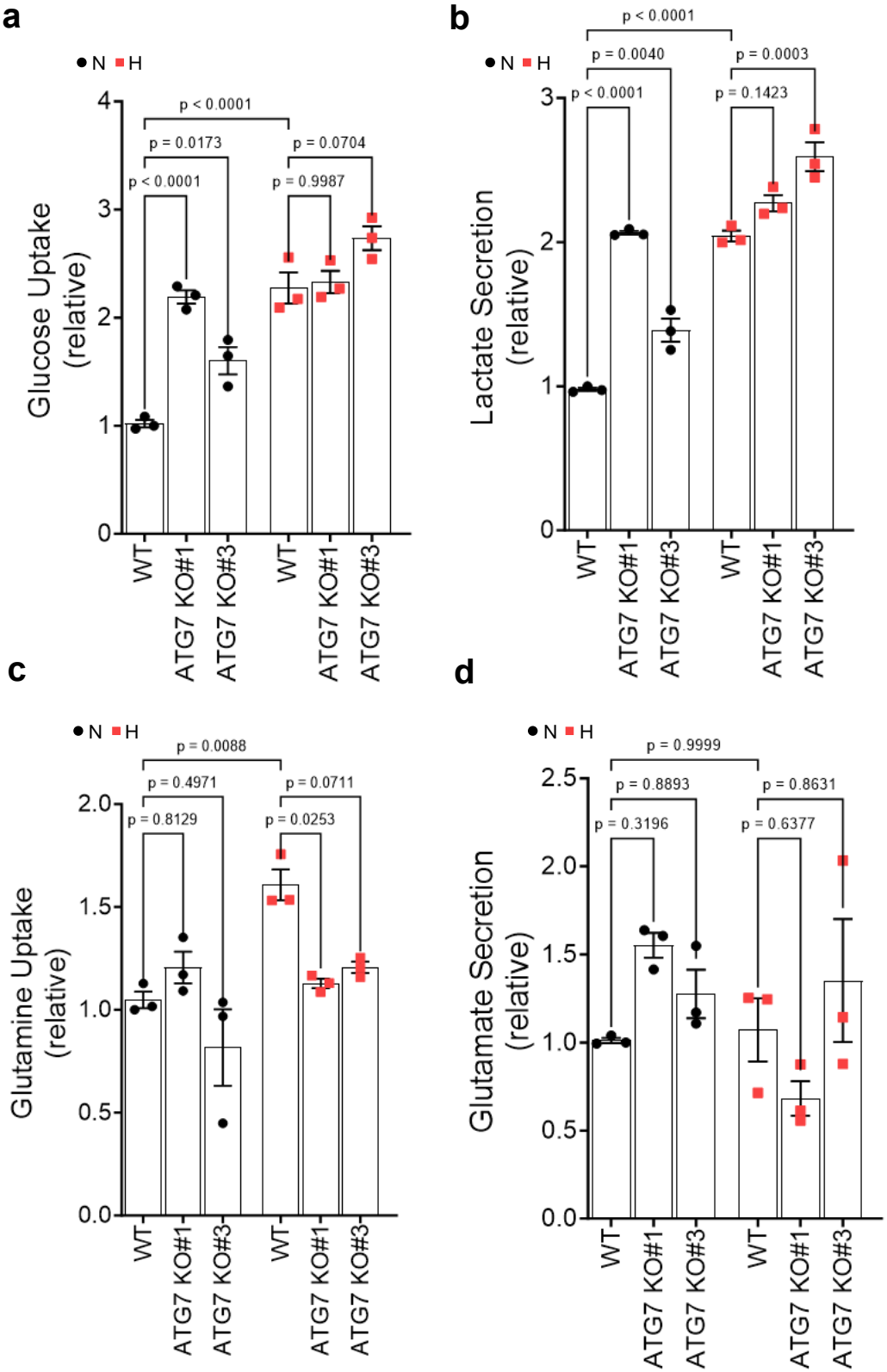
a
N H
Glucose Uptake (relative)
p < 0.0001
p = 0.0173
p < 0.0001
p = 0.0704
p = 0.9987
WT
ATG7 KO#1
ATG7 KO#3
b
N H
Lactate Secretion (relative)
p < 0.0001
p = 0.0040
p < 0.0001
p = 0.0003
p = 0.1423
c
N H
Glutamine Uptake (relative)
p = 0.0088
p = 0.4971
p = 0.8129
p = 0.0711
p = 0.0253
d
N H
Glutamate Secretion (relative)
p = 0.9999
p = 0.8893
p = 0.3196
p = 0.8631
p = 0.6377

Figure 32: General autophagy does not regulate the hypoxia-increased glutamine uptake in CML cells at the same extent as BNIP3 KO. Relative a) glucose uptake, b) lactate secretion c) glutamine uptake and d) glutamate secretion of WT and ATG7 KO (guide#1 and guide#3) K562 cells cultured under 21% O_2 (N) or 0.5% O_2 (H) for 72 hours. Data were plotted as mean ± SEM of n=3 independent cultures. P-values were calculated with ordinary two-way ANOVA with Turkey's multiple comparison test.

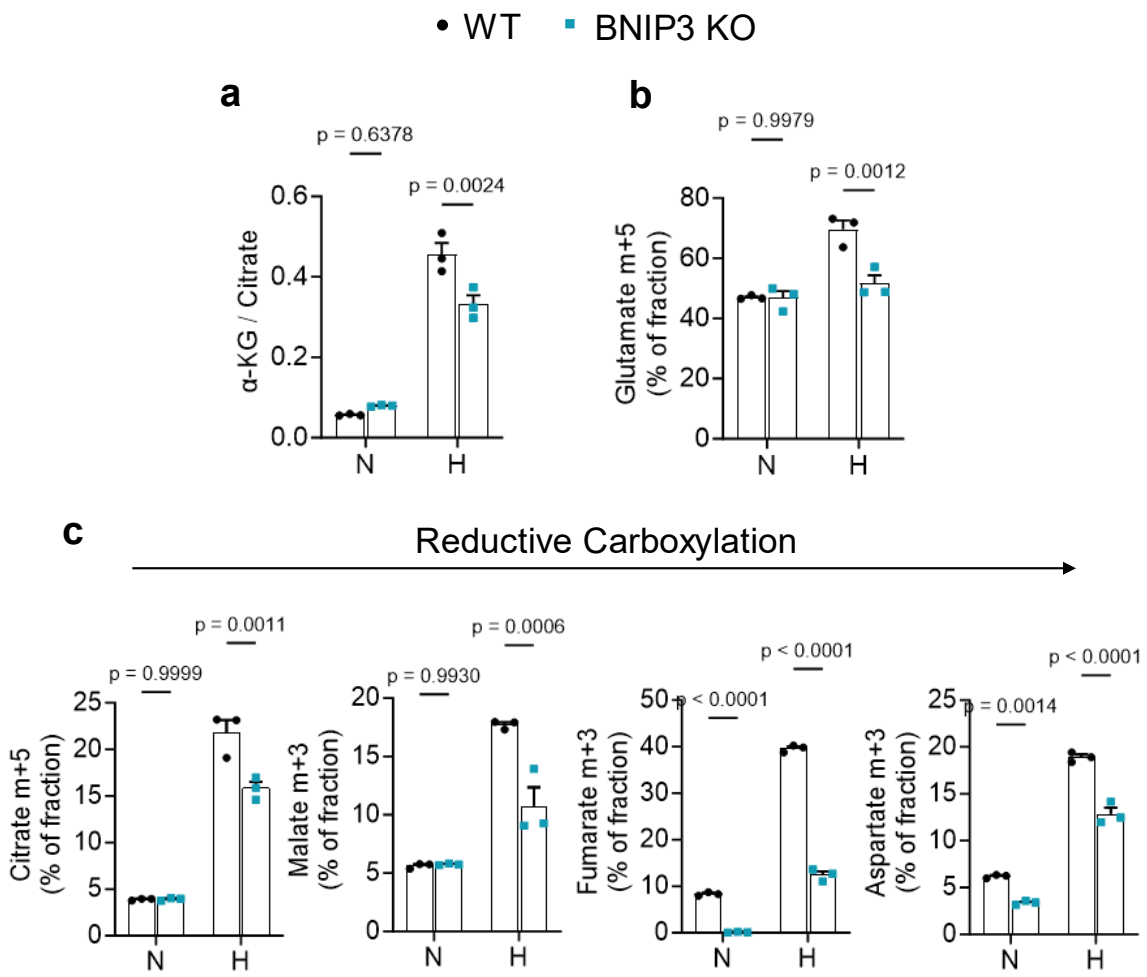

Figure 33: BNIP3 is required for hypoxia-driven glutamine reductive carboxylation. a) Ratio of α-KG/Citrate of WT and BNIP3 KO cells. b) Fractional enrichment of Glutamate m+5 from K562 WT and BNIP3 KO cultured under 21%O_2 (N) or 0.5%O_2 (H) with medium containing $^{13}C_5$-Glutamine for 24 hours (n=3 independent cultures). c) Fractional enrichment of Reductive Carboxylation metabolites (Citrate m+5, Malate m+3, Fumarate m+3 and Aspartate m+3) from K562 WT and BNIP3 KO cultured under 21%O_2 (N) or 0.5%O_2 (H) with medium containing $^{13}C_5$-Glutamine for 24 hours (n=3 technical replicates). Means and P-values in (a), (b) and (c) were calculated using one-way ANOVA with Dunnett's multiple comparisons test.

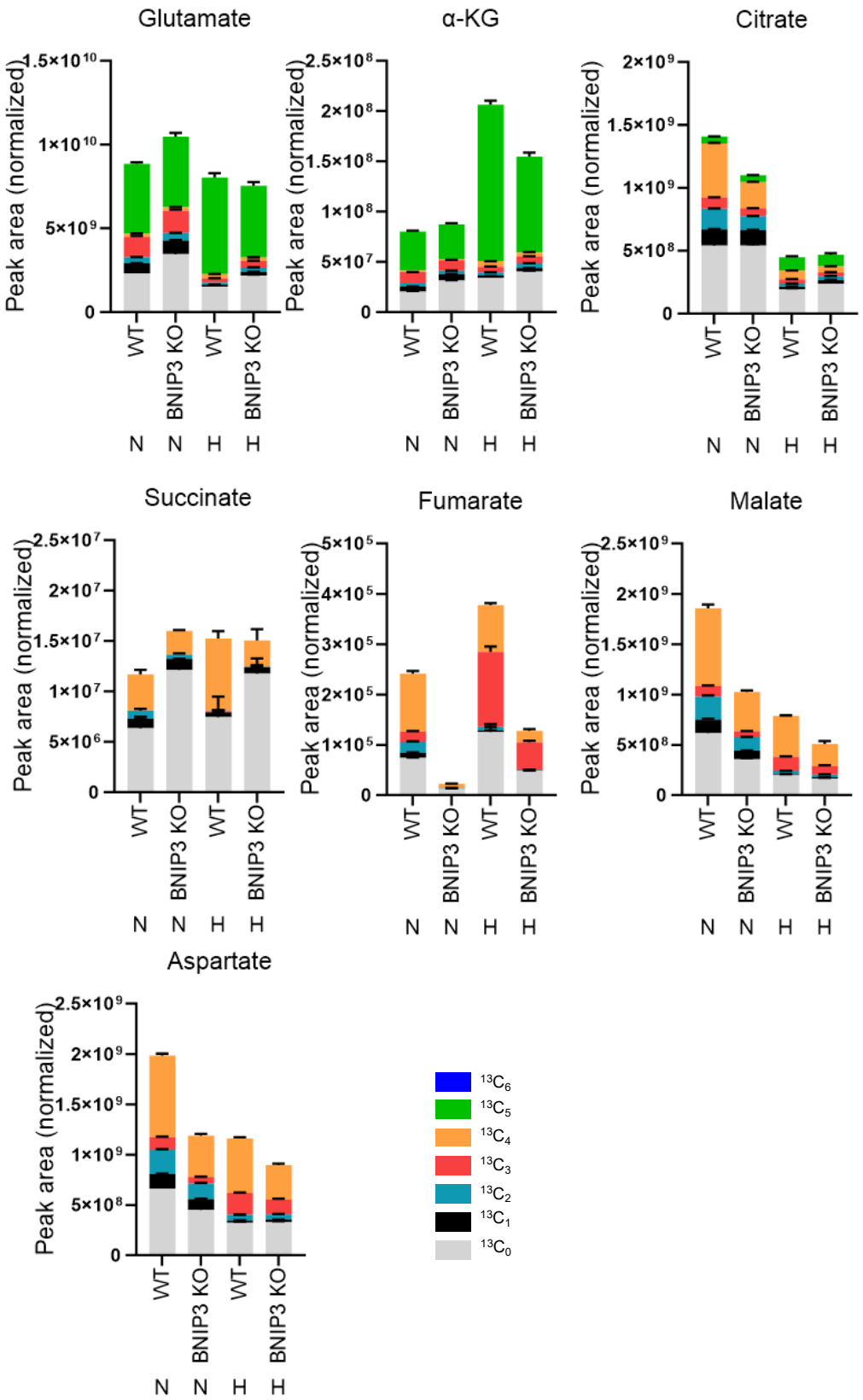
Glutamate
α-KG
Citrate
Succinate
Fumarate
Malate
Aspartate
Peak area (normalized)
WT
BNIP3 KO
WT
BNIP3 KO
N N H H
$^{13}C_6$
$^{13}C_5$
$^{13}C_4$
$^{13}C_3$
$^{13}C_2$
$^{13}C_1$
$^{13}C_0$

Figure 34: BNIP3 sustains glutamine metabolism in CML cells under hypoxia. Isotopolog distribution of the indicated metabolites in K562 WT and BNIP3 KO cells cultured under 21%O_2 (N) or 0.5%O_2 (H) with medium containing $^{13}C_5$-Glutamine for 24 hours (n=3 technical replicates). P values in were calculated using 2-way ANONA using Šídák's multiple comparisons test.

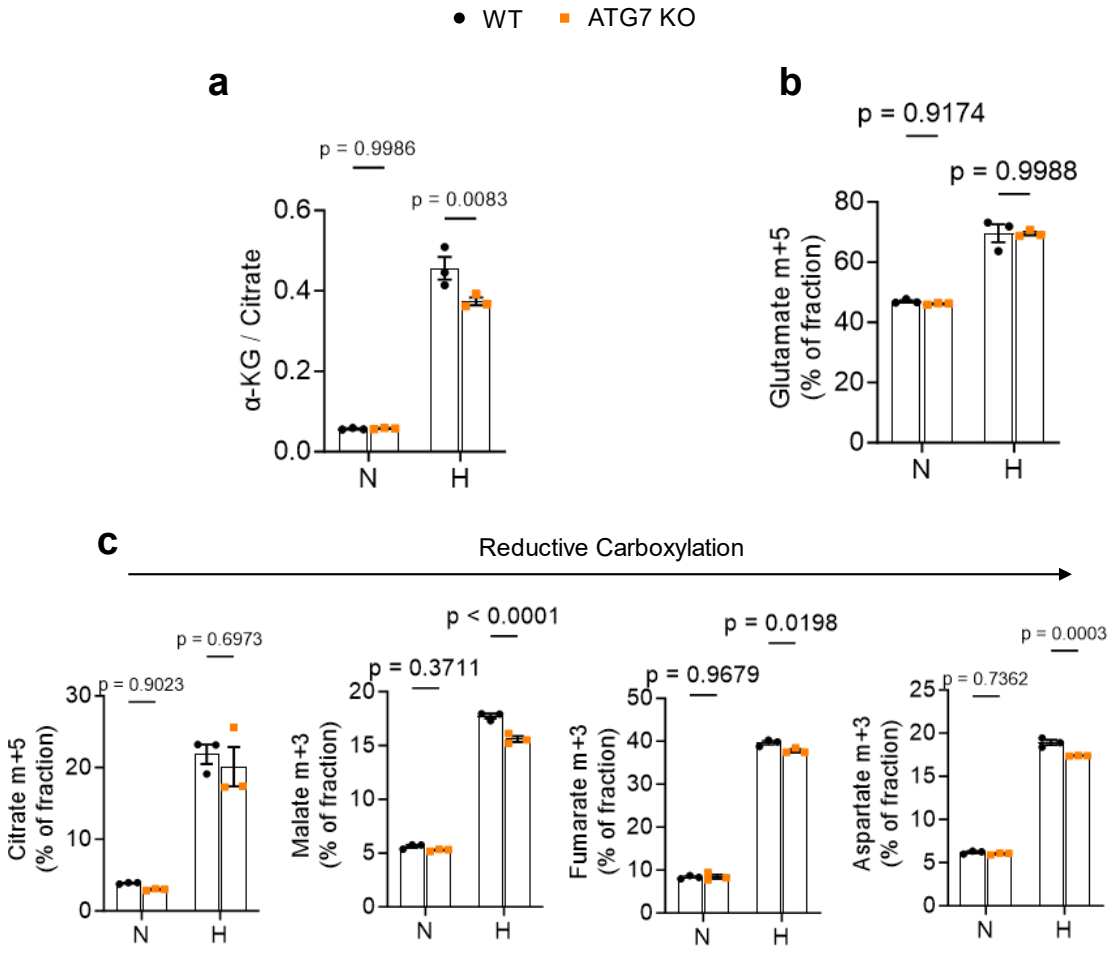
WT
ATG7 KO
a
p = 0.9986
p = 0.0083
α-KG / Citrate
0.6
0.4
0.2
0.0
N
H
b
p = 0.9174
p = 0.9988
Glutamate m+5
(% of fraction)
80
60
40
20
0
N
H
c
Reductive Carboxylation
Citrate m+5
(% of fraction)
p = 0.6973
p = 0.9023
30
20
10
0
N
H
Malate m+3
(% of fraction)
p < 0.0001
p = 0.3711
20
15
10
5
0
N
H
Fumarate m+3
(% of fraction)
p = 0.0198
p = 0.9679
50
40
30
20
10
0
N
H
Aspartate m+3
(% of fraction)
p = 0.0003
p = 0.7362
25
20
15
10
5
0
N
H

Figure 35: ATG7 is not required for hypoxia-driven glutamine reductive carboxylation. a) Ratio of α-KG/Citrate of WT and ATG7 KO cells. b) Fractional enrichment of Glutamate m+5 from K562 WT and ATG7 KO cultured under 21%O_2 (N) or 0.5%O_2 (H) with medium containing $^{13}C_5$-Glutamine for 24 hours (n=3 technical replicates). c) Fractional enrichment of Reductive Carboxylation metabolites (Citrate m+5, Malate m+3, Fumarate m+3 and Aspartate m+3) from K562 WT and ATG7 KO cultured under 21%O_2 (N) or 0.5%O_2 (H) with medium containing $^{13}C_5$-Glutamine for 24 hours (n=3 technical replicates). Means and P-values in (a), (b) and (c) were calculated using one-way ANOVA with Dunnett's multiple comparisons test.

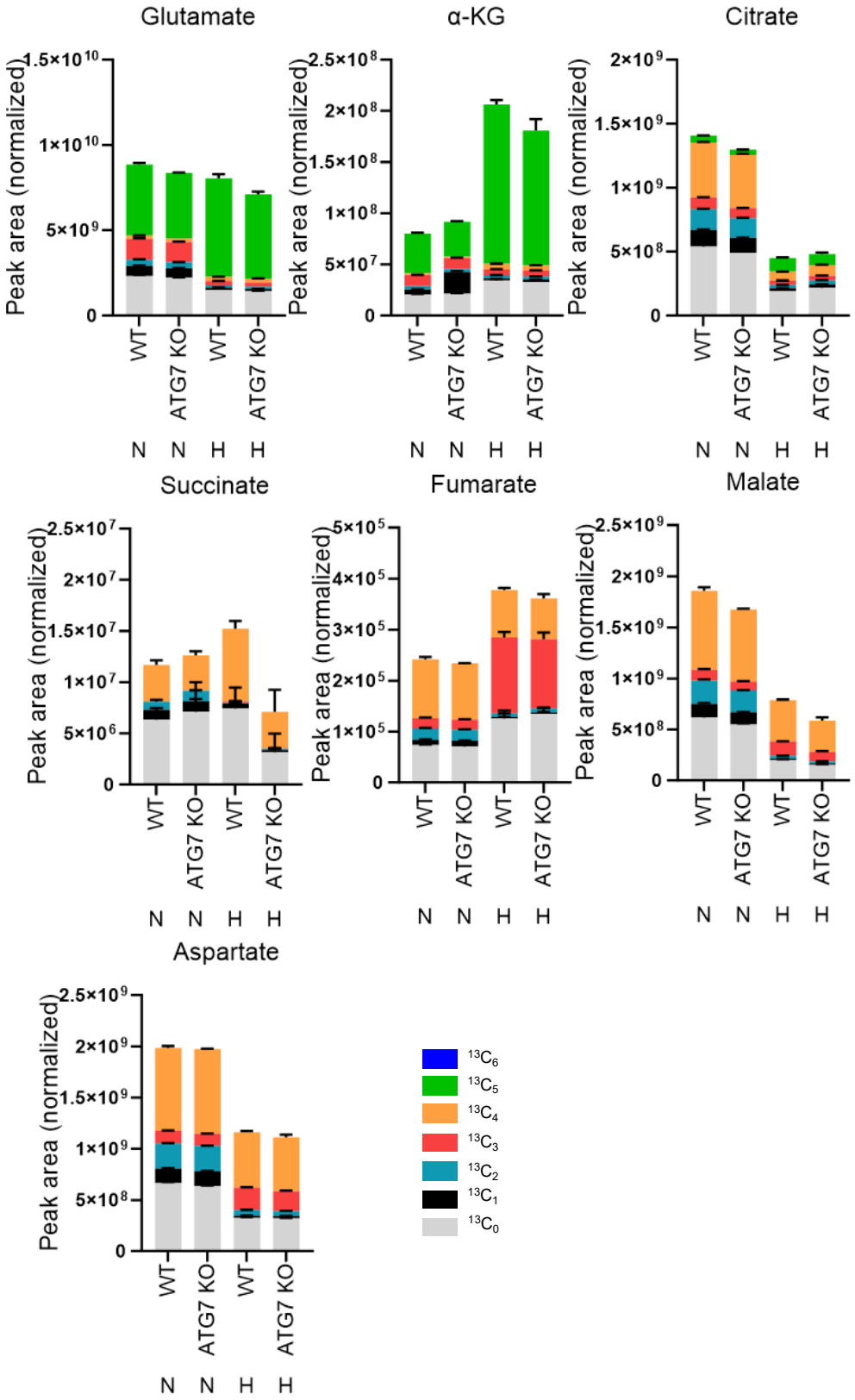

Figure 36: ATG7 does not sustains glutamine metabolism in CML cells under hypoxia. Isotopolog distribution of the indicated metabolites in K562 WT and ATG7 KO cells cultured under 21%O_2 (N) or 0.5%O_2 (H) with medium containing $^{13}C_5$-Glutamine for 24 hours (n=3 technical replicates).

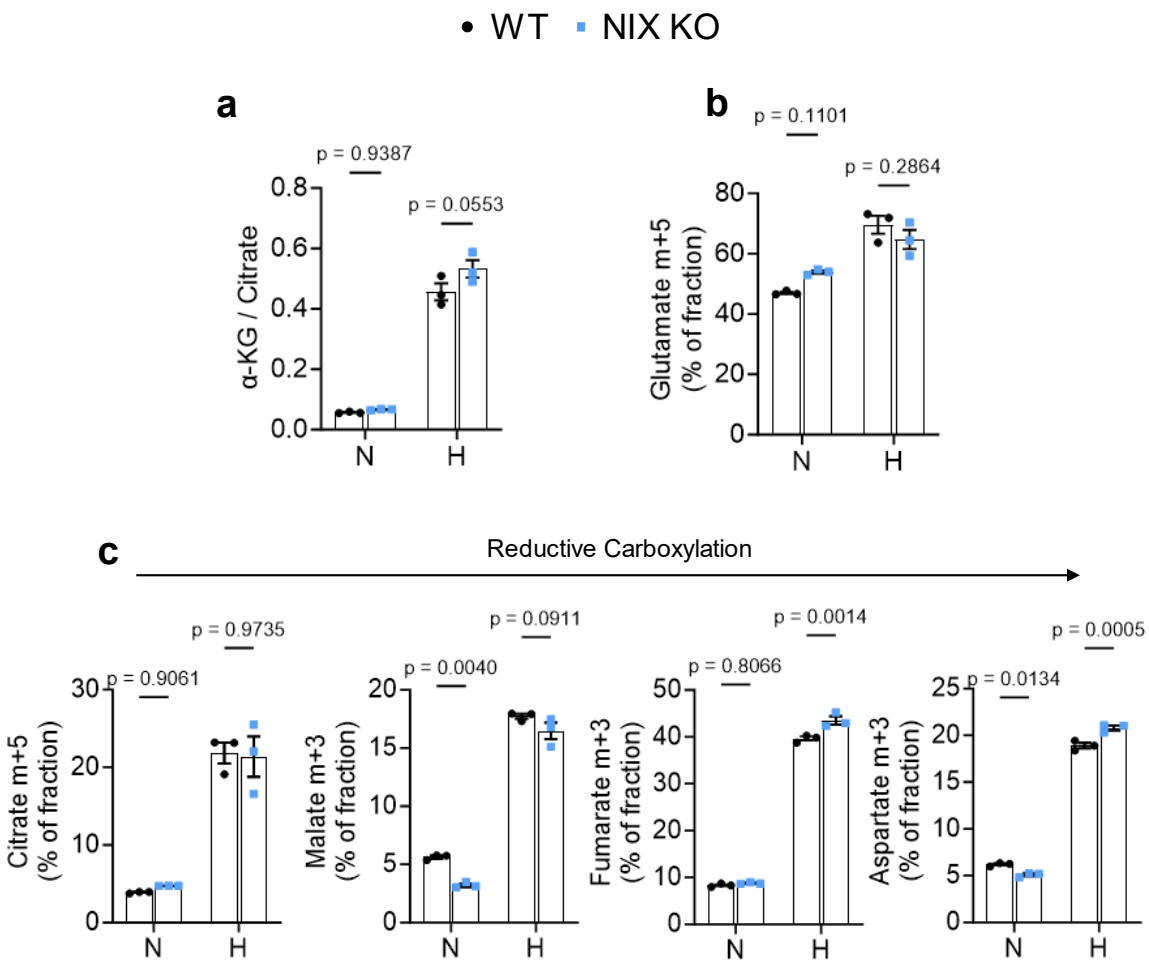

Figure 37: NIX is not required for hypoxia-driven glutamine reductive carboxylation. a) Ratio of α-KG/Citrate of WT and NIX KO cells. b) Fractional enrichment of Glutamate m+5 from K562 WT and NIX KO cultured under 21%O_2 (N) or 0.5%O_2 (H) with medium containing $^{13}C_5$-Glutamine for 24 hours (n=3 technical replicates). c) Fractional enrichment of Reductive Carboxylation metabolites (Citrate m+5, Malate m+3, Fumarate m+3 and Aspartate m+3) from K562 WT and NIX KO cultured under 21%O_2 (N) or 0.5%O_2 (H) with medium containing $^{13}C_5$-Glutamine for 24 hours (n=3 technical replicates). Means and P-values in (a), (b) and (c) were calculated using one-way ANOVA with Dunnett's multiple comparisons test.

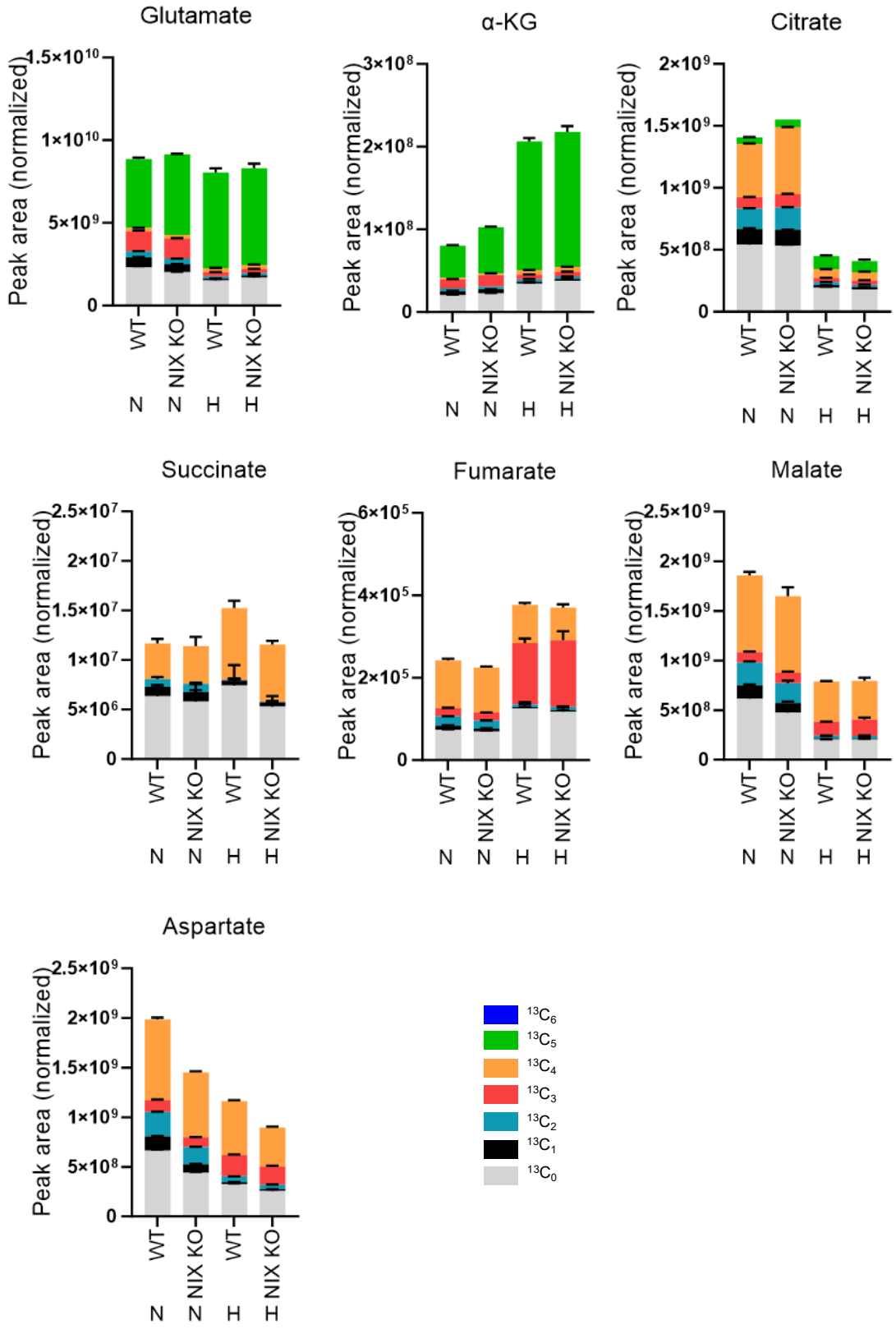

Figure 38: NIX does not sustain glutamine metabolism in CML cells under hypoxia. Isotopologue distribution of the indicated metabolites in K562 WT and NIX KO cells cultured under 21%O_2 (N) or 0.5%O_2 (H) with medium containing $^{13}C_5$-Glutamine for 24 hours (n=3 technical replicates).

4.8 Loss of BNIP3 in CML reduces xenograft formation

Given the antiproliferative and pro-apoptotic effect of BNIP3-mediated mitophagy inhibition in CML cells *in vitro*, we decided to investigate the effect of BNIP3 loss in an *in vivo* setting. KCL22 cells can form extramedullary tumours when transplanted via tail vein injection into immunocompromised mice. Therefore, we transplanted 4 million control and BNIP3 KO cells into NRGW[41] immunocompromised mice via tail vein injection and monitored mice for 12 weeks (schematic shown in figure 39a). Loss of BNIP3 reduced KCL22 tumour xenograft formation and resulted in significantly extended survival of mice when compared to mice transplanted with control WT cells (figure 39b). Furthermore, the tumour burden at experimental endpoint was significantly reduced in mice transplanted with BNIP3 KO KCL22 cells (figure 39c-d).

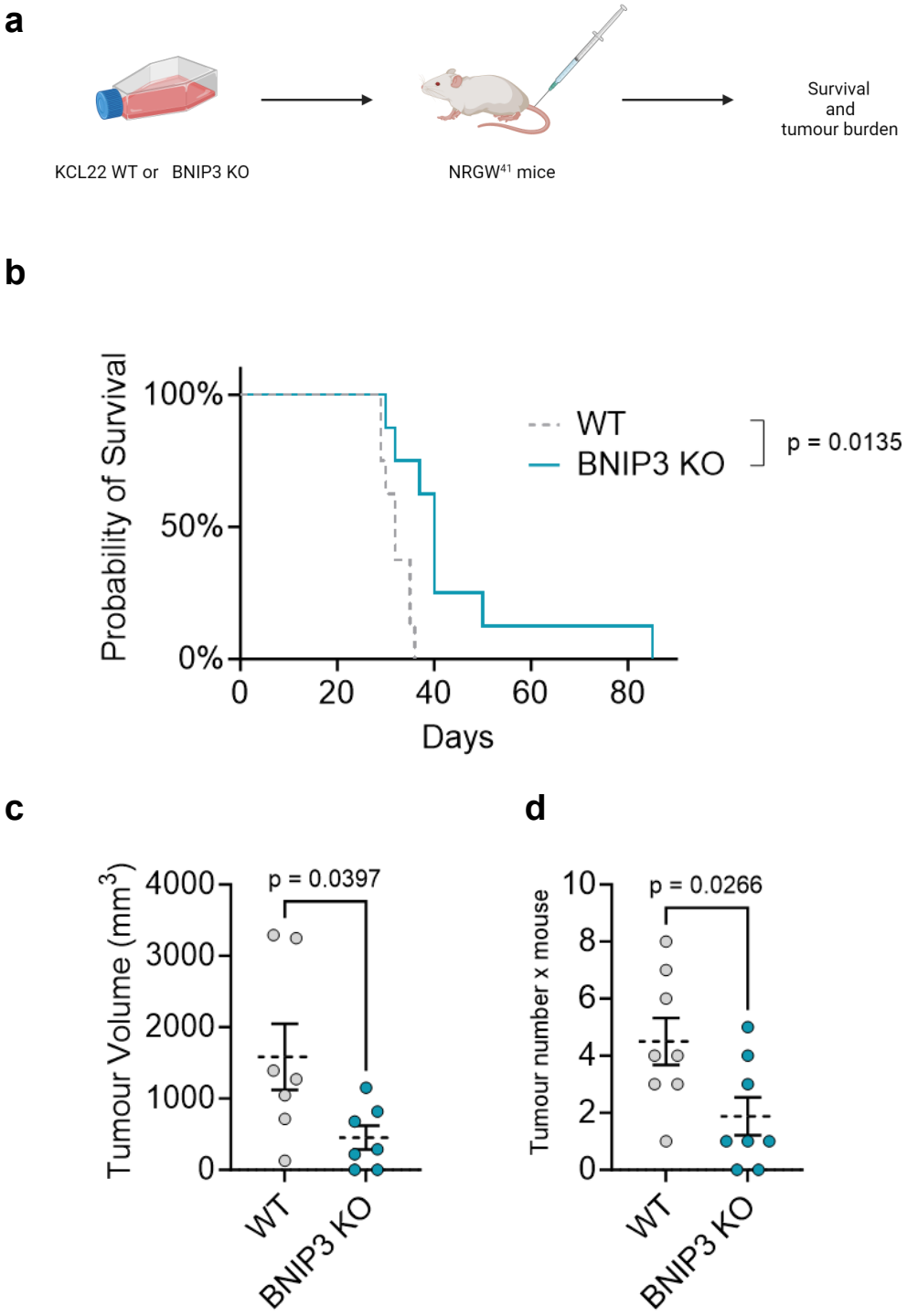

Figure 39: BNIP3 loss impairs xenograft capacity of CML cells. a) Schematic representing WT and BNIP3 KO KCL22 cells transplanted in NRGW[41] male and female mice via tail vein injection. b) Kaplan-Meier analysis comparing survival of mice transplanted with KCL22 WT and BNIP3 KO cells over 85 days. c) Burden of extramedullary tumours harvested from each mouse at experimental end point. P values were calculated using long-rank (Mantel-Cox) test. In (c) P values were calculated with a Mann-Whitney test.

4.9 BNIP3 loss inhibits hypoxia-induced erythroid differentiation

K562 cells can be used as an *in vitro* model to study erythropoiesis. Moreover, mitophagy plays an important role during erythropoiesis thanks to the removal of mitochondria. Therefore, we investigated if hypoxia-induced mitophagy would be involved in this process. Hypoxia is a well-known stimulus to induce erythropoiesis via promoting increased iron uptake and heme biosynthesis[308].

To study erythropoiesis, we used two erythroid markers: CD71 and glycophorin A (GlyA). CD71, also known as transferrin receptor protein 1 (TfR1) is a transmembrane glycoprotein involved in iron-import, while GlyA is sialo glycoprotein localised on the erythrocyte membrane.

Our results showed that hypoxia drives erythroid differentiation as indicated by the increase in the percentage of $CD71^+$ and $GlyA^+$ cells. However, BNIP3 and ATG7 loss significantly reduced the expression of erythroid markers under hypoxic conditions. These results suggested that BNIP3-mediated mitophagy is involved in the differentiation of K562 cells. Surprisingly, NIX deletion showed the opposite effect (as shown in figure 40a-b).

Recently it has been shown that iron/heme levels drive erythroid differentiation via mitophagy induction[309]. Therefore, we sought to investigate if hypoxia promotes the expression of heme-related genes in our model. As shown in figure 41a-c, analysis of publicly available dataset, revealed that hypoxia significantly triggers upregulation of the mitochondrial Mitoferrin-1 (SLC25A37) but not Mitoferrin-2 (SLC25A38). These are two homologous mitochondrial solute carriers mediating iron trafficking. Moreover, Mitoferrin-1 is involved in iron delivery in developing erythrocytes[310]. Our results suggest that Mitoferrin-1 mediated iron delivery in the mitochondria could be a requirement for K562 cells differentiation and perhaps hypoxia-induced mitophagy could play a role during the process. However, further experimental work would be needed to validate this hypothesis.

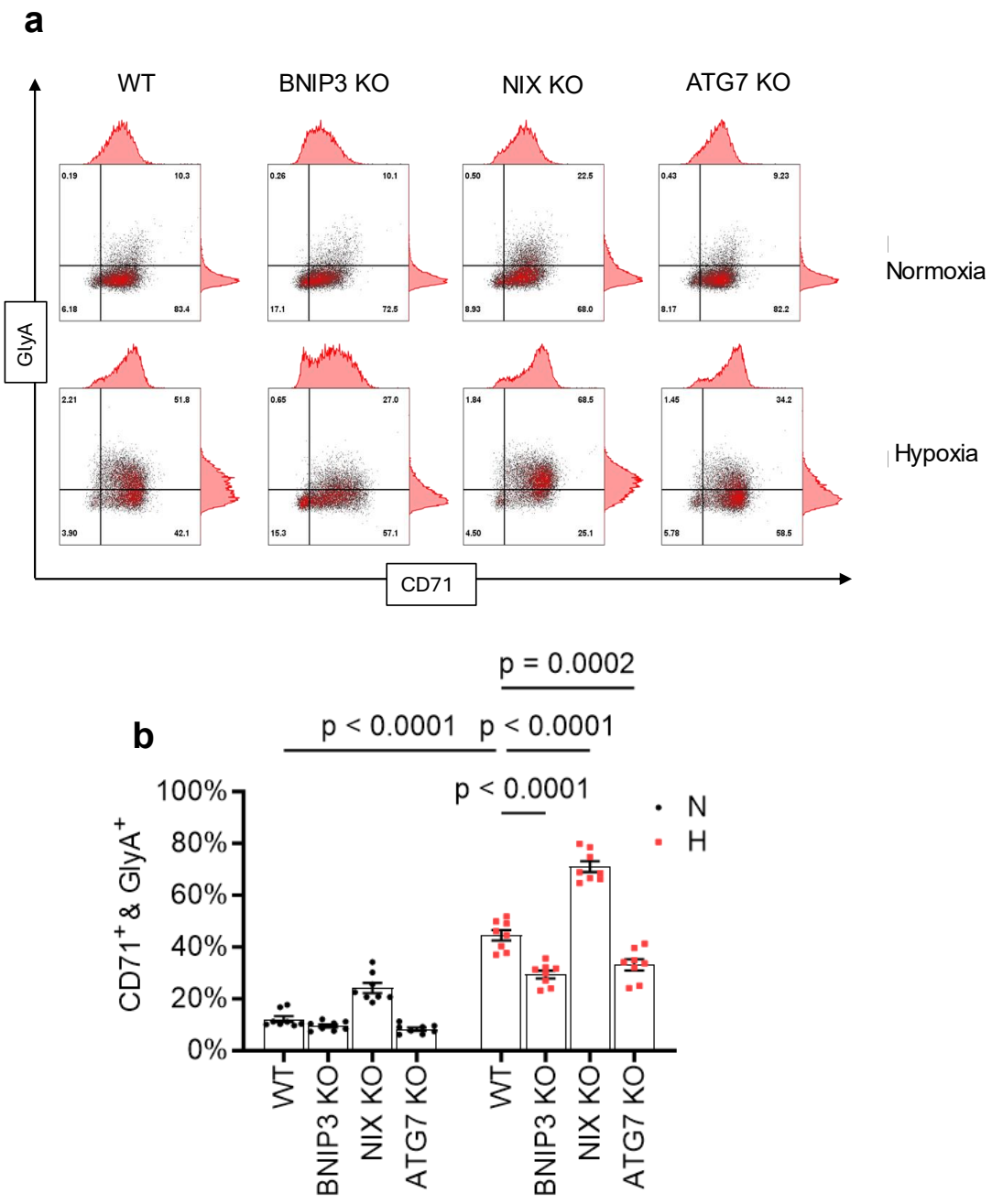

Figure 40: BNIP3 loss impairs hypoxia-induced erythroid differentiation. a) Flow cytometry plots showing expression of erythroid markers CD71 and Glycophorin A (GlyA) in WT and BNIP3, NIX or ATG7 deficient cells. b) percentage of $CD71^{+}GlyA^{+}$ of WT, BNIP3, NIX and ATG7 deficient K562 cells following 72 hours of exposure to 0.5%O_2 (hypoxia) or 21%O_2 (normoxia). Data were plotted as mean ± SEM of n=8 independent cultures. P-values were calculated with ordinary two-way ANOVA with Turkey's multiple comparison test.

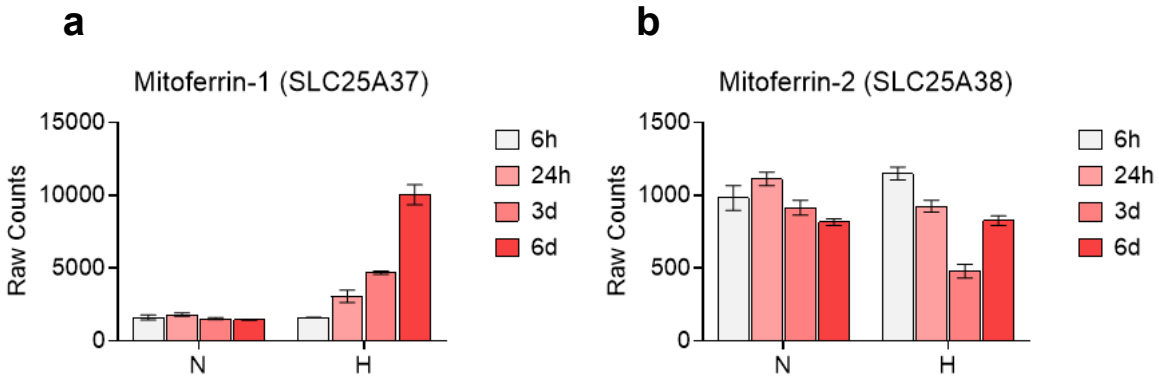

c

$1\%O_2$ vs $21\%O_2$ at 6 days

Gene	Log2FC	Adj.P val.
SLC25A37	2.786067	2.81E-211
SLC25A38	0.018744	0.920748

Figure 41: Hypoxia drives expression of Mitoferrin-1. Graph of raw counts of a) Mitoferrin-1 and b) Mitoferrin-2 of K562 cells exposed to $21\%O_2$ (N) or $1\%O_2$ (H) for 6 hours, 24hours, 3 days and 6 days.c) Table representing Log2FC (= Fold Change) and Adj.P val. (= Adjusted P-values) of SLC25A37 (Mitoferrin-1) or SLC25A38 (Mitoferrin-2) at 6 days of exposure to $1\%O_2$. Data in (a) and (b) were plotted as mean ±SD and are representative of n= 3 independent cultures. Data were taken from GEO: GSE144527. Log2FC and Adj. P val. Values were calculated in R using standard DESeq2 pipeline.

4.10 Discussion

In this chapter we aimed at determining the molecular mechanisms involved in the metabolic switch of CML cells under hypoxia with particular focus to their mitochondrial biology. Via analysis of an unpublished sc-RNA seq. data, we demonstrated that hypoxia reshapes the mitochondrial transcriptome of primitive CML primary cells ($CD34^{+}CD38^{-}CD90^{+}CD93^{+}$) promoting downregulation of most of the mitochondria genes, while inducing the expression of two HIF1α-dependent mitochondrial cargo-receptors: BNIP3 and BNIP3L/NIX. Furthermore, using publicly available data, we demonstrated that BNIP3 expression, but not NIX, is significantly enriched in LSCs versus HSCs. These findings are in line with the current literature demonstrating that cancer cells promote expression of mitophagy-related genes when exposed to low oxygen environment to adapt their metabolic activity.

Via analysis of another publicly available dataset (GSE48294), we also showed that TKI treatment under hypoxia does not affect expression of BNIP3 but significantly increases NIX mRNA levels at both 24 and 96 hours of treatment. However, whether Imatinib drives mitophagy via NIX activation remains to be discovered. Given that BNIP3 gene expression is significantly upregulated in LSCs and further increased upon exposure to hypoxia, these data suggest that BNIP3-mediated mitophagy might be involved in the restructuring of mitochondrial network and metabolism and hence promote survival and persistence of CML cells in the BM microenvironment.

Loss of BNIP3 resulted in increased mitochondrial mass, higher basal levels of mitochondrial ROS and both basal and maximal OCR due to impaired mitophagy flux. Moreover, BNIP3 silencing also resulted in impairment of mitochondrial turnover, given the observed increased accumulation of old mitochondria over time.

In addition, we investigated the metabolic changes upon genetic inhibition of receptor-mediated mitophagy and general autophagy upon exposure of CML cells to hypoxia. Analysis of metabolites amounts in the culture medium revealed that BNIP3 loss impaired glutamine uptake but increased glutamate secretion, while metabolomic analysis showed that BNIP3 KO had decreased intracellular $^{13}C_5$-glutamate levels possibly due to impairment of hypoxia-induced glutaminolysis and reductive glutamine carboxylation, as also suggested by lower α-KG/Citrate ratio and lower intracellular levels of metabolites related to glutamine reductive flux. However, despite the lower levels of glutaminolysis

shown in BNIP3 KO cells, yet BNIP3 KO cells maintain intracellular levels of glutamate (as shown in figure 34) and promote glutamate secretion (figure 31). Therefore, further investigation is needed.

Overall, the observed BNIP3- mediated metabolic rearrangements were not phenocopied by neither ATG7 nor NIX silencing. Altogether, our data suggest that BNIP3-mediated mitophagy is indispensable for CML cells allowing them to promptly adapt to the new metabolic needs under hypoxia via rewiring of their mitochondrial metabolic activity.

Given the antiproliferative effect of BNIP3 loss in CML cells mostly under low oxygen conditions, we investigated the role of BNIP3 loss in mediating the xenograft capacity of leukaemic cells. Since KCL22 cells can form extramedullary tumours when transplanted via tail vein injection into immunocompromised mice, we generated BNIP3 KO KCL22 cells and transplanted WT or BNIP3 KO cells into $NRGW^{41}$ mice. Interestingly, we discovered that BNIP3 ablation significantly impairs engraftment capacity of KCL22 cells, resulting in extended survival of transplanted mice. Moreover, we observed a significantly reduced tumour burden in mice transplanted with BNIP3 KO cells at experimental endpoint. Indeed, most of the mice transplanted with KCL22 BNIP3 KO cells contained few to no tumours, suggesting that loss of BNIP3 not only inhibits metabolic rewiring in CML cells but that also results in impaired tumorigenesis. The extramedullary tumours formed after KCL22 engraftment into immunocompromised mice behave as any other solid tumour, hence they have a hypoxic core. Therefore, the absence of BNIP3 and defective mitophagy might be required for the generation of structured solid tumours from KLC22 cells promoting rewired metabolic activity with a preferential utilization of glutamine to fuel mitochondrial metabolism.

However, the role of BNIP3 in cancer biology is controversial and context dependent. Indeed, higher BNIP3 expression levels can be linked to both good and bad prognosis in cancer patients. For example, in line with our results, BNIP3 loss impaired the growth and cell migration of melanoma cells due to defects in actin function in the cytoskeleton[311]. Again, in melanoma, BNIP3 promoted tumour growth via positive regulation of nuclear receptor coactivator 4 (NCOA4)-mediated ferritinophagy in order to promote HIF1α stabilization and induce glycolysis[312]. Conversely, Berardi et al showed that loss of BNIP3 promoted tumour cell growth and decreased latency in the setting of hepatocellular carcinoma, hence revealing a tumour-suppressing role of BNIP3-mediated mitophagy via regulation of lipid droplets turnover[313].

Lastly, we reported that hypoxia leads to increased levels of erythroid markers (CD71 and GlyA) in K562 cells. To commit to erythroid lineage, HSCs require glutamine uptake and active metabolism and start de novo nucleotide synthesis[314]. Therefore, the hypoxia-driven differentiation of K562 could be a result of increased glutamine uptake and metabolism, condition that we have previously shown. Moreover, hypoxia is a physiological stimulus to drive this differentiation process in the BM microenvironment and mitophagy might be involved in this process, since removal of mitochondria and nuclei represent essential steps of erythrocytes differentiation. Interestingly, it has been recently shown that removal of mitochondria during the late stages of murine red blood cell differentiation depends on levels of iron/heme. More precisely, heme can trigger the expression of GATA1 and, subsequently, induce mitophagy and remove mitochondria[315]. In line with these data, we observed higher expression levels of Mfn-1 (also known as SLC25A37) in K562 exposed to hypoxia after analysis of publicly available data. Mfn-1 is highly expressed in differentiating erythrocytes and is a mitochondrial specific iron transporter which plays a pivotal role in heme biosynthesis promoting the transport ferrous iron from the intermembrane space to the matrix. Moreover, our lab has recently observed that pharmacological inhibition of ULK1 could trigger oxidative-stress-driven differentiation of CML cells[295].

Therefore, we investigated if receptor-mediated mitophagy could be involved in erythroid differentiation in K562 cells. Surprisingly, BNIP3 KO and ATG7 KO cells showed significantly lower expression of erythroid markers when compared to WT cells, while NIX depletion led to higher erythroid markers expression. These preliminary results suggest that hypoxia could drive commitment of K562 cells to the erythroid line, triggering glutamine uptake and glutaminolysis to sustain heme biosynthesis and, subsequently, drive BNIP3- induced mitophagy to promote clearance of mitochondria. However, more experiments would be necessary to demonstrate the link between hypoxia, heme/iron homeostasis and receptor-mediated mitophagy in both K562 and primary CML samples.

Chapter 5 Conclusions and future prospectives

Overall, the aim of this thesis was to investigate the role of hypoxia in CML metabolism, which closely resemble the oxygen availability found in the BM microenvironment. Moreover, we explored hypoxia-induced molecular mechanisms in CML cells. Here, we will discuss our findings considering the current literature, future directions and potential applications of this project.

5.1 Hypoxia and CML cells metabolism

As previously discussed, CML LSCs have been shown to be highly dependent on OXPHOS due to their increased mitochondrial mass and metabolic activity when compared to HSCs[316]. Moreover, results from our lab have previously provided evidence that CML LSCs exploit their increased oxidative anaplerotic metabolism to support aspartate biosynthesis, which directly contributes to nucleotide biosynthesis, and fosters their proliferation and survival when compared to HSCs[316]. Interestingly, pyruvate anaplerosis and purine biosynthesis are targetable vulnerabilities in persistent CML LSCs[265,317].

Hypoxia represents a crucial component of the BM microenvironment, sustains the proper development of HSCs and directs cell-fate decisions via modulation of their mitochondrial metabolism[318]. Moreover, CML LSCs have developed strategies to survive in the hypoxic BM despite inhibition of BCR::ABL1 by TKIs[269,319], suggesting the existence of alternative hypoxia-driven mechanisms involved in their persistence. However, although targeting CML LSCs with HIFs inhibitors has been explored as a possible therapeutic approach[254,319–321], more investigation is required to identify more CML-specific vulnerabilities in low oxygen environments.

One of the effects of hypoxia is induction of metabolic rewiring. Therefore, cancer cells exposed to low oxygen drastically reduce oxidative mitochondrial metabolism, and favour glycolysis and reductive metabolism to sustain their energy demand and proliferation[56–58]. Moreover, another important aspect of hypoxia-induced metabolic changes is represented by the exchange in carbon sources. Indeed, while glucose is the main carbon source to fuel mitochondrial metabolism and OXPHOS in many cancers in highly oxygenated environments, hypoxic cancer cells slow glucose-derived mitochondrial pyruvate uptake down and preferentially increases glutamine uptake, glutaminolysis and glutamine reductive carboxylation[56–58]. In this work we observed that both short-term and long-term

oxygen restriction promotes transcriptional changes in metabolic genes. Moreover, via metabolomics studies, we discovered that CML cells rewire their mitochondrial metabolic activity when exposed to hypoxia. While glucose is mostly used for lactate production and secretion, hypoxic CML cells increase glutamine uptake and use it to fuel the TCA cycle via both oxidative and reductive metabolism. Furthermore, we observed accumulation of fumarate and succinate in CML cells exposed to hypoxia. The accumulation of succinate could be due to reverse activity of SDH, which has been previously shown to occur in conditions that inhibit mitochondrial respiration (including hypoxia). Indeed, fumarate can act as a terminal electron acceptor in the ETC and replace oxygen[322]. However, this does not seem to happen in our experimental setting. In fact, the accumulation of fumarate is to be probably due to the increased glutamine reductive carboxylation, while succinate accumulation could be a consequence of increased glutaminolysis.

However, it would be interesting to assess if CML LSCs use glutamine reductive carboxylation to promote lipid synthesis under hypoxia, as it has been previously shown for other cancers[284].

While we managed to show that $CD34^+$ bulk patient-derived cells reduce glucose oxidation in hypoxia, it would be interesting to study this in more primitive populations, such as $CD34^+CD38^-$ or *in vivo* using CML relevant mouse models. Moreover, it would be of interest to confirm the hypoxia-induced increased glutaminolysis and reductive carboxylation in more clinically relevant models as well.

Intriguingly, we observed that inhibition of GLS1, but not IDH2, significantly induces arrest in cell proliferation and cell death in hypoxic CML cells and that α-KG can be used to rescue both the anti-proliferative and pro-apoptotic effect of CB-839. More studies are required to observe if inhibition of GLS is detrimental for CML LSCs in a more physiological context as it has been demonstrated in the context of AML[286].

Another topic of interest would be to assess the impact of TKI therapy on the hypoxic metabolic rewiring induced in CML LSCs. On this note, it has been shown that Imatinib treatment does not eradicate CML LSCs despite inhibition of BCR::ABL1 downstream signalling, and that Imatinib and hypoxia drive the expression of different sets of genes[269]. Finally, although short-term TKI treatment *in vivo* can inhibit glycolysis, glutaminolysis, the TCA cycle, and OXPHOS, prolonged TKI treatment enriches for metabolically reprogrammed subpopulations overexpressing HIF1[319]. Therefore, the current literature suggests that TKI treatment low effectiveness in eradicating CML LSCs in the hypoxic BM microenvironment could be due to their metabolic reprogramming. Nevertheless, no

one has so far shown if the result of this metabolic rewiring in TKI-resistant CML LSCs is due to increased oxidative and reductive glutamine metabolism.

5.2 Hypoxic CML cells use receptor-mediated mitophagy to regulate mitochondrial turnover

We found that the receptor-mediated mitophagy genes BNIP3 and BNIP3L (NIX) were upregulated in LSCs ($CD34^+CD38^-$) compared to non-CML counterparts. Of clinical relevance, analysis of a publicly available microarray dataset of $CD34^+$ cells exposed to hypoxia for 24 or 96 hours and treated or not with Imatinib, revealed that expression of NIX, but not BNIP3, significantly changes following Imatinib treatment, suggesting that the activation of NIX-mediated mitophagy might be induced following inhibition of BCR::ABL1 downstream signaling, while BNIP3 activation is mostly induced by low oxygen levels.

Previous research from our lab has shown that TKI treatment triggers autophagy[323–326]. Indeed, CML LSCs use autophagy to regulate their metabolic activity as KD of ATG7 (critical component of the LC3 conjugation system) promotes increased mitochondrial metabolism with consequent ROS accumulation and differentiation towards the erythroid lineage[327]. Furthermore, targeting autophagy either with general autophagy inhibitors or using a more selective ULK1 (main component of the initiation step of the autophagy process) inhibitor has been shown to sensitise CML LSCs to TKI treatment, leading to their eradication[328–332]. Therefore, it would be interesting to assess if and how TKI treatment could lead to mitophagy via NIX or other mechanisms to induce mitochondrial turnover and acquire a TKI-resistant metabolic profile. This would also lead to the identification of more selective and potential new druggable targets for the treatment of stem cell driven leukaemias.

However, in this work we show that BNIP3 is required for the complete mitochondrial turnover in CML cell lines even in conditions of atmospheric oxygen levels. Indeed, KO of BNIP3 leads to the accumulation of mature mitochondria with consequent increase in mitochondrial respiration and buildup of mitochondrial ROS. These results suggest that BNIP3 plays a critical role in mitochondrial turnover even at basal culture conditions in CML cells. One possible explanation would be that CML cells have to constantly remove dysfunctional organelles to promptly meet their metabolic needs.

Another interesting topic is the study of BNIP3 and other cargo receptors with other critical proteins of the autophagy machinery. Although it was initially reported that BNIP3 degradation is mediated by ULK1-dependent autophagy after AMPK activation[333], more recently, it has been reported that BNIP3 protein stability and activity could be regulated by direct interaction with ULK1. Indeed, according to Poole *et al*., during hypoxia, ULK1

phosphorylates BNIP3 to protect it from proteasomal degradation, that would happen in normoxic conditions[200]. However, in the previously cited work, only a pharmacological approach was used to inhibit ULK1 kinase activity, while a genetic approach, i.e. KD or KO of ULK1 would be ideal in order to rule out possible drug related off-targets effects. In this study we induced conditional ULK1 KD using the SMARTvector lentiviral technology to observe that ULK1 KD leads to reduction of BNIP3 protein levels in hypoxia. Nevertheless, further experimental results are required to assess more intimate protein-protein interactions between BNIP3 and ULK1 or other kinases. JNK1/2 are kinases that have been reported to promote BNIP3 protein stability and, hence, induce mitophagy under hypoxia[199]. Their phosphorylation activity has been observed also in relation to other BH3-only protein subfamily, such as BH3 interacting-domain death agonist (Bid)[334]. These research articles suggest that there might be different kinases promoting BNIP3 activity and, perhaps, this activation could happen as a multistep or multitemporal process. On this note, for example, NIX was shown to regulate temporal controlled mitochondrial remodelling during the conversion of human embryonic stem cells to induced neurons to finally support metabolic rewiring and OXPHOS[335].

Additionally, we also explored the role of mitophagy in promoting removal of mitochondria during erythroid differentiation. Assessment of the levels of erythroid differentiation markers CD71 and GlyA via flow cytometry, showed us that genetic ablation of BNIP3 and ATG7 but, surprisingly not NIX, significantly reduced the hypoxia-induced erythroid differentiation when compared to WT K562 cells. Moreover, via analysis of a publicly available RNA seq. dataset (GSE144527[336]) of K562 cells exposed to hypoxia, we also observed overexpression of solute carrier family 25 member 37 (SLC25A37/Mitoferrin-1), which is a mitochondrial iron transporter involved in iron delivery in mitochondria during erythrocytes differentiation. Therefore, it would be of interest to assess if BNIP3-induced mitophagy under hypoxia is involved in iron import during this differentiation step.

5.3 BNIP3-mediated mitophagy is required for glutamine anaplerosis and reductive carboxylation in hypoxia

The investigation of the metabolic role of BNIP3 in hypoxic microenvironments is receiving more attention within the scientific community lately. For instance, it was recently reported that BNIP3 loss in nucleus pulposus cells of the intervertebral disc caused significant changes in glycolysis as shown by reduced lactate and ATP production, while glucose derived carbons were redirected to the pentose phosphate pathway and TCA due to increased mitochondrial mass. However, no significant changes in glutamine metabolism were shown in BNIP3 KD cells[337]. Differently, in hepatocellular carcinoma, BNIP3 plays a role as tumour suppressor by promoting the turnover of lipid droplet in an autophagy-dependent manner[209]. Therefore, the metabolic role of BNIP3 is both tissue and pathology related.

Here, via extensive metabolic analysis of K562 cells following genetic inhibition of this mitochondrial cargo receptor, we propose a novel role of BNIP3-dependnet mitophagy in promoting glutamine anaplerosis and reductive carboxylation in CML cells during their adaption to hypoxia. However, microarray data analysis revealed that CML LSCs express higher levels of BNIP3, but not NIX, compared to HSCs even at normal oxygen levels. Given that LSCs also showed increased mitochondrial mass and activity, the higher BNIP3 expression and its role in mitochondrial turnover could suggest that these cells exploit the cargo-receptor to support their metabolic profile via removal of non-functioning mitochondria. However, this hypothesis would need further experimental validation.

Our *in vivo* findings suggest that genetic inhibition of BNIP3-mediated mitophagy is sufficient to inhibit tumorigenesis. These results are in line with previous work from our lab showing that inhibition of autophagy reduces CML growth in transplanted mice[327,328,330,331].

However, it is important to note that NRGW[41] mice transplanted with KCL22 do not develop CML. Therefore, while transplantation with KCL22 BNIP3 KO cells proved the importance of BNIP3-mediated mitophagy in survival and tumour formation in an *in vivo* setting, it does not provide evidence of the importance of BNIP3 mediated mitophagy during and following leukaemia development. To study the role of BNIP3 in leukaemia initiation the SCLtTA/BCR::ABL1 double transgenic model (DTG) could be used. In this model the trans-activator protein tTA is under the control of a 3' enhancer of the murine stem cell leukaemia (SCL) gene and crossed with the TRE-BCR::ABL1 mouse resulting in the generation of the SCLtTA/BCR::ABL1 DTG mouse[278]. Moreover, the effect of BNIP3

on CML development and persistence could be explored via generation of a more complex mouse model, i.e. crossing the SCLtTA/BCR::ABL1 model with a conditional BNIP3 KO mouse model.

An additional limitation to investigate the impact of BNIP3-dependent mitophagy inhibition *in vivo* is that there are not clinically available BNIP3 inhibitors yet, highlighting the need of identifying or developing new and specific inhibitors targeting BNIP3, or its interaction with other key autophagy modulators.

Overall, data generated from this work indicate a novel role of BNIP3-mediated mitophagy in metabolic reprogramming and sustaining the survival of CML cells in the hypoxic microenvironment by promoting reductive carboxylation. To sum up, a schematic representing a summary of our findings is depicted in figure 42.

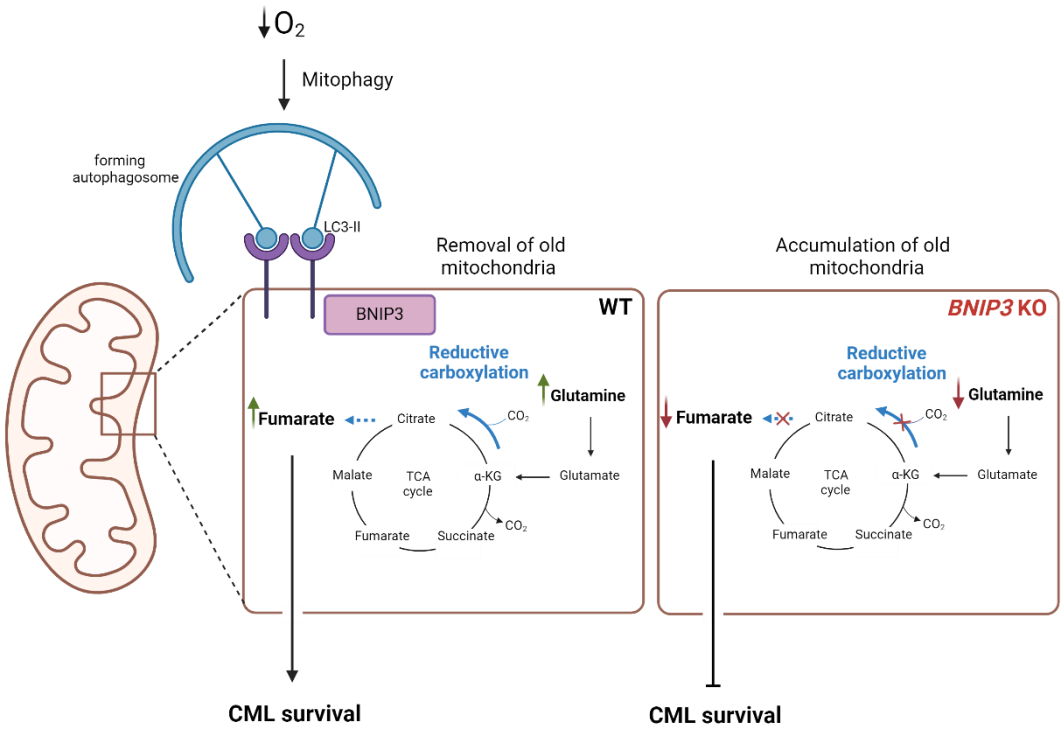

Figure 42 The impact of BNIP3 ablation in hypoxic CML cells.

Chapter 6 Appendix

6.1 CML proteome is affected by hypoxia and BNIP3 expression.

To better understand how BNIP3 expression supports CML cells growth and survival in low oxygen conditions, we explored CML cells proteome. Of note, we are still in the process of analysing and interpreting the results of this experiment as data were provided during the thesis writing.

In brief, BNIP3 KO and WT K562 cells were cultured under hypoxia and normoxia for 48 hours and subsequently processed for protein extraction. Protein containing lysates were then used for mass spectrometry exploiting a tandem mass tag (TMT) workflow. TMT is a quantitative proteomics assay that provides accurate and high-throughput comparisons of up to 18 samples in one mass spectrometry assay.

Principal component analysis (PCA) revealed that all the cells were grouped not only according to oxygen levels but also according BNIP3 expression (figure 43a). These data suggest that the CML cell responses to both hypoxia and BNIP3 expression is largely homogeneous within each experimental arm. Furthermore, the analysis revealed nine independent clusters (figure 43b). Interestingly, cluster 8 identified 48 marker proteins (figure 43c) whose expression depends on both low oxygen levels and BNIP3 expression. Indeed, while WT cells overexpress these proteins when exposed to hypoxia, the same proteins are lowly expressed in hypoxic BNIP3 KO cells. Moreover, BNIP3 depletion significantly downregulates the expression of proteins belonging to cluster 8 in normoxia.

Among this cluster we identified adenylate kinase 4 (AK4), which is expressed in the mitochondrial matrix[338] as being highly expressed in hypoxic WT K562 but not in BNIP3 KO cells. AK4 is a nucleoside monophosphate kinase that catalyses the phosphorylation of nucleosides using mainly ATP or GTP as phosphate donors[338]. Interestingly, in the context of lung adenocarcinoma, it was shown that AK4 expression is related to worse patients' survival. Moreover, AK4 expression promotes HIF1α stability under hypoxia due to increased ROS levels and induces epithelial-to-mesenchymal transition; therefore, AK4 could be used as a biomarker of metastasis in lung cancer[339]. Furthermore, AK4 was also shown to increase breast cancer cells resistance to tamoxifen in a mechanism involving ROS-mediated p38 MAPK stabilization and inhibition of mitochondrial apoptosis[340].

Therefore, it would be of interest to investigate the role of AK4 in CML and study its possible link to BNIP3 and hypoxia-induced mitophagy.

Another interesting protein whose expression was upregulated in WT cells but lowly expressed in BNIP3 KO cells respectively, is a Golgi-associated protein named glioma pathogenesis related 2 (GLIPR2). GLIPR2 has been described as a negative regulator of autophagy[341]. However, the exact role of GLIPR2 in cancer settings has not been thoroughly investigated yet. Therefore, further analysis would be necessary to validate its role in CML cells and BNIP3-induced mitophagy in hypoxia.

With time (beyond the time of this PhD project), we will further investigate the role of the most promising proteins belonging to cluster 8 and other clusters in the future as we believe that this could lead the identification of possible new mechanisms to better explain the role of BNIP3-dependent mitophagy in CML cells.

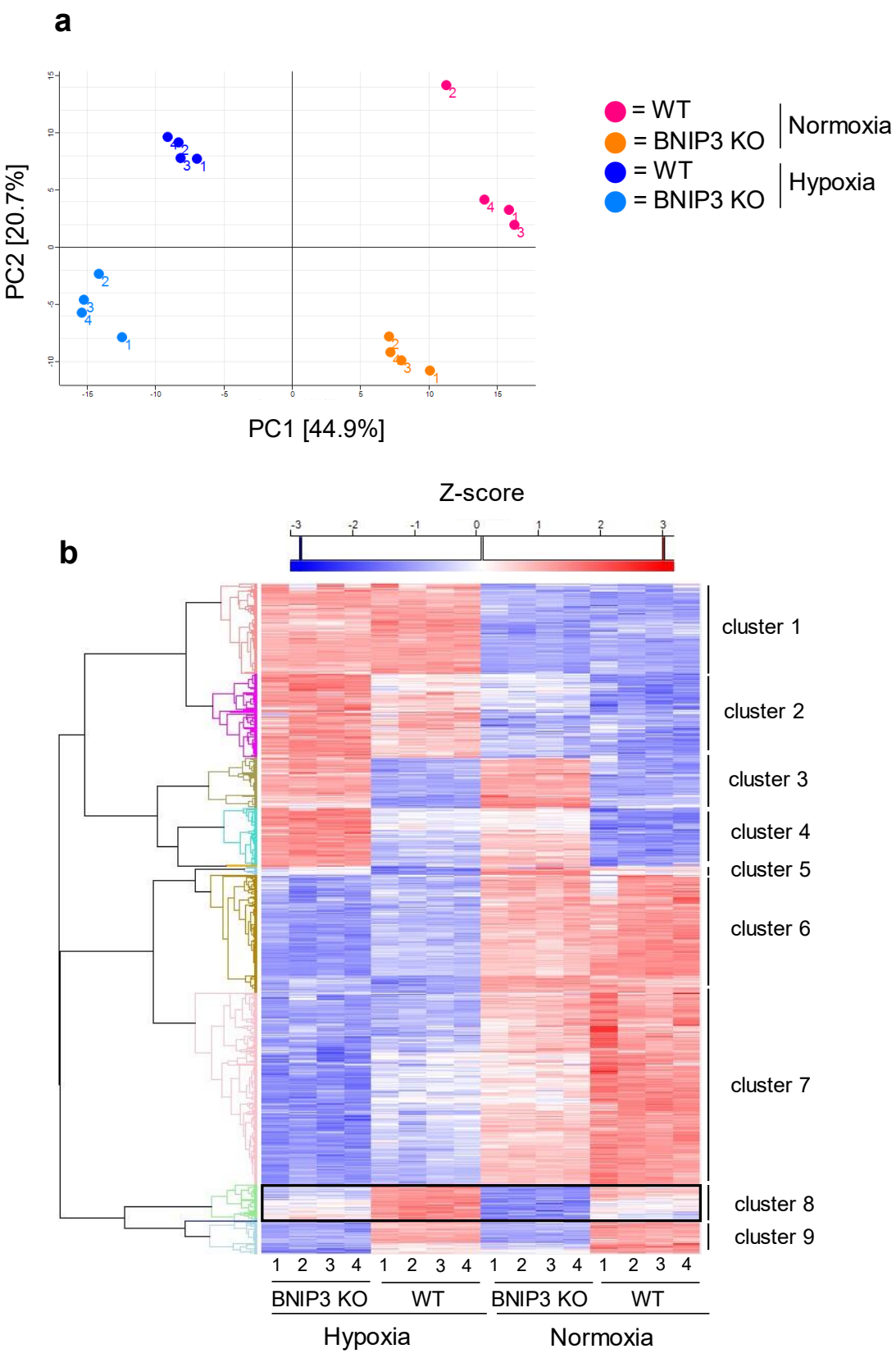
a
PC2 [20.7%]
PC1 [44.9%]
= WT
= BNIP3 KO
Normoxia
= WT
= BNIP3 KO
Hypoxia
b
Z-score
-3 -2 -1 0 1 2 3
cluster 1
cluster 2
cluster 3
cluster 4
cluster 5
cluster 6
cluster 7
cluster 8
cluster 9
1 2 3 4 1 2 3 4 1 2 3 4 1 2 3 4
BNIP3 KO
WT
BNIP3 KO
WT
Hypoxia
Normoxia

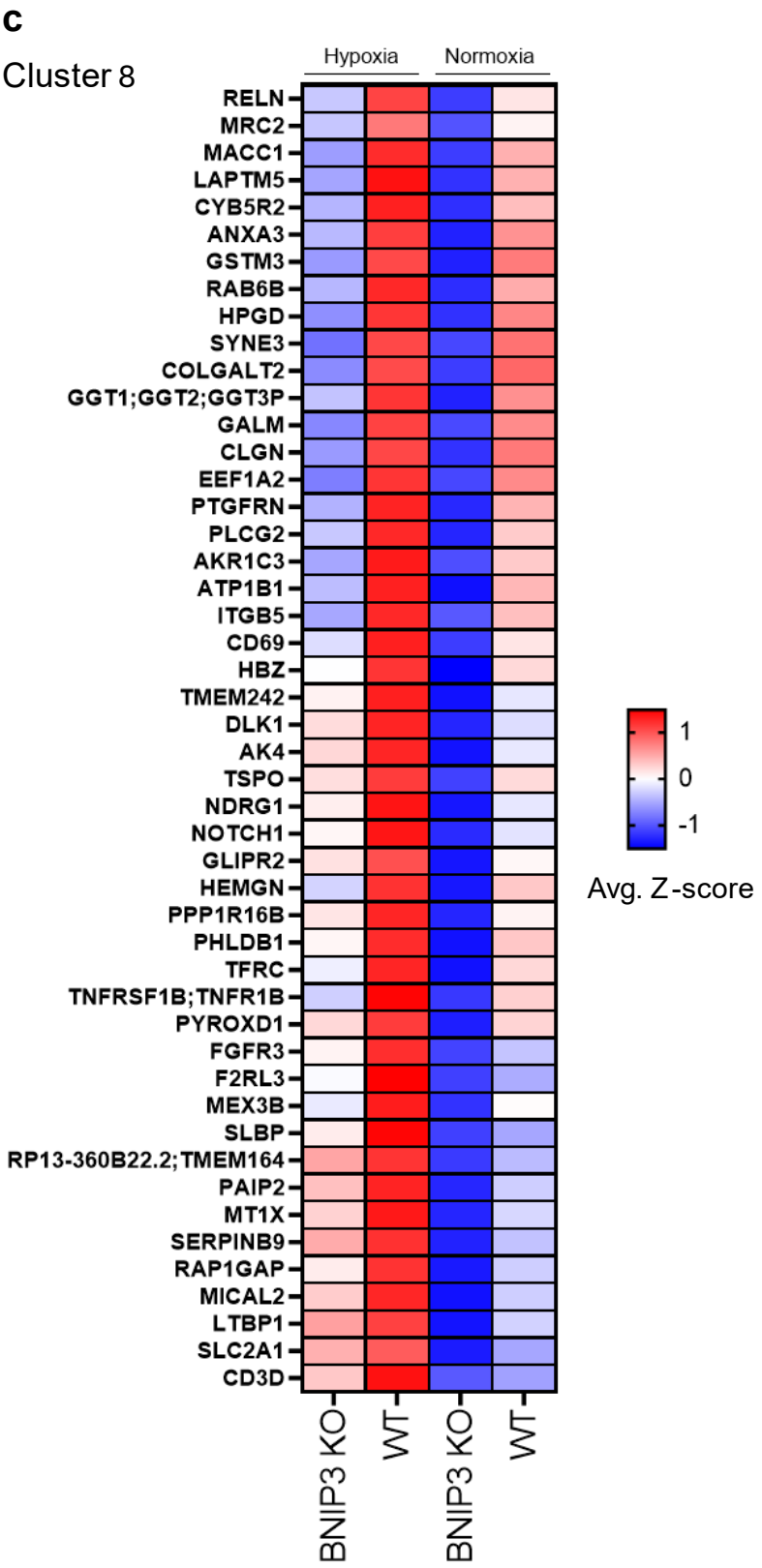

Figure 43 Preliminary TMT proteomics results in K562 cells exposed to hypoxia. a) PCA plot of BNIP3 KO and WT K562 exposed to normoxia (21%O_2) and hypoxia (0.5%O_2) for 48 h. b) Heatmap representing samples, clustering and marker proteins driving clustering. c) Heatmap representing proteins belonging to cluster 8.

List of References

1. Morrison, S. J., Uchida, N. & Weissman, I. L. THE BIOLOGY OF HEMATOPOIETIC STEM CELLS. *Annu. Rev. Cell Dev. Biol* **11**, 35–71 (1995).

2. Lorenz, E., Uphoff, D., Reid, T. R. & Shelton, E. Modification of irradiation injury in mice and guinea pigs by bone marrow injections. *J Natl Cancer Inst* **12**, 197–201 (1951).

3. Jacobson, L. O., Simmons, E. L., Marks, E. K. & Eldredge, J. H. Recovery from Radiation Injury. *Science (1979)* **113**, 510–511 (1951).

4. Till, J. E. & McCulloch, E. A. A Direct Measurement of the Radiation Sensitivity of Normal Mouse Bone Marrow Cells. *Radiat Res* **14**, 213–222 (1961).

5. BECKER, A. J., McCULLOCH, E. A. & TILL, J. E. Cytological Demonstration of the Clonal Nature of Spleen Colonies Derived from Transplanted Mouse Marrow Cells. *Nature* **197**, 452–454 (1963).

6. Muller-Sieburg, C. E., Whitlock, C. A. & Weissman, I. L. Isolation of two early B lymphocyte progenitors from mouse marrow: A committed Pre-Pre-B cell and a clonogenic Thy-1lo hematopoietic stem cell. *Cell* **44**, 653–662 (1986).

7. Ikuta, K. & Weissman, I. L. Evidence that hematopoietic stem cells express mouse c-kit but do not depend on steel factor for their generation. *Proc Natl Acad Sci U S A* **89**, 1502–1506 (1992).

8. Spangrude, G. J., Heimfeld, S. & Weissman, I. L. Purification and Characterization of Mouse Hematopoietic Stem Cells. *Science (1979)* **241**, 58–62 (1988).

9. Morrison, S. J. & Weissman, I. L. The long-term repopulating subset of hematopoietic stem cells is deterministic and isolatable by phenotype. *Immunity* **1**, 661–673 (1994).

10. Ogawa, M. *et al.* Expression and function of c-kit in hemopoietic progenitor cells. *Journal of Experimental Medicine* **174**, 63–71 (1991).

11. Osawa, M., Hanada, K., Hamada, H. & Nakauchi, H. Long-Term Lymphohematopoietic Reconstitution by a Single CD34-Low/Negative Hematopoietic Stem Cell. *Science (1979)* **273**, 242–245 (1996).

12. Christensen, J. L. & Weissman, I. L. Flk-2 is a marker in hematopoietic stem cell differentiation: A simple method to isolate long-term stem cells. *Proc Natl Acad Sci U S A* **98**, 14541–14546 (2001).

13. Smith, L. G., Weissman, I. L. & Heimfeld, S. Clonal analysis of hematopoietic stem-cell differentiation in vivo. *Proceedings of the National Academy of Sciences* **88**, 2788–2792 (1991).

14. Yang, L. *et al.* Identification of Lin–Sca1+kit+CD34+Flt3– short-term hematopoietic stem cells capable of rapidly reconstituting and rescuing myeloablated transplant recipients. *Blood* **105**, 2717–2723 (2005).

15. Morrison, S. J., Wandycz, A. M., Hemmati, H. D., Wright, D. E. & Weissman, I. L. Identification of a lineage of multipotent hematopoietic progenitors. *Development* **124**, 1929–1939 (1997).

16. Zhang, Y., Gao, S., Xia, J. & Liu, F. Special Issue: Stem Cell Biology Hematopoietic Hierarchy-An Updated Roadmap. (2018) doi:10.1016/j.tcb.2018.06.001.

17. Kondo, M., Weissman, I. L. & Akashi, K. Identification of Clonogenic Common Lymphoid Progenitors in Mouse Bone Marrow. *Cell* **91**, 661–672 (1997).

18. Na Nakorn, T., Traver, D., Weissman, I. L. & Akashi, K. Myeloerythroid-restricted progenitors are sufficient to confer radioprotection and provide the majority of day 8 CFU-S. *Journal of Clinical Investigation* **109**, 1579–1585 (2002).

19. Catlin, S. N., Busque, L., Gale, R. E., Guttorp, P. & Abkowitz, J. L. The replication rate of human hematopoietic stem cells in vivo. *Blood* **117**, 4460–4466 (2011).

20. Adolfsson, J. *et al.* Upregulation of Flt3 Expression within the Bone Marrow Lin−Sca1+c-kit+ Stem Cell Compartment Is Accompanied by Loss of Self-Renewal Capacity. *Immunity* **15**, 659–669 (2001).

21. Forsberg, E. C., Serwold, T., Kogan, S., Weissman, I. L. & Passegué, E. New Evidence Supporting Megakaryocyte-Erythrocyte Potential of Flk2/Flt3+ Multipotent Hematopoietic Progenitors. *Cell* **126**, 415–426 (2006).

22. Anjos-Afonso, F. *et al.* CD34− Cells at the Apex of the Human Hematopoietic Stem Cell Hierarchy Have Distinctive Cellular and Molecular Signatures. *Cell Stem Cell* **13**, 161–174 (2013).

23. Link, H. *et al.* Transplantation of allogeneic CD34+ blood cells. *Blood* **87**, 4903–4909 (1996).

24. Terstappen, L. W. M. M., Huang, S., Safford, M., Lansdorp, P. M. & Loken, M. R. Sequential Generations of Hematopoietic Colonies Derived From Single Nonlineage-Committed CD34+CD38- Progenitor Cells. *Blood* **77**, 1218–1227 (1991).

25. Bernitz, J. M., Kim, H. S., MacArthur, B., Sieburg, H. & Moore, K. Hematopoietic Stem Cells Count and Remember Self-Renewal Divisions. *Cell* **167**, 1296-1309.e10 (2016).

26. Crisan, M. & Dzierzak, E. The many faces of hematopoietic stem cell heterogeneity. *Development* **143**, 4571–4581 (2016).

27. Nakamura-Ishizu, A., Ito, K. & Suda, T. Hematopoietic Stem Cell Metabolism during Development and Aging. *Dev Cell* **54**, 239–255 (2020).

28. Cunningham, J. T. *et al.* mTOR controls mitochondrial oxidative function through a YY1–PGC-1α transcriptional complex. *Nature* **450**, 736–740 (2007).

29. Simsek, T. *et al.* The Distinct Metabolic Profile of Hematopoietic Stem Cells Reflects Their Location in a Hypoxic Niche. *Cell Stem Cell* **7**, 380–390 (2010).

30. Vannini, N. *et al.* Specification of haematopoietic stem cell fate via modulation of mitochondrial activity. *Nat Commun* **7**, 13125 (2016).

31. Spencer, J. A. *et al.* Direct measurement of local oxygen concentration in the bone marrow of live animals. (2014) doi:10.1038/nature13034.

32. Takubo, K. *et al.* Regulation of the HIF-1α Level Is Essential for Hematopoietic Stem Cells. *Cell Stem Cell* **7**, 391–402 (2010).

33. Suda, T., Takubo, K. & Semenza, G. L. Metabolic Regulation of Hematopoietic Stem Cells in the Hypoxic Niche. *Cell Stem Cell* **9**, 298–310 (2011).

34. Vukovic, M. *et al.* Adult hematopoietic stem cells lacking Hif-1α self-renew normally. *Blood* **127**, 2841–2846 (2016).

35. Sommerkamp, P. *et al.* Differential Alternative Polyadenylation Landscapes Mediate Hematopoietic Stem Cell Activation and Regulate Glutamine Metabolism. *Cell Stem Cell* **26**, 722-738.e7 (2020).

36. Ito, K. *et al.* A PML–PPAR-δ pathway for fatty acid oxidation regulates hematopoietic stem cell maintenance. *Nat Med* **18**, 1350–1358 (2012).

37. Jang, Y.-Y. & Sharkis, S. J. A low level of reactive oxygen species selects for primitive hematopoietic stem cells that may reside in the low-oxygenic niche. *Blood* **110**, 3056–3063 (2007).

38. Bigarella, C. L., Liang, R. & Ghaffari, S. Stem cells and the impact of ROS signaling. *Development* **141**, 4206–4218 (2014).

39. Mizushima, N. A brief history of autophagy from cell biology to physiology and disease. *Nature Cell Biology* vol. 20 521–527 Preprint at https://doi.org/10.1038/s41556-018-0092-5 (2018).

40. Mizushima, N. & Komatsu, M. Autophagy: Renovation of Cells and Tissues. *Cell* **147**, 728–741 (2011).

41. Ho, T. T. *et al.* Autophagy maintains the metabolism and function of young and old stem cells. *Nature* **543**, 205–210 (2017).

42. Mortensen, M. *et al.* The autophagy protein Atg7 is essential for hematopoietic stem cell maintenance. *Journal of Experimental Medicine* **208**, 455–467 (2011).

43. Ho, T. T. *et al.* Autophagy maintains the metabolism and function of young and old stem cells. *Nature* **543**, 205–210 (2017).

44. Liu, Y. *et al.* Autophagy regulates the maturation of hematopoietic precursors in the embryo. *Nat Commun* **15**, 2255 (2024).

45. Joshi, A. & Kundu, M. Mitophagy in hematopoietic stem cells. *Autophagy 1737 Autophagy* **9**, 1737–1749 (2013).

46. Hu, M. *et al.* Transcription factor Nkx2-3 maintains the self-renewal of hematopoietic stem cells by regulating mitophagy. (1907) doi:10.1038/s41375-023-01907-y.

47. Ito, K. *et al.* Self-renewal of a purified Tie2+ hematopoietic stem cell population relies on mitochondrial clearance. *Science (1979)* **354**, 1156–1160 (2016).

48. Murakami, K. *et al.* OGT Regulates Hematopoietic Stem Cell Maintenance via PINK1-Dependent Mitophagy. *Cell Rep* **34**, 108579 (2021).

49. Berg, J. M., Tymoczko, J. L., Gatto, G. J., Kate, P. & Parker, A. *Biochemestry 8th Edition*.

50. Martínez-Reyes, I. & Chandel, N. S. Mitochondrial TCA cycle metabolites control physiology and disease. *Nature Communications 2020 11:1* **11**, 1–11 (2020).

51. Dimroth, P., Kaim, G. & Matthey, U. Crucial Role of the Membrane Potential for ATP Synthesis by F1Fo ATP Synthases. *Journal of Experimental Biology* **203**, 51–59 (2000).

52. Mitchell, P. & Moyle, J. Chemiosmotic Hypothesis of Oxidative Phosphorylation. *Nature 1967 213:5072* **213**, 137–139 (1967).

53. Eniafe, J. & Jiang, S. The functional roles of TCA cycle metabolites in cancer. *Oncogene 2021 40:19* **40**, 3351–3363 (2021).

54. Semenza, G. L. Hypoxia-Inducible Factors in Physiology and Medicine. *Cell* **148**, 399–408 (2012).

55. Yuan, X., Ruan, W., Bobrow, B., Carmeliet, P. & Eltzschig, H. K. nature reviews drug discovery Targeting hypoxia-inducible factors: therapeutic opportunities and challenges. *Nature Reviews Drug Discovery* | **23**, 175–200 (2024).

56. Lee, P., Chandel, N. S. & Celeste Simon, M. Cellular adaptation to hypoxia through hypoxia inducible factors and beyond. *Nat Rev Mol Cell Biol* doi:10.1038/s41580-020-0227-y.

57. Pouyssegur, J. & López-Barneo, J. Hypoxia in health and disease. *Mol Aspects Med* **47–48**, 1–2 (2016).

58. Wilson, W. R. & Hay, M. P. Targeting hypoxia in cancer therapy. *Nat. Rev. Cancer* **11**, 393–410 (2011).

59. Eales, K. L., Hollinshead, K. E. R. & Tennant, D. A. Hypoxia and metabolic adaptation of cancer cells. *Oncogenesis* **5**, e190–e190 (2016).

60. Warburg, O. On the origin of cancer cells. *Science (1979)* **123**, 309–314 (1956).

61. Luo, Y., Ma, J. & Lu, W. The Significance of Mitochondrial Dysfunction in Cancer. *International Journal of Molecular Sciences 2020, Vol. 21, Page 5598* **21**, 5598 (2020).

62. Heiden, M. G. V., Cantley, L. C. & Thompson, C. B. Understanding the warburg effect: The metabolic requirements of cell proliferation. *Science (1979)* **324**, 1029–1033 (2009).

63. Bertout, J. A., Patel, S. A. & Simon, M. C. The impact of O2 availability on human cancer. *Nat. Rev. Cancer* **8**, 967–975 (2008).

64. Ye, Y. *et al*. Characterization of hypoxia-associated molecular features to aid hypoxia-targeted therapy. *Nature Metabolism 2019 1:4* **1**, 431–444 (2019).

65. Sharp, F. R. & Bernaudin, M. HIF1 and oxygen sensing in the brain. *Nature Reviews Neuroscience* vol. 5 437–448 Preprint at https://doi.org/10.1038/nrn1408 (2004).

66. Wang, G. L., Jiang, B.-H., Rue, E. A. & Semenza, G. L. *Hypoxia-Inducible Factor 1 Is a Basic-Helix-Loop-Helix-PAS Heterodimer Regulated by Cellular 02 Tension (Dioxin Receptor/Erythropoietin/Hypoxia/Transcription)*. *Genetics* vol. 92 (1995).

67. Dengler, V. L., Galbraith, M. D. & Espinosa, J. M. Transcriptional regulation by hypoxia inducible factors. *Crit Rev Biochem Mol Biol* **49**, 1–15 (2014).

68. Hu, C.-J., Wang, L.-Y., Chodosh, L. A., Keith, B. & Simon, M. C. Differential Roles of Hypoxia-Inducible Factor 1α (HIF-1α) and HIF-2α in Hypoxic Gene Regulation. *Mol Cell Biol* **23**, 9361–9374 (2003).

69. Takeda, N. *et al*. Differential activation and antagonistic function of HIF-a isoforms in macrophages are essential for NO homeostasis. doi:10.1101/gad.

70. Tian, H., McKnight, S. L. & Russell, D. W. Endothelial PAS domain protein 1 (EPAS1), a transcription factor selectively expressed in endothelial cells. *Genes Dev* **11**, 72–82 (1997).

71. Taylor, C. T., Doherty, G., Fallon, P. G. & Cummins, E. P. Hypoxia-dependent regulation of inflammatory pathways in immune cells. *J Clin Invest* **126**, 3716–3724 (2016).

72. Markolovic, S., Wilkins, S. E. & Schofield, C. J. Protein Hydroxylation Catalyzed by 2-Oxoglutarate-dependent Oxygenases*. *Journal of Biological Chemistry* **290**, 20712–20722 (2015).

73. Keith, B., Johnson, R. S. & Simon, M. C. HIF1α and HIF2α: sibling rivalry in hypoxic tumour growth and progression. *Nat Rev Cancer* **12**, 9–22 (2012).

74. Kaelin, W. G. & Ratcliffe, P. J. Oxygen Sensing by Metazoans: The Central Role of the HIF Hydroxylase Pathway. *Mol Cell* **30**, 393–402 (2008).

75. Zhang, N. *et al.* The Asparaginyl Hydroxylase Factor Inhibiting HIF-1α Is an Essential Regulator of Metabolism. *Cell Metab* **11**, 364–378 (2010).

76. Cockman, M. E., Webb, J. D., Kramer, H. B., Kessler, B. M. & Ratcliffe, P. J. Proteomics-based Identification of Novel Factor Inhibiting Hypoxia-inducible Factor (FIH) Substrates Indicates Widespread Asparaginyl Hydroxylation of Ankyrin Repeat Domain-containing Proteins. *Molecular & Cellular Proteomics* **8**, 535–546 (2009).

77. Lando, D., Peet, D. J., Whelan, D. A., Gorman, J. J. & Whitelaw, M. L. Asparagine Hydroxylation of the HIF Transactivation Domain: A Hypoxic Switch. *Science (1979)* **295**, 858–861 (2002).

78. Brunelle, J. K. *et al.* Oxygen sensing requires mitochondrial ROS but not oxidative phosphorylation. *Cell Metab* **1**, 409–414 (2005).

79. Chandel, N. S. *et al.* Reactive Oxygen Species Generated at Mitochondrial Complex III Stabilize Hypoxia-inducible Factor-1α during Hypoxia: A MECHANISM OF O2 SENSING*. *Journal of Biological Chemistry* **275**, 25130–25138 (2000).

80. Guzy, R. D. *et al.* Mitochondrial complex III is required for hypoxia-induced ROS production and cellular oxygen sensing. *Cell Metab* **1**, 401–408 (2005).

81. Chandel, N. S. *et al.* Mitochondrial reactive oxygen species trigger hypoxia-induced transcription. *Proceedings of the National Academy of Sciences* **95**, 11715–11720 (1998).

82. Lee, G. *et al.* Oxidative Dimerization of PHD2 is Responsible for its Inactivation and Contributes to Metabolic Reprogramming via HIF-1α Activation. *Sci Rep* **6**, 18928 (2016).

83. Selak, M. A. *et al.* Succinate links TCA cycle dysfunction to oncogenesis by inhibiting HIF-α prolyl hydroxylase. *Cancer Cell* **7**, 77–85 (2005).

84. Pollard, P. J. *et al.* Accumulation of Krebs cycle intermediates and over-expression of HIF1α in tumours which result from germline FH and SDH mutations. *Hum Mol Genet* **14**, 2231–2239 (2005).

85. King, A., Selak, M. A. & Gottlieb, E. Succinate dehydrogenase and fumarate hydratase: linking mitochondrial dysfunction and cancer. *Oncogene* **25**, 4675–4682 (2006).

86. Intlekofer, A. M. *et al.* L-2-Hydroxyglutarate production arises from noncanonical enzyme function at acidic pH. *Nat Chem Biol* **13**, 494–500 (2017).

87. Fukuda, R. *et al.* HIF-1 Regulates Cytochrome Oxidase Subunits to Optimize Efficiency of Respiration in Hypoxic Cells. *Cell* **129**, 111–122 (2007).

88. Tello, D. *et al.* Induction of the Mitochondrial NDUFA4L2 Protein by HIF-1α Decreases Oxygen Consumption by Inhibiting Complex I Activity. *Cell Metab* **14**, 768–779 (2011).

89. Samanta, D. & Semenza, G. L. Maintenance of redox homeostasis by hypoxia-inducible factors. (2017) doi:10.1016/j.redox.2017.05.022.

90. Papandreou, I., Cairns, R. A., Fontana, L., Lim, A. L. & Denko, N. C. HIF-1 mediates adaptation to hypoxia by actively downregulating mitochondrial oxygen consumption. *Cell Metab* **3**, 187–197 (2006).

91. Kim, J., Tchernyshyov, I., Semenza, G. L. & Dang, C. V. HIF-1-mediated expression of pyruvate dehydrogenase kinase: A metabolic switch required for cellular adaptation to hypoxia. *Cell Metab* **3**, 177–185 (2006).

92. Birsoy, K. *et al.* An Essential Role of the Mitochondrial Electron Transport Chain in Cell Proliferation Is to Enable Aspartate Synthesis. *Cell* **162**, (2015).

93. Sullivan, L. B. *et al.* Supporting Aspartate Biosynthesis Is an Essential Function of Respiration in Proliferating Cells. *Cell* **162**, (2015).

94. Garcia-Bermudez, J. *et al.* Aspartate is a limiting metabolite for cancer cell proliferation under hypoxia and in tumours. *Nat Cell Biol* (2018) doi:10.1038/s41556-018-0118-z.

95. Hoefflin, R. *et al.* HIF-1α and HIF-2α differently regulate tumour development and inflammation of clear cell renal cell carcinoma in mice. doi:10.1038/s41467-020-17873-3.

96. Gordan, J. D. *et al.* HIF-α Effects on c-Myc Distinguish Two Subtypes of Sporadic VHL-Deficient Clear Cell Renal Carcinoma. *Cancer Cell* **14**, 435–446 (2008).

97. Pouysségur, J. *et al.* 'Warburg effect' controls tumor growth, bacterial, viral infections and immunity – Genetic deconstruction and therapeutic perspectives. *Semin Cancer Biol* **86**, 334–346 (2022).

98. Luo, X. *et al.* Emerging roles of lipid metabolism in cancer metastasis. doi:10.1186/s12943-017-0646-3.

99. Furuta, E. *et al.* Fatty Acid Synthase Gene Is Up-regulated by Hypoxia via Activation of Akt and Sterol Regulatory Element Binding Protein-1. *Cancer Res* **68**, 1003–1014 (2008).

100. Gao, X. *et al.* Acetate functions as an epigenetic metabolite to promote lipid synthesis under hypoxia. *Nature Communications 2016 7:1* **7**, 1–14 (2016).

101. Keenan, M. M. *et al.* ACLY and ACC1 Regulate Hypoxia-Induced Apoptosis by Modulating ETV4 via α-ketoglutarate. (2015) doi:10.1371/journal.pgen.1005599.

102. Melana, J. P. *et al.* The Hypoxic Microenvironment Induces Stearoyl-CoA Desaturase-1 Overexpression and Lipidomic Profile Changes in Clear Cell Renal Cell Carcinoma. *Cancers (Basel)* **13**, (2021).

103. Zhang, Y., Wang, H., Zhang, J., Lv, J. & Huang, Y. Positive feedback loop and synergistic effects between hypoxia-inducible factor-2α and stearoyl-CoA desaturase-1 promote tumorigenesis in clear cell renal cell carcinoma. *Cancer Sci* **104**, 416–422 (2013).

104. Savino, A. M. *et al.* Metabolic adaptation of acute lymphoblastic leukemia to the central nervous system microenvironment depends on stearoyl-CoA desaturase. *Nat Cancer* **1**, 998–1009 (2020).

105. Bacigalupa, Z. A. *et al.* HIF-2α expression and metabolic signaling require ACSS2 in clear cell renal cell carcinoma. *Journal of Clinical Investigation* **134**, (2024).

106. Bergström, J., Fürst, P., Norée, L. O. & Vinnars, E. Intracellular free amino acid concentration in human muscle tissue. *J Appl Physiol* **36**, 693–697 (1974).

107. Yuneva, M., Zamboni, N., Oefner, P., Sachidanandam, R. & Lazebnik, Y. Deficiency in glutamine but not glucose induces MYC-dependent apoptosis in human cells . *Journal of Cell Biology* **178**, 93–105 (2007).

108. Li, T., Copeland, C. & Le, A. Glutamine Metabolism in Cancer. *Adv Exp Med Biol* **1311**, 17–38 (2021).

109. Yoo, H. C. *et al.* A Variant of SLC1A5 Is a Mitochondrial Glutamine Transporter for Metabolic Reprogramming in Cancer Cells. *Cell Metab* **31**, 267-283.e12 (2020).

110. Lin, T. C. *et al.* Autophagy. *Autophagy* **8**, 1477–1493 (2012).

111. Strohecker, A. M. *et al.* Autophagy Sustains Mitochondrial Glutamine Metabolism and Growth of Braf V600E-Driven Lung Tumors. (1273) doi:10.1158/2159-8290.CD-13-0397.

112. Altman, B. J., Stine, Z. E. & Dang, C. V. From Krebs to clinic: glutamine metabolism to cancer therapy. *Nat Rev Cancer* **16**, 619–634 (2016).

113. Schulte, M. L. *et al.* Pharmacological blockade of ASCT2-dependent glutamine transport leads to antitumor efficacy in preclinical models. *Nat Med* **24**, 194–202 (2018).

114. Wahi, K. & Holst, J. ASCT2: a potential cancer drug target. *Expert Opin Ther Targets* **23**, 555–558 (2019).

115. Nicklin, P. *et al.* Bidirectional Transport of Amino Acids Regulates mTOR and Autophagy. *Cell* **136**, 521–534 (2009).

116. Timmerman, L. A. *et al.* Glutamine Sensitivity Analysis Identifies the xCT Antiporter as a Common Triple-Negative Breast Tumor Therapeutic Target. *Cancer Cell* **24**, 450–465 (2013).

117. Jin, J., Byun, J.-K., Choi, Y.-K. & Park, K.-G. Targeting glutamine metabolism as a therapeutic strategy for cancer. doi:10.1038/s12276-023-00971-9.

118. Wise, D. R. *et al.* Myc regulates a transcriptional program that stimulates mitochondrial glutaminolysis and leads to glutamine addiction. *Proc Natl Acad Sci U S A* **105**, 18782–18787 (2008).

119. Gao, P. *et al.* c-Myc suppression of miR-23a/b enhances mitochondrial glutaminase expression and glutamine metabolism. *Nature 2009 458:7239* **458**, 762–765 (2009).

120. Hu, W. *et al.* Glutaminase 2, a novel p53 target gene regulating energy metabolism and antioxidant function. *Proc Natl Acad Sci U S A* **107**, 7455–7460 (2010).

121. Srinivasan, M., Kalousek, F. & Curthoys, N. P. In vitro characterization of the mitochondrial processing and the potential function of the 68-kDa subunit of renal glutaminase. *Journal of Biological Chemistry* **270**, 1185–1190 (1995).

122. Elgadi, K. M., Meguid, R. A., Qian, M., Souba, W. W. & Abcouwer, S. F. Cloning and analysis of unique human glutaminase isoforms generated by tissue-specific alternative splicing. (1999).

123. Cassago, A. *et al*. Mitochondrial localization and structure-based phosphate activation mechanism of Glutaminase C with implications for cancer metabolism. *Proc Natl Acad Sci U S A* **109**, 1092–1097 (2012).

124. Feng, S., Aplin, C., Nguyen, T.-T. T., Milano, S. K. & Cerione, R. A. Filament formation drives catalysis by glutaminase enzymes important in cancer progression. *Nat Commun* **15**, 1971 (2024).

125. Adamoski, D. *et al*. Molecular mechanism of glutaminase activation through filamentation and the role of filaments in mitophagy protection. *Nat Struct Mol Biol* **30**, 1902–1912 (2023).

126. Curthoys, N. P. & Watford, M. REGULATION OF GLUTAMINASE ACTIVITY AND GLUTAMINE METABOLISM. *Annu. Rev. Nutr. J99S. JS* 33–42.

127. Colombo, S. L. *et al*. Molecular basis for the differential use of glucose and glutamine in cell proliferation as revealed by synchronized HeLa cells. *Proc Natl Acad Sci U S A* **108**, 21069–21074 (2011).

128. Polletta, L. *et al*. SIRT5 regulation of ammonia-induced autophagy and mitophagy. *Autophagy* **11**, 253–270 (2015).

129. Lu, W., Zuo, Y., Feng, Y. & Zhang, M. SIRT5 facilitates cancer cell growth and drug resistance in non-small cell lung cancer. *Tumour Biol* **35**, 10699–10705 (2014).

130. Hebert, A. S. *et al*. Calorie Restriction and SIRT3 Trigger Global Reprogramming of the Mitochondrial Protein Acetylome. *Mol Cell* **49**, 186–199 (2013).

131. Wróblewski, F. & Ladue, J. S. Serum glutamic pyruvic transaminase in cardiac with hepatic disease. *Proc Soc Exp Biol Med* **91**, 569–571 (1956).

132. Sorbi, D., Boynton, J. & Lindor, K. D. The ratio of aspartate aminotransferase to alanine aminotransferase: potential value in differentiating nonalcoholic steatohepatitis from alcoholic liver disease. *Am J Gastroenterol* **94**, 1018–1022 (1999).

133. Moreadith, R. W. & Lehninger, A. L. The pathways of glutamate and glutamine oxidation by tumor cell mitochondria. Role of mitochondrial NAD(P)+-dependent malic enzyme. *Journal of Biological Chemistry* **259**, 6215–6221 (1984).

134. Welbourne, T. C. Ammonia production and glutamine incorporation into glutathione in the functioning rat kidney. *Can J Biochem* **57**, 233–237 (1979).

135. Hensley, C. T., Wasti, A. T. & DeBerardinis, R. J. Glutamine and cancer: cell biology, physiology, and clinical opportunities. *J Clin Invest* **123**, 3678–3684 (2013).

136. Schofield, C. J. & Ratcliffe, P. J. Oxygen sensing by HIF hydroxylases. *Nature Reviews Molecular Cell Biology* vol. 5 343–354 Preprint at https://doi.org/10.1038/nrm1366 (2004).

137. DeBerardinis, R. J. *et al.* Beyond aerobic glycolysis: Transformed cells can engage in glutamine metabolism that exceeds the requirement for protein and nucleotide synthesis. *Proc Natl Acad Sci U S A* **104**, 19345–19350 (2007).

138. Wang, Y.-P. *et al.* Malic enzyme 2 connects the Krebs cycle intermediate fumarate to mitochondrial biogenesis. *Cell Metab* **33**, 1027-1041.e8 (2021).

139. Yang, W.-H., Qiu, Y., Stamatatos, O., Janowitz, T. & Lukey, M. J. Enhancing the Efficacy of Glutamine Metabolism Inhibitors in Cancer Therapy. *Trends Cancer* **7**, 790–804 (2021).

140. Erickson, J. W. & Cerione, R. A. Glutaminase: A Hot Spot For Regulation Of Cancer Cell Metabolism? *Oncotarget* **1**, 734–740 (2010).

141. Shukla, K. *et al.* Design, Synthesis, and Pharmacological Evaluation of Bis-2-(5-phenylacetamido-1,2,4-thiadiazol-2-yl)ethyl Sulfide 3 (BPTES) Analogs as Glutaminase Inhibitors. *J Med Chem* **55**, 10551–10563 (2012).

142. Hudson, C. D. *et al.* Altered glutamine metabolism in platinum resistant ovarian cancer. *Oncotarget* **7**,.

143. Biancur, D. E. *et al.* ARTICLE Compensatory metabolic networks in pancreatic cancers upon perturbation of glutamine metabolism. (2017) doi:10.1038/ncomms15965.

144. Wicker, C. A. *et al.* Glutaminase inhibition with telaglenastat (CB-839) improves treatment response in combination with ionizing radiation in head and neck squamous cell carcinoma models. *Cancer Lett* **502**, 180–188 (2021).

145. Varghese, S. *et al.* The Glutaminase Inhibitor CB-839 (Telaglenastat) Enhances the Antimelanoma Activity of T-Cell-Mediated Immunotherapies. doi:10.1158/1535-7163.MCT-20-0430.

146. Hensley, C. T., Wasti, A. T. & DeBerardinis, R. J. Glutamine and cancer: cell biology, physiology, and clinical opportunities. *J Clin Invest* **123**, 3678–3684 (2013).

147. Xiao, D. *et al.* The glutamine-alpha-ketoglutarate (AKG) metabolism and its nutritional implications. *Amino Acids* **48**, 2067–2080 (2016).

148. Jiang, L. *et al.* Reductive carboxylation supports redox homeostasis during anchorage-independent growth. *Nature* **532**, 255–258 (2016).

149. Reitman, Z. J. & Yan, H. Isocitrate Dehydrogenase 1 and 2 Mutations in Cancer: Alterations at a Crossroads of Cellular Metabolism. *JNCI: Journal of the National Cancer Institute* **102**, 932–941 (2010).

150. Metallo, C. M. *et al.* Reductive glutamine metabolism by IDH1 mediates lipogenesis under hypoxia. *Nature* **481**, 380–384.

151. Mullen, A. R. *et al.* Reductive carboxylation supports growth in tumour cells with defective mitochondria. *Nature 2011 481:7381* **481**, 385–388 (2011).

152. Dai, W. *et al.* FASN deficiency induces a cytosol-to-mitochondria citrate flux to mitigate detachment-induced oxidative stress. *Cell Rep* **42**, 112971 (2023).

153. Kapitsinou, P. P. & Haase, V. H. The VHL tumor suppressor and HIF: insights from genetic studies in mice. *Cell Death Differ* **15**, 650–659 (2008).

154. Gameiro, P. A. *et al.* In Vivo HIF-Mediated Reductive Carboxylation Is Regulated by Citrate Levels and Sensitizes VHL-Deficient Cells to Glutamine Deprivation. *Cell Metab* **17**, 372–385 (2013).

155. Mullen, A. R. *et al.* Oxidation of Alpha-Ketoglutarate Is Required for Reductive Carboxylation in Cancer Cells with Mitochondrial Defects. *Cell Rep* **7**, 1679–1690 (2014).

156. Jaccard, A. *et al.* Reductive carboxylation epigenetically instructs T cell differentiation. doi:10.1038/s41586-023-06546-y.

157. Jiang, H. *et al.* MOLECULAR CANCER RESEARCH | Mitochondrial Uncoupling Inhibits Reductive Carboxylation in Cancer Cells. doi:10.1158/1541-7786.MCR-23-0049.

158. Youle, R. J. & Narendra, D. P. *Mechanisms of Mitophagy*. www.nature.com/reviews/molcellbio (2011) doi:10.1038/nrm3028.

159. Palikaras, K., Lionaki, E. & Tavernarakis, N. Mechanisms of mitophagy in cellular homeostasis, physiology and pathology. *Nature Cell Biology* vol. 20 1013–1022 Preprint at https://doi.org/10.1038/s41556-018-0176-2 (2018).

160. Tal, R., Winter, G., Ecker, N., Klionsky, D. J. & Abeliovich, H. Aup1p, a Yeast Mitochondrial Protein Phosphatase Homolog, Is Required for Efficient Stationary Phase Mitophagy and Cell Survival*. *Journal of Biological Chemistry* **282**, 5617–5624 (2007).

161. Schweers, R. L. *et al.* NIX is required for programmed mitochondrial clearance during reticulocyte maturation. *Proceedings of the National Academy of Sciences* **104**, 19500–19505 (2007).

162. Kundu, M. *et al.* Ulk1 plays a critical role in the autophagic clearance of mitochondria and ribosomes during reticulocyte maturation. *Blood* **112**, 1493–1502 (2008).

163. Narendra, D., Tanaka, A., Suen, D.-F. & Youle, R. J. Parkin is recruited selectively to impaired mitochondria and promotes their autophagy . *Journal of Cell Biology* **183**, 795–803 (2008).

164. Ashrafi, G. & Schwarz, T. L. The pathways of mitophagy for quality control and clearance of mitochondria. *Cell Death Differ* **20**, 31–42 (2013).

165. Twig, G. & Shirihai, O. S. The Interplay Between Mitochondrial Dynamics and Mitophagy. *Antioxid. Redox Signal* **14**, 1939–1951.

166. Twig, G. *et al.* Fission and selective fusion govern mitochondrial segregation and elimination by autophagy. *EMBO J* **27**, 433–446 (2008).

167. Westermann, B. Mitochondrial fusion and fission in cell life and death. *Nat Rev Mol Cell Biol* **11**, 872–884 (2010).

168. Krantz, S. *et al.* Mitophagy mediates metabolic reprogramming of induced pluripotent stem cells undergoing endothelial differentiation. *Journal of Biological Chemistry* **297**, 101410 (2021).

169. Yamashita, S. I. *et al.* Mitochondrial division occurs concurrently with autophagosome formation but independently of Drp1 during mitophagy. *J Cell Biol* **215**, 649 (2016).

170. Harper, J. W., Ordureau, A. & Heo, J.-M. Building and decoding ubiquitin chains for mitophagy. *Nat Rev Mol Cell Biol* **19**, 93–108 (2018).

171. Sekine, S. *et al*. Reciprocal Roles of Tom7 and OMA1 during Mitochondrial Import and Activation of PINK1 Article Reciprocal Roles of Tom7 and OMA1 during Mitochondrial Import and Activation of PINK1. *Mol Cell* **73**, (2019).

172. Youle, R. J. & Narendra, D. P. *Mechanisms of Mitophagy*. *Nature Publishing Group* www.nature.com/reviews/molcellbio (2011) doi:10.1038/nrm3028.

173. Jin, S. M. & Youle, R. J. PINK1- and Parkin-mediated mitophagy at a glance. *J Cell Sci* **125**, 795–799 (2012).

174. Imai, Y. & Lu, B. Mitochondrial Dynamics and Mitophagy in Parkinson's Disease: Disordered cellular power plant becomes a big deal in a major movement disorder. (2011) doi:10.1016/j.conb.2011.10.016.

175. Lazarou, M. *et al*. The ubiquitin kinase PINK1 recruits autophagy receptors to induce mitophagy. doi:10.1038/nature14893.

176. Tanida, I. Autophagosome Formation and Molecular Mechanism of Autophagy. *Antioxid Redox Signal* **14**, 2201–2214 (2010).

177. Kim, K.-Y. *et al*. Parkin is a lipid-responsive regulator of fat uptake in mice and mutant human cells. *J Clin Invest* **121**, 3701–3712 (2011).

178. Zhang, C. *et al*. Parkin, a p53 target gene, mediates the role of p53 in glucose metabolism and the Warburg effect. *Proceedings of the National Academy of Sciences* **108**, 16259–16264 (2011).

179. Li, C. *et al*. PINK1 and PARK2 Suppress Pancreatic Tumorigenesis through Control of Mitochondrial Iron-Mediated Immunometabolism In Brief Developmental Cell Article PINK1 and PARK2 Suppress Pancreatic Tumorigenesis through Control of Mitochondrial Iron-Mediated Immunometabolism. *Dev Cell* **46**, 441–455 (2018).

180. McWilliams, T. G. *et al*. Basal Mitophagy Occurs Independently of PINK1 in Mouse Tissues of High Metabolic Demand. *Cell Metab* **27**, 439-449.e5 (2018).

181. Birgisdottir, Å. B., Lamark, T. & Johansen, T. The LIR motif – crucial for selective autophagy. *J Cell Sci* **126**, 3237–3247 (2013).

182. Ding, W. X. & Yin, X. M. Mitophagy: Mechanisms, pathophysiological roles, and analysis. *Biol Chem* **393**, 547–564 (2012).

183. Xian, H. & Liou, Y.-C. Functions of outer mitochondrial membrane proteins: mediating the crosstalk between mitochondrial dynamics and mitophagy Given the interplay of distinct molecular pathways of mitophagy, what signal in physiological contexts would stimulate specific route of mitochondrial elimination? *Cell Death Differ* doi:10.1038/s41418-020-00657-z.

184. Chen, M. *et al*. Mitophagy receptor FUNDC1 regulates mitochondrial dynamics and mitophagy. *Autophagy* **12**, 689–702 (2016).

185. Killackey, S. A., Philpott, D. J. & Girardin, S. E. Mitophagy pathways in health and disease. *J Cell Biol* **219**, (2020).

186. Macleod, K. F. Mitophagy and Mitochondrial Dysfunction in Cancer. *Annu. Rev. Cancer Biol* **4**, 41–60 (2020).

187. Xu, Z., Yang, L., Xu, S., Zhang, Z. & Cao, Y. The receptor proteins: pivotal roles in selective autophagy. *Acta Biochim Biophys Sin (Shanghai)* **47**, 571–580 (2015).

188. Marinković, M. & Novak, I. A brief overview of BNIP3L/NIX receptor-mediated mitophagy. *FEBS Open Bio* **11**, 3230 (2021).

189. Zhang, J. & Ney, P. A. Role of BNIP3 and NIX in cell death, autophagy, and mitophagy BCL2 and adenovirus E1B 19 kDa-interacting protein 3; LC3, microtubule-associated protein 1 light chain 3; MPTP, mitochondrial permeability transition pore; NIX, NIP3-like protein X; ULK1, Unc51-like kinase. *Cell Death Differ* **16**, 939–946 (2009).

190. Ney, P. A. Mitochondrial autophagy: Origins, significance, and role of BNIP3 and NIX. *Biochimica et Biophysica Acta (BBA) - Molecular Cell Research* **1853**, 2775–2783 (2015).

191. Glick, D. *et al.* BNip3 Regulates Mitochondrial Function and Lipid Metabolism in the Liver. *Mol Cell Biol* **32**, 2570–2584 (2012).

192. Marinković, M., Šprung, M. & Novak, I. Dimerization of mitophagy receptor BNIP3L/NIX is essential for recruitment of autophagic machinery. (2020) doi:10.1080/15548627.2020.1755120.

193. Ohi, N. *et al.* A novel adenovirus E1B19K-binding protein B5 inhibits apoptosis induced by Nip3 by forming a heterodimer through the C-terminal hydrophobic region. *Cell Death Differ* **6**, 314–325 (1999).

194. Rodger, C. E., McWilliams, T. G. & Ganley, I. G. Mammalian mitophagy – from in vitro molecules to in vivo models. *FEBS Journal* **285**, 1185–1202 (2018).

195. Zhao, J.-F., Rodger, C. E., Allen, G. F. G., Weidlich, S. & Ganley, I. G. HIF1α-dependent mitophagy facilitates cardiomyoblast differentiation. *Cell Stress* **4**, (2020).

196. Melser, S. *et al.* Rheb Regulates Mitophagy Induced by Mitochondrial Energetic Status. *Cell Metab* **17**, 719–730 (2013).

197. Li, Y. *et al.* Bnip3 Mediates the Hypoxia-induced Inhibition on Mammalian Target of Rapamycin by Interacting with Rheb*. *Journal of Biological Chemistry* **282**, 35803–35813 (2007).

198. Vyas, S., Zaganjor, E. & Haigis, M. C. Leading Edge Review Mitochondria and Cancer. doi:10.1016/j.cell.2016.07.002.

199. He, Y.-L. *et al.* Title: BNIP3 phosphorylation by JNK1/2 promotes mitophagy via enhancing its stability under hypoxia 2 Running title: JNK1/2 regulates BNIP3-mediated mitophagy 3. doi:10.1101/2020.08.27.271270.

200. Poole, L. P., Bock-Hughes, A., Berardi, D. E. & Macleod, K. F. ULK1 promotes mitophagy via phosphorylation and stabilization of BNIP3. *Sci Rep* **11**, (2021).

201. Wu, W. *et al.* ULK1 translocates to mitochondria and phosphorylates FUNDC1 to regulate mitophagy. *EMBO Rep* **15**, 566–575 (2014).

202. Nguyen-Dien, G. T. *et al.* FBXL4 suppresses mitophagy by restricting the accumulation of NIX and BNIP3 mitophagy receptors. *EMBO J* e112767 (2023) doi:10.15252/EMBJ.2022112767.

203. Sandoval, H. *et al.* Essential role for Nix in autophagic maturation of erythroid cells. *Nature* **454**, 232–235 (2008).

204. Humpton, T. J. *et al.* Oncogenic KRAS induces NIX-mediated mitophagy to promote pancreatic cancer. *Cancer Discov* **9**, 1268–1287 (2019).

205. Jung, J. *et al.* Molecular Cell Biology Mitochondrial NIX Promotes Tumor Survival in the Hypoxic Niche of Glioblastoma. (2019) doi:10.1158/0008-5472.CAN-19-0198.

206. Wilhelm, L. P. *et al.* BNIP3L / NIX regulates both mitophagy and pexophagy . *EMBO J* **41**, (2022).

207. Sandoval, H. *et al.* Essential role for Nix in autophagic maturation of erythroid cells. *Nature* **454**, 232–235 (2008).

208. Springer, M. Z. *et al.* BNIP3-dependent mitophagy promotes cytosolic localization of LC3B and metabolic homeostasis in the liver. *Autophagy* **17**, 3530–3546 (2021).

209. Berardi, D. E. *et al.* Lipid droplet turnover at the lysosome inhibits growth of hepatocellular carcinoma in a BNIP3-dependent manner. *Sci Adv* **8**, 2510 (2022).

210. Maes, H. *et al.* BNIP3 supports melanoma cell migration and vasculogenic mimicry by orchestrating the actin cytoskeleton. *Cell Death Dis* **5**, e1127–e1127 (2014).

211. Vara-Pérez, M. *et al.* BNIP3 promotes HIF-1α-driven melanoma growth by curbing intracellular iron homeostasis. *EMBO J* **40**, (2021).

212. ROWLEY, J. D. A New Consistent Chromosomal Abnormality in Chronic Myelogenous Leukaemia identified by Quinacrine Fluorescence and Giemsa Staining. *Nature* **243**, 290–293 (1973).

213. Heisterkamp, N. *et al.* Localization of the c-abl oncogene adjacent to a translocation break point in chronic myelocytic leukaemia. *Nature* **306**, 239–242 (1983).

214. Faderl, S. *et al.* The Biology of Chronic Myeloid Leukemia. *New England Journal of Medicine* **341**, 164–172 (1999).

215. Apperley, J. F. Chronic myeloid leukaemia. *The Lancet* **385**, 1447–1459 (2015).

216. Höglund, M., Sandin, F. & Simonsson, B. Epidemiology of chronic myeloid leukaemia: an update. *Ann Hematol* **94**, 241–247 (2015).

217. Pendergast, A. M., Muller, A. J., Havlik, M. H., Maru, Y. & Witte, O. N. BCR sequences essential for transformation by the BCR-ABL oncogene bind to the ABL SH2 regulatory domain in a non-phosphotyrosine-dependent manner. *Cell* **66**, 161–171 (1991).

218. Melo, J. V & Deininger, M. W. N. Biology of chronic myelogenous leukemia—signaling pathways of initiation and transformation. *Hematol Oncol Clin North Am* **18**, 545–568 (2004).

219. Cilloni, D. & Saglio, G. Molecular Pathways: BCR-ABL. (2011) doi:10.1158/1078-0432.CCR-10-1613.

220. He, Y. *et al.* The coiled-coil domain and Tyr177 of bcr are required to induce a murine chronic myelogenous leukemia–like disease by bcr/abl. *Blood* **99**, 2957–2968 (2002).

221. Hochhaus, A. *et al.* Expert opinion—management of chronic myeloid leukemia after resistance to second-generation tyrosine kinase inhibitors. *Leukemia* **34**, 1495–1502 (2020).

222. Hochhaus, A. *et al.* European LeukemiaNet 2020 recommendations for treating chronic myeloid leukemia. *Leukemia* **34**, 966–984 (2020).

223. O'Hare, T. *et al.* AP24534, a Pan-BCR-ABL Inhibitor for Chronic Myeloid Leukemia, Potently Inhibits the T315I Mutant and Overcomes Mutation-Based Resistance. *Cancer Cell* **16**, 401–412 (2009).

224. Mahon, F. X. *et al.* Discontinuation of imatinib in patients with chronic myeloid leukaemia who have maintained complete molecular remission for at least 2 years: the prospective, multicentre Stop Imatinib (STIM) trial. *Lancet Oncol* **11**, 1029–1035 (2010).

225. Michor, F. *et al.* Dynamics of chronic myeloid leukaemia. *Nature* **435**, 1267–1270 (2005).

226. Chomel, J. C. *et al.* Leukemic stem cell persistence in chronic myeloid leukemia patients with sustained undetectable molecular residual disease. *Blood* **118**, 3657–3660 (2011).

227. Bhatia, R. *et al.* Persistence of malignant hematopoietic progenitors in chronic myelogenous leukemia patients in complete cytogenetic remission following imatinib mesylate treatment. *Blood* **101**, 4701–4707 (2003).

228. Liu, J., Pei, J. & Lai, L. A combined computational and experimental strategy identifies mutations conferring resistance to drugs targeting the BCR-ABL fusion protein. doi:10.1038/s42003-019-0743-5.

229. Thomas, J., Wang, L., Clark, R. E. & Pirmohamed, M. Active transport of imatinib into and out of cells: implications for drug resistance. (2004) doi:10.1182/blood-2003-12-4276.

230. Vetrie, D., Helgason, G. V. & Copland, M. The leukaemia stem cell: similarities, differences and clinical prospects in CML and AML. *Nature Reviews Cancer* vol. 20 158–173 Preprint at https://doi.org/10.1038/s41568-019-0230-9 (2020).

231. Hamilton, A. *et al.* Chronic myeloid leukemia stem cells are not dependent on Bcr-Abl kinase activity for their survival. (2012) doi:10.1182/blood.

232. Corbin, A. S. *et al.* Human chronic myeloid leukemia stem cells are insensitive to imatinib despite inhibition of BCR-ABL activity. *Journal of Clinical Investigation* **121**, 396–409 (2011).

233. Andreas, H. *et al.* Asciminib in Newly Diagnosed Chronic Myeloid Leukemia. *New England Journal of Medicine* **0**, (2024).

234. Manley, P. W., Barys, L. & Cowan-Jacob, S. W. The specificity of asciminib, a potential treatment for chronic myeloid leukemia, as a myristate-pocket binding ABL inhibitor and analysis of its interactions with mutant forms of BCR-ABL1 kinase. *Leuk Res* **98**, 106458 (2020).

235. Cortes, J. E. *et al.* Asciminib monotherapy in patients with chronic-phase chronic myeloid leukemia with the T315I mutation after ≥1 prior tyrosine kinase inhibitor: 2-year follow-up results. *Leukemia* **38**, 1522–1533 (2024).

236. De Beauchamp, L., Himonas, E. & Vignir Helgason, G. Mitochondrial metabolism as a potential therapeutic target in myeloid leukaemia. doi:10.1038/s41375-021-01416-w.

237. Rattigan, K. M., Zarou, M. M. & Helgason, G. V. Metabolism in stem cell–driven leukemia: parallels between hematopoiesis and immunity. *Blood* **141**, 2553–2565 (2023).

238. Flis, K., Irvine, D., Copland, M., Bhatia, R. & Skorski, T. Chronic myeloid leukemia stem cells display alterations in expression of genes involved in oxidative phosphorylation. *Leuk Lymphoma* **53**, 2474–2478 (2012).

239. Kuntz, E. M. *et al.* Targeting mitochondrial oxidative phosphorylation eradicates therapy-resistant chronic myeloid leukemia stem cells. *Nat Med* **23**, 1234–1240 (2017).

240. Abraham, A. *et al.* SIRT1 regulates metabolism and leukemogenic potential in CML stem cells. *Journal of Clinical Investigation* **129**, 2685–2701 (2019).

241. Giustacchini, A. *et al.* Single-cell transcriptomics uncovers distinct molecular signatures of stem cells in chronic myeloid leukemia. *Nat Med* **23**, 692–702 (2017).

242. Reed, G. A. *et al.* A Phase 1 study of intravenous infusions of tigecycline in patients with acute myeloid leukemia. *Cancer Med* **5**, 3031–3040 (2016).

243. Molina, J. R. *et al.* An inhibitor of oxidative phosphorylation exploits cancer vulnerability. doi:10.1038/s41591-018-0052-4.

244. Yap, T. A. *et al.* Complex I inhibitor of oxidative phosphorylation in advanced solid tumors and acute myeloid leukemia: phase I trials. *Nat Med* **29**, 115–126 (2023).

245. Rattigan, K. M. *et al.* Pyruvate anaplerosis is a targetable vulnerability in persistent leukaemic stem cells. doi:10.1038/s41467-023-40222-z.

246. Rendina-Ruedy, E. & Rosen, C. J. Lipids in the Bone Marrow: An Evolving Perspective. *Cell Metabolism* vol. 31 219–231 Preprint at https://doi.org/10.1016/j.cmet.2019.09.015 (2020).

247. Woolthuis, C. M. *et al.* Leukemic Stem Cells Evade Chemotherapy by Metabolic Adaptation to an Adipose Tissue Niche. *Cell Stem Cell* **19**, 23–37 (2016).

248. Jain, I. H. *et al.* Genetic Screen for Cell Fitness in High or Low Oxygen Highlights Mitochondrial and Lipid Metabolism. *Cell* **181**, 716-727.e11 (2020).

249. Zarou, M. M. *et al.* Inhibition of mitochondrial folate metabolism drives differentiation through mTORC1 mediated purine sensing. doi:10.1038/s41467-024-46114-0.

250. Desplat, V. *et al.* Hypoxia Modifies Proliferation and Differentiation of CD34+ CML Cells. *Stem Cells* **20**, 347–354 (2002).

251. Ng, K. P. *et al.* Physiologic hypoxia promotes maintenance of CML stem cells despite effective BCR-ABL1 inhibition Key Points • Hypoxia mediates TKI resistance. • Hypoxia enhances CML stem cell maintenance. (2014) doi:10.1182/blood-2013-07-511907.

252. Cheloni, G. *et al.* Targeting chronic myeloid leukemia stem cells with the hypoxia-inducible factor inhibitor acriflavine. *Blood* **130**, 655–665 (2017).

253. Qiu, S. *et al.* Metabolic adaptation to tyrosine kinase inhibition in leukemia stem cells. *Blood* **142**, 574–588 (2023).

254. Wang, J. *et al.* HIF-2α inhibition disrupts leukemia stem cell metabolism and impairs vascular microenvironment to enhance chronic myeloid leukemia treatment. *Cancer Lett* **597**, 217060 (2024).

255. Panuzzo, C. *et al.* mTORC2 Is Activated under Hypoxia and Could Support Chronic Myeloid Leukemia Stem Cells. *Int J Mol Sci* **24**, 1234 (2023).

256. Lawson, H. *et al.* The selective prolyl hydroxylase inhibitor IOX5 stabilizes HIF-1α and compromises development and progression of acute myeloid leukemia. *Nature Cancer* | **5**, 916–937 (2024).

257. Voorde, J. Vande *et al.* Improving the metabolic fidelity of cancer models with a physiological cell culture medium. *Sci Adv* **5**, eaau7314 (2019).

258. Um, J. H., Kim, Y. Y., Finkel, T. & Yun, J. Sensitive Measurement of Mitophagy by Flow Cytometry Using the pH-dependent Fluorescent Reporter mt-Keima. *J. Vis. Exp* 58099 doi:10.3791/58099.

259. Hernandez, G. *et al.* MitoTimer. *Autophagy* **9**, 1852–1861 (2013).

260. Hernandez, G. *et al.* MitoTimer: A novel tool for monitoring mitochondrial turnover. *Autophagy* **9**, 1852–1861 (2013).

261. Ferree, A. W. *et al.* MitoTimer probe reveals the impact of autophagy, fusion, and motility on subcellular distribution of young and old mitochondrial protein and on relative mitochondrial protein age. *Autophagy* **9**, 1887 (2013).

262. O'Prey, J. *et al.* Chapter Six - Application of CRISPR/Cas9 to Autophagy Research. in *Molecular Characterization of Autophagic Responses, Part B* (eds. Galluzzi, L., Bravo-San Pedro, J. M. & Kroemer, G. B. T.-M. in E.) vol. 588 79–108 (Academic Press, 2017).

263. Medicine, O. & Longevity, C.-L. Corrigendum Corrigendum to 'Slower Dynamics and Aged Mitochondria in Sporadic Alzheimer's Disease'. *Hindawi Oxidative Medicine and Cellular Longevity* **2017**, (2017).

264. Mahmood, M. *et al.* Mitochondrial DNA mutations drive aerobic glycolysis to enhance checkpoint blockade response in melanoma. *Nature Cancer 2024 5:4* **5**, 659–672 (2024).

265. Rattigan, K. M. *et al.* Pyruvate anaplerosis is a targetable vulnerability in persistent leukaemic stem cells. doi:10.1038/s41467-023-40222-z.

266. Miller, P. H. *et al.* Analysis of parameters that affect human hematopoietic cell outputs in mutant c-kit-immunodeficient mice. (2017) doi:10.1016/j.exphem.2016.12.012.

267. An end to end workflow for differential gene expression using Affymetrix microarrays. https://bioconductor.org/packages/devel/workflows/vignettes/maEndToEnd/inst/doc/MA-Workflow.html#.

268. Dawson, A. An Investigation into the Myeloid Leukaemic Bone Marrow. (2017).

269. Ng, K. P. *et al.* Physiologic hypoxia promotes maintenance of CML stem cells despite effective BCR-ABL1 inhibition. *Blood* (2014) doi:10.1182/blood-2013-07-511907.

270. Parmar, K., Mauch, P., Vergilio, J.-A., Sackstein, R. & Down, J. D. *Distribution of Hematopoietic Stem Cells in the Bone Marrow According to Regional Hypoxia*. (2007).

271. Azab, A. K. *et al.* The influence of hypoxia on CML trafficking through modulation of CXCR4 and E-cadherin expression. *Leukemia* vol. 27 961–964 Preprint at https://doi.org/10.1038/leu.2012.353 (2013).

272. Mohyeldin, A., Garzón-Muvdi, T. & Quiñones-Hinojosa, A. Oxygen in stem cell biology: A critical component of the stem cell niche. *Cell Stem Cell* vol. 7 150–161 Preprint at https://doi.org/10.1016/j.stem.2010.07.007 (2010).

273. Wang, Y. *et al*. Coordinative metabolism of glutamine carbon and nitrogen in proliferating cancer cells under hypoxia. *Nature Communications 2019 10:1* **10**, 1–14 (2019).

274. Yoo, H. C. *et al*. A Variant of SLC1A5 Is a Mitochondrial Glutamine Transporter for Metabolic Reprogramming in Cancer Cells. *Cell Metab* **31**, 267-283.e12 (2020).

275. Fendt, S. M. *et al*. Reductive glutamine metabolism is a function of the α-ketoglutarate to citrate ratio in cells. *Nat Commun* **4**, 1–11 (2013).

276. DeBerardinis, R. J., Lum, J. J., Hatzivassiliou, G. & Thompson, C. B. The Biology of Cancer: Metabolic Reprogramming Fuels Cell Growth and Proliferation. *Cell Metabolism* vol. 7 11–20 Preprint at https://doi.org/10.1016/j.cmet.2007.10.002 (2008).

277. Gallipoli, P. *et al*. Glutaminolysis is a metabolic dependency in FLT3ITD acute myeloid leukemia unmasked by FLT3 tyrosine kinase inhibition. *Blood* **131**, 1639–1653 (2018).

278. Schubert, C. *et al*. The SCLtTAxBCR-ABL transgenic mouse model closely reflects the differential effects of dasatinib on normal and malignant hematopoiesis in chronic phase-CML patients. (2017).

279. Spinelli, J. B. *et al*. Fumarate is a terminal electron acceptor in the mammalian electron transport chain.

280. Mashimo, T. *et al*. Article Acetate Is a Bioenergetic Substrate for Human Glioblastoma and Brain Metastases. doi:10.1016/j.cell.2014.11.025.

281. García-Cañaveras, J. C. *et al*. SHMT inhibition is effective and synergizes with methotrexate in T-cell acute lymphoblastic leukemia. *Leukemia* **35**, 377–388 (2021).

282. Losman, J.-A., Koivunen, P. & Kaelin, W. G. 2-Oxoglutarate-dependent dioxygenases in cancer. doi:10.1038/s41568-020-00303-3.

283. Wise, D. R. *et al*. Hypoxia promotes isocitrate dehydrogenase-dependent carboxylation of α-ketoglutarate to citrate to support cell growth and viability. doi:10.1073/pnas.1117773108.

284. Metallo, C. M. *et al*. Reductive glutamine metabolism by IDH1 mediates lipogenesis under hypoxia. *Nature 2011 481:7381* **481**, 380–384 (2011).

285. Intlekofer, A. M. *et al*. Hypoxia Induces Production of L-2-Hydroxyglutarate. *Cell Metab* **22**, 304–311 (2015).

286. Gallipoli, P. *et al*. Glutaminolysis is a metabolic dependency in FLT3ITD acute myeloid leukemia unmasked by FLT3 tyrosine kinase inhibition. *Blood* **131**, 1639–1653 (2018).

287. Lee, P. *et al*. Targeting glutamine metabolism slows soft tissue sarcoma growth. doi:10.1038/s41467-020-14374-1.

288. Jin, J., Byun, J.-K., Choi, Y.-K. & Park, K.-G. Targeting glutamine metabolism as a therapeutic strategy for cancer. doi:10.1038/s12276-023-00971-9.

289. Altman, B. J., Stine, Z. E. & Dang, C. V. From Krebs to clinic: Glutamine metabolism to cancer therapy. *Nature Reviews Cancer* vol. 16 619–634 Preprint at https://doi.org/10.1038/nrc.2016.71 (2016).

290. Metallo, C. M. *et al.* Reductive glutamine metabolism by IDH1 mediates lipogenesis under hypoxia. *Nature* **481**, 380–384.

291. Kinstrie, R. *et al.* CD93 is expressed on chronic myeloid leukemia stem cells and identifies a quiescent population which persists after tyrosine kinase inhibitor therapy. *Leukemia* **34**, 1613–1625 (2020).

292. Dawson, A. An Investigation into the Myeloid Leukaemic Bone Marrow. (2017).

293. Ding, W. X. & Yin, X. M. Mitophagy: Mechanisms, pathophysiological roles, and analysis. *Biol Chem* **393**, 547–564 (2012).

294. Zhang, J. & Ney, P. A. Role of BNIP3 and NIX in cell death, autophagy, and mitophagy BCL2 and adenovirus E1B 19 kDa-interacting protein 3; LC3, microtubule-associated protein 1 light chain 3; MPTP, mitochondrial permeability transition pore; NIX, NIP3-like protein X; ULK1, Unc51-like kinase. *Cell Death Differ* **16**, 939–946 (2009).

295. Ianniciello, A. *et al.* ULK1 inhibition promotes oxidative stress-induced differentiation and sensitizes leukemic stem cells to targeted therapy. *Sci. Transl. Med* **13**, 5016 (2021).

296. Baquero, P. *et al.* Targeting quiescent leukemic stem cells using second generation autophagy inhibitors. *Leukemia* **33**, 981–994 (2019).

297. Liu, L., Sakakibara, K., Chen, Q. & Okamoto, K. Receptor-mediated mitophagy in yeast and mammalian systems. *REVIEW npg Cell Research* **24**, 787–795 (2014).

298. Marinković, M. & Novak, I. A brief overview of BNIP3L/NIX receptor-mediated mitophagy. *FEBS Open Bio* **11**, 3230 (2021).

299. Macleod, K. F. Mitophagy and Mitochondrial Dysfunction in Cancer. *Annu. Rev. Cancer Biol* **4**, 41–60 (2020).

300. Marinković, M., Šprung, M. & Novak, I. Dimerization of mitophagy receptor BNIP3L/NIX is essential for recruitment of autophagic machinery. (2020) doi:10.1080/15548627.2020.1755120.

301. Um, J. H., Kim, Y. Y., Finkel, T. & Yun, J. Sensitive Measurement of Mitophagy by Flow Cytometry Using the pH-dependent Fluorescent Reporter mt-Keima. *J. Vis. Exp* 58099 doi:10.3791/58099.

302. Liu, W. J. *et al.* p62 links the autophagy pathway and the ubiqutin–proteasome system upon ubiquitinated protein degradation. *Cell Mol Biol Lett* **21**, 29 (2016).

303. Poole, L. P., Bock-Hughes, A., Berardi, D. E. & Macleod, K. F. ULK1 promotes mitophagy via phosphorylation and stabilization of BNIP3. *Sci Rep* **11**, (2021).

304. Hernandez, G. *et al.* MitoTimer: A novel tool for monitoring mitochondrial turnover. *Autophagy* **9**, 1852–1861 (2013).

305. Ferree, A. W. *et al.* MitoTimer probe reveals the impact of autophagy, fusion, and motility on subcellular distribution of young and old mitochondrial protein and on relative mitochondrial protein age. *Autophagy* **9**, 1887 (2013).

306. Krantz, S. *et al.* Mitophagy mediates metabolic reprogramming of induced pluripotent stem cells undergoing endothelial differentiation. *Journal of Biological Chemistry* **297**, 101410 (2021).

307. Liu, L., Li, Y., Chen, G. & Chen, Q. Crosstalk between mitochondrial biogenesis and mitophagy to maintain mitochondrial homeostasis. *J Biomed Sci* **30**, 86 (2023).

308. Haase, V. H. Regulation of erythropoiesis by hypoxia-inducible factors. (2012) doi:10.1016/j.blre.2012.12.003.

309. Ikeda, M. *et al.* Heme-dependent induction of mitophagy program during differentiation of murine erythroid cells. *Exp Hematol* **118**, 21–30 (2023).

310. Paradkar, P. N., Zumbrennen, K. B., Paw, B. H., Ward, D. M. & Kaplan, J. Regulation of Mitochondrial Iron Import through Differential Turnover of Mitoferrin 1 and Mitoferrin 2. *Mol Cell Biol* **29**, 1007–1016 (2009).

311. Maes, H. *et al.* BNIP3 supports melanoma cell migration and vasculogenic mimicry by orchestrating the actin cytoskeleton. *Cell Death Dis* **5**, e1127–e1127 (2014).

312. Vara-Pérez, M. *et al.* BNIP3 promotes HIF-1α-driven melanoma growth by curbing intracellular iron homeostasis. *EMBO J* **40**, (2021).

313. Berardi, D. E. *et al.* Lipid droplet turnover at the lysosome inhibits growth of hepatocellular carcinoma in a BNIP3-dependent manner. *Sci Adv* **8**, 2510 (2022).

314. Oburoglu, L. *et al.* Cell Stem Cell Article Glucose and Glutamine Metabolism Regulate Human Hematopoietic Stem Cell Lineage Specification. (2014) doi:10.1016/j.stem.2014.06.002.

315. Ikeda, M. *et al.* Heme-dependent induction of mitophagy program during differentiation of murine erythroid cells. *Exp Hematol* **118**, 21–30 (2023).

316. Kuntz, E. M. *et al.* Targeting mitochondrial oxidative phosphorylation eradicates therapy-resistant chronic myeloid leukemia stem cells. *Nat Med* **23**, 1234–1240 (2017).

317. Zarou, M. M. *et al.* Inhibition of mitochondrial folate metabolism drives differentiation through mTORC1 mediated purine sensing. doi:10.1038/s41467-024-46114-0.

318. Bargiela, D., Burr, S. P. & Chinnery, P. F. Mitochondria and Hypoxia: Metabolic Crosstalk in Cell-Fate Decisions. *Trends in Endocrinology & Metabolism* **29**, 249–259 (2018).

319. Qiu, S. *et al.* Metabolic adaptation to tyrosine kinase inhibition in leukemia stem cells. *Blood* **142**, 574–588 (2023).

320. Cheloni, G. *et al.* Targeting chronic myeloid leukemia stem cells with the hypoxia-inducible factor inhibitor acriflavine. *Blood* **130**, 655–665 (2017).

321. Zhao, F. *et al.* Imatinib resistance associated with BCR-ABL upregulation is dependent on HIF-1α-induced metabolic reprograming. *Oncogene* **29**, 2962–2972 (2010).

322. Spinelli, J. B. *et al.* Fumarate is a terminal electron acceptor in the mammalian electron transport chain.

323. Carroll, B., Helgason, G. V., Ianniciello, A. & Rattigan, K. M. Citation: Ianniciello A, Rattigan KM and Helgason GV (2018) The Ins and Outs of Autophagy and Metabolism in Hematopoietic and Leukemic Stem Cells: Food for Thought The Ins and Outs of Autophagy and Metabolism in Hematopoietic and Leukemic Stem Cells: Food. *Front. Cell Dev. Biol* **6**, 120 (2018).

324. Helgason, G. V., Karvela, M. & Holyoake, T. L. Kill one bird with two stones: Potential efficacy of BCR-ABL and autophagy inhibition in CML. *Blood* vol. 118 2035–2043 Preprint at https://doi.org/10.1182/blood-2011-01-330621 (2011).

325. Helgason, G. V., Young, G. A. R. & Holyoake, T. L. Targeting chronic myeloid leukemia stem cells. *Curr Hematol Malig Rep* **5**, 81–87 (2010).

326. Helgason, G. V., Holyoake, T. L., Ryan, K. M. & O'gorman, P. 1 Role of autophagy in cancer prevention, development and therapy. *Essays Biochem* **55**, 2013 (2020).

327. Karvela, M. *et al*. ATG7 regulates energy metabolism, differentiation and survival of Philadelphia-chromosome-positive cells. *Autophagy* **12**, (2016).

328. Ianniciello, A. *et al*. ULK1 inhibition promotes oxidative stress-induced differentiation and sensitizes leukemic stem cells to targeted therapy. *Sci. Transl. Med* **13**, 5016 (2021).

329. Bellodi, C. *et al*. Targeting autophagy potentiates tyrosine kinase inhibitor-induced cell death in Philadelphia chromosome-positive cells, including primary CML stem cells. *Journal of Clinical Investigation* **119**, 1109–1123 (2009).

330. Baquero, P. *et al*. Targeting quiescent leukemic stem cells using second generation autophagy inhibitors. *Leukemia* **33**, 981–994 (2019).

331. Mitchell, R. *et al*. Targeting BCR-ABL-independent TKI resistance in chronic myeloid leukemia by mTOR and autophagy inhibition. *J Natl Cancer Inst* **110**, 467–478 (2018).

332. Horne, G. A. *et al*. Chronic myelogenous leukaemia A randomised phase II trial of hydroxychloroquine and imatinib versus imatinib alone for patients with chronic myeloid leukaemia in major cytogenetic response with residual disease. *Leukemia* **34**, 1775–1786 (2020).

333. Park, C. W. *et al*. BNIP3 is degraded by ULK1-dependent autophagy via MTORC1 and AMPK View supplementary material. *www.landesbioscience.com Autophagy* **345**, 345–360 (2013).

334. Prakasam, A. *et al*. JNK1/2 regulate Bid by direct phosphorylation at Thr59 in response to ALDH1L1. *Cell Death Dis* **5**, e1358–e1358 (2014).

335. Ordureau, A. *et al*. Temporal proteomics during neurogenesis reveals large-scale proteome and organelle remodeling via selective autophagy. *Mol Cell* **81**, 5082-5098.e11 (2021).

336. Jain, I. H. *et al*. Genetic Screen for Cell Fitness in High or Low Oxygen Highlights Mitochondrial and Lipid Metabolism. *Cell* **181**, 716-727.e11 (2020).

337. Madhu, V. *et al*. The mitophagy receptor BNIP3 is critical for the regulation of metabolic homeostasis and mitochondrial function in the nucleus pulposus cells of the intervertebral disc. (2023) doi:10.1080/15548627.2022.2162245.

338. Panayiotou, C., Solaroli, N., Johansson, M. & Karlsson, A. Evidence of an intact N-terminal translocation sequence of human mitochondrial adenylate kinase 4. *Int J Biochem Cell Biol* **42**, 62–69 (2010).

339. Jan, Y.-H. *et al*. Adenylate kinase 4 modulates oxidative stress and stabilizes HIF-1α to drive lung adenocarcinoma metastasis. doi:10.1186/s13045-019-0698-5.

340. Liu, X. *et al.* Adenylate Kinase 4 Modulates the Resistance of Breast Cancer Cells to Tamoxifen through an m 6 A-Based Epitranscriptomic Mechanism. (2020) doi:10.1016/j.ymthe.2020.09.007.

341. Zhao, Y. *et al.* GLIPR2 is a negative regulator of autophagy and the BECN1-ATG14-containing phosphatidylinositol 3-kinase complex. *Autophagy* **17**, 2891–2904 (2021).